

Donor functionalized BODIPYs

Ph.D. Thesis

By

BHAUSAHEB KASHINATH DHOKALE



**DEPARTMENT OF CHEMISTRY
INDIAN INSTITUTE OF TECHNOLOGY
INDORE**

May, 2015

Donor functionalized BODIPYs

A THESIS

*Submitted in partial fulfillment of the
requirements for the award of the degree
of*
DOCTOR OF PHILOSOPHY

By

BHAUSAHEB KASHINATH DHOKALE



**DISCIPLINE OF CHEMISTRY
INDIAN INSTITUTE OF TECHNOLOGY
INDORE**

May, 2015



INDIAN INSTITUTE OF TECHNOLOGY INDORE

CANDIDATE'S DECLARATION

I hereby certify that the work which is being presented in the thesis entitled **Donor functionalized BODIPYs** for the partial fulfillment of the requirements for the award of the degree of **DOCTOR OF PHILOSOPHY** and submitted in the **DISCIPLINE OF CHEMISTRY, Indian Institute of Technology Indore**, is an authentic record of my own work carried out during the time period from JULY, 2010 to APRIL, 2015 under the supervision Dr. Rajneesh Misra, Associate Professor.

The matter presented in this thesis has not been submitted by me for the award of any other degree of this or any other institute.

Signature of the student with date
(**BHAUSAHEB KASHINATH DHOKALE**)

This is to certify that the above statement made by the candidate is correct to the best of my knowledge.

Signature of Thesis Supervisor with date
(**Dr. RAJNEESH MISRA**)

BHAUSAHEB KASHINATH DHOKALE has successfully given his Ph.D. Oral Examination held on

Signature of Thesis Supervisor
Date:

Convener, DPGC
Date:

Signature of PSPC Member #1
Date:

Signature of PSPC Member #1
Date:

Signature of External Examiner
Date:

ACKNOWLEDGEMENTS

It is my great pleasure to express my deep sense of gratitude to my supervisor Dr. Rajneesh Misra, for the wonderful opportunity to pursue research with colorful world of chemistry and believing my research abilities. His constant guidance, support and motivation has been immensely helpful to complete this journey. His assurance at the time of crisis, especially for standing by me when chemistry did not work, is humbly acknowledged/ appreciated. I am really honored to be his first Ph.D. student. His enthusiasm and dedication has always inspired me.

I specially thank to Dr. Shaikh M. Mobin for single crystal X-ray support and his guidance. Further I would like to thank my PSpC members Dr. Sanjay Kumar Singh and Dr. Santosh Kumar Vishwakarma for their valuable suggestions and support.

I wish to express my gratitude to Prof. Pradeep Mathur, Director, IIT Indore for his continuous encouragement, help and support in every aspect.

I am grateful to Dr. Chelvam Venkatesh (Head, Discipline of Chemistry, Indian Institute of Technology Indore) for his suggestions and guidance in various aspects. I am also grateful to Dr. Anjan Chakraborty, Dr. Tridib Kumar Sarma, Dr. Suman Mukhopadhyay, Dr. Apurba Kumar Das, Dr. Sampak Samantha, Dr. Biswarup Pathak, Dr. Sanjay Singh, Dr. Tushar Kanti Mukherjee and Dr. Satya S. Bulusu for their guidance and help during various activities.

I would like to extend my sincere thanks to Dr. Deepa Dey and Dr. Pradeep Kumar Jaiswal for their kind and friendly nature and help in dealing with difficulties.

I extend my deep thanks to my group members Prabhat, Thaksen, Rekha, Ramesh, Yuvraj, Manideep, Dr. Sheshenshena Reddy and Dr. Rakesh Kumar Gupta for their selfless co-operation and help to make my work successful. I also thank to project students Adarsh, Apoorva and Pragya and Jayprakash for their help and support.

I would also like to thank technical staff from Sophisticated Instrumentation Center (SIC), IIT Indore, Ms. Sarita Batra, Mr. Kinny Pandey, Mr. Ghanshyam Bhavsar and Mr. Manish Kushwaha for their patience and timely technical support without which it was impossible to continue with my work. I would also like to thank Ms. Anjali Bandiwadekar, Mr. Gati Krishna Nayak, Mr. Rajesh Kumar, Mr. Lala Ram Ahirwar and other library staff and Ms. Jaya Vakade, Mr. Prahalad Singh Panwar, Mr. Manoj

Pal, Mr. Nithin Bhate, and other technical and non-technical staff for their constant help, whenever required.

I personally want to extend my thanks to my batch mates and friends Bhagwati, Dr. Rajendar, Dr. Raina, Tamalika, Dr. Dnyanesh, Dr. Indrajit, Mahesh, Ajay Panwar, Dr. Varun Bajaj and Dr. Yogesh Pandya who were always there and never let me down during these Ph.D. days.

Here, it is to be specially mentioned that, it has been wonderful to work with many friends together during my Ph.D. On this occasion I would like to record my thanks to Shivendra, Anvita, Veenu, Sonam, Debashis, Anupam, Maruthi, Anuradha, Biju, Surajit, Arpan, Roopali, Manideepa, Mriganka, Rohit, Deepika, Sagar, Arup, Priyanka, Novina, Anubha, Deepali and Bishnubasu for their generous co-operation and help.

I would like to take an opportunity to express my respect; love and gratitude to all the teachers from Z. P. Primary school and Nutan Madhyamik Vidyalaya, Khadakwadi, Shri Baleshwar Junior College, Sarole Pathar, Adv. M. N. Deshmukh College, Rajur and Fergusson College, Pune. My special thanks to Dr. R. S. Konde Deshmukh, Dr. Bhatwadekar, Dr. Mamulakar, Prof. Firke, Prof. Dhanmane, Prof. Vankate, Principal T. N. Kanawade, Prof. J. D. Arote, Dr. V. N Gite, Prof. B. K. Tapale, and Prof. B. K. Tambe.

Most importantly none of this would have been possible without the support of my family and I deeply express my love and gratitude to my lovable father Mr. Kashinath Dhokale and mothers Ms. Indubai and Ms. Alka, who are my inspiration for their indefinite love and support and my dear sisters Sujata and Sheetal, and dear brother Vaibhav who are my strengths. I am thankful to my brother in laws Dr. Sanjay Thorat, and my uncles Mr. Santosh Jadhav, Mr. Sonaba Dhokale and Late Bhaguji Dhokale for their love and care and I must have to mention youngest members of our family Siddhi and Atharva for their smiley support.

Finally I would like to express my thanks to IIT Indore for infrastructure and Council of Scientific and Industrial Research (CSIR), New Delhi for my Fellowship and all others who helped and supported me directly or indirectly.

BHAUSAHEB KASHINATH DHOKALE

Dedicated to

My Motherland and India

and

its

FARMERS, Teachers,
soldiers and Researchers

-Bhau Sahab

SYNOPSIS

In recent years research on BODIPY dyes has gained momentum. BODIPY dyes outdistance themselves from contemporary fluorophores due to their spectacular photonic properties and diverse applications. They exhibit strong absorption, high fluorescence quantum yield and excellent thermal and photochemical stability. Their diverse functionalization ability makes them one of the most explored fluorophore. The photonic properties of BODIPYs can be tuned by incorporating suitable functionality at the appropriate position. Their high electron affinity makes them strong acceptor. Incorporation of donor groups on the BODIPYs results in donor-acceptor (D-A) systems.

Donor-acceptor (D-A) molecules are highly polarized molecular systems, which exhibit intramolecular charge transfer and strong non-linear optical behaviour. The strength of the donor-acceptor interaction depends on the electron donating ability of the donor, electron affinity of the acceptor and nature of the spacer.

The ferrocene is undoubtedly strong electron donor and exhibits high thermal and photochemical stability. The reversible oxidation of metal centre from Fe(II) to Fe(III) makes ferrocene a highly reversible redox centre and an ideal candidate for diverse electrochemical studies. Ferrocene is widely studied donor in D-A systems, and coupled with various acceptors like porphyrin, perylenediimide, benzothiazole, triazene and many more.

The BODIPYs can be functionalized at α , β and *meso* positions. The functionalization at these positions perturbs the photonic properties of BODIPYs significantly. We have functionalized various positions of BODIPYs with ferrocenyl group through varying length of spacers and evaluated different positions of BODIPY for their superior electronic communication and further applications into efficient D-A systems.

The main objectives of the present study are,

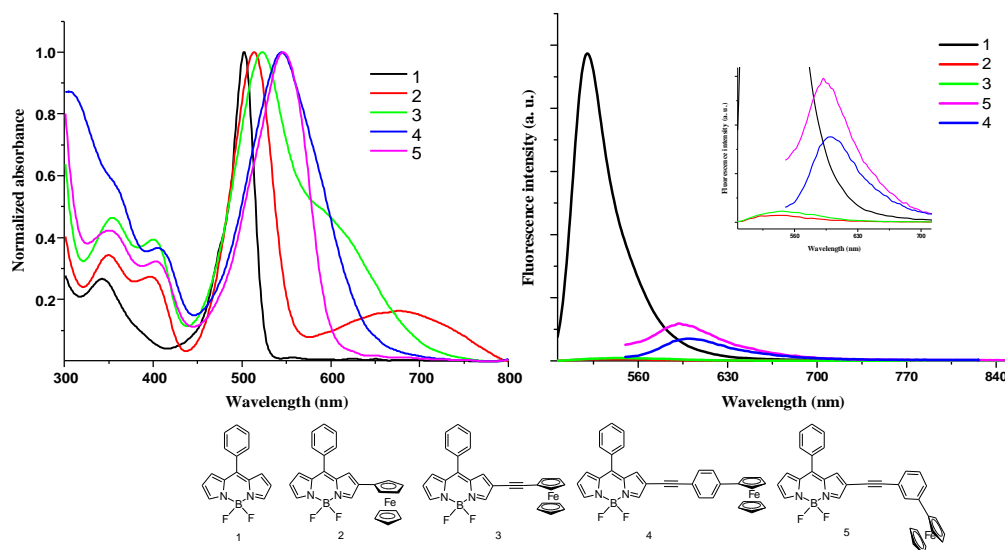
- To design and synthesise β -substituted ferrocenyl BODIPYs connected through different spacers and study their D-A interaction.

- To design and synthesise *meso* alkynylated ferrocenyl BODIPYs and to compare the effect of alkynylation of BODIPYs at α , β and *meso* positions.
- To explore the alkynylation at *meso* position of the BODIPYs for the design and synthesis of different D-A systems, and to study their quenching of fluorescence as an indicator of donor strength of different aryl substituents.
- To design and synthesise heteroatom connected ferrocenyl BODIPYs and study the effect of heteroatom substitution on their properties.
- To study the reactivity and electron deficient nature of 8-chloro BODIPY for the synthesis of *meso* enamine substituted BODIPYs.

The first Chapter describes the detailed historical development of various synthetic, and functionalization strategies of BODIPYs, and their utility in diverse fields. The recent functionalization strategies are summarized and further explored into D-A systems in subsequent Chapters.

The second Chapter summarizes general experimental methods, characterization techniques and the details of instruments used for characterization.

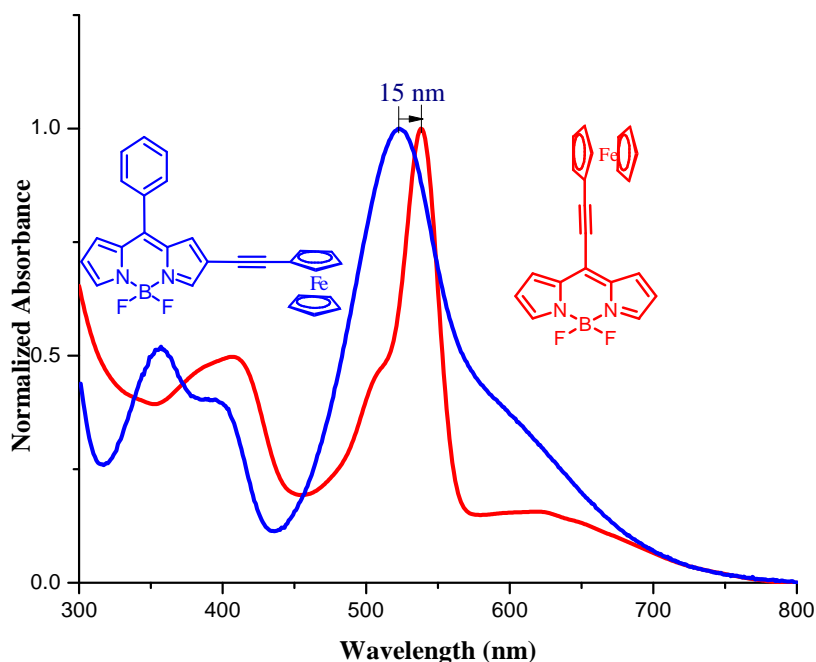
Chapter 3: Donor-acceptor β -substituted ferrocenyl BODIPYs.



In this chapter a series of donor-acceptor ferrocenyl substituted BODIPYs have been designed, and synthesized via palladium-catalysed Suzuki, and Sonogashira cross-coupling reactions. The ferrocene and BODIPYs were connected through varying length of spacers. The UV-visible absorption results indicate intramolecular

charge transfer from the ferrocene to the BODIPY. The incorporation of ferrocenyl group on BODIPY reduces the fluorescence quantum yield. The fluorescence quantum yields were drastically reduced, where the ferrocenyl group was strongly communicating with the BODIPY. Whereas the fluorescence quantum yields were relatively better where the ferrocenyl group was attached through the poorly communicating *meta* linkage. The single crystal X-ray structure of ferrocenyl BODIPYs reveals that the conformations of the two cyclopentadienyl rings of the ferrocene are the function of conjugation length, and steric crowding. The ferrocenyl moiety directly attached to BODIPY unit by single bond, shows staggered conformation, whereas the ferrocenyl moiety attached to BODIPY via phenylacetylene linkage, shows eclipsed conformation.

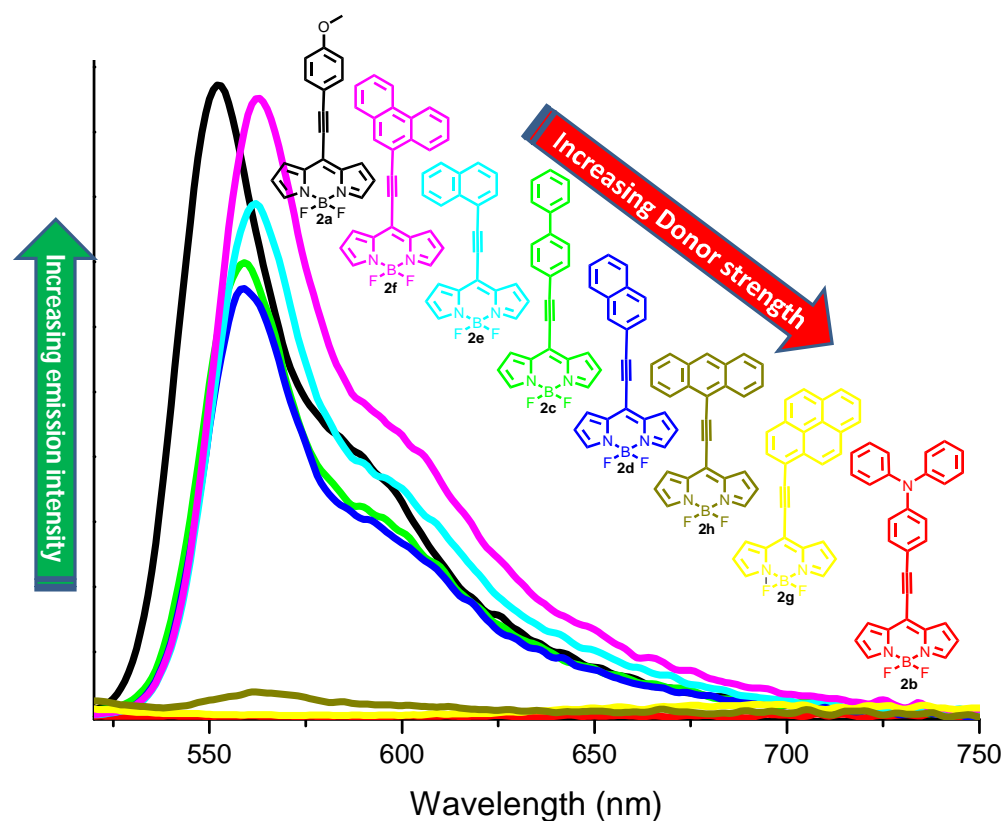
Chapter 4: Donor–acceptor *meso*-alkynylated ferrocenyl BODIPYs.



In order to evaluate the effect of alkylation on the α , β and *meso* positions of BODIPYs, *meso*-alkynylated ferrocenyl BODIPYs with varying conjugation length were designed, and synthesized using the palladium-catalyzed Sonogashira cross-coupling reaction of 8-chloro BODIPY with the corresponding ferrocenylethynes. These BODIPYs have been designed to improve the electronic communication between the donor ferrocene, and the acceptor BODIPY. The photonic, and electrochemical properties indicate strong charge transfer (CT) from ferrocene to the BODIPY. The *meso* alkynylated ferrocenyl BODIPYs exhibit red

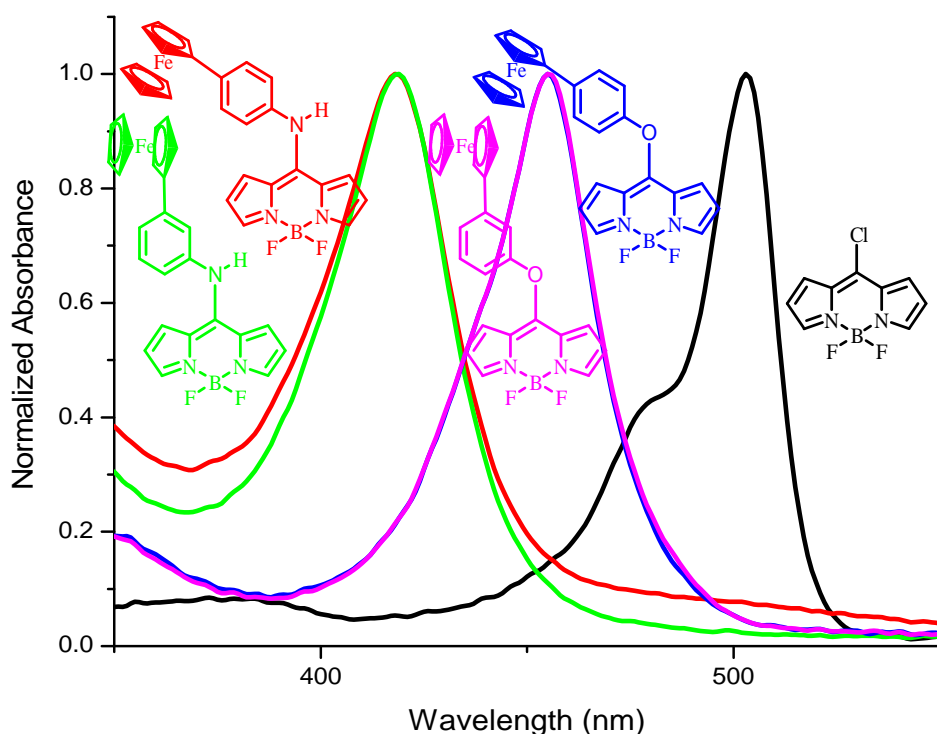
shifted absorption than the α and β alkynylated ferrocenyl BODIPYs, reflecting better electronic conjugation in *meso* alkynylated BODIPYs.

Chapter 5: Quenching of fluorescence as an indicator of donor-strength in *meso* arylethynyl BODIPYs.



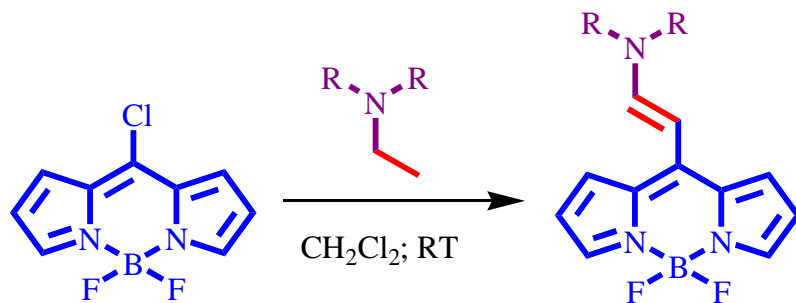
A series of *meso* arylethynyl BODIPYs were designed and synthesized by the Pd-catalyzed Sonogashira cross-coupling reaction. The effects of donor on the photophysical properties of the BODIPYs were explored. The DFT optimized structures and crystal structures show planar orientation of the donor group with respect to the acceptor BODIPY, which favors high degree of conjugation and induces strong donor-acceptor interaction. The quenching of fluorescence was correlated with the electron donating strength of the donor. Stronger the donor poor will be the quantum yield and *vice versa*. The anthracene, pyrene and triphenylamine moieties were found to have stronger electron donating ability than p-methoxyphenyl, phenanthrene, 1-naphthalene, biphenyl, and 2-naphthalene moieties. This was further supported by computational calculations and electrochemical analysis.

Chapter 6: Heteroatom connected ferrocenyl BODIPYs.



A series of heteroatom connected ferrocenyl BODIPYs were designed and synthesized by the nucleophilic aromatic substitution reaction of 8-chloro BODIPY, with ferrocenyl anilines and ferrocenyl phenols. The effects of heteroatom substitution at the *meso* position on the optical and electrochemical properties of the BODIPYs were studied. The absorption spectra of the BODIPYs containing nitrogen at the *meso* position show blue shift of 80 nm, whereas the BODIPYs containing oxygen at the *meso* position show blue shift of 50 nm compared to 8-chloro BODIPY. The DFT calculations reveal strong donor acceptor interactions. The TD-DFT studies indicate that the ferrocenyl group perturbs the HOMO energy levels and induces the absorption from HOMO-n energy levels, whereas the nature of heteroatom does not affect the HOMO but perturbs the LUMO energy level significantly.

Chapter 7: Oxidation of aliphatic *tert*-amines by 8-chloro BODIPY.



The electron deficient nature of 8-chloro BODIPY promotes the oxidation of aliphatic amines to enamines and *in situ* cross-coupling. This has been explored for the synthesis of various *meso* enamine substituted BODIPYs. The reaction conditions were optimized to achieve better yields. The reaction works well with aliphatic *tert*-amines bearing *N*-(CH-CH-) backbone. The *N*-alkyl substituents have strong influence on the properties of enamine substituted BODIPYs. The incorporation of enamines quenches the fluorescence of BODIPYs through intramolecular charge-transfer from enamine to the BODIPY.

LIST OF PUBLICATIONS

1. **Dhokale, B.**, Jadhav, T., Mobin, S. M., Misra, R.,* (2014), *Meso* enamine substituted BODIPYs, *Chem. Commun.*, 50, 9119 (DOI: 10.1039/C4CC03857F).†
2. Misra, R.,* **Dhokale, B.**, Jadhav, T., Mobin, S. M., (2014), Heteroatom-Connected Ferrocenyl BODIPYs: Synthesis, Structure, and Properties, *Organometallics*, 33, 1867–1877 (DOI: 10.1021/om5002292).†
3. Misra, R.,* **Dhokale, B.**, Jadhav, T., Mobin, S. M., (2014), The quenching of fluorescence as an indicator of donor-strength in *meso* arylethynyl BODIPYs, *Dalton Trans.*, 43, 4854-4861 (DOI: 10.1039/C3DT53056F).†
4. Misra, R.,* **Dhokale, B.**, Jadhav, T., Mobin, S. M., (2013), Donor–acceptor *meso*-alkynylated ferrocenyl BODIPYs: synthesis, structure, and properties, *Dalton Trans.*, 42, 13658 (DOI: 10.1039/C3DT51374B).†
5. **Dhokale, B.**, Gautam, P., Mobin, S. M., Misra, R.,* (2013), Donor–acceptor, ferrocenyl substituted BODIPYs with marvelous supramolecular interactions, *Dalton Trans.*, 42, 1512 (DOI: 10.1039/C2DT31632C).†
6. Misra, R.,* Jadhav, T., **Dhokale, B.**, Gautam, P., Sharma, R., Maragani, R., Mobin, S. M., (2014) Carbazole-BODIPY conjugates: design, synthesis, structure and properties, *Dalton Trans.*, 43, 13076-13086 (DOI: 10.1039/c4dt00983e).
7. Jadhav, T., **Dhokale, B.**, Mobin, S. M., Misra, R.,* (2015), Mechanochromism and aggregation induced emission in benzothiazole substituted tetraphenylethylenes: a structure function correlation, *RSC Adv.*, 5, 29878-29884 (DOI: 10.1039/C5RA04881H).
8. **Dhokale, B.**, Jadhav, T., Mobin, S. M., Misra, R.,* (2015), *Meso* enyne substituted BODIPYs: synthesis, structure and properties, *Dalton Trans.*, (DOI: 10.1039/C5DT00565E).
9. Misra, R.,* Jadhav, T., **Dhokale, B.**, Mobin, S. M., (2014), Reversible mechanochromism and enhanced AIE in tetraphenylethene substituted phenanthroimidazoles, *Chem. Commun.*, 50, 9076-9078 (DOI: 10.1039/C4CC02824D).

10. Misra, R.,* **Dhokale, B.**, Jadhav, T., Mobin, S. M., (2014), *Meso*-aryloxy and *meso*-arylaza linked BODIPY dimers: synthesis, structure and properties, *New J. Chem.*, 38, 3579-3585 (DOI: 10.1039/C4NJ00354C).
11. Gautam, P., **Dhokale, B.**, Mobin, S. M., Misra, R.,* (2012), Ferrocenyl BODIPYs: synthesis, structure and properties, *RSC Adv.*, 2, 12105-12107 (DOI: 10.1039/C2RA21964F).
12. **Dhokale, B.**, Gautam, P., Misra, R.,* (2012), Donor–acceptor perylenediimide–ferrocene conjugates: synthesis, photophysical, and electrochemical properties, *Tetrahedron Letters*, 53, 2352–2354 (DOI:10.1016/j.tetlet.2012.02.107).
13. Gautam, P., **Dhokale, B.**, Shukla, V., Singh, C. P., Bindra, K. S., Misra, R.,* (2012), Optical limiting performance of *meso*-tetraferrocenyl porphyrin and its metal derivatives, *Journal of Photochemistry and Photobiology A: Chemistry*, 239, 24–27 (DOI: <http://dx.doi.org/10.1016/j.jphotochem.2012.04.020>).

†Papers pertaining to the thesis.

CONFERENCE PRESENTATION

1. **Dhokale, B.**, Jadhav, T., Misra, R., Synthesis and properties of *meso* enamine substituted BODIPYs, 8th Asian Photochemistry conference (APC-2014), Trivandrum, India (10-13th Nov, 2014); Poster presented.
2. Jadhav, T., **Dhokale, B.**, Misra, R., Mechanochromic and AIE active tetraphenylethene substituted phenanthroimidazoles, 8th Asian Photochemistry conference (APC-2014), Trivandrum, India (10-13th Nov, 2014); Poster Authored.

TABLE OF CONTENTS

1. List of Figures	xvii
2. List of Schemes	xxi
3. List of Tables	xxii
4. Acronyms	xxiv
5. Nomenclature	xxvi
Chapter 1: General Introduction and Background	
1.1. BODIPYs	1
1.2. Synthesis of BODIPYs	3
1.2.1. History	3
1.2.2. From pyrroles and acid chlorides	4
1.2.3. From pyrroles and aldehydes	4
1.2.4. From pyrroles and acid anhydride	5
1.2.5. Synthesis of parent unsubstituted BODIPY	5
1.2.6. Synthesis of asymmetric BODIPY dyes	7
1.3. Functionalization of the BODIPY framework	7
1.3.1. Knoevenagel condensation reaction	7
1.3.2. Halogenation	8
1.3.2.1. Halogenation of dipyrromethane core	9
1.3.2.2. Halogenation of BODIPYs	10
1.3.3. Through 8-(methylthio)-BODIPY	12
1.3.4. Modification at the boron center	14
1.3.5. Fused BODIPYs for extension of conjugation	15
1.3.6. Oxidative nucleophilic reactions via C–H activation	16
1.3.7. Similar systems like BODIPY	16
1.3.7.1. Aza-BODIPY	16
1.3.7.2. BOPHY	16
1.4. Donor-Acceptor system	17
1.5. Fluorescence of BODIPY dyes and charge transfer interactions	19

1.6.	Organization of thesis	20
	References	21
Chapter 2: Materials and Experimental Techniques		
2.1.	Introduction	39
2.2.	Chemicals used for synthesis	39
2.3.	Spectroscopic Measurements	40
2.4.	Electrochemical Studies	41
2.5.	Elemental Analysis	41
2.6.	Computational Calculations	41
2.7.	Single Crystal X-ray Diffraction Studies	41
	References	42
Chapter 3: Donor-Acceptor β-Substituted Ferrocenyl BODIPYs		
3.1.	Introduction	43
3.2.	Results and discussion	44
3.3.	Photophysical properties	45
3.4.	Single Crystal X-ray Diffraction Studies	47
3.5.	Experimental Section	52
3.6.	Conclusions	54
	References	55
Chapter 4: <i>Meso</i>-alkynylated ferrocenyl BODIPYs		
4.1.	Introduction	59
4.2.	Results and Discussion	60
4.3.	Photophysical Properties	62
4.4.	Electrochemical properties	65
4.5.	Computational Calculations	65
4.6.	Single crystal X-ray diffraction studies	67
4.7.	Experimental section	70
4.8.	Conclusion	72
	References	72
Chapter 5: Quenching of fluorescence as an indicator of donor strength in meso arylethynyl BODIPYs		
5.1.	Introduction	83
5.2.	Results and Discussion	84

5.3.	Photophysical Properties	85
5.4.	Electrochemical properties	88
5.5.	Theoretical Calculations	89
5.6.	Single crystal X-ray diffraction studies	90
5.7.	Experimental section	94
5.8.	Conclusion	97
	References	97
Chapter 6: Heteroatom connected ferrocenyl BODIPYs		
6.1.	Introduction	103
6.2.	Results and Discussion	104
6.3.	Thermogravimetric Analysis	105
6.4.	Photophysical Properties	106
6.5.	Electrochemical properties	108
6.6.	Theoretical Calculations	109
6.7.	Single crystal X-ray diffraction studies	113
6.8.	Experimental section	121
6.9.	Conclusion	122
	References	123
Chapter 7: Oxidation of aliphatic <i>tert</i>-amines by 8-chloro BODIPY and in situ cross-coupling		
7.1.	Introduction	129
7.2.	Results and Discussion	130
7.3.	Single crystal X-ray diffraction studies	133
7.4.	Photophysical Properties	134
7.5.	Experimental section	135
7.6.	Conclusion	137
	References	137
Conclusions and future scope		143

LIST OF FIGURES

Chapter-1: General Introduction and Background

Figure 1.1.	The Scopus analysis of the research on BODIPY fluorophore.	1
Figure 1.2.	Colors of BODIPY derivatives in day light (A) and under UV light (B).	3
Figure 1.3.	Versatility of halogenated precursors in synthesis.	9
Figure 1.4.	The blue shift in the absorption spectra of heteroatom substituted BODIPYs (Adapted with permission from ref ^[43] . Copyright © (2013) American Chemical Society.)	14
Figure 1.5.	Schematic representation of Donor-Acceptor system and the effect of orbital couplings on the HOMO-LUMO gap.	17
Figure 1.6.	Fate of excited state electron depends on the nature of substituent.	20

Chapter-3: Donor-Acceptor β -Substituted Ferrocenyl BODIPYs

Figure 3.1.	(A) Normalized electronic absorption spectra of compounds 1 – 5 , recorded in toluene. (B) Fluorescence spectra of 1 – 5 at 0.1 absorption, excited at 487 nm (for 1-3) and 540 nm (for 4 – 5) in toluene. Inset shows enlarged view.	45
Figure 3.2.	X-ray structures of BODIPYs 1' , 2 , 3 and 4 . (a) Front view, and (b) top view.	48
Figure 3.3.	Crystal packing of 1' showing hydrogen bonded 2D network. Secondary interactions are shown by dashed lines.	49
Figure 3.4.	Crystal packing of 2 along b-axis.	50
Figure 3.5.	Crystal packing of 4 along b-axis, showing sheet like structure, both sides are covered by ferrocenes.	50
Figure 3.6.	Crystal Packing of 3 showing zigzag pattern, along a-axis.	51

Chapter 4: *Meso*-alkynylated ferrocenyl BODIPYs

Figure 4.1.	TGA plot of the BODIPYs 2 – 6 .	61
Figure 4.2.	(A) UV-vis absorption spectra of BODIPYs 2 – 6 recorded in toluene. (B) Emission Spectra of 2 – 6 recorded in toluene, inset shows enlarged view (Excited at respective $\lambda_{S0 \rightarrow S1}$ at concentration of 0.1 absorbance).	62

Figure 4.3.	BODIPYs 2-6 in toluene at concentration of 10^{-4} M.	63
Figure 4.4.	Positive solvatochromism in BODIPY 3 .	63
Figure 4.5.	Overlaid CV and DPV plots of BODIPYs 2 – 6 .	65
Figure 4.6.	HOMO, and LUMO frontier orbitals of BODIPYs at the B3LYP/6-31+G** for C, N, B, F, H, and Lanl2DZ for Fe level.	66
Figure 4.7.	Crystal structures of 2' , 3 , and 6 (a) Front view, (b) Side view.	67
Figure 4.8.	Crystal packing of 3 along tilted <i>b</i> -axis.	68
Figure 4.9.	<i>Zigzag</i> arrangement of molecules in the crystal packing of 6 along <i>a</i> -axis.	68
Figure 4.10.	Complex 3-D crystal packing structure of 2' .	69
Chapter 5: Quenching of fluorescence as an indicator of donor strength of meso arylethynyl BODIPYs		
Figure 5.1.	TGA plot of the <i>meso</i> arylethynyl BODIPYs 2a – 2h .	85
Figure 5.2.	BODIPYs 2a – 2h in dichloromethane at concentration of 10^{-4} M (a) in day light and (b) in UV light.	85
Figure 5.3.	Normalized UV-vis absorption spectra of <i>meso</i> -arylethynyl BODIPYs 2a – 2h recorded in dichloromethane, inset show the enlarged view.	86
Figure 5.4.	Emission spectra of the <i>meso</i> -arylethynyl BODIPYs 2a – 2h , recorded in dichloromethane.	87
Figure 5.5.	Overlaid CV and DPV plots of the <i>meso</i> -arylethynyl BODIPY 2a – 2h .	89
Figure 5.6.	HOMO and LUMO frontier molecular orbitals of the <i>meso</i> -arylethynyl BODIPYs at the B3LYP/6-31G (d).	90
Figure 5.7.	Single crystals of BODIPYs 2d and 2e , front view and side view.	92
Figure 5.8.	Crystal packing of 2d .	93
Figure 5.9.	Crystal packing of 2e along tilted <i>b</i> -axis.	94
Chapter 6: Meso Heteroatom connected ferrocenyl BODIPYs.		
Figure 6.1.	TGA plots of the heteroatom connected ferrocenyl BODIPYs 2a, 2b, 3c and 3d recorded at the heating rate of $10\text{ }^{\circ}\text{C min}^{-1}$	105

under nitrogen atmosphere.

- Figure 6.2.** 8-chloro BODIPY **1**, and heteroatom connected ferrocenyl BODIPYs **2a**, **2b**, **3c** and **3d**, in dichloromethane at 10^{-4} M concentration. 107
- Figure 6.3.** Normalized electronic absorption spectra of the 8-chloro BODIPY **1** and the heteroatom connected ferrocenyl BODIPYs **2a**, **2b**, **3c** and **3d** in dichloromethane. 108
- Figure 6.4.** Cyclic voltammogram and differential pulse voltammogram of the heteroatom connected ferrocenyl BODIPY **2a**, **2b**, **3c** and **3d**. 109
- Figure 6.5.** Comparison of selected bond lengths of the crystal structures and DFT optimized structures of the heteroatom connected ferrocenyl BODIPYs **2a**, **2b**, **3c** and **3d** (x and y represents two different molecules in an asymmetric unit). 110
- Figure 6.6.** Comparison of the planarity of the BODIPY central ring in the crystal structure and the DFT optimized structure of **2a** (top view). 111
- Figure 6.7.** Energy level diagram of the frontier molecular orbitals of the BODIPYs **1**, **4**, **2a**, **2b**, **5**, **3c** and **3d** estimated by DFT calculations. 112
- Figure 6.8.** Electrostatic potential map of heteroatom connected ferrocenyl BODIPYs **2a**, **2b**, **3c** and **3d**. Red = lowest potential (electron-rich) and blue = highest potential (electron-poor). Calculated by Gaussian 09W. 111
- Figure 6.9.** Frontier molecular orbitals of BODIPYs **5**, **3c**, **3d**, **4**, **2a** and **2b** at the B3LYP/6-31 G** for C, N, B, F, H, O and Lanl2DZ for Fe level. 113
- Figure 6.10.** Crystal structures of the BODIPY **2a**, **2b**, **2c** and **3d**, (A) front view and (B) side view (x and y represents two different molecules in an asymmetric unit). 114
- Figure 6.11.** Torsional angles in cyclopentadienyl ring in the crystal structures of heteroatom connected ferrocenyl BODIPYs **2a**, **2b**, **3c** and **3d**. 115

Figure 6.12.	Packing diagram of the heteroatom connected ferrocenyl BODIPY 2a (red and green color represent two different molecules in asymmetric unit).	116
Figure 6.13.	Packing diagram of the heteroatom connected ferrocenyl BODIPY 2b .	117
Figure 6.14.	Packing diagram of the heteroatom connected ferrocenyl BODIPY 3c .	117
Figure 6.15.	Packing diagram of the heteroatom connected ferrocenyl BODIPY 3d .	118
Chapter 7: Oxidation of aliphatic <i>tert</i>-amines by 8-chloro BODIPY and <i>in situ</i> cross-coupling.		
Figure 7.1.	Single crystal structures of BODIPYs 2 , 4a , 4b and 5a . Front view (above) and Side view (below).	134
Figure 7.2.	Normalized electronic absorption spectra of BODIPYs 1 – 5 in dichloromethane.	135

LIST OF CHARTS

Chapter-1: General Introduction and Background

Chart 1.1.	Nomenclature of <i>s</i> -indacene, dipyrromethane, dipyrromethaene and BODIPY.	2
Chart 1.2.	Boron functionalized BODIPYs.	14
Chart 1.3.	Fused BODIPYs.	15
Chart 1.4.	Fused BODIPYs.	15
Chart 1.5.	BOPHY and its derivative for pH sensing.	16
Chart 1.6.	Frequently used donors.	18
Chart 1.7.	Frequently used acceptors.	19

Chapter 4: *Meso*-alkynylated ferrocenyl BODIPYs.

Chart 4.1.	Structures of previously reported ferrocenyl BODIPYs.	64
-------------------	---	----

Chapter 6: *Meso* Heteroatom connected ferrocenyl BODIPYs.

Chart 6.1.	Previously reported aniline and phenol substituted BODIPYs.	105
-------------------	---	-----

LIST OF SCHEMES

Chapter-1: General Introduction and Background

Scheme 1.1.	Serendipitous discovery of BODIPY.	4
Scheme 1.2.	Synthesis of BODIPYs from Pyrroles and acid chlorides.	4
Scheme 1.3.	Synthesis of BODIPYs from pyrroles and aldehydes.	5
Scheme 1.4.	Synthesis of BODIPYs from pyrroles and acid anhydride.	5
Scheme 1.5.	Synthesis of Parent unsubstituted BODIPY.	6
Scheme 1.6.	Synthesis of asymmetric BODIPY dyes.	7
Scheme 1.7.	Knoevenagel condensation reaction of methylated BODIPYs.	8
Scheme 1.8.	Halogenation of Dipyrrromethane core.	9
Scheme 1.9.	Bromination of BODIPY at multiple positions.	10
Scheme 1.10.	Halogenation at β' -position.	10
Scheme 1.11.	Halogenated of <i>meso</i> aryl substituent.	11
Scheme 1.12.	Synthesis of <i>meso</i> halogenated BODIPYs.	11
Scheme 1.13.	Synthesis of 8-chloro BODIPYs.	12
Scheme 1.14.	Synthesis of 8-(methylthio)-BODIPY and its synthetic utility.	13
Scheme 1.15.	Synthesis of aza-BODIPYs.	16

Chapter-3: Donor-Acceptor β -Substituted Ferrocenyl BODIPYs.

Scheme 3.1	Synthesis of Bromo BODIPY 1' .	44
Scheme 3.2	Synthetic route for the synthesis of BODIPYs 2 – 5 .	44

Chapter 4: *Meso*-alkynylated ferrocenyl BODIPYs.

Scheme 4.1.	Synthesis of 8-chloro BODIPY 2 .	60
Scheme 4.2.	Synthesis of the ferrocenyl BODIPYs 3 – 6 .	60
Scheme 4.3.	Formation of BODIPY 2' from 2 .	67

Chapter 5: Quenching of fluorescence as an indicator of donor strength of *meso* arylethynyl BODIPYs.

Scheme 5.1.	Synthesis of <i>meso</i> -arylethynyl BODIPYs 2a – 2h .	84
--------------------	--	----

Chapter 6: *Meso* Heteroatom connected ferrocenyl BODIPYs.

Scheme 6.1.	Synthesis of heteroatom connected ferrocenyl BODIPYs 2a , 2b , 3c and 3d .	104
--------------------	--	-----

LIST OF TABLES

Chapter-3: Donor-Acceptor β -Substituted Ferrocenyl BODIPYs

Table 3.1.	Photophysical properties of BODIPYs 1 – 5 .	46
Table 3.2.	Crystal data and structure refinement parameters.	47
Table 3.3.	Distance and angle of intermolecular interactions in the crystal structures.	52

Chapter 4: *Meso*-alkynylated ferrocenyl BODIPYs.

Table 4.1.	Photophysical & electrochemical properties of BODIPYs 2 – 6 .	64
Table 4.2.	Crystal data and structure refinement parameters.	70

Chapter 5: Quenching of fluorescence as an indicator of donor strength of *meso* arylethynyl BODIPYs.

Table 5.1.	Photophysical and thermal properties of <i>meso</i> -arylethynyl BODIPYs 2a – 2h .	88
Table 5.2.	Electrochemical properties of the <i>meso</i> -arylethynyl BODIPYs 2a – 2h .	88
Table 5.3.	Crystal structure and data refinement parameters.	91
Table 5.4.	Distance and angle of intermolecular of interactions in the crystal structures.	92

Chapter 6: *Meso* Heteroatom connected ferrocenyl BODIPYs.

Table 6.1.	Optical, electrochemical and thermal properties of the BODIPYs 1, 2a, 2b, 3c and 3d .	106
Table 6.2.	Computed vertical transitions and their oscillator strengths and configurations of BODIPY 3c .	109
Table 6.3.	Crystal structure and data refinement parameters.	119
Table 6.4.	Distance and angle of intermolecular interactions in the crystal structure of BODIPYs 2a, 2b, 3c and 3d .	120

Chapter 7: Oxidation of aliphatic *tert*-amines by 8-chloro BODIPY and *in situ* cross-coupling.

Table 7.1.	Screening results of reaction optimization.	130
Table 7.2.	Screening of the substrates and optical properties of the BODIPYs 1 – 5 .	131
Table 7.3.	Crystal data and structure refinement parameters.	133

ACRONYMS

D-A	Donor-acceptor
NLO	Non-linear Optical
pH	The negative logarithm of hydronium-ion concentration ($-\log_{10} [\text{H}_3\text{O}^+]$)
SCXRD	Single Crystal X-ray diffraction
PXRD	Powder X-ray diffraction
NMR	Nuclear Magnetic Resonance
PPh ₃	Triphenylphosphine
DMF	Dimethylformamide
DCM	Dichloromethane
TGA	Thermogravimetric Analysis
Ph	phenyl
IR	Infrared
UV-Vis	UV-Visible Spectroscopy
...	Represents interaction
Calcd.	Calculated
CDCl ₃	Chloroform-d
ESI-MS	Electrospray Ionization- Mass Spectrometry
EtOH	Ethanol
MeOH	Methanol
THF	Tetrahydrofuran
TFA	Trifluoroacetic Acid

TLC	Thin Layer Chromatography
TEA	Triethylamine
DIEPA	<i>N,N</i> -Di-isopropyl-ethylamine
DIPA	<i>N,N</i> -Di-isopropylamine
DBU	1,8-Diazabicyclo[5.4.0]undec-7-ene

NOMENCLATURE

λ	Wavelength
ε	Extinction coefficient
α	Alfa
β	Beta
γ	Gamma
π	Pi
Φ	Fluorescence quantum yield
σ	Sigma
\AA	Angstrom
nm	Nanometer
cm	Centimeter
$^{\circ}$	Degree
$^{\circ}\text{C}$	Degree Centigrade
mmol	Millimol
mL	Milliliter
μL	Microliter
a. u.	Arbitrary Unit

Chapter 1

General Introduction and Background

1.1.BODIPYs

In recent years research on BODIPY fluorophore has gained momentum due to its spectacular photonic properties.^[1] They outdistance themselves from contemporary fluorophores due to strong absorption throughout the UV-Visible region, sharp fluorescence with high quantum yield, and excellent photochemical and thermal stability.^[2] These unique properties make them an attractive candidate for wide range of applications in organic electronics, chemosensors, photovoltaics, NLO, bioimaging and photodynamic therapy.^[3] The photonic properties of BODIPY fluorophore can be tuned by incorporating suitable functionality at appropriate position.^[4] Thus the functionalization of BODIPYs is of interest to achieve the fluorophores of desired properties for specific applications.^[5]

The Scopus search on BODIPY reveals, substantial share of BODIPYs in scientific literature (Figure 1.1). About 2200 documents were published on BODIPYs in 2014. The Scopus analysis further highlights the applicability of BODIPYs in chemistry, biochemistry, materials science, engineering, physics, electronics, various therapeutic applications and many more fields.

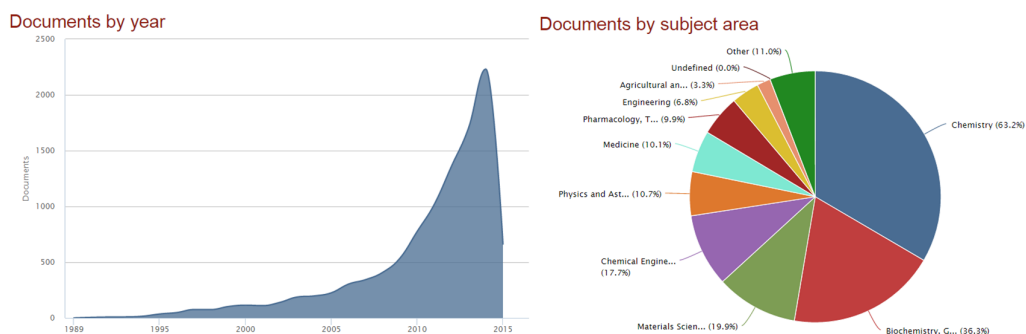


Figure 1.1. The Scopus analysis of the research on BODIPY fluorophore.

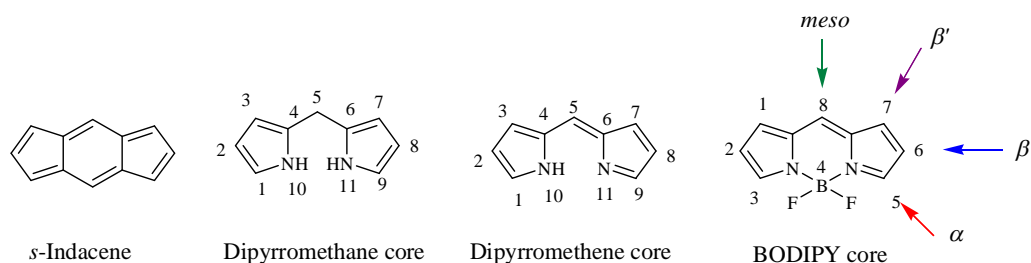


Chart 1.1. Nomenclature of *s*-indacene, dipyrromethane, dipyrromethene and BODIPY.

The BODIPY consists of dipyrromethene moiety complexed with BF_2 unit. The dipyrromethene is a bidentate ligand used in various metal complexes and exists in *cis-trans* isomeric forms. The complexation of dipyrromethene with BF_2 makes it constrained into cyanine dyes and gives rigidity to the BODIPY framework, which prevents *cis-trans* isomerization. The BODIPYs are highly planar; but in certain BODIPYs the boron atom is slightly deviated from the average plane.^[6]

The IUPAC numbering system for 4,4-Difluoro-4-bora-3a,4a-diaza-*s*-indacene (BODIPY) dye is different than that used for dipyrromethane and dipyrromethene (Chart 1.1). However, the terms α , β and *meso*- are used in the same way for both dipyrromethene and BODIPYs. These nomenclature systems are widely used in recent literature and accepted worldwide.^[7]

The BODIPYs exhibit strong and narrow $S_0 \rightarrow S_1$ ($\pi \rightarrow \pi^*$) absorption band in the region of 500 – 525 nm ($\epsilon = 40000 - 80000 \text{ M}^{-1} \cdot \text{cm}^{-1}$) with a shoulder at high energy region corresponding vibrational transition.^[8] It also exhibits a weak absorption band around 375 nm corresponding to $S_0 \rightarrow S_2$ ($\pi \rightarrow \pi^*$) transition.^[9] The BODIPYs emit a narrow band in the region of 530 – 560 nm. The emission is independent of excitation wavelength and mirror image of the absorption band. The BODIPY exhibits high thermal and photochemical stability and good solubility in wide range of solvents. The BODIPY derivatives show a range of colors in day light as well as under UV light (Figure 1.2). The BODIPY fluorophore have high electron affinity, which makes them a strong acceptor for donor-acceptor (D-A) systems.^[10]

The photonic properties of BODIPY fluorophore can be tuned by functionalization with appropriate substituent at α , β and *meso* positions. The

numerous synthetic methodologies and diverse functionalization ability makes them most studied fluorophore. In summary, the BODIPYs are a fluorophore of wide interest for their spectacular properties like;

- Strong absorption throughout visible region, and extending into near-IR region.
- High molar extinction coefficient.
- Strong fluorescence, which results in high fluorescence quantum yield.
- Excellent photochemical and thermal stability.
- High electron affinity.
- Tunable photonic properties.
- Ease of synthetic functionalization.

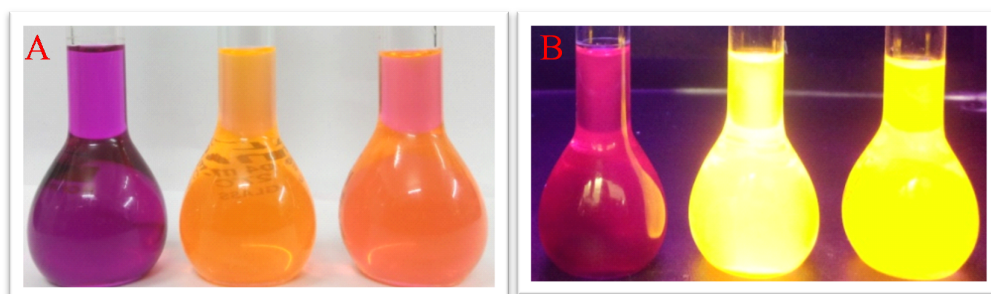


Figure 1.2. Colors of BODIPY derivatives in day light (A) and under UV light (B).

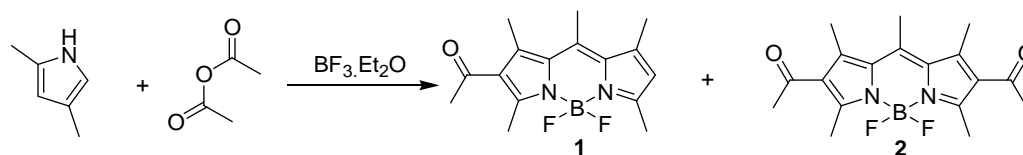
1.2. Synthesis of BODIPYs

The researchers are continuously exploring the BODIPYs for desirable properties. The BODIPY have emerged as fluorophore of interest for their application in the tunable laser dyes,^[11] fluorescent labels for biomolecules and cellular imaging,^[12] energy transfer cassettes,^[13] fluorescent switches,^[14] photosensitizers,^[15] light-emitting devices,^[16] drug delivery agents,^[17] chemosensors^[18] and solar cells.^[19] The Life technologies (Formerly Molecular Probes) have commercially prepared vast number of BODIPY bio-conjugate derivatives.^[20] The researchers from diverse fields have contributed immensely for the functionalization of BODIPY fluorophores. Milestones of these functionalization strategies are summarized in the following sections.

1.2.1. History

The BODIPY fluorophore was first discovered by Treibs and Kreuzer serendipitously in 1968. The reaction of 2,4-dimethylpyrrole with acetic anhydride

in the presence of $\text{BF}_3 \cdot \text{OEt}_2$ resulted mixture of mono- and di-acetylated BODIPY fluorophores, **1** and **2** (Scheme 1.1).^[21]

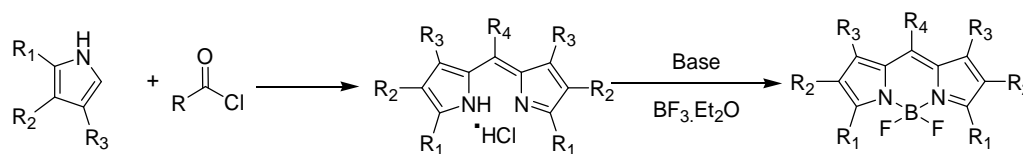


Scheme 1.1. Serendipitous discovery of BODIPY.

The first water-soluble BODIPY fluorophore was synthesized by Wories and colleagues in 1985,^[22] followed by significant work by Haugland and Kang on the BODIPY as fluorescent materials.^[23]

1.2.2. From pyrroles and acid chlorides

The BODIPYs were synthesized from the dipyrromethene, which in turn was synthesized by the condensation reaction of the acid chloride and pyrrole.^[24] The complexation of dipyrromethene with BF_3 -etherate in the presence of tertiary base results the BODIPY (Scheme 1.2). The substituted pyrroles and substituted acid chlorides were used to synthesize different BODIPY derivatives.

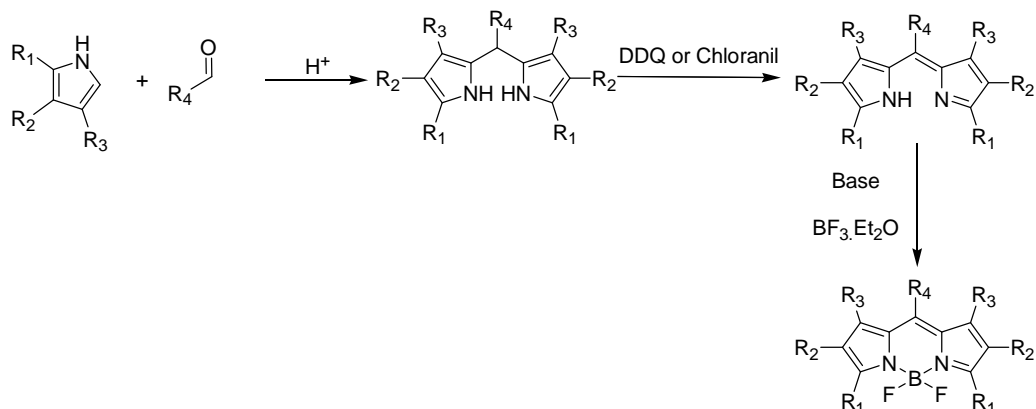


Scheme 1.2. Synthesis of BODIPYs from pyrroles and acid chlorides.

1.2.3. From pyrroles and aldehydes

This is the regularly used, classical route for the synthesis of BODIPYs. The acid catalyzed condensation reaction of aldehyde with pyrrole results dipyrromethane, which on oxidation with DDQ or *p*-chloranil result the dipyrromethene (Scheme 1.3).^[25] The dipyrromethenes are unstable but on complexation with BF_3 -etherate in the presence of tertiary amine result the stable BODIPY fluorophore. The overall yield, by this method is about 40 – 60 %. The wide ranges of functional groups are compatible with these reaction conditions, but the use of aliphatic aldehydes has been not reported may be due to the experimental

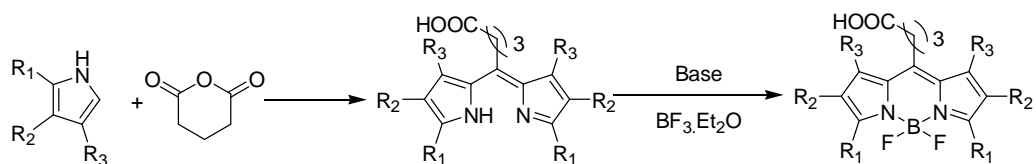
complications with oxidizing agents. The use of substituted pyrroles and aldehydes resulted wide range of functionalized BODIPYs.



Scheme 1.3. Synthesis of BODIPYs from pyrroles and aldehydes.

1.2.4. From pyrroles and acid anhydride

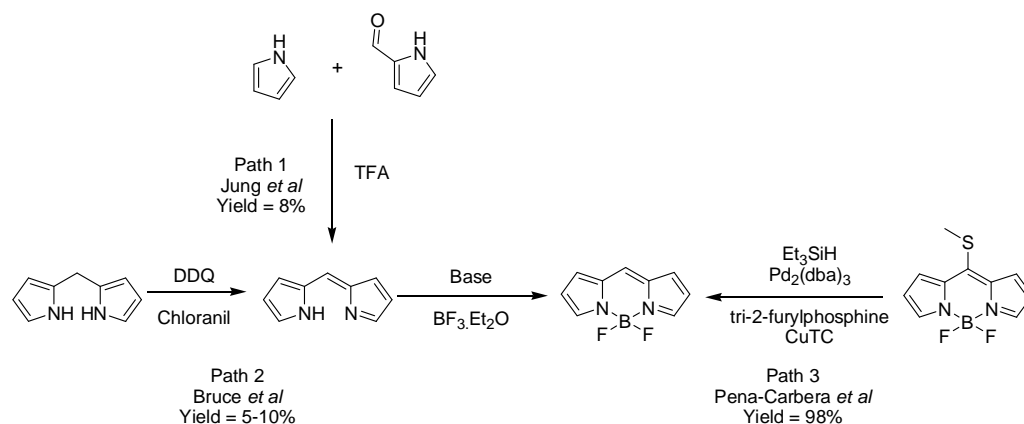
The dipyrromethene can also be synthesized by condensation reaction of pyrroles with acid anhydride.^[26] The dipyrromethene on complexation with BF₃·etherate in the presence of tertiary amine results the BODIPY (Scheme 1.4). The important feature of synthesizing BODIPYs from acid anhydrides is that, the free carboxylic acid is produced, which may be used to attach the probe to target molecules.



Scheme 1.4. Synthesis of BODIPYs from pyrroles and acid anhydride.

1.2.5. Synthesis of parent unsubstituted BODIPY

Although wide range of BODIPYs were reported, their parent unsubstituted BODIPY was not reported until recently. Their precursor dipyrromethene is highly unstable and its unblocked pyrrolic carbons are susceptible for electrophilic attack. In 2008-2009, three different routes for the synthesis of unsubstituted parent BODIPY were reported independently (Scheme 1.5).



Scheme 1.5. Synthesis of Parent unsubstituted BODIPY.

In the first report (December, 2008) Jung and co-workers,^[27] reacted pyrrole-2-carboxaldehyde and unsubstituted pyrrole, in acidic conditions; followed by complexation with $\text{BF}_3 \cdot \text{Et}_2\text{O}$ in the presence of a base (Path 1). The overall yield by this route was only 8 %.

In the second report (March, 2009), Bruce and co-workers^[28] (Path 2), carried out the oxidation of dipyrromethane to dipyrromethene by DDQ at -78°C under inert atmosphere; followed by in situ complexation with $\text{BF}_3 \cdot \text{Et}_2\text{O}$ in the presence of base DBU. The yield by this route was only 5-10 %. The structure of parent unsubstituted BODIPY was confirmed by ^1H , ^{13}C , ^{11}B and ^{19}F NMR and single crystal X-ray analysis.

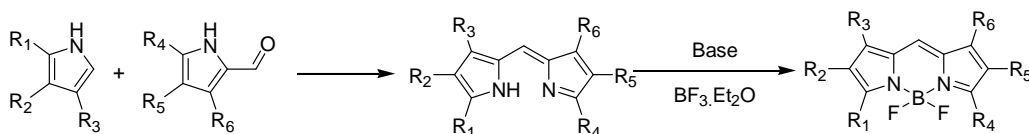
In the third report (July, 2009), Pena-Cabrera and co-workers (Path 3),^[29] reacted 8-thiomethyl BODIPY and triethylsilane in presence of a catalytic amount of palladium and a stoichiometric amount of copper (I) thiophene-2-carboxylate (CuTc) in THF at 55°C for 45 min. This route resulted parent unsubstituted BODIPY in 98 % yield.

1.2.5.1. Properties of parent unsubstituted BODIPY

The parent unsubstituted BODIPY exhibits high photostability ($\tau = 7.2$ ns) but poor thermal stability. It decomposes above 50°C temperature. It absorbs at 503 nm and emits at 512 nm with green fluorescence and high quantum yield (up to 93 %) in nonpolar and polar solvents, including water.

1.2.6. Synthesis of asymmetric BODIPY dyes

The acid catalyzed MacDonald coupling-reaction of pyrrole-2-carboxaldehyde with α -free pyrrole resulted asymmetric dipyrromethene.^[30] The dipyrromethene is generally isolated in its salt form, which on complexation with BF₃·etherate in presence of base, usually a tertiary amine, affords the desired asymmetric BODIPY dye (Scheme 1.6). The yield of this reaction was high enough, but reduced significantly for electron deficient pyrroles due to self-condensation of pyrrole-2-carboxaldehyde.



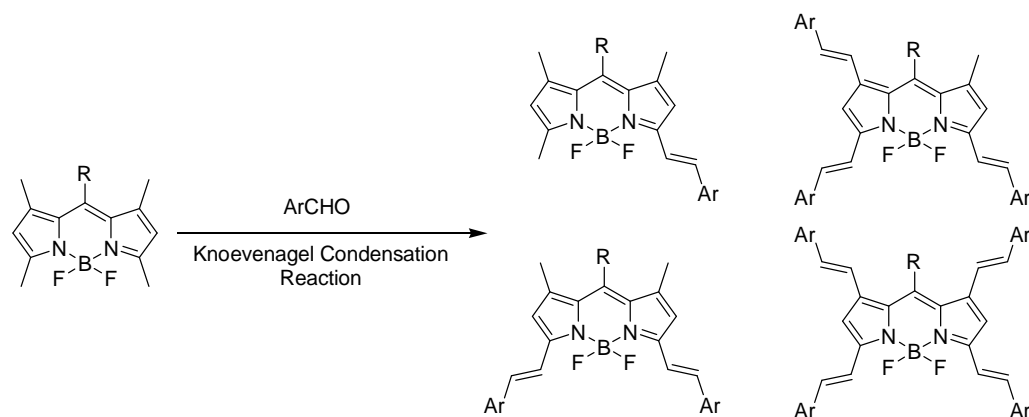
Scheme 1.6. Synthesis of asymmetric BODIPY dyes.

1.3. Functionalization of the BODIPY framework

The photonic properties of BODIPYs can be tuned by substituting it with suitable functionality at appropriate position. Variety of strategies have been developed for the functionalization of the BODIPY scaffold at the 8- (*meso*-), 2, 6-, 3, 5-, 1, 7-positions and at the boron center. Numerous research groups are developing materials for various optoelectronic applications, and they have established several routes for the functionalization of BODIPYs. Some of them are discussed here.

1.3.1. Knoevenagel condensation reaction

The methyl substituents on the BODIPY core are acidic enough to participate in Knoevenagel condensation reaction with different aldehydes. The reaction resulted vinyl substituted BODIPYs (Scheme 1.7). The reaction is simple, straight forward and compatible with wide range of substituted aldehydes.^[31] The BODIPYs can be decorated at α , β , β' and *meso* positions with different substituents to get near IR shifted absorption and emission. The methyl groups can be treated in stepwise manner by controlling the amount of aldehyde, concentration of reaction mixture and reaction time.



Scheme 1.7. Knoevenagel condensation reaction of methylated BODIPYs.

1.3.2. Halogenation

The halogenation gives extremely useful precursors for the transition metal catalyzed C-C and C-heteroatom bond formation reactions. Several halogenating agents and methodologies have been developed in recent decades.^[32] The Figure 1.3 describes the different Pd-catalyzed coupling reactions. Most of these reactions involve the four important steps.

1. Oxidative addition
2. Transmetallation
3. Rearrangement
4. Reductive elimination

The halogenated precursors can be used for wide variety of functionalization. The various halogenation strategies have been developed for the halogenation of BODIPYs. The halogenation of dipyrromethane results halogenation at α -position selectively, whereas the halogenation of BODIPY framework results halogenation at β -position selectively.^[33]

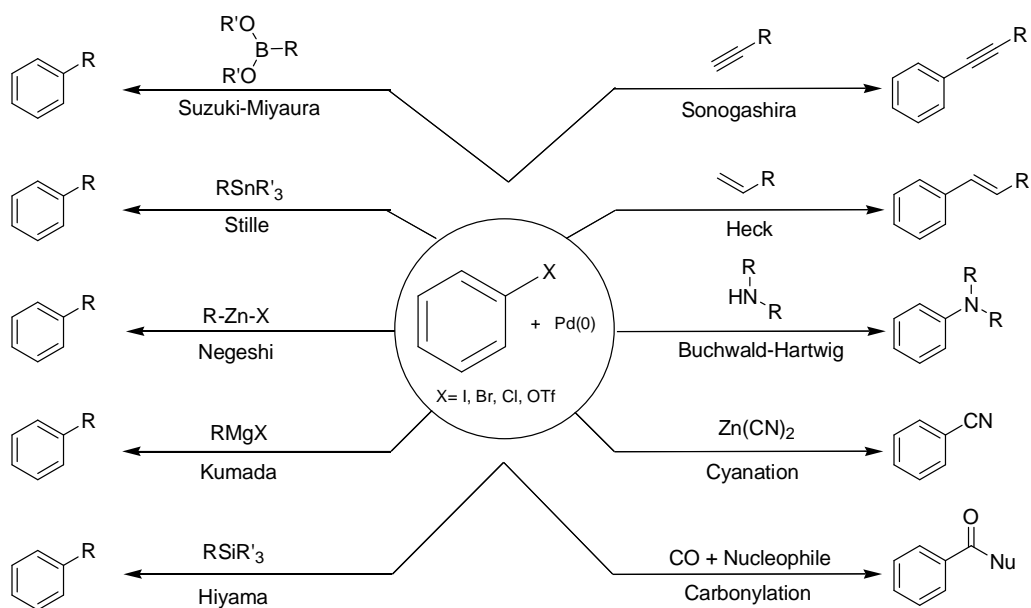
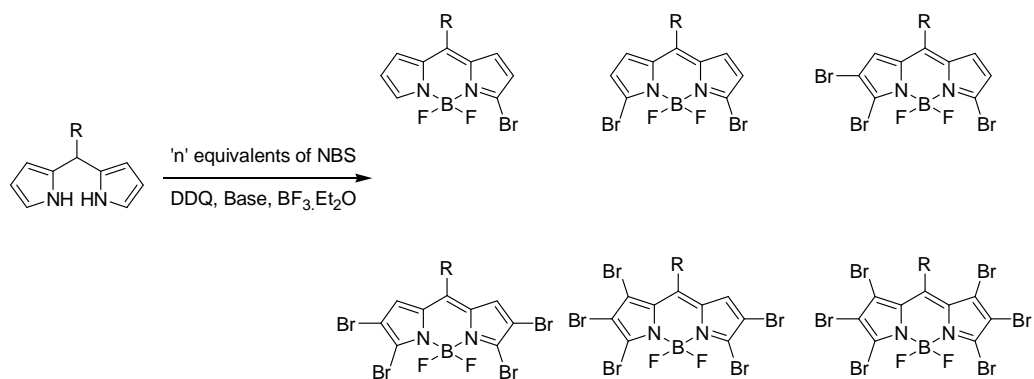


Figure 1.3. Versatility of halogenated precursors in synthesis.

1.3.2.1. Halogenation of dipyrromethane core

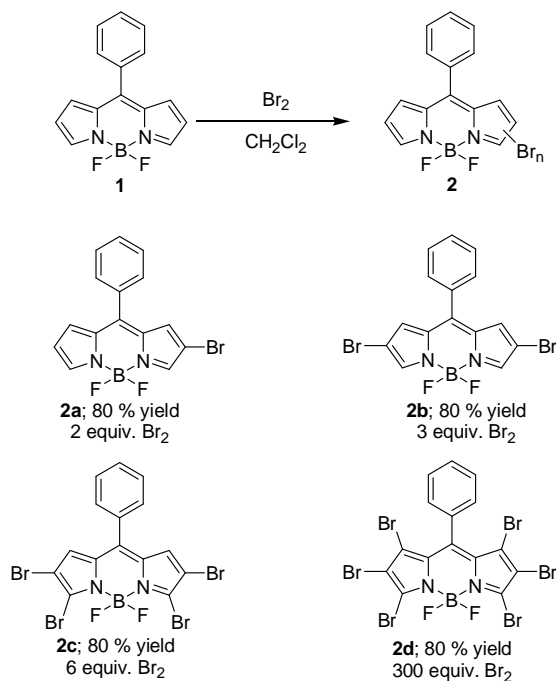


Scheme 1.8. Halogenation of dipyrromethane core.

The α halogenated BODIPYs can be obtained by the halogenation of dipyrromethane core. The halogenation occurs selectively at α -position and varying the amount of *N*-bromo succinimide (NBS), the mono, di or tri-bromo BODIPYs can be obtained. Excess use of NBS gives tetra, penta and hexa-bromo BODIPYs. Several reports use the bromine as halogenating agent instead of NBS. The α -chlorinated BODIPYs were also synthesized by reacting dipyrromethane with NCS. The oxidation of halogenated dipyrromethane to dipyrromethene by DDQ or *p*-

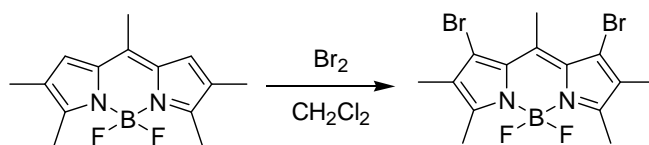
chloranil, followed by treatment with base and complexation with $\text{BF}_3 \cdot \text{etherate}$ results the halogenated BODIPYs.^[34]

1.3.2.2. Halogenation of BODIPYs



Scheme 1.9. Bromination of BODIPY at multiple positions.

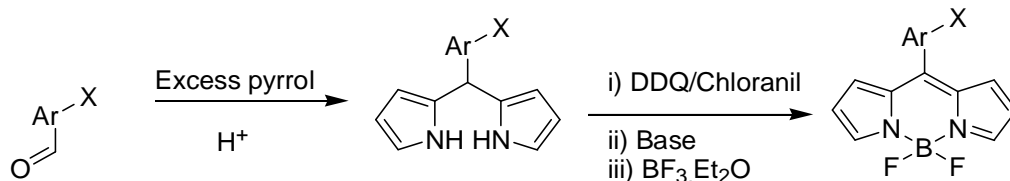
The BODIPYs are susceptible to electrophilic halogenation at the β -pyrrolic positions. Using different procedures they can be brominated or iodinated to get β -halogenated BODIPYs. The halogenation of BODIPYs initially occurs at β -position followed by at α and β' -positions (Scheme 1.9). Various halogenating reagents like NBS, Br_2 , ICl , NIS and $\text{I}_2\text{-HIO}_3$ have been employed for the halogenation of BODIPY. The alkylation of unwanted position of BODIPY is useful strategy for selective halogenation at expected position. Using this strategy the BODIPYs have been selectively brominated at β' position (Scheme 1.10).^[35]



Scheme 1.10. Halogenation at β' -position.

1.3.2.2.1. Halogenation at *meso* position

i) With halogenated aryl substituents (aldehyde)

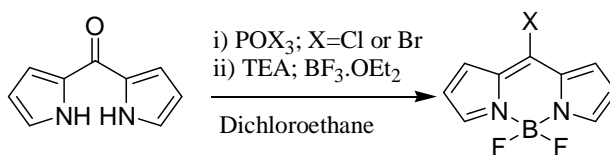


Scheme 1.11. BODIPYs with halogenated *meso* aryl substituents.

The functionalization of BODIPYs at *meso* position with halogenated aryl substituents is relatively easy and widely used method. The use of halogenated aromatic aldehydes or acyl chlorides results the *meso* aryl halogenated BODIPYs (Scheme 1.11). Various electron donating and withdrawing groups have been introduced at this position and their photophysical properties are studied in depth.^[36]

ii) Halogenation at *meso* position

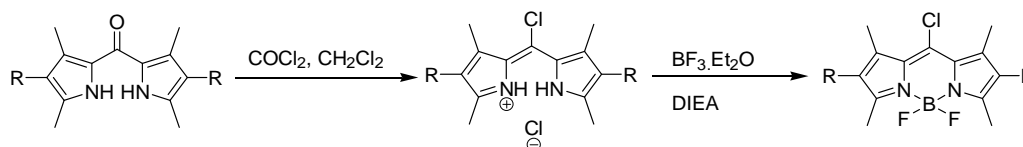
Wim Dehaen and Kevin M. Smith have developed the synthetic routes for *meso* halogenated BODIPYs. Wim Dehaen *et al.* synthesized 8-chloro and 8-bromo BODIPYs from dipyrromethane, by incorporation of the chloro and bromo groups through deoxygenative substitution using POCl₃ and POBr₃ respectively, followed by *in situ* deprotonation, and complexation with BF₃·etherate (Scheme 1.12).^[37] The 8-chloro BODIPY was further used for the synthesis of 8-iodo BODIPY by halogen exchange with NaI.



Scheme 1.12. Synthesis of *meso* halogenated BODIPYs.

Kelvin M. Smith *et al.* synthesized 8-chloro BODIPY by the reaction of dipyrromethane with phosgene followed by treatment with BF₃·etherate and *N,N*-diisopropylethylamine (Scheme 1.13).^[38] The *meso* halogenated BODIPYs enable the

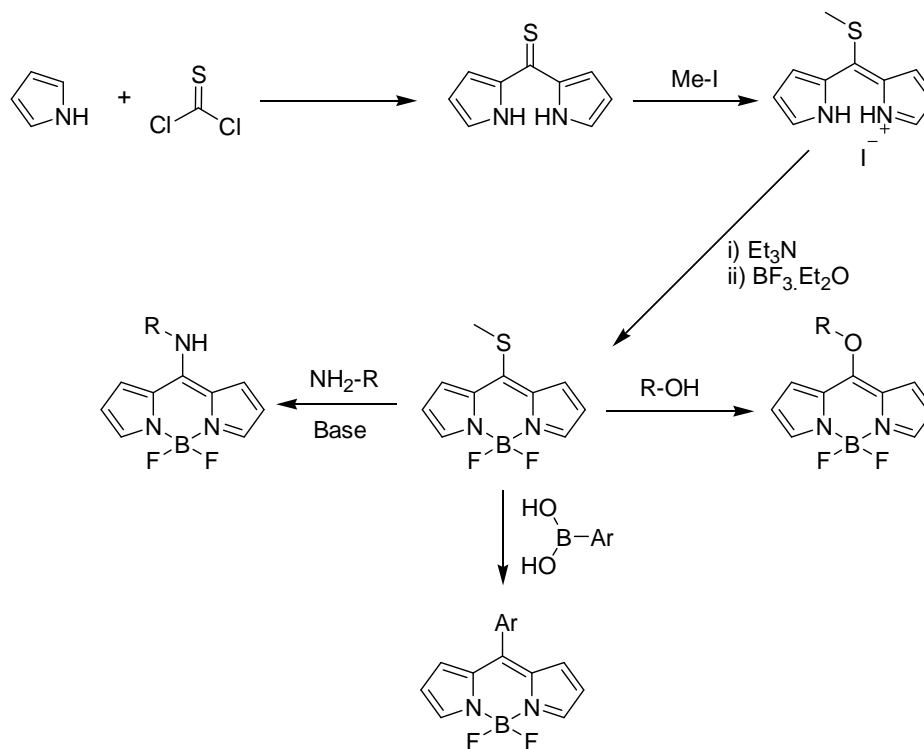
introduction of alkyne linkage at the *meso* position by Sonogashira cross-coupling reaction. The *meso* alkynylated BODIPYs ensures the planarity of *meso* substituent with BODIPY, which is not possible in the case of *meso* aryl substituted BODIPYs. Hiroshi Nishihara and coworkers have synthesized the *meso* alkynylated BODIPYs from alkynylated aldehydes and compared the effect of alkynylation at the *meso* position of BODIPYs with respect to *meso* aryl substituted BODIPYs.^[39]



Scheme 1.13. Synthesis of 8-chloro BODIPYs.

1.3.3. Through 8-(methylthio)-BODIPY

The 8-(methylthio)-BODIPY is an important precursor for the functionalization of BODIPYs at the *meso* position.^[40] The synthesis of 8-(methylthio)-BODIPY is outlined in Scheme 1.14.^[41] The condensation reaction of pyrrole with thiophosgene results dipyrrothioketone. The dipyrrothioketone on further reaction with methyl iodide gives an intermediate which on treatment with base followed by complexation with BF_3 ·etherate results 8-(methylthio)-BODIPY. The 8-(methylthio)-BODIPY is widely explored for the substitution reactions with N- and O- nucleophiles. It is also an useful intermediate for Liebeskind-Srogl cross-coupling reactions with various boronic acids.^[42]



Scheme 1.14. Synthesis of 8-(methylthio)-BODIPY and its synthetic utility.

The substitution of amines at the *meso* position of the BODIPY gives highly fluorescent blue emitting laser dyes, whereas substitution with anilines results in quenching of fluorescence. The BODIPYs substituted with the alcohol and phenol at *meso* position show green fluorescence with good to moderate fluorescence quantum yields.

The heteroatom substitution at the *meso* position of the BODIPY blue shifts the absorption by ~ 50 nm (for O-) and ~ 80 nm (for N-) compared to unsubstituted BODIPY (Figure 1.4). This has been assigned to the destabilization of LUMO and formation of merocyanine and hemicyanine type conjugated system.

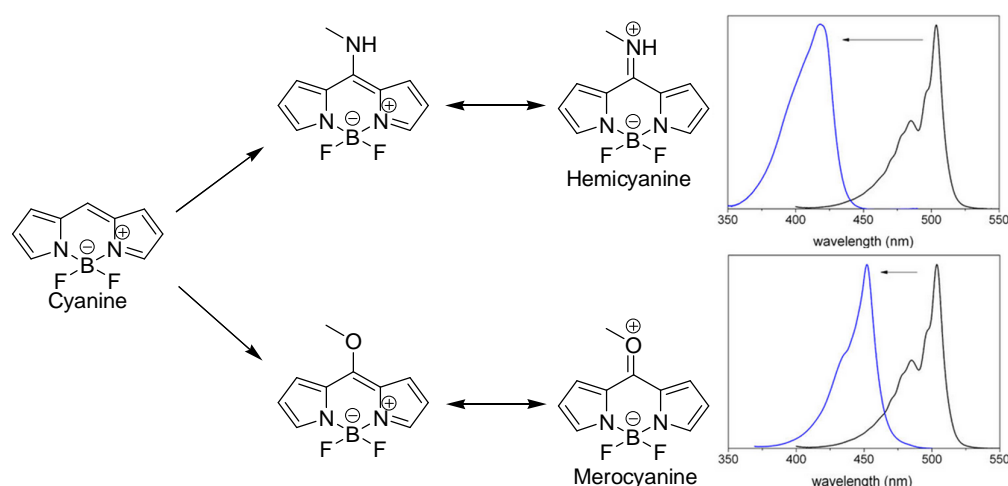


Figure 1.4. The blue shift in the absorption spectra of heteroatom substituted BODIPYs (Adapted with permission from ref ^[43]. Copyright © (2013) American Chemical Society).

1.3.4. Modification at the boron center

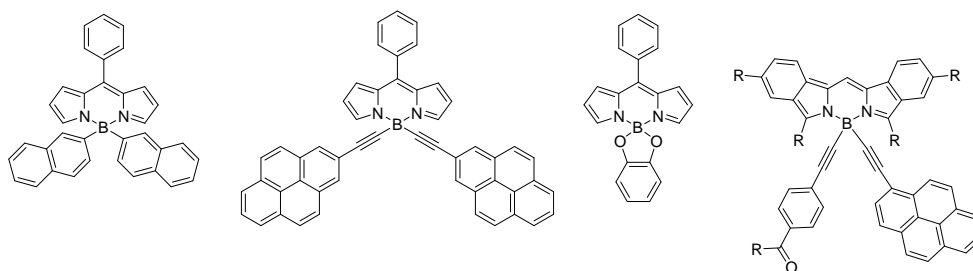


Chart 1.2. Boron functionalized BODIPYs.

The two fluorine atoms on boron of BODIPY can be replaced by different C- and O- substituents (Chart 1.2). This family of B-substituted BODIPYs is named according to the substituents on it, like aryl (C-BODIPY), ethynyl (E-BODIPY) or alkoxide (O-BODIPY). This family of BODIPYs exhibit high Stokes shift and high fluorescence quantum yield. The fluorine atoms have been replaced by strongly fluorescent aromatic cores and studied for through space energy transfer cassettes. Ziessel, Ulrich, Harriman and Ortiz^[44] have synthesized such molecular dyads for photovoltaics, electroluminescent devices and energy transfer cassettes.

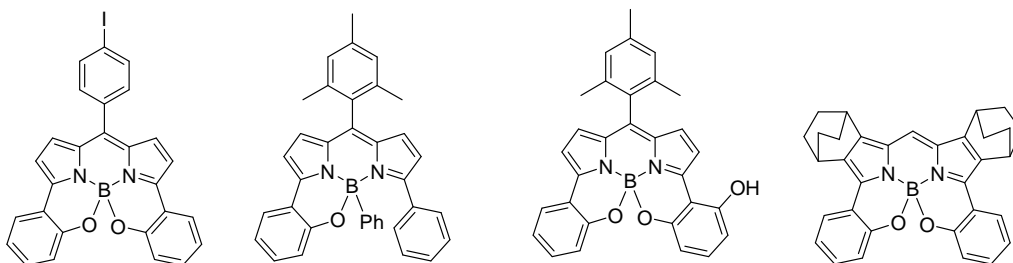


Chart 1.3. Fused BODIPYs.

The aryl or alkynyl substituents on the boron atom are not in conjugation with BODIPY fluorophore hence the absorption spectrum of these BODIPYs are restricted to visible region only, but the B-functionalization of fused BODIPYs exhibits highly red shifted absorption and emission (Chart 1.3).^[45] Burgess and Ravikanth have fused α -substituted aryl moieties with the boron atom of BODIPYs to get rigidified ring fused BODIPYs, with near IR absorption and fluorescence. These constrained BODIPYs exhibit higher fluorescence quantum yields than their unconstrained derivatives due to the restricted molecular rotations and steric crowding.

1.3.5. Fused BODIPYs for extension of conjugation

The aromatic ring fused BODIPYs can be synthesized using aromatic ring fused pyrroles. Another way to get fused BODIPYs is to use metal catalyzed C-H activation to couple the aromatic substituents like anthracene, perylene or porphyrin (Chart 1.4).^[46] The fused BODIPYs can absorb above 900 nm region.

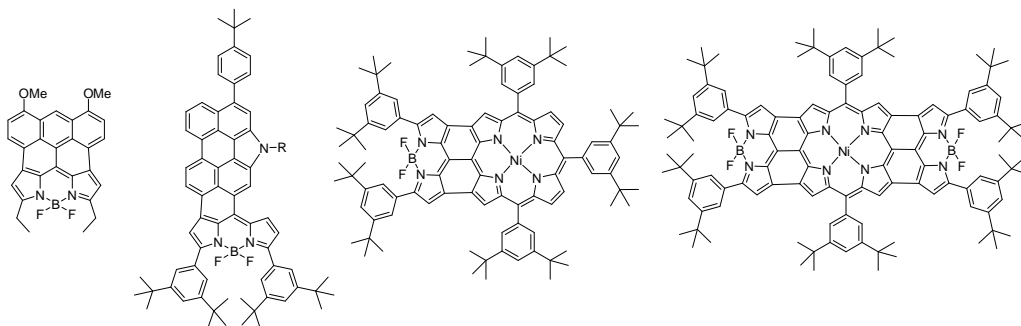


Chart 1.4. Fused BODIPYs.

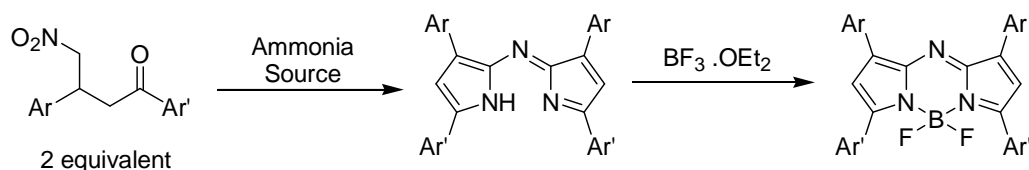
1.3.6. Oxidative nucleophilic reactions via C–H activation

The α unsubstituted BODIPYs are susceptible to the nucleophilic attack through C-H activation under oxygen atmosphere. The metal catalyzed C-H activation results α -substituted BODIPYs without any pre-functionalization step.^[47] The ring fused BODIPYs can also be synthesized through C-H activation.

1.3.7. Similar systems like BODIPY

1.3.7.1. Aza-BODIPY

The introduction of nitrogen at the *meso* position of BODIPYs results the aza-BODIPYs (Scheme 1.15).^[48] They exhibit ~ 100 nm red shifted absorption than the BODIPYs, with excellent fluorescence quantum yields. The aza-BODIPYs are being explored for wide range of applications.



Scheme 1.15. Synthesis of aza-BODIPYs.

1.3.7.2. BOPHY

Recently Ziegler^[49] and Hao^[50] reported a class of BODIPY type highly fluorescent dyes which they called bis(difluoroboron)1,2-bis((1H-pyrrol-2-yl)methylene)hydrazine (BOPHY) (Chart 1.5). The BOPHY derivatives are highly fluorescent in solution, film and solid state with large stokes shifts. The methylated BOPHY was further explored for Knoevenagel condensation reaction with *N,N*-dimethyl-(4-formyl)-aniline, and utilized for pH sensing.^[51]

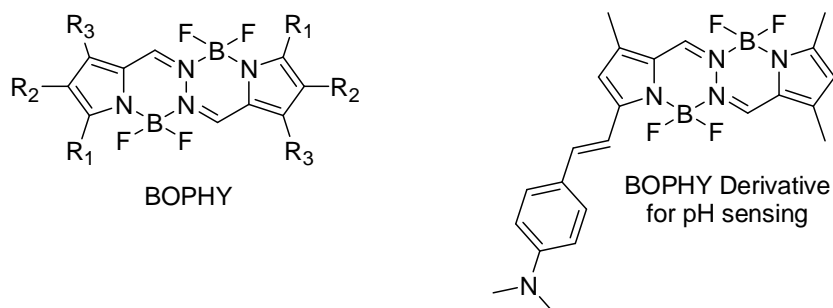


Chart 1.5. BOPHY and its derivative for pH sensing.

1.4. Donor-Acceptor system

The combination of electron rich moiety (Donor) and electron deficient moiety (Acceptor) through appropriate spacer are known as Donor-Acceptor (D-A) systems (Figure 1.5). They are relative in nature. The electron rich moiety, with the ability to donate the electrons to another moiety is known as donor. The moieties bearing heteroatoms with lone pair of electrons, amines, alcohols, sulphides, metallocene derivatives (like ferrocene and ruthenocene), or aromatic carbocycles are well known donors (Chart 1.6).

The electron deficient moieties which have capacity to withdraw the electrons from donors are known as acceptor. The strength of acceptors to withdraw the electrons from donor depends on the energy levels of LUMO. Lower the LOMO, stronger will be the accepting power of acceptor and *vice versa*. The anhydrides, nitrogen rich heterocycles, boron complexes, ketones, amides, nitriles and esters are examples of acceptors (Chart 1.7).

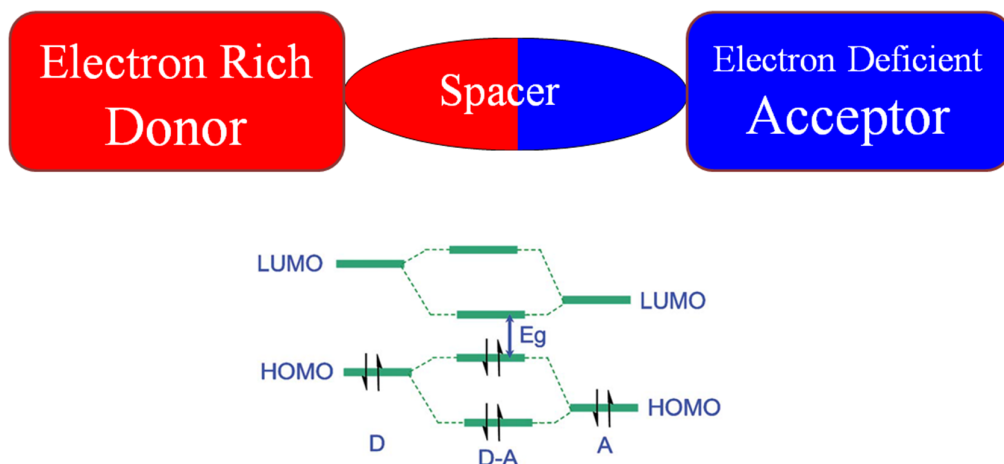


Figure 1.5. Schematic representation of Donor-Acceptor system and the effect of orbital couplings on the HOMO-LUMO gap.

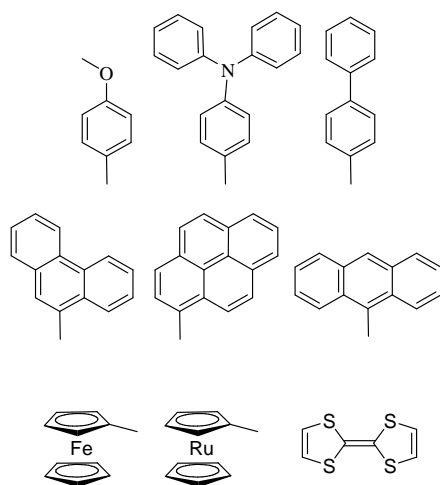


Chart 1.6. Frequently used donors.

The HOMO of D-A system becomes destabilized than that of individual donor and acceptor whereas the LUMO becomes stabilized than that of individual donor and acceptor. This results in overall lowering of the HOMO-LUMO gap and red shift in the absorption spectra. The strength of acceptor to withdraw the electrons and strength of donor to donate the electrons decides the strength of D-A system.

The donors and acceptors are coupled to each other through conjugated or non-conjugated spacers like single, double or triple bond, aromatic, hetero-aromatic ring(s) etc. The nature of spacer has key role in tuning the properties of D-A systems. The D-A systems have wide range of applications in diverse areas like;

- Non-Linear Optics (NLO) and Optical Limiting Materials
- Fluorescence Resonance Energy Transfer (FRET)
- Two Photon Absorption
- Solar Cell
- Photodynamic Therapy
- Organic Light Emitting Diodes (OLEDs)
- Mechanochromism

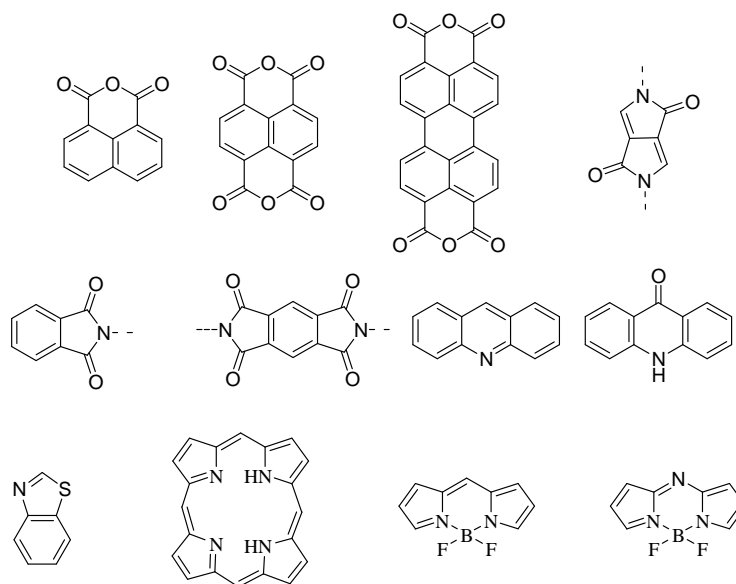


Chart 1.7. Frequently used acceptors.

1.5. Fluorescence of BODIPY dyes and charge transfer interactions

The fluorescence quantum yield of the fluorophore strongly depends on the nature of substituents and, can be tuned by systematic variation in the nature of substituents. Depending on the oxidation potential or reduction potential of the substituents relative to the excited state of fluorophore Nagano *et al.* rationalized the principles for modulating the fluorescence quantum yield of fluorescein derivatives^[52] and applied to the *meso* aryl substituted BODIPYs.^[53] The excited state electron can return to the ground state via fluorescence, phosphorescence, non-radiative pathway or quenching of fluorescence either by energy transfer or by electron transfer. In photoinduced electron transfer the excited state can behave as donor or as an acceptor. In D-A systems due to electron transfer the fluorescence is quenched by reductive photoinduced electron transfer (Figure 1.6B). Whereas if the LUMO of substituent is at appropriate energy to accept the excited state electron of fluorophore the fluorescence is quenched through oxidative photoinduced electron transfer (Figure 1.6C).

In energy transfer process the excited state electrons of the donor return to the ground state with emission of radiation, which is again absorbed by the acceptor unit with photoexcitation.^[54] The excited state electron of this acceptor can exhibit emission with very high Stoke's shift.

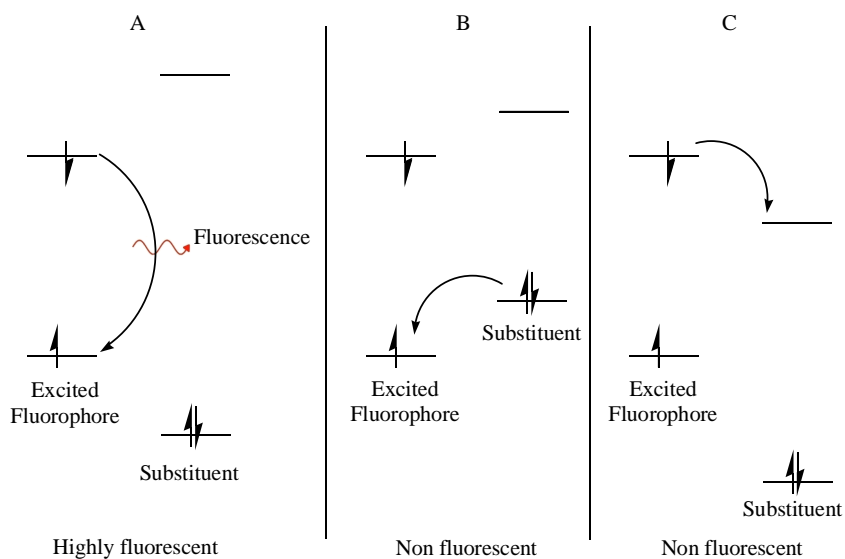


Figure 1.6. Fate of excited state electron depends on the nature of substituent.

1.6. Organization of thesis

Chapter 1 gives the detailed introduction about the historical development of various synthetic and functionalization strategies of BODIPYs and their utility in diverse fields. The recent functionalization strategies have been summarized and further explored in D-A systems in the subsequent chapters.

Chapter 2 Summarizes the instrumentation and general methods used for the present study.

In **Chapter 3** a series of donor-acceptor ferrocenyl substituted BODIPYs have been designed, and synthesized via palladium catalysed Suzuki, and Sonogashira cross-coupling reactions. The effect of ferrocenyl group on the photophysical properties of BODIPYs were studied as function of varying spacer length.

In **Chapter 4**, for the evaluation of the effect of alkynylation on the α , β and *meso* positions of BODIPYs the *meso*-alkynylated ferrocenyl BODIPYs with varying conjugation length were designed, and synthesized. The *meso* alkynylated ferrocenyl BODIPYs exhibit red shifted absorption than the α and β alkynylated ferrocenyl BODIPYs, which indicates better electronic conjugation in *meso* alkynylated BODIPYs.

In **Chapter 5** a series of *meso* arylethynyl BODIPYs were designed and synthesized to study the effects of donor on the photophysical properties of the BODIPYs. The quenching of fluorescence was correlated with the electron donating strength of different donors.

In **Chapter 6** a set of heteroatom connected ferrocenyl BODIPYs were designed and synthesized by the nucleophilic aromatic substitution reaction of 8-chloro BODIPY, with ferrocenyl anilines and ferrocenyl phenols. The effects of heteroatom and ferrocenyl group on the optical and electrochemical properties of the BODIPYs were studied.

In **Chapter 7**, the electron deficient nature of 8-chloro BODIPY leads to the oxidation of aliphatic amines to enamines and *in situ* cross coupling. This has been explored for the synthesis of *meso* enamine substituted BODIPYs.

References

- [1] (a) Bessette, A., and Hanan, G. S. (2014). Design, synthesis and photophysical studies of dipyrromethene-based materials: insights into their applications in organic photovoltaic devices. *Chemical Society Reviews*, 43(10), 3342–3405. <http://doi.org/10.1039/C3CS60411J>; (b) Lu, H., Mack, J., Yang, Y., and Shen, Z. (2014). Structural modification strategies for the rational design of red/NIR region BODIPYs. *Chemical Society Reviews*, 43(13), 4778–4823. <http://doi.org/10.1039/C4CS00030G>.
- [2] (a) Nepomnyashchii, A. B., and Bard, A. J. (2012). Electrochemistry and Electrogenenerated Chemiluminescence of BODIPY Dyes. *Accounts of Chemical Research*, 45(11), 1844–1853. <http://doi.org/10.1021/ar200278b>; (b) Chibani, S., Le Guennic, B., Charaf-Eddin, A., Laurent, A. D., and Jacquemin, D. (2013). Revisiting the optical signatures of BODIPY with ab initio tools. *Chemical Science*, 4(5), 1950–1963. <http://doi.org/10.1039/C3SC22265A>; (c) Benniston, A. C., & Copley, G. (2009). Lighting the way ahead with boron dipyrromethene (Bodipy) dyes. *Physical Chemistry Chemical Physics*, 11(21), 4124–4131. <http://doi.org/10.1039/B901383K>.

-
- [3] (a) Karolin, J., Johansson, L. B.-A., Strandberg, L., and Ny, T. (1994). Fluorescence and Absorption Spectroscopic Properties of Dipyrrometheneboron Difluoride (BODIPY) Derivatives in Liquids, Lipid Membranes, and Proteins. *Journal of the American Chemical Society*, 116(17), 7801–7806. <http://doi.org/10.1021/ja00096a042>; (b) Tan, K., Jaquinod, L., Paolesse, R., Nardis, S., Di Natale, C., Di Carlo, A., Prodi, L., Montalti, M., Zaccheroni, N. and Smith, K. M. (2004). Synthesis and characterization of β -fused porphyrin-BODIPY® dyads. *Tetrahedron*, 60(5), 1099–1106. <http://doi.org/http://dx.doi.org/10.1016/j.tet.2003.11.072>; (c) Fa, M., Bergström, F., Hägglöf, P., Wilczynska, M., Johansson, L. B.-A., and Ny, T. (2000). The structure of a serpin–protease complex revealed by intramolecular distance measurements using donor–donor energy migration and mapping of interaction sites. *Structure*, 8(4), 397–405. [http://doi.org/http://dx.doi.org/10.1016/S0969-2126\(00\)00121-0](http://doi.org/http://dx.doi.org/10.1016/S0969-2126(00)00121-0); (d) Kamkaew, A., Lim, S. H., Lee, H. B., Kiew, L. V., Chung, L. Y., and Burgess, K. (2013). BODIPY dyes in photodynamic therapy. *Chemical Society Reviews*, 42(1), 77–88. <http://doi.org/10.1039/C2CS35216H>; (e) Awuah, S. G., and You, Y. (2012). Boron dipyrromethene (BODIPY)-based photosensitizers for photodynamic therapy. *RSC Advances*, 2(30), 11169–11183. <http://doi.org/10.1039/C2RA21404K>; (f) Ni, Y. and Wu, J. (2014). Far-red and near infrared BODIPY dyes: synthesis and applications for fluorescent pH probes and bio-imaging. *Organic & Biomolecular Chemistry*, 12, 3774–3791. DOI: 10.1039/c3ob42554a.
- [4] (a) Boens, N., Leen, V., and Dehaen, W. (2012). Fluorescent indicators based on BODIPY. *Chemical Society Reviews*, 41(3), 1130–1172. <http://doi.org/10.1039/C1CS15132K>; (b) Benstead, M., Mehl, G. H., & Boyle, R. W. (2011). 4,4'-Difluoro-4-bora-3a,4a-diaza-s-indacenes (BODIPYs) as components of novel light active materials. *Tetrahedron*, 67(20), 3573–3601. <http://doi.org/http://dx.doi.org/10.1016/j.tet.2011.03.028>.
- [5] (a) Ulrich, G., Zissel, R., and Harriman, A. (2008). The Chemistry of Fluorescent Bodipy Dyes: Versatility Unsurpassed. *Angewandte Chemie International Edition*, 47(7), 1184–1201. <http://doi.org/10.1002/anie.200702070>; (b) Loudet, A., and Burgess, K. (2007). BODIPY Dyes and Their

Derivatives: Syntheses and Spectroscopic Properties. *Chemical Reviews*, 107(11), 4891–4932. <http://doi.org/doi:10.1021/cr078381n>.

- [6] Tram, K., Yan, H., Jenkins, H. A., Vassiliev, S., and Bruce, D. (2009). The synthesis and crystal structure of unsubstituted 4,4-difluoro-4-bora-3a,4a-diaza-s-indacene (BODIPY). *Dyes and Pigments*, 82(3), 392–395. <http://doi.org/http://dx.doi.org/10.1016/j.dyepig.2009.03.001>.
- [7] Moss G P. (1987). Nomenclature of tetrapyrroles (Recommendations 1986) . *Pure and Applied Chemistry*. <http://doi.org/10.1351/pac198759060779>.
- [8] (a) Zheng, Q., Xu, G., and Prasad, P. N. (2008). Conformationally Restricted Dipyrromethene Boron Difluoride (BODIPY) Dyes: Highly Fluorescent, Multicolored Probes for Cellular Imaging. *Chemistry – A European Journal*, 14(19), 5812–5819. <http://doi.org/10.1002/chem.200800309>; (b) Wang, Y.-W., Descalzo, A. B., Shen, Z., You, X.-Z., and Rurack, K. (2010). Dihydronaphthalene-Fused Boron–Dipyrromethene (BODIPY) Dyes: Insight into the Electronic and Conformational Tuning Modes of BODIPY Fluorophores. *Chemistry – A European Journal*, 16(9), 2887–2903. <http://doi.org/10.1002/chem.200902527>.
- [9] (a) Qin, W., Baruah, M., De Borggraeve, W. M., and Boens, N. (2006). Photophysical properties of an on/off fluorescent pH indicator excitable with visible light based on a borondipyrromethene-linked phenol. *Journal of Photochemistry and Photobiology A: Chemistry*, 183(1–2), 190–197. <http://doi.org/http://dx.doi.org/10.1016/j.jphotochem.2006.03.015>; (b) Li, L., Nguyen, B., and Burgess, K. (2008). Functionalization of the 4,4-difluoro-4-bora-3a,4a-diaza-s-indacene (BODIPY) core. *Bioorganic and Medicinal Chemistry Letters*, 18(10), 3112–3116. <http://doi.org/http://dx.doi.org/10.1016/j.bmcl.2007.10.103>; (c) Thivierge, C., Bandichhor, R., and Burgess, K. (2007). Spectral Dispersion and Water Solubilization of BODIPY Dyes via Palladium-Catalyzed C–H Functionalization. *Organic Letters*, 9(11), 2135–2138. <http://doi.org/10.1021/ol0706197>.

-
- [10] (a) El-Khouly, M. E., Fukuzumi, S., and D'Souza, F. (2014). Photosynthetic Antenna–Reaction Center Mimicry by Using Boron Dipyrromethene Sensitizers. *ChemPhysChem*, 15(1), 30–47. <http://doi.org/10.1002/cphc.201300715>.
- [11] (a) Mula, S., Ray, A. K., Banerjee, M., Chaudhuri, T., Dasgupta, K., and Chattopadhyay, S. (2008). Design and Development of a New Pyrromethene Dye with Improved Photostability and Lasing Efficiency: Theoretical Rationalization of Photophysical and Photochemical Properties. *The Journal of Organic Chemistry*, 73(6), 2146–2154. <http://doi.org/10.1021/jo702346s>; (b) Chen, T., Boyer, J. H., and Trudell, M. L. (1997). Synthesis of 2,6-diethyl-3-methacroyloxymethyl-1,5,7,8-tetramethylpyrromethene-BF₂ for the preparation of new solid-state laser dyes. *Heteroatom Chemistry*, 8(1), 51–54. [http://doi.org/10.1002/\(SICI\)1098-1071\(1997\)8:1<51::AID-HC7>3.0.CO;2-5](http://doi.org/10.1002/(SICI)1098-1071(1997)8:1<51::AID-HC7>3.0.CO;2-5); (c) Girard, P.-M., Graindorge, D., Smirnova, V., Rigolet, P., Francesconi, S., Scanlon, S., and Sage, E. (2013). Oxidative Stress in Mammalian Cells Impinges on the Cysteines Redox State of Human XRCC3 Protein and on Its Cellular Localization. *PLoS ONE*, 8(10), e75751. <http://doi.org/10.1371/journal.pone.0075751>.
- [12] (a) Merino, E. J., and Weeks, K. M. (2005). Facile Conversion of Aptamers into Sensors Using a 2'-Ribose-Linked Fluorophore. *Journal of the American Chemical Society*, 127(37), 12766–12767. <http://doi.org/10.1021/ja053189t>; (b) Meng, Q., Kim, D. H., Bai, X., Bi, L., Turro, N. J., and Ju, J. (2006). Design and Synthesis of a Photocleavable Fluorescent Nucleotide 3'-O-Allyl-dGTP-PC-Bodipy-FL-510 as a Reversible Terminator for DNA Sequencing by Synthesis. *The Journal of Organic Chemistry*, 71(8), 3248–3252. <http://doi.org/10.1021/jo060300k>; (c) Peters, C., Billich, A., Ghobrial, M., Högenauer, K., Ullrich, T., and Nussbaumer, P. (2007). Synthesis of Borondipyrromethene (BODIPY)-Labeled Sphingosine Derivatives by Cross-metathesis Reaction. *The Journal of Organic Chemistry*, 72(5), 1842–1845. <http://doi.org/10.1021/jo062347b>.

-
- [13] (a) Burghart, A., Thoresen, L. H., Chen, J., Burgess, K., Bergstrom, F., and Johansson, L. B.-A. (2000). Energy transfer cassettes based on BODIPY dyes. *Chemical Communications*, (22), 2203-2204. <http://doi.org/10.1039/B006769P>; (b) Ziessel, R., and Harriman, A. (2011). Artificial light-harvesting antennae: electronic energy transfer by way of molecular funnels. *Chemical Communications*, 47(2), 611-631. <http://doi.org/10.1039/C0CC02687E>.
- [14] (a) Ulrich, G., Goze, C., Guardigli, M., Roda, A., and Ziessel, R. (2005). Pyrromethene Dialkynyl Borane Complexes for “Cascatelle” Energy Transfer and Protein Labeling. *Angewandte Chemie International Edition*, 44(24), 3694-3698. <http://doi.org/10.1002/anie.200500808>; (b) Loudet, A., Bandichhor, R., Wu, L., and Burgess, K. (2008). Functionalized BF₂ chelated azadipyrromethene dyes. *Tetrahedron*, 64(17), 3642-3654. <http://doi.org/http://dx.doi.org/10.1016/j.tet.2008.01.117>; (c) Li, F., Yang, S. I., Ciringh, Y., Seth, J., Martin, C. H., Singh, D. L., Kim, D., Birge, R. R., Bocian, D. F., Holten, D. and Lindsey, J. S. (1998). Design, Synthesis, and Photodynamics of Light-Harvesting Arrays Comprised of a Porphyrin and One, Two, or Eight Boron-Dipyrin Accessory Pigments. *Journal of the American Chemical Society*, 120(39), 10001-10017. <http://doi.org/10.1021/ja9812047>.
- [15] (a) He, H., Lo, P.-C., Yeung, S.-L., Fong, W.-P., and Ng, D. K. P. (2011). Synthesis and in Vitro Photodynamic Activities of Pegylated Distyryl Boron Dipyrromethene Derivatives. *Journal of Medicinal Chemistry*, 54(8), 3097-3102. <http://doi.org/10.1021/jm101637g>; (b) Bura, T., Retailleau, P., Ulrich, G., and Ziessel, R. (2011). Highly Substituted Bodipy Dyes with Spectroscopic Features Sensitive to the Environment. *The Journal of Organic Chemistry*, 76(4), 1109-1117. <http://doi.org/10.1021/jo102203f>; (c) Yogo, T., Urano, Y., Ishitsuka, Y., Maniwa, F., and Nagano, T. (2005). Highly Efficient and Photostable Photosensitizer Based on BODIPY Chromophore. *Journal of the American Chemical Society*, 127(35), 12162-12163. <http://doi.org/10.1021/ja0528533>.
- [16] (a) Ziessel, R., Ulrich, G., and Harriman, A. (2007). The chemistry of Bodipy: A new El Dorado for fluorescence tools. *New Journal of Chemistry*, 31(4),

-
- 496–501. <http://doi.org/10.1039/B617972J>; (b) Lammi, R. K., Ambroise, A., Balasubramanian, T., Wagner, R. W., Bocian, D. F., Holten, D., and Lindsey, J. S. (2000). Structural Control of Photoinduced Energy Transfer between Adjacent and Distant Sites in Multiporphyrin Arrays. *Journal of the American Chemical Society*, 122(31), 7579–7591. <http://doi.org/10.1021/ja001031x>; (c) Ambroise, A., Kirmaier, C., Wagner, R. W., Loewe, R. S., Bocian, D. F., Holten, D., and Lindsey, J. S. (2002). Weakly Coupled Molecular Photonic Wires: Synthesis and Excited-State Energy-Transfer Dynamics. *The Journal of Organic Chemistry*, 67(11), 3811–3826. <http://doi.org/10.1021/jo025561i>.
- [17] Erbas, S., Gorgulu, A., Kocakusakogullari, M., and Akkaya, E. U. (2009). Non-covalent functionalized SWNTs as delivery agents for novel Bodipy-based potential PDT sensitizers. *Chemical Communications*, (33), 4956–4958. <http://doi.org/10.1039/B908485A>.
- [18] (a) Coskun, A., and Akkaya, E. U. (2005). Ion Sensing Coupled to Resonance Energy Transfer: A Highly Selective and Sensitive Ratiometric Fluorescent Chemosensor for Ag(I) by a Modular Approach. *Journal of the American Chemical Society*, 127(30), 10464–10465. <http://doi.org/10.1021/ja052574f>; (b) Zeng, L., Miller, E. W., Pralle, A., Isacoff, E. Y., and Chang, C. J. (2006). A Selective Turn-On Fluorescent Sensor for Imaging Copper in Living Cells. *Journal of the American Chemical Society*, 128(1), 10–11. <http://doi.org/10.1021/ja055064u>; (c) Peng, X., Du, J., Fan, J., Wang, J., Wu, Y., Zhao, J., Sun, S. and Xu, T. (2007). A Selective Fluorescent Sensor for Imaging Cd²⁺ in Living Cells. *Journal of the American Chemical Society*, 129(6), 1500–1501. <http://doi.org/10.1021/ja0643319>; (d) Krumova, K., Oleynik, P., Karam, P., and Cosa, G. (2009). Phenol-Based Lipophilic Fluorescent Antioxidant Indicators: A Rational Approach. *The Journal of Organic Chemistry*, 74(10), 3641–3651. <http://doi.org/10.1021/jo900335z>; (e) Yuan, M., Zhou, W., Liu, X., Zhu, M., Li, J., Yin, X., Zheng, H., Zuo, Z., Ouyang, C., Liu, H., Li, Y. and Zhu, D. (2008). A Multianalyte Chemosensor on a Single Molecule: Promising Structure for an Integrated Logic Gate. *The Journal of Organic Chemistry*, 73(13), 5008–5014. <http://doi.org/10.1021/jo8005683>; (f) Hargrove, A. E., Nieto, S., Zhang, T., Sessler, J. L., and

Anslyn, E. V. (2011). Artificial receptors for the recognition of phosphorylated molecules. *Chemical Reviews*, 111(11), 6603–6782. <http://doi.org/10.1021/cr100242s>.

[19] (a) Kim, B., Ma, B., Donuru, V. R., Liu, H., and Frechet, J. M. J. (2010). Bodipy-backboned polymers as electron donor in bulk heterojunction solar cells. *Chemical Communications*, 46(23), 4148–4150. <http://doi.org/10.1039/B927350F>; (b) Rousseau, T., Cravino, A., Bura, T., Ulrich, G., Ziessel, R., and Roncali, J. (2009). BODIPY derivatives as donor materials for bulk heterojunction solar cells. *Chemical Communications*, (13), 1673–1675. <http://doi.org/10.1039/B822770E>; (c) Rousseau, T., Cravino, A., Ripaud, E., Leriche, P., Rihn, S., De Nicola, A., Ziessel, R. and Roncali, J. (2010). A tailored hybrid BODIPY-oligothiophene donor for molecular bulk heterojunction solar cells with improved performances. *Chemical Communications*, 46(28), 5082–5084. <http://doi.org/10.1039/C0CC01144D>; (d) Mao, M., Wang, J.-B., Xiao, Z.-F., Dai, S.-Y., and Song, Q.-H. (2012). New 2,6-modified BODIPY sensitizers for dye-sensitized solar cells. *Dyes and Pigments*, 94(2), 224–232. <http://doi.org/http://dx.doi.org/10.1016/j.dyepig.2012.01.011>.

[20] <https://www.lifetechnologies.com/in/en/home.html>.

[21] (a) Treibs, A., and Kreuzer, F.-H. (1968). Difluoroboryl-Komplexe von Di- und Tripyrrylmethenen. *Justus Liebigs Annalen Der Chemie*, 718(1), 208–223. <http://doi.org/10.1002/jlac.19687180119>; (b) Wood, T. E., and Thompson, A. (2007). Advances in the Chemistry of Dipyrins and Their Complexes. *Chemical Reviews*, 107(5), 1831–1861. <http://doi.org/10.1021/cr050052c>.

[22] Wories, H. J., Koek, J. H., Lodder, G., Lugtenburg, J., Fokkens, R., Driessen, O., and Mohn, G. R. (1985). A novel water-soluble fluorescent probe: Synthesis, luminescence and biological properties of the sodium salt of the 4-sulfonato-3,3',5,5'-tetramethyl-2,2'-pyrromethen-1,1'-BF₂ complex. *Recueil Des Travaux Chimiques Des Pays-Bas*, 104(11), 288–291. <http://doi.org/10.1002/recl.19851041104>.

-
- [23] (a) Sathyamoorthi, G., Boyer, J. H., Allik, T. H., and Chandra, S. (1994). Laser active cyanopyrromethene-BF₂ complexes. *Heteroatom Chemistry*, 5(4), 403–407. <http://doi.org/10.1002/hc.520050413>; (b) Bañuelos, J., Martín, V., Gómez-Durán, C. F. A., Córdoba, I. J. A., Peña-Cabrera, E., García-Moreno, I., Costela, Á., Pérez-Ojeda, M. E., Arbeloa, T. and Arbeloa, Í. L. (2011). New 8-Amino-BODIPY Derivatives: Surpassing Laser Dyes at Blue-Edge Wavelengths. *Chemistry – A European Journal*, 17(26), 7261–7270. <http://doi.org/10.1002/chem.201003689>; (c) Johnson, I. D., Kang, H. C., and Haugland, R. P. (1991). Fluorescent membrane probes incorporating dipyrrometheneboron difluoride fluorophores. *Analytical Biochemistry*, 198(2), 228–237. [http://doi.org/http://dx.doi.org/10.1016/0003-2697\(91\)90418-S](http://doi.org/http://dx.doi.org/10.1016/0003-2697(91)90418-S); (d) Schade, S. Z., Jolley, M. E., Sarauer, B. J., and Simonson, L. G. (1996). BODIPY- α -Casein, a pH-Independent Protein Substrate for Protease Assays Using Fluorescence Polarization. *Analytical Biochemistry*, 243(1), 1–7. <http://doi.org/http://dx.doi.org/10.1006/abio.1996.0475>.
- [24] (a) Shah, M., Thangaraj, K., Soong, M. -L., Wolford, L. T., Boyer, J. H., Politzer, I. R., and Pavlopoulos, T. G. (1990). Pyrromethene-BF₂ complexes as laser dyes:1. *Heteroatom Chemistry*, 1(5), 389–399. <http://doi.org/10.1002/hc.520010507>; (b) Boyer, J. H., Haag, A. M., Sathyamoorthi, G., Soong, M.-L., Thangaraj, K., and Pavlopoulos, T. G. (1993). Pyrromethene-BF₂ complexes as laser dyes: 2. *Heteroatom Chemistry*, 4(1), 39–49. <http://doi.org/10.1002/hc.520040107>.
- [25] Wagner R W, and Lindsey J S. (1996). Boron-dipyrromethene dyes for incorporation in synthetic multi-pigment light-harvesting arrays. *Pure and Applied Chemistry*. <http://doi.org/10.1351/pac199668071373>.
- [26] Li, Z., Mintzer, E., and Bittman, R. (2006). First Synthesis of Free Cholesterol - BODIPY Conjugates. *The Journal of Organic Chemistry*, 71(4), 1718–1721. <http://doi.org/10.1021/jo052029x>.
- [27] Schmitt, A., Hinkeldey, B., Wild, M., and Jung, G. (2009). Synthesis of the Core Compound of the BODIPY Dye Class: 4,4'-Difluoro-4-bora-(3a,4a)-

diaza-s-indacene. *Journal of Fluorescence*, 19(4), 755–758. <http://doi.org/10.1007/s10895-008-0446-7>.

- [28] Tram, K., Yan, H., Jenkins, H. A., Vassiliev, S., and Bruce, D. (2009). The synthesis and crystal structure of unsubstituted 4,4-difluoro-4-bora-3a,4a-diaza-s-indacene (BODIPY). *Dyes and Pigments*, 82(3), 392–395. <http://doi.org/http://dx.doi.org/10.1016/j.dyepig.2009.03.001>.
- [29] Arroyo, I. J., Hu, R., Merino, G., Tang, B. Z., and Peña-Cabrera, E. (2009). The Smallest and One of the Brightest. Efficient Preparation and Optical Description of the Parent Borondipyrromethene System. *The Journal of Organic Chemistry*, 74(15), 5719–5722. <http://doi.org/10.1021/jo901014w>.
- [30] (a) Lim, S. H., Thivierge, C., Nowak-Sliwinska, P., Han, J., van den Bergh, H., Wagnières, G., Burgess, K. and Lee, H. B. (2010). In Vitro and In Vivo Photocytotoxicity of Boron Dipyrromethene Derivatives for Photodynamic Therapy. *Journal of Medicinal Chemistry*, 53(7), 2865–2874. <http://doi.org/10.1021/jm901823u>; (b) Uppal, T., Hu, X., Fronczek, F. R., Maschek, S., Bobadova-Parvanova, P., and Vicente, M. G. H. (2012). Synthesis, Computational Modeling, and Properties of Benzo-Appended BODIPYs. *Chemistry – A European Journal*, 18(13), 3893–3905. <http://doi.org/10.1002/chem.201103002>; (c) Ziessel, R., Bonardi, L., and Ulrich, G. (2006). Boron dipyrromethene dyes: a rational avenue for sensing and light emitting devices. *Dalton Transactions*, (23), 2913–2918. <http://doi.org/10.1039/B516222J>.
- [31] (a) Buyukcakil, O., Bozdemir, O. A., Kolemen, S., Erbas, S., and Akkaya, E. U. (2009). Tetrastaryl-Bodipy Dyes: Convenient Synthesis and Characterization of Elusive Near IR Fluorophores. *Organic Letters*, 11(20), 4644–4647. <http://doi.org/10.1021/ol9019056>; (b) Rurack, K., Kollmannsberger, M., and Daub, J. (2001). Molecular Switching in the Near Infrared (NIR) with a Functionalized Boron–Dipyrromethene Dye. *Angewandte Chemie International Edition*, 40(2), 385–387. [http://doi.org/10.1002/1521-3773\(20010119\)40:2<385::AID-ANIE385>3.0.CO;2-F](http://doi.org/10.1002/1521-3773(20010119)40:2<385::AID-ANIE385>3.0.CO;2-F); (c) Bura, T., Hablot, D., and Ziessel, R.

-
- (2011). Fluorescent boron dipyrromethene (Bodipy) dyes having two and four vinyl residues. *Tetrahedron Letters*, 52(18), 2370–2374. <http://doi.org/http://dx.doi.org/10.1016/j.tetlet.2011.02.094>; (d) Zhu, S., Zhang, J., Vegesna, G., Tiwari, A., Luo, F.-T., Zeller, M., Luck, R., Li, H., Green, S. and Liu, H. (2012). Controlled Knoevenagel reactions of methyl groups of 1,3,5,7-tetramethyl BODIPY dyes for unique BODIPY dyes. *RSC Advances*, 2(2), 404–407. <http://doi.org/10.1039/C1RA00678A>.
- [32] (a) Johansson Seechurn, C. C. C., Kitching, M. O., Colacot, T. J., and Snieckus, V. (2012). Palladium-Catalyzed Cross-Coupling: A Historical Contextual Perspective to the 2010 Nobel Prize. *Angewandte Chemie International Edition*, 51(21), 5062–5085. <http://doi.org/10.1002/anie.201107017>; (b) Peña-Cabrera, E., Aguilar-Aguilar, A., González-Domínguez, M., Lager, E., Zamudio-Vázquez, R., Godoy-Vargas, J., and Villanueva-García, F. (2007). Simple, General, and Efficient Synthesis of *Meso*-Substituted Borondipyrromethenes from a Single Platform. *Organic Letters*, 9(20), 3985–3988. <http://doi.org/10.1021/ol7016615>; (c) Suzuki, A. (2011). Cross-Coupling Reactions Of Organoboranes: An Easy Way To Construct C-C Bonds (Nobel Lecture). *Angewandte Chemie International Edition*, 50(30), 6722–6737. <http://doi.org/10.1002/anie.201101379>; (d) Negishi, E. (2011). Magical Power of Transition Metals: Past, Present, and Future (Nobel Lecture). *Angewandte Chemie International Edition*, 50(30), 6738–6764. <http://doi.org/10.1002/anie.201101380>; (e) Cross-Coupling Arylations: Precedents and Rapid Historical Review of the Field. (2014). In *Catalytic Arylation Methods* (pp. 1–94). Wiley-VCH Verlag GmbH and Co. KGaA. <http://doi.org/10.1002/9783527672707.ch1>.
- [33] (a) Jiao, L., Pang, W., Zhou, J., Wei, Y., Mu, X., Bai, G., and Hao, E. (2011). Regioselective Stepwise Bromination of Boron Dipyrromethene (BODIPY) Dyes. *The Journal of Organic Chemistry*, 76(24), 9988–9996. <http://doi.org/10.1021/jo201754m>; (b) Lakshmi, V., and Ravikanth, M. (2012). Brominated boron dipyrins: synthesis, structure, spectral and electrochemical properties. *Dalton Transactions*, 41(19), 5903–5911. <http://doi.org/10.1039/C2DT00019A>.

-
- [34] (a) Rao, M. R., Mobin, S. M., and Ravikanth, M. (2010). Boron-dipyrromethene based specific chemodosimeter for fluoride ion. *Tetrahedron*, 66(9), 1728–1734. <http://doi.org/http://dx.doi.org/10.1016/j.tet.2009.12.039>; (b) Baruah, M., Qin, W., Basarić, N., De Borggraeve, W. M., and Boens, N. (2005). BODIPY-Based Hydroxyaryl Derivatives as Fluorescent pH Probes. *The Journal of Organic Chemistry*, 70(10), 4152–4157. <http://doi.org/10.1021/jo0503714>; (c) Rohand, T., Baruah, M., Qin, W., Boens, N., and Dehaen, W. (2006). Functionalisation of fluorescent BODIPY dyes by nucleophilic substitution. *Chemical Communications*, (3), 266–268. <http://doi.org/10.1039/B512756D>. (d) Lakshmi, V., Rao, M., R. and Ravikanth, M. (2015). Halogenated boron-dipyrromethenes: synthesis, properties and applications. *Organic & Biomolecular Chemistry*, (13), 2501. DOI: 10.1039/c4ob02293a.
- [35] (a) Meng, G., Velayudham, S., Smith, A., Luck, R., and Liu, H. (2009). Color Tuning of Polyfluorene Emission with BODIPY Monomers. *Macromolecules*, 42(6), 1995–2001. <http://doi.org/10.1021/ma8023975>; (b) Lu, H., Wang, Q., Gai, L., Li, Z., Deng, Y., Xiao, X., Lai, G. and Shen, Z. (2012). Tuning the Solid-State Luminescence of BODIPY Derivatives with Bulky Arylsilyl Groups: Synthesis and Spectroscopic Properties. *Chemistry – A European Journal*, 18(25), 7852–7861. <http://doi.org/10.1002/chem.201200169>.
- [36] (a) Zhang, X., Xiao, Y., He, L., and Zhang, Y. (2014). Through-Bond Energy Transfer Cassettes for Multicolor Encoding. *The Journal of Organic Chemistry*, 79(13), 6315–6320. <http://doi.org/10.1021/jo500653r>; (b) Nano, A., Ziessel, R., Stachelek, P., Alamiry, M. A. H., and Harriman, A. (2014). Exciplex Emission from a Boron Dipyrromethene (Bodipy) Dye Equipped with a Dicyanovinyl Appendage. *ChemPhysChem*, 15(1), 177–186. <http://doi.org/10.1002/cphc.201300805>; (c) Rao, M. R., Kumar, K. V. P., and Ravikanth, M. (2010). Synthesis of boron-dipyrromethene–ferrocene conjugates. *Journal of Organometallic Chemistry*, 695(6), 863–869. <http://doi.org/http://dx.doi.org/10.1016/j.jorganchem.2010.01.009>; (d) Hu, R., Gomez-Duran, C. F. A., Lam, J. W. Y., Belmonte-Vazquez, J. L., Deng, C., Chen, S., Chen, S., Ye, R., Pena-Cabrera, E., Zhong, Y., Wong, K. S. and Tang, B. Z. (2012). Synthesis,

-
- solvatochromism, aggregation-induced emission and cell imaging of tetraphenylethene-containing BODIPY derivatives with large Stokes shifts. *Chemical Communications*, 48(81), 10099–10101. <http://doi.org/10.1039/C2CC35188A>.
- [37] Leen, V., Yuan, P., Wang, L., Boens, N., and Dehaen, W. (2012). Synthesis of *Meso*-Halogenated BODIPYs and Access to *Meso*-Substituted Analogues. *Organic Letters*, 14(24), 6150–6153. <http://doi.org/10.1021/ol3028225>.
- [38] Wang, H., Vicente, M. G. H., Fronczek, F. R., and Smith, K. M. (2014). Synthesis and Transformations of 5-Chloro-2,2'-Dipyrrins and Their Boron Complexes, 8-Chloro-BODIPYs. *Chemistry – A European Journal*, 20(17), 5064–5074. <http://doi.org/10.1002/chem.201304310>.
- [39] Kusaka, S., Sakamoto, R., Kitagawa, Y., Okumura, M., and Nishihara, H. (2013). *meso*-Alkynyl BODIPYs: Structure, Photoproperties, π -Extension, and Manipulation of Frontier Orbitals. *Chemistry – An Asian Journal*, 8(4), 723–727. <http://doi.org/10.1002/asia.201201176>.
- [40] (a) Lager, E., Liu, J., Aguilar-Aguilar, A., Tang, B. Z., and Peña-Cabrera, E. (2009). Novel *meso*-Polyarylamine-BODIPY Hybrids: Synthesis and Study of Their Optical Properties. *The Journal of Organic Chemistry*, 74(5), 2053–2058. <http://doi.org/10.1021/jo802519b>; (b) Esnal, I., Urías-Benavides, A., Gómez-Durán, C. F. A., Osorio-Martínez, C. A., García-Moreno, I., Costela, A., Bañuelos, J., Epelde, N., López A. I., Hu, R., Zhong T. B. and Peña-Cabrera, E. (2013). Reaction of Amines with 8-Methylthio BODIPY: Dramatic Optical and Laser Response to Amine Substitution. *Chemistry – An Asian Journal*, 8(11), 2691–2700. <http://doi.org/10.1002/asia.201300760>; (c) Martinez-Gonzalez, M. R., Urías-Benavides, A., Alvarado-Martínez, E., Lopez, J. C., Gómez, A. M., del Rio, M., Garcia, I., Costela, A., Bañuelos, J., Arbeloa, T., Lopez A. I. and Peña-Cabrera, E. (2014). Convenient Access to Carbohydrate-BODIPY Hybrids by Two Complementary Methods Involving One-Pot Assembly of “Clickable” BODIPY Dyes. *European Journal of Organic Chemistry*, 2014(26), 5659–5663. <http://doi.org/10.1002/ejoc.201402767>; (d) Poe, A. M.,

-
- Della Pelle, A. M., Subrahmanyam, A. V., White, W., Wantz, G., and Thayumanavan, S. (2014). Small molecule BODIPY dyes as non-fullerene acceptors in bulk heterojunction organic photovoltaics. *Chemical Communications*, 50(22), 2913–2915. <http://doi.org/10.1039/C3CC49648A>; (e) Roacho, R. I., Metta-Magana, A., Pena-Cabrera, E., and Pannell, K. (2015). Unprecedented one-pot sequential thiolate substitutions under mild conditions leading to a red emissive BODIPY dye 3,5,8-tris(PhS)-BODIPY. *Organic and Biomolecular Chemistry*, 13(4), 995–999. <http://doi.org/10.1039/C4OB01892C>; (f) Roacho, R. I., Metta-Magaña, A., Portillo, M. M., Peña-Cabrera, E., and Pannell, K. H. (2013). 8-Amino-BODIPYs: Structural Variation, Solvent-Dependent Emission, and VT NMR Spectroscopic Properties of 8-R₂N-BODIPY. *The Journal of Organic Chemistry*, 78(9), 4245–4250. <http://doi.org/10.1021/jo302758a>.
- [41] (a) Kim, D., Yamamoto, K., and Ahn, K. H. (2012). A BODIPY-based reactive probe for ratiometric fluorescence sensing of mercury ions. *Tetrahedron*, 68(26), 5279–5282. <http://doi.org/http://dx.doi.org/10.1016/j.tet.2012.01.091>; (b) Santschi, N., Cvengroš, J., Matthey, C., Otth, E., and Antonio Togni, and. (2014). Rapid and Selective Electrophilic Trifluoromethylation of the 4,4-Difluoro-4-bora-3a,4a-diaza-s-indacene (BODIPY) Scaffold. *European Journal of Organic Chemistry*, 2014(29), 6371–6375. <http://doi.org/10.1002/ejoc.201402874>.
- [42] (a) Goud, T. V., Tutar, A., and Biellmann, J.-F. (2006). Synthesis of 8-heteroatom-substituted 4,4-difluoro-4-bora-3a,4a-diaza-s-indacene dyes (BODIPY). *Tetrahedron*, 62(21), 5084–5091. <http://doi.org/http://dx.doi.org/10.1016/j.tet.2006.03.036>; (b) Arroyo, I. J., Hu, R., Tang, B. Z., López, F. I., and Peña-Cabrera, E. (2011). 8-Alkenylborondipyrromethene dyes. General synthesis, optical properties, and preliminary study of their reactivity. *Tetrahedron*, 67(38), 7244–7250. <http://doi.org/http://dx.doi.org/10.1016/j.tet.2011.07.067>.
- [43] Flores-Rizo, J. O., Esnal, I., Osorio-Martínez, C. A., GómezDurán, C. F. A., Bañuelos, J., López Arbeloa, I., Pannell, K. H., Metta-Magaña, A. J. and Peña-

-
- Cabrera, E. (2013). 8-Alkoxy- and 8-Aryloxy-BODIPYs: Straightforward Fluorescent Tagging of Alcohols and Phenols. *The Journal of Organic Chemistry*, 78(12), 5867–5877. <http://doi.org/10.1021/jo400417h>.
- [44] (a) Duran-Sampedro, G., Esnal, I., Agarrabeitia, A. R., Bañuelos Prieto, J., Cerdán, L., García-Moreno, I., Costela, A., Lopez-Arbeloa, I. and Ortiz, M. J. (2014). First Highly Efficient and Photostable E and C Derivatives of 4,4-Difluoro-4-bora-3a,4a-diaza-s-indacene (BODIPY) as Dye Lasers in the Liquid Phase, Thin Films, and Solid-State Rods. *Chemistry – A European Journal*, 20(9), 2646–2653. <http://doi.org/10.1002/chem.201303579>; (b) Lundrigan, T., Cameron, T. S., and Thompson, A. (2014). Activation and deprotection of F-BODIPYs using boron trihalides. *Chemical Communications*, 50(53), 7028–7031. <http://doi.org/10.1039/C4CC02706J>; (c) Harriman, A., Izzet, G., and Ziessel, R. (2006). Rapid Energy Transfer in Cascade-Type Bodipy Dyes. *Journal of the American Chemical Society*, 128(33), 10868–10875. <http://doi.org/10.1021/ja0631448>; (d) Goze, C., Ulrich, G., and Ziessel, R. (2007). Tetrahedral Boron Chemistry for the Preparation of Highly Efficient “Cascatelle” Devices. *The Journal of Organic Chemistry*, 72(2), 313–322. <http://doi.org/10.1021/jo060984w>; (e) Tahtaoui, C., Thomas, C., Rohmer, F., Klotz, P., Duportail, G., Mély, Y., Bonnet, D. and Hibert, M. (2007). Convenient Method To Access New 4,4-Dialkoxy- and 4,4-Diaryloxy-diaza-s-indacene Dyes: Synthesis and Spectroscopic Evaluation. *The Journal of Organic Chemistry*, 72(1), 269–272. <http://doi.org/10.1021/jo061567m>.
- [45] (a) Chen, J., Burghart, A., Derecskei-Kovacs, A., and Burgess, K. (2000). 4,4-Difluoro-4-bora-3a,4a-diaza-s-indacene (BODIPY) Dyes Modified for Extended Conjugation and Restricted Bond Rotations. *The Journal of Organic Chemistry*, 65(10), 2900–2906. <http://doi.org/10.1021/jo991927o>; (b) Loudet, A., Bandichhor, R., Burgess, K., Palma, A., McDonnell, S. O., Hall, M. J., and O’Shea, D. F. (2008). B,O-Chelated Azadipyromethenes as Near-IR Probes. *Organic Letters*, 10(21), 4771–4774. <http://doi.org/10.1021/ol8018506>; (c) Kim, H., Burghart, A., B. Welch, M., Reibenspies, J., and Burgess, K. (1999). Synthesis and spectroscopic properties of a new 4-bora-3a,4a-diaza-s-indacene

(BODIPY[registered sign]) dye. *Chemical Communications*, (18), 1889–1890. <http://doi.org/10.1039/A905739K>.

- [46] (a) Zeng, L., Jiao, C., Huang, X., Huang, K.-W., Chin, W.-S., and Wu, J. (2011). Anthracene-Fused BODIPYs as Near-Infrared Dyes with High Photostability. *Organic Letters*, 13(22), 6026–6029. <http://doi.org/10.1021/ol202493c>; (b) Jiao, C., Zhu, L., and Wu, J. (2011). BODIPY-Fused Porphyrins as Soluble and Stable Near-IR Dyes. *Chemistry – A European Journal*, 17(24), 6610–6614. <http://doi.org/10.1002/chem.201100619>; (c) Jiao, C., Huang, K.-W., and Wu, J. (2011). Perylene-Fused BODIPY Dye with Near-IR Absorption/Emission and High Photostability. *Organic Letters*, 13(4), 632–635. <http://doi.org/10.1021/ol102879g>.
- [47] (a) Luo, L., Wu, D., Li, W., Zhang, S., Ma, Y., Yan, S., and You, J. (2014). Regioselective Decarboxylative Direct C–H Arylation of Boron Dipyrromethenes (BODIPYs) at 2,6-Positions: A Facile Access to a Diversity-Oriented BODIPY Library. *Organic Letters*, 16(23), 6080–6083. <http://doi.org/10.1021/ol502883x>; (b) Leen, V., Van der Auweraer, M., Boens, N., and Dehaen, W. (2011). Vicarious Nucleophilic Substitution of α -Hydrogen of BODIPY and Its Extension to Direct Ethenylation. *Organic Letters*, 13(6), 1470–1473. <http://doi.org/10.1021/ol200148u>; (c) Leen, V., Qin, W., Yang, W., Cui, J., Xu, C., Tang, X., Liu, W., Robeyns, K., Van Meervelt, L., Beljonne, D., Lazzaroni, R., Tonnelé, C., Boens, N. and Dehaen, W. (2010). Synthesis, Spectroscopy, Crystal Structure Determination, and Quantum Chemical Calculations of BODIPY Dyes with Increasing Conformational Restriction and Concomitant Red-Shifted Visible Absorption and Fluorescence Spectra. *Chemistry – An Asian Journal*, 5(9), 2016–2026. <http://doi.org/10.1002/asia.201000248>; (d) Rao, M. R., Tiwari, M. D., Bellare, J. R., and Ravikanth, M. (2011). Synthesis of BF₂ Complexes of Prodigiosin Type Oligopyrroles. *The Journal of Organic Chemistry*, 76(17), 7263–7268. <http://doi.org/10.1021/jo201183s>.
- [48] (a) Díaz-Moscoso, A., Emond, E., Hughes, D. L., Tizzard, G. J., Coles, S. J., and Cammidge, A. N. (2014). Synthesis of a Class of Core-Modified Aza-

-
- BODIPY Derivatives. *The Journal of Organic Chemistry*, 79(18), 8932–8936. <http://doi.org/10.1021/jo501863t>; (b) Prusty, D. K., Kwak, M., Wildeman, J., and Herrmann, A. (2012). Modular Assembly of a Pd Catalyst within a DNA Scaffold for the Amplified Colorimetric and Fluorimetric Detection of Nucleic Acids. *Angewandte Chemie International Edition*, 51(47), 11894–11898. <http://doi.org/10.1002/anie.201206006>; (c) Fan, G., Yang, L., and Chen, Z. (2014). Water-soluble BODIPY and aza-BODIPY dyes: synthetic progress and applications. *Frontiers of Chemical Science and Engineering*, 8(4), 405–417. <http://doi.org/10.1007/s11705-014-1445-7>.
- [49] Tamgho, I.-S., Hasheminasab, A., Engle, J. T., Nemykin, V. N., and Ziegler, C. J. (2014). A New Highly Fluorescent and Symmetric Pyrrole–BF₂ Chromophore: BOPHY. *Journal of the American Chemical Society*, 136(15), 5623–5626. <http://doi.org/10.1021/ja502477a>.
- [50] Yu, C., Jiao, L., Zhang, P., Feng, Z., Cheng, C., Wei, Y., Mu, X. and Hao, E. (2014). Highly Fluorescent BF₂ Complexes of Hydrazine–Schiff Base Linked Bispyrrole. *Organic Letters*, 16(11), 3048–3051. <http://doi.org/10.1021/ol501162f>.
- [51] Jiang, X.-D., Su, Y., Yue, S., Li, C., Yu, H., Zhang, H., Sun, C. -L. and Xiao, L.-J. (2015). Synthesis of mono-(p-dimethylamino)styryl-containing BOPHY dye for a turn-on pH sensor. *RSC Advances*, 5(22), 16735–16739. <http://doi.org/10.1039/C4RA15914D>.
- [52] Ueno, T., Urano, Y., Setsukinai, K., Takakusa, H., Kojima, H., Kikuchi, K., Ohkubo, K., Fukuzumi, S. and Nagano, T. (2004). Rational Principles for Modulating Fluorescence Properties of Fluorescein. *Journal of the American Chemical Society*, 126(43), 14079–14085. <http://doi.org/10.1021/ja048241k>.
- [53] Sunahara, H., Urano, Y., Kojima, H., and Nagano, T. (2007). Design and Synthesis of a Library of BODIPY-Based Environmental Polarity Sensors Utilizing Photoinduced Electron-Transfer-Controlled Fluorescence ON/OFF Switching. *Journal of the American Chemical Society*, 129 (17), 5597–5604. <http://doi.org/10.1021/ja068551y>.

-
- [54] Fan, J., Hu, M., Zhan, P., and Peng, X. (2013). Energy transfer cassettes based on organic fluorophores: construction and applications in ratiometric sensing. *Chemical Society Reviews*, 42(1), 29–43. <http://doi.org/10.1039/C2CS35273G>.

Chapter 2

Materials and Experimental Techniques

2.1. Introduction

In this chapter the materials used, general synthetic procedures, characterization techniques and the instrumentation employed in this thesis are discussed.

2.2. Chemicals for synthesis

Common solvents used for syntheses were purified according to known procedures.^[1] Pyrrole, Benzaldehyde, thiophosgene, Phosphorus oxychloride and Boron trifluoride etherate were obtained from Spectrochem India. Triethylamine, *N,N*-Di-isopropylethylamine, were obtained from S.D.Fine chem. Ltd. *N,N*-Dimethylethylamine, *N*-ethylpyrrolidine, CuI, Pd(PPh₃)₄, PdCl₂(PPh₃)₂, ferrocene, tetrabutylammonium hexafluorophosphate (TBAF₆), 4-ethynylaniline, 3-ethynylaniline, Ethynyl ferrocene, chloranil, DDQ and trifluoroacetic acid (TFA) were procured from Aldrich chemicals USA. Aluminum oxide (neutral) and silica gel (100 – 200 mesh and 230 – 400 mesh) were purchased from Rankem chemicals, India. TLC pre-coated silica gel plates (Kieselgel 60F254, Merck) were obtained from Merck, India.

Dry solvents dichloromethane, chloroform, tetrahydrofuran (THF), *N,N*-dimethylformamide (DMF), dioxane and methanol were obtained from spectrochem and S.D.Fine chem. Ltd. All oxygen or moisture sensitive reactions were performed under nitrogen/argon atmosphere using standard schlenk method.

The solvents and reagents were used as received unless otherwise indicated. The pyrrole was distilled before use. Photophysical and electrochemical studies were performed with spectroscopic grade solvents.

2.3. Spectroscopic Measurements

2.3.1. NMR Spectroscopy

^1H NMR (400 MHz), ^{13}C NMR (100 MHz), ^{11}B NMR (128.37 MHz), and ^{19}F NMR (376.49 MHz) spectra were recorded on the Bruker Avance (III) 400 MHz, using CDCl_3 and acetone- d_6 as solvent. Chemical shifts in ^1H , ^{13}C , ^{11}B and ^{19}F NMR spectra were reported in parts per million (ppm). In ^1H NMR chemical shifts are reported relative to the residual solvent peak (CDCl_3 , 7.26 ppm). Multiplicities are given as: s (singlet), d (doublet), t (triplet), q (quartet), dd (doublet of doublets), m (multiplet), and the coupling constants J , are given in Hz. ^{13}C NMR chemical shifts are reported relative to the solvent residual peak (CDCl_3 , 77.36 ppm).

2.3.2. Mass Spectrometry

High resolution mass spectra (HRMS) were recorded on Bruker-Daltonics, micrOTOF-Q II mass spectrometer using positive and negative mode electrospray ionizations.

2.3.3. UV-Vis Spectroscopy

UV-Vis absorption spectra were recorded using a Varian Cary100 Bio UV-Vis and PerkinElmer LAMBDA 35 UV/Vis spectrophotometer.

2.3.4. Fluorescence Spectroscopy

Fluorescence emission spectra were recorded upon specific excitation wavelength on a Horiba Scientific Fluoromax-4 spectrophotometer. The slit width for the excitation and emission was set at 2 nm.

The fluorescence quantum yields (ϕ_F)

The fluorescence quantum yields (ϕ_F) of compounds **1-4** were calculated by the steady-state comparative method using following equation,

$$\phi_F = \phi_{st} \times S_u/S_{st} \times A_{st} / A_u \times n_{Du}^2/n_{Dst}^2 \dots\dots\dots (\text{Eq. 1})$$

Where ϕ_F is the emission quantum yield of the sample, ϕ_{st} is the emission quantum yield of the standard, A_{st} and A_u represent the absorbance of the standard and sample at the excitation wavelength, respectively, while S_{st} and S_u are the integrated emission band areas of the standard and sample, respectively, and n_{Dst} and n_{Du} the solvent refractive index of the standard and sample, u and st refer to the unknown and standard, respectively.

2.4. Electrochemical Studies

Cyclic voltamograms (CVs) and Differential Pulse Voltamograms (DPVs) were recorded on CHI620D electrochemical analyzer using Glassy carbon as working electrode, Pt wire as the counter electrode, and Saturated Calomel Electrode (SCE) as the reference electrode. The scan rate was 100 mVs⁻¹. A solution of tetrabutylammonium hexafluorophosphate (TBAPF₆) in CH₂Cl₂ (0.1 M) was employed as the supporting electrolyte.

2.5. Elemental Analysis

Elemental analyses for elements carbon, hydrogen, nitrogen and sulphur were performed on the Thermo Scientific FLASH 2000 (formerly the Flash EA1112) elemental analyser.

2.6. Computational Calculations

The density functional theory (DFT) calculation were carried out at the B3LYP/6-31G** level for B, F, C, N, O, H, and Lanl2DZ level for Fe in the Gaussian 09 program.²

2.7. Single Crystal X-ray Diffraction Studies.

Single crystal X-ray diffraction studies were performed on SUPER NOVA diffractometer. The strategy for the Data collection was evaluated by using the CrysAlisPro CCD software. The data were collected by the standard 'phi-omega scan techniques, and were scaled and reduced using CrysAlisPro RED software. The structures were solved by direct methods using SHELXS-97, and refined by full matrix least-squares with SHELXL-97, refining on F^2 .¹ The positions of all the atoms were obtained by direct methods. All non-hydrogen atoms were refined anisotropically. The remaining hydrogen atoms were placed in geometrically constrained positions, and refined with isotropic temperature factors, generally 1.2 U_{eq} of their parent atoms. The CCDC numbers contain the respective supplementary crystallographic data. These data can be obtained free of charge via www.ccdc.cam.ac.uk/conts/retrieving.html (or from the Cambridge Crystallographic

Data Centre, 12 union Road, Cambridge CB21 EZ, UK; Fax: (+44) 1223-336-033; or deposit@ccdc.cam.ac.uk).

References

- [1] (a) Vogel, A. I., Tatchell, A. R., Furnis, B. S., Hannaford, A. J., & Smith, P. W. G. (1996). *Vogel's Textbook of Practical Organic Chemistry (5th Edition)* (5th ed.); (b) Wei Ssberger, A. Proskraner, E. S. Riddick, J. A. Toppos Jr., E. F. (1970). *Organic Solvents in Techniques of Organic Chemistry*, Vol. IV, 3rd Edition, Inc. New York.
- [2] (a) Frisch, M. J.; Trucks, G. W.; Schlegel, H. B.; Scuseria, G. E.; Robb, M. A.; Cheeseman, J. R.; Scalmani, G.; Barone, V.; Mennucci, B.; Petersson, G. A.; Nakatsuji, H.; Caricato, M.; Li, X.; Hratchian, H. P.; Izmaylov, A. F.; Bloino, J.; Zheng, G.; Sonnenberg, J. L.; Hada, M.; Ehara, M.; Toyota, K.; Fukuda, R.; Hasegawa, J.; Ishida, M.; Nakajima, T.; Honda, Y.; Kitao, O.; Nakai, H.; Vreven, T.; Montgomery, J. A. Jr.; Peralta, J. E.; Ogliaro, F.; Bearpark, M.; Heyd, J. J.; Brothers, E.; Kudin, K. N.; Staroverov, V. N.; Kobayashi, R.; Normand, J.; Raghavachari, K.; Rendell, A.; Burant, J. C.; Iyengar, S. S.; Tomasi, J.; Cossi, M.; Rega, N.; Millam, N. J.; Klene, M.; Knox, J. E.; Cross, J. B.; Bakken, V.; Adamo, C.; Jaramillo, J.; Gomperts, R.; Stratmann, R. E.; Yazyev, O.; Austin, A. J.; Cammi, R.; Pomelli, C.; Ochterski, J. W.; Martin, R. L.; Morokuma, K.; Zakrzewski, V. G.; Voth, G. A.; Salvador, P.; Dannenberg, J. J.; Dapprich, S.; Daniels, A. D.; Farkas, O.; Foresman, J. B.; Ortiz, J. V.; Cioslowski, J.; Fox, D. J. (2009). *Gaussian 09, revision A.02*; *Gaussian, Inc.*: Wallingford, CT. (b) Lee, C., Yang, W., & Parr, R. G. (1988). Development of the Colle-Salvetti correlation-energy formula into a functional of the electron density. *Physical Review B*, 37(2), 785–789. **DOI:** 10.1103/PhysRevB.37.785; (c) A.D. Becke (1993). A new mixing of Hartree-Fock and local density-functional theories. *J. Chem. Phys.* 98 (2), 1372–377. **DOI:** 10.1063/1.464304.

Chapter 3

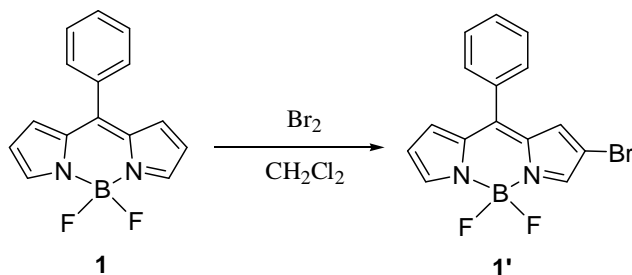
Donor-Acceptor β -Substituted Ferrocenyl BODIPYs

3.1 Introduction

There has been myriad of reports on the design, and synthesis of materials with enhanced nonlinear optical (NLO) properties.^[1] It has been established that the donor-acceptor (D-A) type of molecular systems, show promising results.^[2] 4, 4-difluoroboradiaza-s-indacene, widely known as boron dipyrromethene (BODIPY), is a unique luminophore. The BODIPY dyes exhibit strong absorption, with large absorption coefficient, and high luminescence efficiencies.^[3] They are thermally, and photochemically inert, which makes them attractive candidate for variety of applications such as chemosensors, NIR-absorbing dyes, photovoltaic devices, and NLO materials.^[4] The electronic properties of BODIPY can be tuned by functionalization at *meso*-position, as well as at the pyrrolic position. However functionalization at later position perturbs the electronic properties more significantly.^[5] Therefore substituting the donor groups at the pyrrolic position will result in the donor-acceptor (D-A) system.

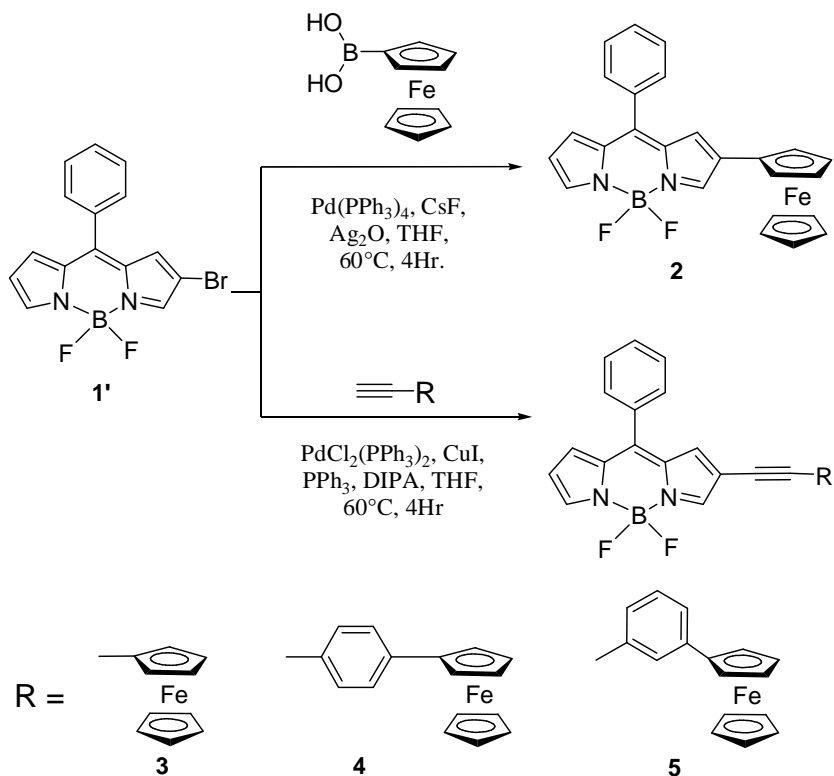
There are many reports, where the donor group is attached, at the pyrrolic position of the BODIPY.^[6] We were interested to substitute the donor group at only one β -pyrrolic position of the BODIPY,^[7] which will result in donor-acceptor (D-A) system. Ferrocene is undoubtedly strong electron donor.^[8] The ferrocenyl derivatives are thermally, and photochemically stable. There are few reports, where the ferrocenyl derivatives are connected to the BODIPY at different positions.^[9] In this report, we have attached the ferrocenyl group at one of the pyrrolic position of the BODIPY moiety directly, via ethynyl bond, and phenylethynyl bond. We were interested to explore the photophysical, electrochemical, and the structural properties of these molecular systems.

3.2 Results and discussion



Scheme 3.1: Synthesis of Bromo BODIPY **1'**.

The 2-bromo BODIPY (**1'**) was synthesized by the bromination reaction of parent 4,4-difluoro-8-phenyl-4-bora-3a,4a-diaza-s-indacene (**1**) (Scheme 1).^[10] The ferrocenyl substituted BODIPYs (**2-5**) were synthesised by the Suzuki, and Sonogashira coupling reactions of mono-bromo BODIPY **1'**, with the ferrocenyl boronic acid, and the ferrocenyl substituted ethyne respectively (Scheme 2).



Scheme 3.2: Synthetic route for the synthesis of BODIPYs **2 – 5**.

The bromo substituted BODIPY **1'** was reacted with the ferrocenyl boronic acid under the Suzuki coupling reaction conditions to give compound **2** in 45 % yield. The Sonogashira coupling reaction of bromo BODIPY **1'** with ethynylferrocene, 4-ferrocenylphenylacetylene, and 3-ferrocenylphenylacetylene resulted **3**, **4**, and **5** in

78%, 58%, and 42% yields respectively. All compounds were well characterized by ^1H , ^{13}C NMR, and HRMS techniques. Compounds **1'**, **2**, **3**, and **4** were also characterized by single crystal X-ray technique.

3.3 Photophysical properties

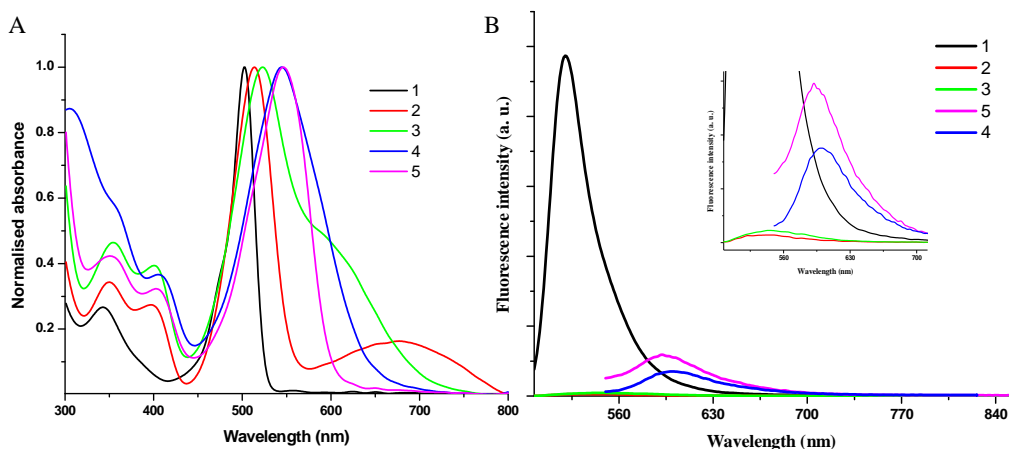


Figure 3.1. (A) Normalized electronic absorption spectra of compounds **1** – **5**, recorded in toluene. (B) Fluorescence spectra of **1** – **5** at 0.1 absorption, excited at 487 nm (for **1** – **3**) and 540 nm (for **4** – **5**) in toluene. Inset shows enlarged view.

The electronic absorption and emission spectra of compounds **1** – **5** was recorded in toluene at room temperature (Table 1), and displayed in Figure 6. Generally, BODIPY dyes exhibit strong absorption band around 500 nm along with a broad transition at higher energy region. The BODIPYs **1** – **5** show characteristic strong absorption band at 502-544 nm corresponding to $S_0 \rightarrow S_1$ transition, the weak-band at 345 nm in compound **1** is assigned to $S_0 \rightarrow S_2$ transition of BODIPY, this band shows considerable red shift to 405, 404, 412 and 409 nm in compounds **2** – **5** respectively.^[5] Another weak band is observed in compounds **2** – **5** at ~350 nm which can be assigned to the absorption of substituted ferrocenyl moiety.^[11, 5] The absorption maxima of BODIPYs **2** – **5** is considerably red shifted by 11 nm, 21 nm, 41 nm, and 42 nm respectively compared to the absorption maxima at about 500 nm for BODIPY **1** (Table 3.1). The sequential enhancement in π -conjugation from **2** – **5** leads to sequential red shift in the absorption spectra. The π -conjugation increases in the order **2** < **3** < **4** < **5**.

The ferrocenyl substituted BODIPYs **2** – **5** show moderate extinction coefficients. The compound **2** shows charge transfer (CT), **3** shows in the form of shoulder,

while **4** and **5** show that CT band is merged with $S_0 \rightarrow S_1$ absorption (evidenced from broadening of $S_0 \rightarrow S_1$ absorption band)^[9a] from this data we can interpret that the charge transfer is more effective in **2**, because the donor ferrocene is directly attached to BODIPY by single bond, and gradually decreases for **3** where ferrocene is attached via the triple bond, and the CT becomes moderate for **4** and **5** where ferrocene is attached via extended π -conjugated spacers.

Table 3.1. Photophysical properties of BODIPYs **1** – **5**.

Compound ^a	$\lambda_{(S_0 \rightarrow S_1)}$ (nm)	ϵ (M ⁻¹ cm ⁻¹)	λ_{em} (nm) ^b	Φ^c
1	502	62400	520	0.050
2	513	32300	535	0.001
3	523	32400	546	0.002
4	543	35900	590	0.009
5	544	35700	591	0.018

^a Recorded in toluene. ^b Exited at $\lambda_{S_0 \rightarrow S_1}$. ^c Determined by using Rhodamine 6G as standard ($\Phi_{st} = 0.88$, ethanol).^[12]

The ferrocenyl substituted BODIPYs **2** – **5** show substantial decrease in the fluorescence intensity compared to the BODIPY **1**, which indicates that there is fast non-radiative deactivation of the excited state with intramolecular charge transfer.^[13] The trend in the red shift in absorption spectrum of BODIPYs **2** – **5** is followed in the fluorescence emission also. The emission spectrum of BODIPYs **2** – **5** show red shift of 15 nm, 26 nm, 70 nm, and 71 nm respectively compared to BODIPY **1**. The quantum yields of **4** and **5** (0.009 and 0.018) are much higher than that of **2** and **3** (0.001 and 0.002), which indicate that, the electronic communication between ferrocenyl moiety and the BODIPY unit is poor in compounds **4** and **5** than in compounds **2** and **3**. As result the fluorescence of **4** and **5** is relatively reduced while in **2** and **3** it is quenched.

Quenching of fluorescence is in correlation with position of charge transfer band. In compounds **2** and **3**, where CT band is distinctly observable at low energy region, shows maximum fluorescence quenching, while in case of **4** and **5** where the CT band is merged with main absorption band, shows much intense fluorescence than **2** and **3**.

3.4 Single Crystal X-ray Diffraction Studies

Table 3.2. Crystal data and structure refinement parameters.

Compound	1'	2	3	4
Empirical formula	C ₃₀ H ₂₀ B ₂ Br ₂ F ₄ N ₄	C ₂₅ H ₁₉ BF ₂ FeN ₂	C ₂₇ H ₁₉ BF ₂ FeN ₂	C ₃₃ H ₂₃ BF ₂ FeN ₂
Formula weight	693.94	452.08	476.10	552.19
Temperature/K	293(2) K	150(2) K	150(2) K	150(2) K
Crystal system	Monoclinic	Monoclinic	Monoclinic	Monoclinic
Space group	<i>P</i> 2 ₁ /n	<i>P</i> 2 ₁ /n	<i>P</i> 2 ₁ /c	<i>P</i> 2 ₁ /c
Unit cell dimensions				
<i>a</i> /Å	10.2069(5)	10.7269(5)	10.9439(11)	16.1854(5)
<i>a</i> /°	90	90	90	90
<i>b</i> /Å	21.3250(9)	7.6282(4)	6.9521(4)	13.5186(5)
<i>β</i> /°	110.414(5)	100.154(4)	93.478(7)	95.882(3)
<i>c</i> /Å	13.6329(6)	24.6682(12)	28.5370(19)	11.6565(4)
<i>γ</i> /°	90	90	90	90
Volume/ Å ³	2781.0(2)	1986.91(17)	2167.2(3)	2537.06(15)
<i>Z</i>	4	4	4	4
Calculated density/ Mg/m ³	1.657	1.511	1.459	1.446
Absorption coefficient/mm ⁻¹	2.971	0.793	0.731	0.636
<i>F</i> (000)	1376	928	976	1136
Crystal size/mm	0.32 × 0.28 × 0.24	0.23 × 0.16 × 0.13	0.26 × 0.21 × 0.18	0.33 × 0.28 × 0.23
<i>θ</i> range from data collection/°	2.86 to 25.00	3.15 to 25.00	3.02 to 25.00	2.95 to 25.00
Reflections collected/unique	20420 / 4893 [<i>R</i> (int) = 0.0451]	13949 / 3488 [R(int) = 0.0574]	16579 / 3804 [R(int) = 0.0990]	18721 / 4459 [R(int) = 0.0691]
Absorption correction	Semi-empirical from equivalents	Semi-empirical from equivalents	Semi-empirical from equivalents	Semi-empirical from equivalents
Data/restraints/parameters	4893 / 0 / 379	3488 / 0 / 280	3804 / 96 / 344	4459 / 0 / 352
Goodness-of-fit on <i>F</i> ²	1.058	1.085	1.068	1.040
Final <i>R</i> indices [<i>I</i> > 2σ(<i>I</i>)]	<i>R</i> ₁ = 0.0430, <i>wR</i> ₂ = 0.0992	<i>R</i> ₁ = 0.0350, <i>wR</i> ₂ = 0.0809	<i>R</i> ₁ = 0.0618, <i>wR</i> ₂ = 0.1419	<i>R</i> ₁ = 0.0482, <i>wR</i> ₂ = 0.1178
<i>R</i> indices (all data)	<i>R</i> ₁ = 0.0646, <i>wR</i> ₂ = 0.1110	<i>R</i> ₁ = 0.0440, <i>wR</i> ₂ = 0.0867	<i>R</i> ₁ = 0.1132, <i>wR</i> ₂ = 0.1737	<i>R</i> ₁ = 0.0678, <i>wR</i> ₂ = 0.1318
Largest diff. peak and hole/e Å ⁻³	0.554 and -0.504	0.330 and -0.370	0.347 and -0.404	0.356 and -0.388
CCDC number	888341	888338	888337	888336

The single crystals of **1'**, **3**, and **4** were grown by slow evaporation of mixture of chloroform and ethanol (7:3 ratio), whereas the single crystal of **2** was grown from the mixture of chloroform and hexane (1:1 ratio). The crystal and refinement data are summarized in Table 1. The interplanar angle between the *meso*-phenyl ring, and the BF(1)F(2) mean plane is 38.65 ° in **1'**, 38.47° in **2**, 33.52° in **3** and 39.12° in **4**, while in case of unsubstituted BODIPY this angle is 28.16°.

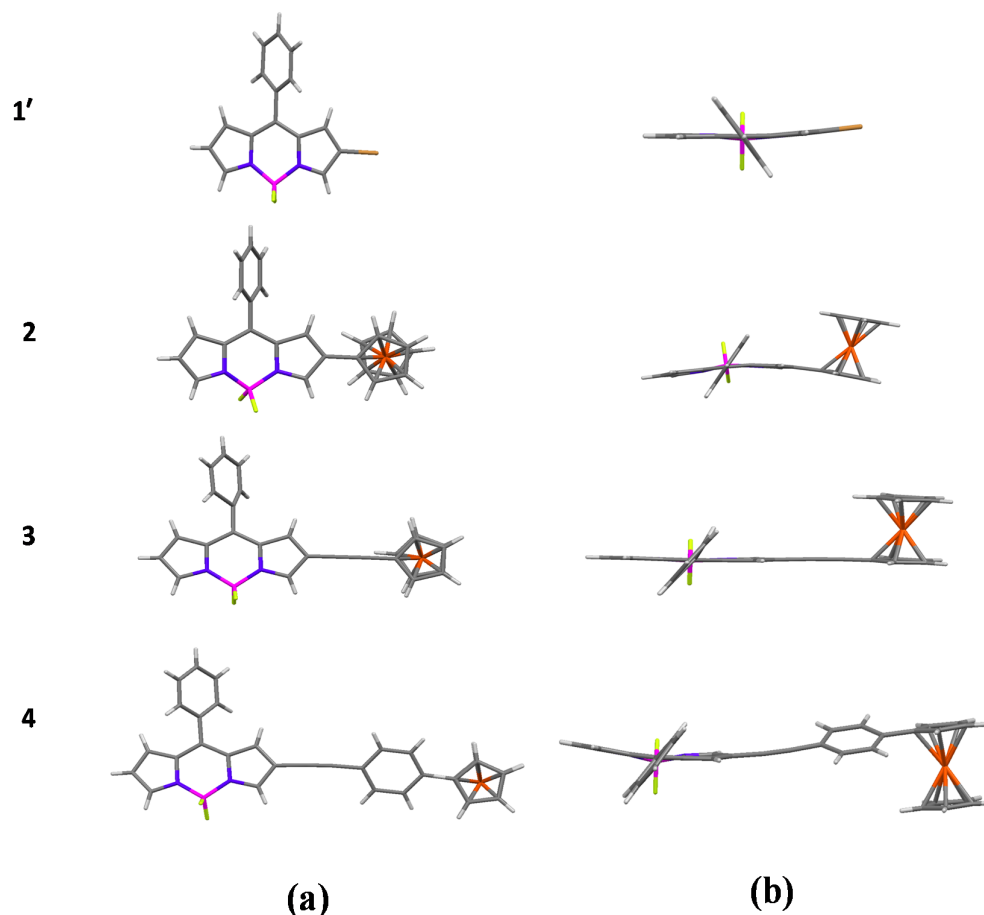


Figure 3.2: X-ray structures of BODIPYs **1'**, **2**, **3** and **4**. (a) Front view, and (b) top view.

The huge deviation in this interplanar angle indicates huge steric hindrance in the substituted BODIPYs (Figure 2). The two cyclopentadienyl rings of ferrocene are staggered in **2**, because of huge steric hindrance due to direct connectivity with the BODIPY core. Whereas in the case of **3**, and **4** the two cyclopentadienyl rings of ferrocene are eclipsed, as the ferrocenyl group is away from BODIPY core. This is also supported by the top view of the crystal, which shows bending in the structure of **2**, while in the case of compound **1'** and **3** the crystal structures show highly planar structure, and the compound **4** is slightly deviated from the planarity. The inter planar angle between the planes containing unsubstituted pyrrole ring of the BODIPY, and substituted ferrocenyl cyclopentadienyl ring is 4.69° , 16.67° and 20.96° for **3**, **4** and **2** respectively, which also support the deviation from planarity.

Single crystal structure packing

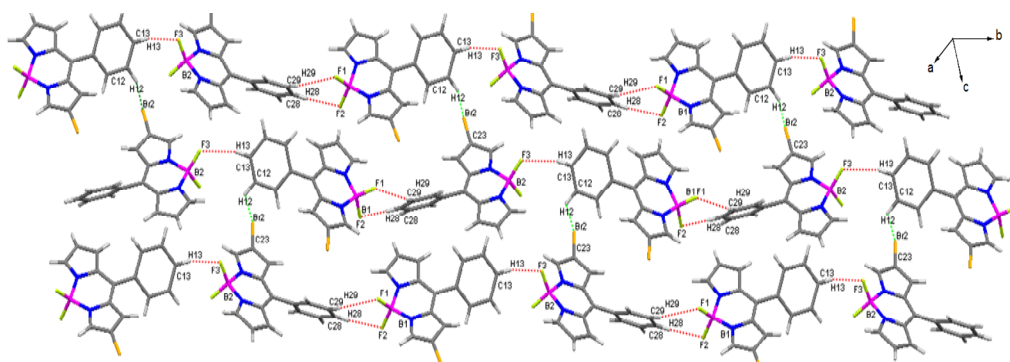


Figure 3.3. Crystal packing of **1'** showing hydrogen bonded 2D network. Secondary interactions are shown by dashed lines.

The crystal structures of **1'**, **2**, **3**, and **4** show interesting supramolecular interactions through intermolecular hydrogen bonding. The intermolecular interactions in the crystals are displayed in Table 3. The crystal structure of **1'** consists of two molecules in asymmetric unit. The packing diagram reveals intermolecular C-H...F, and C-H...Br hydrogen bonding (Figure 3). The two molecules in asymmetric unit are interconnected via fluorine of one unit, and phenyl protons of another unit, C(29)-H(29)...F(1) (2.636 Å), C(28)-H(28)...F(2) (2.481 Å) forming a hydrogen bonded dimer, which is further linked through C(13)-H(13)...F(3) (2.510 Å) leading to formation of 1D-polymeric chain along b-axis (interactions are shown with dashed lines in red colour). Moreover, each 1D-chain is further connected to neighbouring 1D-chain via C(12)-H(12)...Br(2) (3.092 Å) (interactions are shown with dashed lines in green colour) leading to the formation of hydrogen bonded 2D-network along c-axis, and along a-axis it is connected via C(17)-H(17)...F(2) (2.531 Å).

In the crystal structure of **2**, the packing diagram shows the intermolecular C-H...F, and C-H... π interactions (Figure 4), which leads to the formation of hydrogen bonded dimer. The C-H...F interactions are between pyrrolic hydrogen, and fluorines C(9)-H(9)...F(1) (2.641 Å), and C(9)-H(9)...F(2) (2.500 Å) forming hydrogen bonded dimer, and this dimer is further linked to neighbouring molecule along c-axis via C-H... π interaction of H(21) with ferrocenyl centroids at distance of 3.202 Å forming a 2D-network.

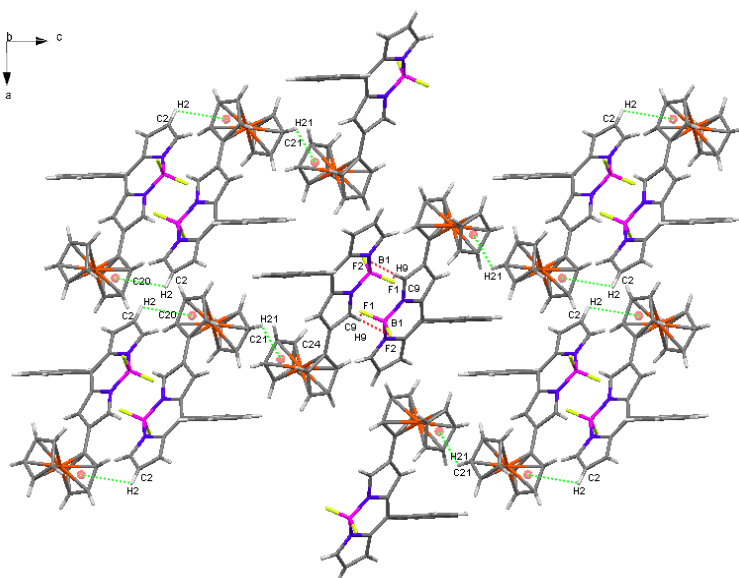


Figure 3.4. Crystal packing of **2** along b-axis.

The packing diagram of **3** exhibits intermolecular C-H...F, and C-H... π hydrogen bonding interactions (Figure 6). The fluorine holds two ferrocenyl hydrogens of two different neighboring molecules, via C(19)-H(19)...F(1) (2.561 Å) and C(15)-H(15)...F(2) (155.14 Å) interactions. Further it is extended through C(20)-H(20)...F(2) (135.15 Å) interactions forming linear chain. Moreover this linear chain is connected to neighboring molecules via C(2)-H(2)... π (Fc) (3.128 Å) interaction between C-H of pyrrole, and π electrons of another pyrrole leading to the formation of 1D zigzag chain. Overall it shows sheet like structure along b-axis, and zigzag packing along a-axis.

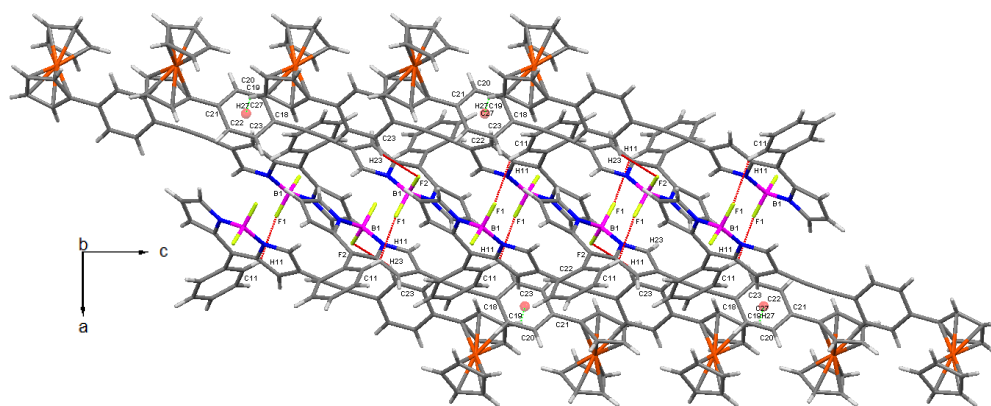


Figure 3.5. Crystal packing of **4** along b-axis, showing sheet like structure, both sides are covered by ferrocenes.

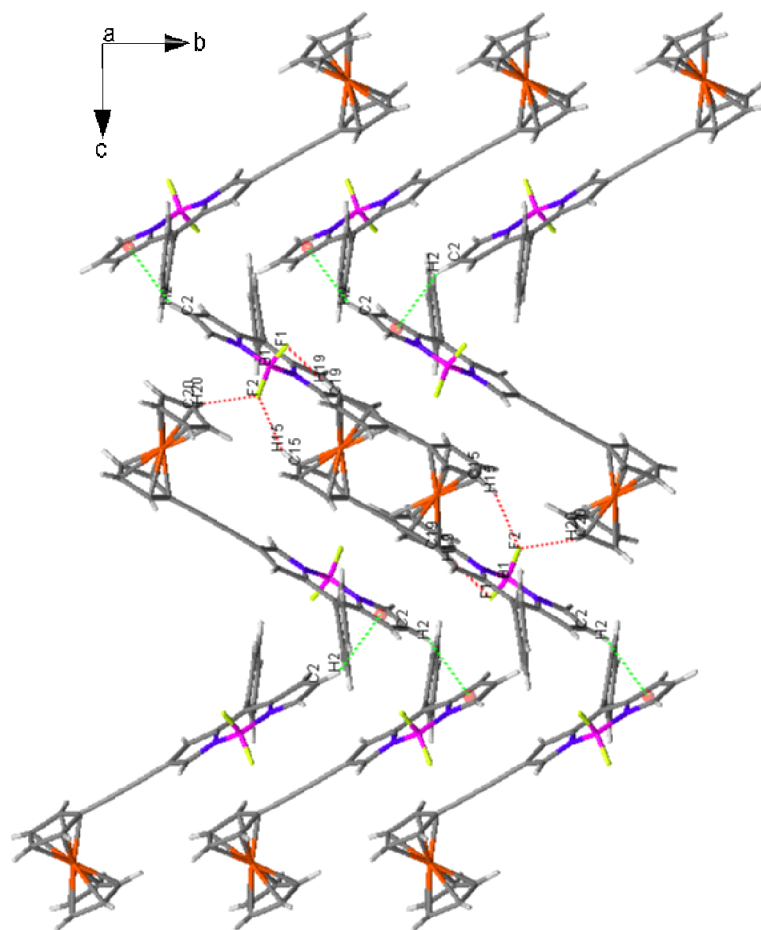


Figure 3.6. Crystal Packing of **3** showing zigzag pattern, along *a*-axis.

The packing diagram of crystal **4** reveals intermolecular C-H...F hydrogen bonding, and C-H... π interactions (Figure 4). The C-H...F interactions involve between F(2) of one molecule, and the aromatic H of two neighbouring molecule, these molecules are further interlinked through C-H... π interactions forming 1D polymeric chain.

Table 3.3. Distance and angle of intermolecular interactions in the crystal structures.

	Interaction	Distance Å	(Angle °)
1'	C(29)- H(29)---F(1)	2.636	145.03
	C(28)- H(28)---F(2)	2.481	144.59
	C(13)- H(13)---F(3)	2.510	152.31
	C(12)-H(12)---Br(2)	3.092	101.30
	C(17)- H(17)---F(2)	2.531	124.80
2	C(9)- H(9)---F(1)	2.641	134.98
	C(9)- H(9)---F(2)	2.500	172.99
	C(11)- H(11)---F(2)	2.429	147.51
	C(2)- H(2)--- π (Fc)	3.128	
	C(21)- H(21)--- π (Fc)	3.202	
3	C(19)- H(19)---F(1)	2.561	171.70
	C(15)- H(15)---F(2)	2.555	155.14
	C(20)- H(20)---F(2)	2.437	135.15
	C(2)- H(2)--- π (Fc)	2.785	
4	C(11)- H(11)---F(1)	2.350	140.91
	C(22)- H(22)---F(2)	2.659	166.39
	C(23)- H(23)---F(2)	2.658	146.36

3.5 Experimental Section

General methods- Chemicals were used as received unless otherwise indicated. All oxygen or moisture sensitive reactions were performed under nitrogen/argon atmosphere using standard schlenk method. Diisopropylamine (DIPA) was received from commercial source, and distilled on KOH prior to use. ^1H NMR (400 MHz), and ^{13}C NMR (100MHz) spectra were recorded on the Bruker Avance (III) 400 MHz, using CDCl_3 as solvent. Chemical shifts in ^1H , and ^{13}C NMR spectra were reported in parts per million (ppm) with TMS (0 ppm), and CDCl_3 (77.23 ppm) as standards. UV-visible absorption spectra of all compounds in toluene were recorded on a Carry-100 Bio UV-visible Spectrophotometer. Fluorescence spectra of all the compounds were recorded on a Horiba Jobin Yvon Floromax 4P spectrophotometer. HRMS was recorded on Brucker-Daltonics, microTOF-Q II mass spectrometer.

Synthesis and Characterization:

2-Ferrocenyl-4,4-difluoro-8-phenyl-4-bora-3a,4a-diaza-s-indacene (2)

2-Bromo-4,4-difluoro-8-phenyl-4-bora-3a,4a-diaza-s-indacene (**1'**) (150mg, 0.4323 mmol), ferrocenylboronic acid (119.24 mg, 0.5188 mmol), CsF (131.14 mg, 0.8646 mmol), Ag₂O (111.1819 mg, 0.4798 mmol), and Pd(PPh₃)₄ (5.495 mg, 0.0047 mmol) were dissolved in dry THF (9 mL) and the solution was degassed with argon. After stirring at 60°C for 4 h the solvent was removed under reduced pressure, and the residue was purified by column chromatography on silica gel (230-400 mesh size) with hexane, and CH₂Cl₂ mixture (1:1 ratio), and recrystallized from chloroform, and hexane mixture to yield the desired product as violet crystals in 45% yield. ¹H NMR (CDCl₃, 400 MHz, ppm): δ= 8.02 (s, 1H), 7.91 (s, 1H), 7.61 (m, 5H), 6.90 (s, 1H), 6.79 (s, 1H), 6.54 (s, 1H), 4.61 (s, 2H), 4.42 (s, 1H), 4.17 (s, 5H). ¹³C NMR (CDCl₃, 100 MHz, ppm): 145.41, 143.45, 142.67, 135.80, 135.25, 134.92, 134.08, 130.64, 130.49, 128.53, 127.67, 124.71, 117.87, 77.81, 69.82, 69.14, 66.50. HRMS m/z = 452.0956 (calculated for C₂₅H₁₉BF₂FeN₂= 452.0959). UV-vis (in toluene): λ_{max} (ε [M⁻¹cm⁻¹]): 513 nm (32300).

General procedure for Sonogashira reaction for compounds 3-5

2-Bromo-4,4-difluoro-8-phenyl-4-bora-3a,4a-diaza-s-indacene (**1'**) (50mg, 0.1445 mmol), respective ferrocenyl substituted ethyne (0.2167 mmol), PdCl₂(PPh₃)₂ (5 mg, 0.0072 mmol), CuI (2.75 mg, 0.014 mmol) and triphenylphosphine (3.79 mg, 0.014 mmol) were dissolved in a mixture of dry THF (2 mL), and dry *N,N*-diisopropylamine (1 mL) under argon atmosphere. And the reaction mixture was stirred at 60°C for 4 h. Following cooling to room temperature, the solvent was removed under reduced pressure, and the residue was purified by column chromatography on silica gel (230-400 mesh size) in 1:1 mixture of chloroform and hexane, and recrystallized in mixture of chloroform and ethanol to yield the desired product.

2-Ferrocenylethenyl-4,4-difluoro-8-phenyl-4-bora-3a,4a-diaza-s-indacene (3)

Yield: 78 %. ¹H NMR (CDCl₃, 400 MHz, ppm): δ 7.95 (s, 1H), 7.91 (s, 1H), 7.50 (m, 5H), 6.90 (s, 2H), 6.50 (s, 1H), 4.38 (t, 2H), 4.16 (t, 2H), 4.15 (s, 5H). ¹³C NMR (CDCl₃, 100 MHz, ppm): 147.05, 145.93, 145.10, 139.30, 135.54, 134.31, 133.60, 132.22, 131.47, 130.98, 130.50, 128.58, 119.05, 114.11, 91.33, 78.27, 71.37, 70.03, 68.97, 64.91. HRMS (ESI) m/z = 476.0924 (calculated for C₂₇H₁₉BF₂FeN₂ =

476.0958). UV-vis (in toluene): λ_{max} (ϵ [$\text{M}^{-1}\text{cm}^{-1}$]): 523nm (32400).

2-((4-Ferrocenyl)-phenylethenyl)-4,4-difluoro-8-phenyl-4-bora-3a,4a-diaza-s-indacene (4)

Yield: 58 %. ^1H NMR (CDCl_3 , 400 MHz, ppm): δ 7.97 (s, 1H), 7.93 (s, 1H), 7.51 (m, 5H), 7.25 (s, 2H), 7.17 (s, 2H), 6.94 (s, 1H), 6.91 (s, 1H), 6.52 (d, 1H), 4.87 (s, 2H), 4.55 (s, 2H), 4.19 (s, 5H). ^{13}C NMR (CDCl_3 , 100 MHz, ppm): 144.70, 144.52, 143.11, 139.07, 134.59, 134.21, 133.26, 132.51, 131.53, 130.70, 130.42, 130.01, 129.50, 127.57, 124.87, 107.14, 90.28, 69.02, 68.52, 67.94, 65.61. HRMS (ESI) m/z = 552.1279 (calculated for $\text{C}_{33}\text{H}_{23}\text{BF}_2\text{FeN}_2$ = 552.1272). UV-vis (in toluene): λ_{max} (ϵ [$\text{M}^{-1}\text{cm}^{-1}$]): 543 nm (35900).

2-((3-Ferrocenyl)-phenylethenyl)-4,4-difluoro-8-phenyl-4-bora-3a,4a-diaza-s-indacene (5)

Yield: 42 %. ^1H NMR (CDCl_3 , 400 MHz, ppm): δ 8.02 (s, 1H), 7.94 (s, 1H), 7.45-7.55 (m, 7H), 7.36 (d, $J=8\text{Hz}$, 2H), 6.99 (s, 1H), 6.945 (d, $J=4\text{Hz}$, 1H), 6.535 (d, $J=4\text{Hz}$, 1H), 4.58 (s, 2H), 4.26 (s, 2H), 3.98 (s, 5H). ^{13}C NMR (CDCl_3 , 100 MHz, ppm): 146.39, 144.70, 144.53, 138.79, 138.23, 134.21, 132.46, 131.14, 131.03, 130.05, 129.49, 127.86, 127.59, 127.47, 126.65, 125.14, 122.79, 113.07, 91.21, 80.86, 68.65, 68.17, 65.47. HRMS (ESI) m/z = 552.1293 (calculated for $\text{C}_{33}\text{H}_{23}\text{BF}_2\text{FeN}_2$ = 552.1272). UV-vis (in toluene): λ_{max} (ϵ [$\text{M}^{-1}\text{cm}^{-1}$]): 544 nm (35700).

3.6 Conclusions

In summary we have designed and synthesized donor-acceptor ferrocenyl BODIPYs by the palladium catalyzed Suzuki and Sonogashira cross-coupling reactions. The red shift in the absorption and emission maxima is in agreement with an increase in the effective conjugation length. The photophysical studies show intramolecular charge transfer from the donor ferrocene to the acceptor BODIPY. The crystal structures of **1'-4** exhibit interesting supramolecular structures. We have shown how the optical properties of BODIPYs can be tuned by attaching appropriate electroactive group.

References

- [1] (a) Laoudet, A., Burgess, K., (2007), BODIPY Dyes and Their Derivatives: Syntheses and Spectroscopic Properties, *Chem. Rev.*, 107, 4891-4932, (DOI: 10.1021/cr078381n); (b) Gautam, P., Dhokale, B., Shukla, V., Singh, C. P., Bindra, K. S., Misra, R., (2012), Optical limiting performance of *meso*-tetraferrocenyl porphyrin and its metal derivatives, *J. Photochem. Photobiol., A*, 239, 24-27, (DOI:10.1016/j.jphotochem.2012.04.020); (c) Boens, N., Leen, V., Dehaen, W., (2012), Fluorescent indicators based on BODIPY, *Chem. Soc. Rev.*, 41, 1130-1172, (DOI: 10.1039/C1CS15132K).
- [2] (a) Dong, Y.; Bolduc, A. A.; McGregor, N.; Skene, W. G., (2011), Push-Pull Aminobithiophenes - Highly Fluorescent Stable Fluorophores, *Org. Lett.*, 13, 1844-1847, (DOI: 10.1021/ol200353k); (b) Barsu, C.; Cheaib, R.; Chambert, S.; Queneau, Y.; Maury, O.; Cottet, D.; Wege, H.; Douady, J.; Bretonniere, Y.; Andraud, (2010), Neutral push-pull chromophores for nonlinear optical imaging of cell membranes, *C. Org. Biomol. Chem.*, 8, 142-150, (DOI: 10.1039/B915654B).
- [3] Nepomnyashchii, A. B.; Bard, A. J., (2012), Electrochemistry and Electrogenenerated Chemiluminescence of BODIPY Dyes, *Acc. of Chem. Res.*, 45, 1844-1853, (DOI: 10.1021/ar200278b).
- [4] (a) Cheng, T.; Wang, T.; Zhu, W.; Chen, X.; Yang, Y.; Xu, Y.; Qian, X., (2011), Red-Emission Fluorescent Probe Sensing Cadmium and Pyrophosphate Selectively in Aqueous Solution, *Org. Lett.*, 13, 3656, (DOI: 10.1021/ol201305d); (b) Bozdemir, O. A.; Guliyev, R.; Buyukcakil, O.; Selcuk, S.; Kolemen, S.; Gulseren, G.; Nalbantoglu, T.; Boyaci, H.; Akkaya, E. U., (2010), Selective Manipulation of ICT and PET Processes in Styryl-Bodipy Derivatives: Applications in Molecular Logic and Fluorescence Sensing of Metal Ions, *J. Am. Chem. Soc.*, 132, 8029, (DOI: 10.1021/ja1008163); (c) Kim, H. S.; Pham, T. C. T.; Yoon, K. B., (2012), A novel class of nonlinear optical materials based on host-guest composites: zeolites as inorganic crystalline hosts *Chem. Commun.*, 48, 4659-4673, (DOI: 10.1039/C2CC30919J); (d) Benstead M.; Mehl, G. H.; Boyle, R. W., (2011), 4,4'-Difluoro-4-bora-3a,4a-diaza-s-

indacenes (BODIPYs) as components of novel light active materials, *Tetrahedron*, *67*, 3573-3601, (**DOI**:10.1016/j.tet.2011.03.028); (e) Zhou, Y.; Xiao, Y.; Chi, S.; Qian, X., (2008), Isomeric Boron-Fluorine Complexes with Donor-Acceptor Architecture: Strong Solid/Liquid Fluorescence and Large Stokes Shift, *Org. Lett.*, *10*, 633-636, (**DOI**: 10.1021/ol702963w); (f) Lord, S. J.; Conley, N. R.; Lee, H. I. D.; Samuel, R.; Liu, N.; Twieg, R. J.; Moerner, W. E., (2008), A Photoactivatable Push-Pull Fluorophore for Single-Molecule Imaging in Live Cells, *J. Am. Chem. Soc.*, *130*, 9204-9205, (**DOI**: 10.1021/ja802883k); (g) West, R., Panagabko, C., Atkinson, J., (2010), Synthesis and Characterization of BODIPY- α -Tocopherol: A Fluorescent Form of Vitamin E, *J. Org. Chem.*, *75*, 2883, (**DOI**: 10.1021/jo100095n); (h) Descalzo, A. B., Xu, H. J., Xue, Z. L., Hoffmann, K., Shen, Z., Weller, M. G., You, X. Z., Rurack, K., (2008), Phenanthrene-Fused Boron-Dipyrromethenes as Bright Long-Wavelength Fluorophores, *Org. Lett.*, *10*, 1581, (**DOI**: 10.1021/ol800271e); (i) Marder, S. R., Kippelen, B., Jen, A. K. Y., Peyghambarian, N., (1997), Design and synthesis of chromophores and polymers for electro-optic and photorefractive applications, *Nature*, *388*, 845-851, (**DOI**: 10.1038/42190); (j) LeCours, S. M., Guan, H.-W., DiMaggio, S. G., Wang, C. H., Therien, M. J., (1996), Push-Pull Arylethynyl Porphyrins: New Chromophores That Exhibit Large Molecular First-Order Hyperpolarizabilities, *J. Am. Chem. Soc.*, *118*, 1497-1503, (**DOI**: 10.1021/ja953610l).

- [5] (a) Chen, J.; Mizumura, M.; Shinokubo, H.; Osuka, A., (2009), Functionalization of Boron Dipyrin (BODIPY) Dyes through Iridium and Rhodium Catalysis: A Complementary Approach to α - and β -Substituted BODIPYs, *Chem. Eur. J.*, *15*, 5942-5949, (**DOI**: 10.1002/chem.200802541); (b) Schmidt, E. Y.; Trofimov, B. A.; Mikhaleva, A. I.; Zorina, N. V.; Protzuk, N. I.; Petrushenko, K. B.; Ushakov, I. A.; Dvorko, M. Y.; Meallet-Renault, R.; Clavier, G.; Vu, T. T.; Tran, H. T. T.; Pansu, R. B., (2009), Synthesis and Optical Properties of 2-(Benzo[b]thiophene-3-yl)pyrroles and a New BODIPY Fluorophore (BODIPY=4,4-Difluoro-4-bora-3a,4a-diaza-s-indacene), *Chem. Eur. J.*, *15*, 5823-5830, (**DOI**: 10.1002/chem.200802467); (c) Ulrich, G.; Ziessel, R.; Harriman, A., (2008), The

-
- Chemistry of Fluorescent Bodipy Dyes: Versatility Unsurpassed, *Angew. Chem. Int. Ed.*, **47**, 1184-1201, (DOI: 10.1002/anie.200702070).
- [6] Yu, C.; Xu, Y.; Jiao, L.; Zhou, J.; Wang, Z.; Hao E., (2012), Isoindole-BODIPY dyes as red to near-infrared fluorophores, *Chem. Eur. J.*, **18**, 6437-6442, (doi: 10.1002/chem.201200398).
- [7] Boens, N.; Leen, V.; Dehaen, W., (2012), Fluorescent indicators based on BODIPY, *Chem. Soc. Rev.*, **41**, 1130–1172, (DOI: 10.1039/C1CS15132K).
- [8] Green, M. L. H.; Marder, S. R.; Thompson, M. E.; Bandy, J. A.; Bloor, D.; Kolinsky, P. V.; Jones, R. J., (1987), Synthesis and structure of (cis)-[1-ferrocenyl-2-(4-nitrophenyl)ethylene], an organotransition metal compound with a large second-order optical nonlinearity, *Nature*, **330**, 360, (DOI:10.1038/330360a0).
- [9] (a) Ziessel, R.; Retailleau, P.; Elliott K. J.; Harriman A., (2009), Boron Dipyrin Dyes Exhibiting “Push–Pull–Pull” Electronic Signatures, *Chem. Eur. J.*, **15**, 10369–10374, (DOI: 10.1002/chem.200901725); (b) Khan, T. K., Pissurlenkar, R. R. S., Shaikh M. S., Ravikanth M., (2012), Synthesis and studies of covalently linked *meso*-furyl boron-dipyrromethene-ferrocene conjugates, *J. Organomet. Chem.*, **697**, 65-73, (DOI: <http://dx.doi.org/10.1016/j.jorganchem.2011.10.016>); (c) Yin, X., Li, Y., Li, Y., Zhu, Y., Tang, X., Zheng, H., Zhu, D., (2009), Electrochromism based on the charge transfer process in a ferrocene–BODIPY molecule, *Tetrahedron*, **65**, 8373–8377, (DOI: <http://dx.doi.org/10.1016/j.tet.2009.08.008>); (d) Yin, X., Li, Y., Zhu, Y., Jing, X., Li, Y., Zhu, D., (2010), A highly sensitive viscosity probe based on ferrocene-BODIPY dyads, *Dalton Trans.*, **39**, 9929–9935, (DOI: 10.1039/C0DT00309C).
- [10] Jiao, L., Pang, W., Zhou, J., Wei, Y., Mu, X., Bai, G., Hao, E., (2011), Regioselective Stepwise Bromination of Boron Dipyrromethene (BODIPY) Dyes, *J. Org. Chem.*, **76**, 9988–9996, (DOI: 10.1021/jo201754m).
- [11] Kee, H. L., Kirmaier, C., Yu, L., Thamyongkit, P., Youngblood, W. J., Calder, M. E., Ramos, L., Noll, B. C., Bocian, D. F., Scheidt, W. R., Birge, R. R.,

-
- Lindsey, J. S., Holten, D., (2005), Structural Control of the Photodynamics of Boron–Dipyrin Complexes, *J. Phys. Chem. B*, **109**, 20433–20443, (DOI: 10.1021/jp0525078).
- [12] Zhang, R. L., Wang, Z. L., Wu, Y. S., Fu, H. B., Yao, J. N., (2008), A Novel Redox-Fluorescence Switch Based on a Triad Containing Ferrocene and Perylene Diimide Units, *Org. Lett.*, **10**, 3065, (DOI: 10.1021/ol801053t).
- [13] (a) Rao, M. R., Pavan Kumar K. V., Ravikanth, M., (2010), Synthesis of boron-dipyrromethene–ferrocene conjugates, *J. Organomet. Chem.*, **695**, 863–869, (<http://dx.doi.org/10.1016/j.jorganchem.2010.01.009>); (b) Misra, R., Kumar, R., PrabhuRaja, V., Chandrashekar, T. K., (2005), Modified push–pull expanded corroles: Syntheses, structure and nonlinear optical properties, *J. Photochem. Photobiol. A*, **175**, 108–117, (DOI: <http://dx.doi.org/10.1016/j.jphotochem.2005.04.024>); (c) Dhokale, B., Gautam, P., Misra, R., (2012), Donor–acceptor perylenediimide–ferrocene conjugates: synthesis, photophysical, and electrochemical properties, *Tetrahedron Lett.*, **53**, 2352–2354, (DOI: <http://dx.doi.org/10.1016/j.tetlet.2012.02.107>); (d) Fery-Forgues, S., Delavaux-Nicot, B., (2000), Ferrocene and ferrocenyl derivatives in luminescent systems *J. Photochem. Photobiol., A*, **132**, 137–159, (DOI: [http://dx.doi.org/10.1016/S1010-6030\(00\)00213-6](http://dx.doi.org/10.1016/S1010-6030(00)00213-6)); (e) Nadtochenko, V. A., Denisov, N. N., Gak, V. Y., Abramova, N. V., Loim, N. M., (1999), Photochemical and photophysical properties of *meso*-tetraferrocenylporphyrin. Quenching of *meso*-tetraphenylporphyrin by ferrocene, *Russ. Chem. Bull.*, **148**, 1900, (DOI: 10.1007/BF02494744); (f) Barlow, S., Marder, S. R., (2000), Electronic and optical properties of conjugated group 8 metallocene derivatives, *Chem. Commun.*, 1555–1562, (DOI: 10.1039/B004907G).

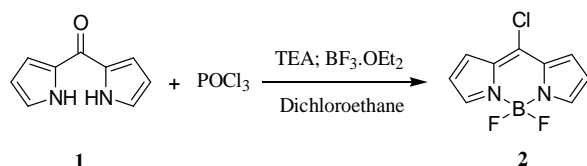
Chapter 4

***Meso*-alkynylated ferrocenyl BODIPYs**

4.1. Introduction

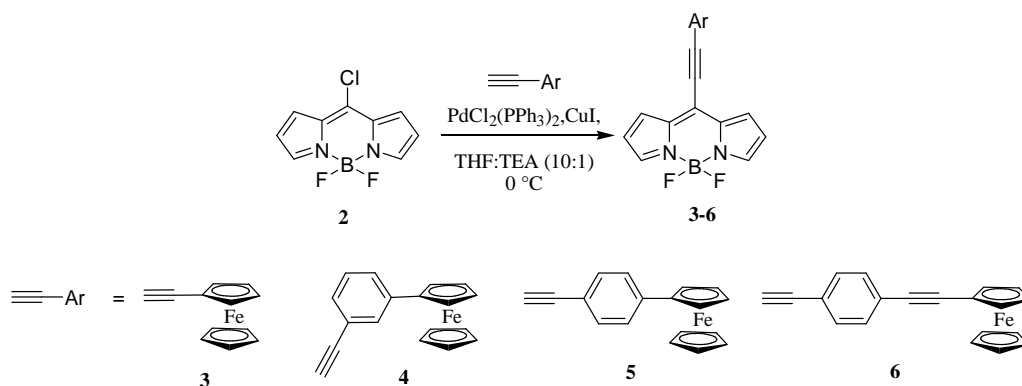
Borondipyrromethene (BODIPY) dyes are unique fluorophores with spectacular properties.^[1] They are extensively used for photovoltaics,^[2] optoelectronics,^[3] nonlinear optics,^[4] bioimaging or sensing,^[5] and photodynamic therapy.^[6] The chemistry of the BODIPY molecular systems has gained momentum, which is reflected in the large number of publications on the BODIPYs.^[7] The electronic and photonic properties of the BODIPYs have been explored widely.^[8] The BODIPY unit acts as an acceptor.^[9] Recently new synthetic strategies have been developed for the functionalisation of the BODIPY dyes at the α , β , and *meso* positions.^[10] Halogenation at these positions provides a platform for further modification *via* substitution, and cross-coupling reactions.^[11] The Wim Dehaen group has reported the synthesis of *meso*-halogenated BODIPYs, which is an important intermediate for further derivatization.^[12] The *meso* functionalized BODIPYs are mostly synthesized by the acid catalyzed condensation reaction of an aromatic aldehyde with pyrrole. The *meso* substituent in these BODIPYs shows poor electronic communication, due to a large dihedral angle between the *meso* phenyl ring and the BODIPY core. The electronic communication between the *meso* substituent and the BODIPY can be improved by reducing the dihedral angle. A convenient strategy to increase the electronic communication between the *meso* substituent and the BODIPY is introduction of a triple bond at the *meso* position.^[13] Our group is interested in the design and synthesis of donor–acceptor (D–A) molecular systems.^[14] We have incorporated a donor ferrocenyl group with different ethynyl spacers at the *meso* position of the BODIPY. Here our aim was to explore the effect of substituting the donor ferrocenyl group *via* ethynyl linkages, at the *meso* position, and to explore its photonic and electronic properties.

4.2. Results and Discussion



Scheme 4.1. Synthesis of 8-chloro BODIPY **2**.

The ferrocenyl BODIPYs **3** – **6** were synthesized by the Pd-catalyzed Sonogashira cross-coupling reaction of 8-chloro BODIPY **2**, with the respective ferrocenylethyne as outlined in Scheme 4.2. The key intermediate, *meso*-chloro BODIPY **2**, was synthesized from the dipyrromethane **1**, by incorporation of the chloro group through deoxygenative substitution, followed by *in situ* deprotonation, and complexation with BF₃·etherate (Scheme 4.1).¹² The dipyrromethane **1**, in turn, was synthesized by the condensation reaction of thiophosgene, and pyrrole, followed by oxidation with KOH–H₂O₂.^[15] The ferrocenylethyne, 3-(ferrocenyl)phenylethyne, 4-(ferrocenyl)phenylethyne, and 4-(ferrocenylethynyl)phenylethyne, were synthesized by reported procedures.^[16]



The BODIPYs **3** and **6** were also characterized by single crystal X-ray diffraction technique.

A typical ^1H NMR spectrum of the BODIPYs **3** – **6**, shows the following types of protons: (a) a singlet at ~ 7.8 ppm for two α -pyrrolic protons, (b) a broad peak at ~ 6.5 ppm for two β -pyrrolic protons, (c) a broad peak at ~ 7.4 ppm for two β' -pyrrolic protons, (d) the phenyl ring protons in ferrocenyl BODIPYs **5** and **6** are exhibited as two doublets between 7.5 – 7.6 ppm, (e) the phenyl ring protons in the ferrocenyl BODIPY **4** exhibit a typical *meta*-substitution pattern in the region 7.3–7.7 ppm, (f) the ferrocenyl group exhibits three different signals. The unsubstituted cyclopentadienyl ring of the ferrocene exhibited a sharp singlet around 4.2 ppm for five protons, and the mono substituted cyclopentadienyl ring exhibits two broad singlets for BODIPYs **4** – **6**, and triplets for BODIPY **3** around 4.5 ppm, and 4.7 ppm for four protons.

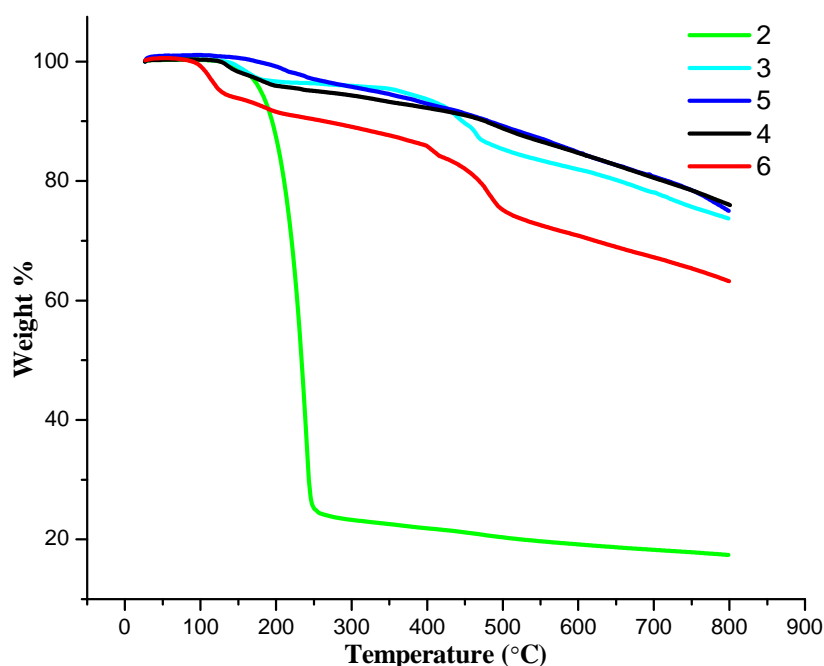


Figure 4.1. TGA plot of the BODIPYs **2** – **6**.

Thermal properties of the BODIPYs **2** – **6** were investigated by thermogravimetric analysis (TGA) at a heating rate of $10\text{ }^{\circ}\text{C min}^{-1}$, under a nitrogen atmosphere (Figure 4.1). BODIPY **2** shows 10 % weight loss at $193\text{ }^{\circ}\text{C}$, and 75 % weight loss at $\sim 248\text{ }^{\circ}\text{C}$, while **3** – **5** show 10 % weight loss between 440 – $490\text{ }^{\circ}\text{C}$, and only 25% weight loss even at $800\text{ }^{\circ}\text{C}$. The thermal decomposition temperature (T_d) shows that the ferrocenyl BODIPYs **3** – **6** are more

stable than the 8-chloro BODIPY **2** (Table 1). Ferrocenyl BODIPY **6**, was found to be the least stable, and shows 10 % weight loss at only 266 °C.

4.3. Photophysical Properties

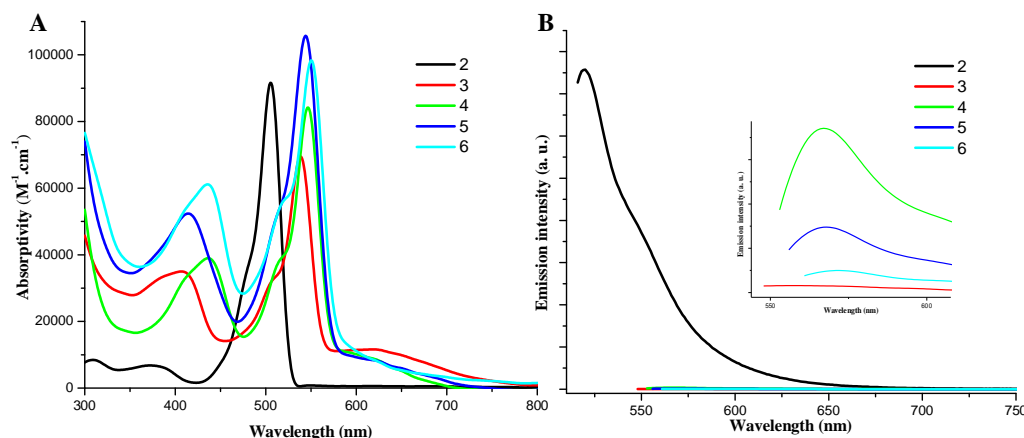


Figure 4.2. (A) UV-vis absorption spectra of BODIPYs **2** – **6** recorded in toluene. (B) Emission Spectra of **2** – **6** recorded in toluene, inset shows enlarged view (Excited at respective $\lambda_{S_0 \rightarrow S_1}$ at concentration of 0.1 absorbance).

The UV-vis absorption spectra and emission of the BODIPYs **2** – **6** were recorded in toluene (Figure 4.2), and the corresponding data are shown in Table 4.1. The BODIPYs **2** – **6** show a strong absorption band between 500 to 551 nm corresponding to the $S_0 \rightarrow S_1$ transition, and a shoulder in the higher energy region corresponding to the respective vibronic transition. The BODIPYs **3** – **6** show a successive red shift in the $S_0 \rightarrow S_1$ absorption band by 32, 38, 40, and 45 nm compared to BODIPY **2** (Table 4.1).

The weak band at ~ 370 nm in the BODIPY **2** spectrum, corresponds to the $S_0 \rightarrow S_2$ transition, and this band is red shifted to ~ 430 nm in BODIPYs **3** – **6**. The red shift in the absorption band is consistent with the increase in conjugation length in the order of **6** > **5** > **4** > **3**. All the ferrocenyl BODIPYs show a broad charge transfer (CT) band between 600–650 nm. The presence of a CT band is confirmed from the positive solvatochromic effect (Figure 4.3). The CT band in ferrocenyl BODIPY **3** is more prominent than others, which indicates strong electronic coupling between the donor ferrocene, and the acceptor BODIPY.

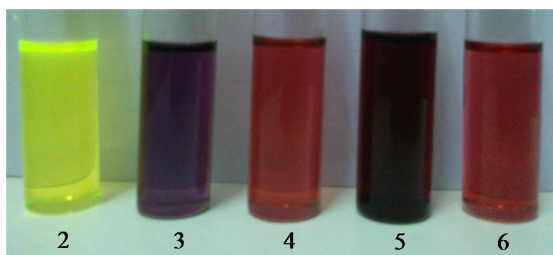


Figure 4.3. BODIPYs **2-6** in toluene at concentration of 10^{-4} M.

The CT in the ferrocenyl BODIPYs **3 – 6** shows a pronounced effect on their color pattern in toluene (Figure 4.3). The solution of *meso*-chloro BODIPY **2** has a fluorescent yellow-green color while ferrocenyl BODIPYs **3 – 6** show color variations from red to purple.

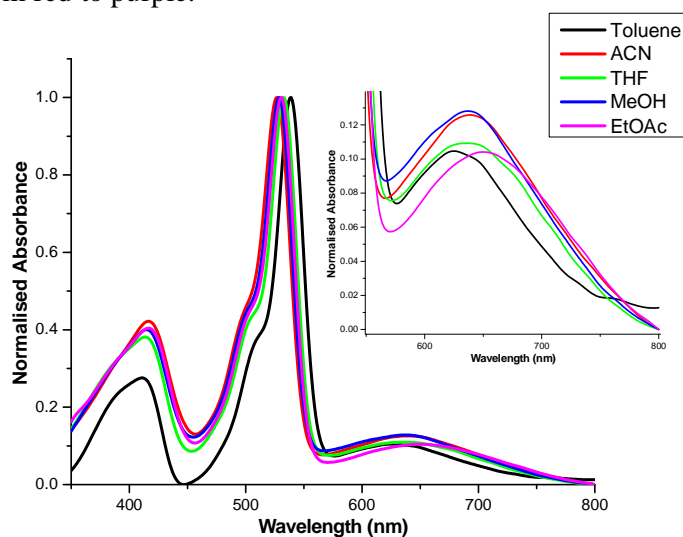


Figure 4.4. Positive solvatochromism in BODIPY **3**.

The comparison of the absorption spectra of the ferrocenyl BODIPY **3** with the previously reported ferrocenyl BODIPYs (Chart 4.1), where the ferrocenyl unit is attached to BODIPY (via an ethynyl linkage) at the α -pyrrolic position **3a**,^[17a] and the β -pyrrolic position **3b**,^[14e] shows a red shift of 8 and 15 nm respectively. The ferrocenyl BODIPYs **3**, **3a**, and **3b** show extinction coefficients of 74 622, 46 773, and 32 400 ($\text{mol}^{-1} \text{cm}^{-1}$) respectively. The red shift in the absorption wavelength and increase in extinction coefficient values are attributed to the increase in conjugation, which follows the order **3** > **3a** > **3b**. Hence BODIPY **3** has superior electronic communication between the donor and acceptor units compared to **3a** and **3b**.

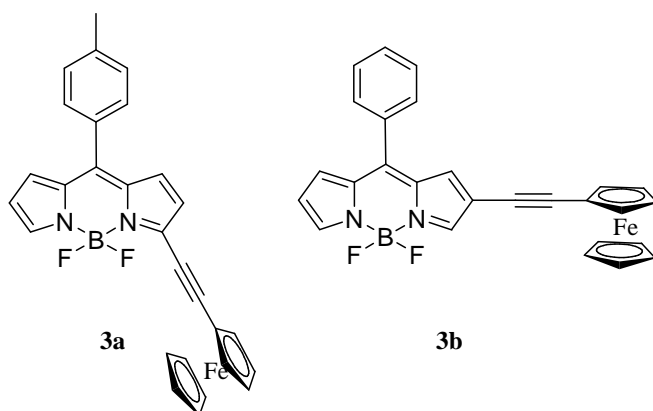


Chart 4.1. Structures of previously reported ferrocenyl BODIPYs.

The emission spectra of the BODIPYs **2** – **6** were recorded in toluene at 0.1 absorbance (Figure 4.2; Table 4.1). Compound **3** is non-emissive in nature. The emission spectra of BODIPYs **4** – **6** show a red shift of ~ 70 nm compared to that of **2**, due to enhanced conjugation. The fluorescence studies revealed that the incorporation of the ferrocenyl moiety into the BODIPY results in quenching of the fluorescence due to fast non-radiative deactivation of the excited state with intramolecular charge transfer from the donor ferrocenyl unit to the acceptor BODIPY moiety,^[17] which further supports the strong interaction between the donor and acceptor. The fluorescence quantum yield values follow the order **4** > **6** > **5** > **3**. The trend observed in the quenching of fluorescence depends upon the nature of the spacer unit. The ferrocenyl BODIPY **3**, linked by an ethynyl spacer is non-emissive in nature due to maximum electronic communication. The *meta* linkage in the ferrocenyl BODIPY **4** disrupts the extended π -conjugation compared to other phenylethynyl spacers, therefore exhibits better fluorescence than **3**, **6** and **5**.

Table 4.1. Photophysical and electrochemical^f properties of BODIPYs **2** – **6**.

BODIPY	$\lambda_{S_0 \rightarrow S_1}$ (nm)	ϵ^a (Mol ⁻¹ .cm ⁻¹)	λ_{em}^b (nm)	Φ_F^c	T _d ^d (°C)	E _{oxid} ^g (BODIPY)	E _{oxid} ^h (Fc)	E ¹ Red ^g	E ² Red ^g
2	506	102801	519	0.4700	193	1.31	--	-0.96	-1.32
3^e	538	74622	-	-	446	1.03	0.25	-1.01	-1.28
4	544	108769	566	0.0012	478	1.09	0.08	-0.95	-1.34
5	546	88977	567	0.0001	480	1.11	0.07	-0.93	-1.32
6	551	103285	571	0.0010	266	1.12	0.11	-0.94	-1.34

^arecorded at $S_0 \rightarrow S_1$, ^bExcited at $\lambda_{S_0 \rightarrow S_1}$, ^cdetermined by using Rhodamine 6G as standard ($\Phi=0.88$, in ethanol), ^dDecomposition temperature at 10% weight loss, determined by TGA. ^eferrocenyl BODIPY is non emissive in nature. ^felectrochemical analysis was performed, in 0.1 M solution of Bu₄NPF₆ in DCM at 100 mVs⁻¹ scan rate, versus Fc/Fc⁺. ^girreversible wave, ^hreversible wave.

4.4. Electrochemical properties

The electrochemical properties of BODIPY **2**, and the ferrocenyl BODIPYs **3** – **6** were explored by cyclic voltammetric (CV) analysis. The overlaid CV and DPV of BODIPYs **2** – **6** is shown in Figure 4.5, and the data are listed in Table 4.1. All potentials are corrected against Fc/Fc^+ , as required by IUPAC.^[18]

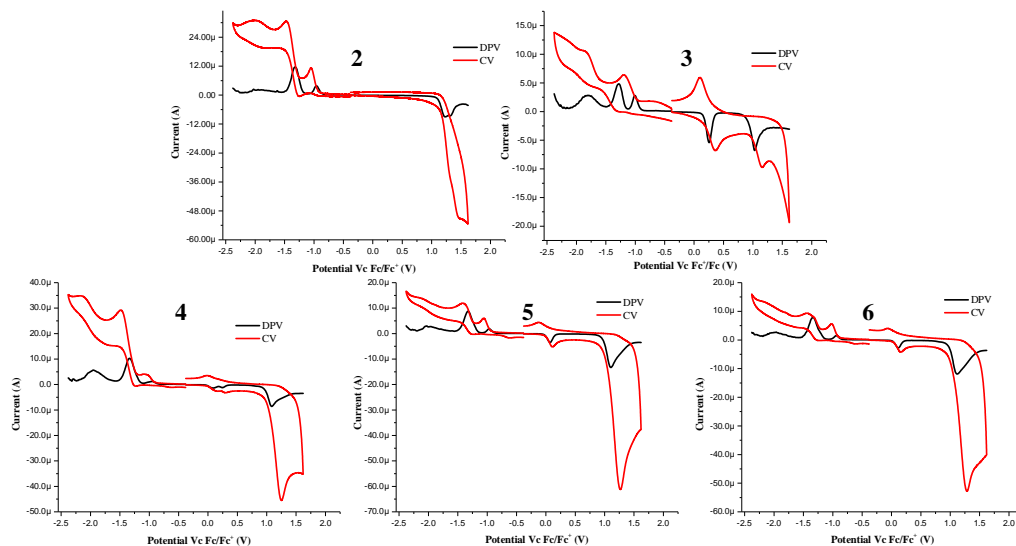


Figure 4.5. Overlaid CV and DPV plots of BODIPYs **2** – **6**.

The ferrocenyl BODIPYs **3** – **6** show one reversible oxidation wave corresponding to the ferrocenyl unit, along with one irreversible oxidation wave corresponding to the BODIPY moiety. From the ferrocenyl oxidation potentials of ferrocenyl BODIPYs **3** – **6**, in the region 0.07 – 0.25 V, the ferrocenyl oxidation is becoming harder than for the free ferrocene. This is attributed to the delocalization of the donor ferrocenyl electrons on the acceptor BODIPY core. The first reduction potential values indicate that the reduction is becoming harder in case of **3**, while in other ferrocenyl BODIPYs **4** – **6** it is not much affected compared to chloro BODIPY **2**. This supports the stronger electronic coupling between donor and acceptor units in **3** than other ferrocenyl BODIPYs.

4.5. Computational Calculations

In order to explore the electronic structure of the ferrocenyl BODIPYs **3** – **6**, DFT calculations were performed at the B3LYP/6-31+G** level for C, N, B, F, H,

and the Lanl2DZ level for Fe.^[3d] The frontier molecular orbital (FMO) plots of BODIPYs **3** – **6** are shown in Figure 4.6.

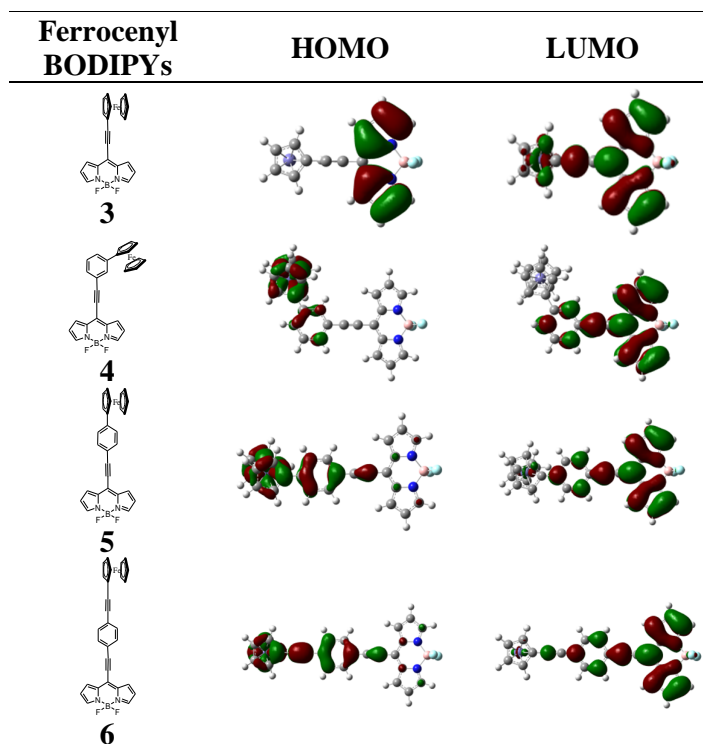
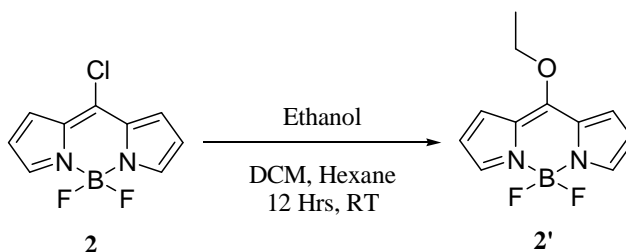


Figure 4.6. HOMO, and LUMO frontier orbitals of BODIPYs at the B3LYP/6-31+G** for C, N, B, F, H, and Lanl2DZ for Fe level.

In BODIPYs **4** – **6** the plots of HOMO, and LUMO reveal that the maximum density in the HOMO exists on the donor part of the molecule, whereas the maximum density in the LUMO exists on the acceptor part of the molecule. This shows a typical donor–acceptor (D–A) system, with charge transfer process^[19] The detailed analysis of the HOMO and LUMO in **4** – **6** reveals that the phenylethynyl group, which is acting as a π -bridge plays a key role in the HOMO and LUMO.

In the HOMO of the ferrocenyl BODIPY **3**, there is a node at the *meso* carbon, hence, there is no contribution from the ethynylferrocene group. The LUMO of ferrocenyl BODIPY **3** is spread over the entire molecule, which shows appreciable delocalization over the entire molecule.

4.6. Single crystal X-ray diffraction studies



Scheme 4.3. Formation of BODIPY **2'** from **2**.

The single crystals of BODIPYs **3** and **6** were grown by the slow evaporation of a mixture of chloroform, hexane, and ethanol solution (7 : 2 : 1 ratio). Efforts to grow the single crystals of 8-chloro BODIPY **2** with the same solvent combination resulted in substitution of the chloro group with ethanol (Scheme 4.3), this indicates, that the chloro group is highly labile for substitution by the nucleophile.^[7] The BODIPYs **2'**, **3** and **6** crystallize in the space groups *P*, *P2₁/c*, and *P2₁/n* respectively.

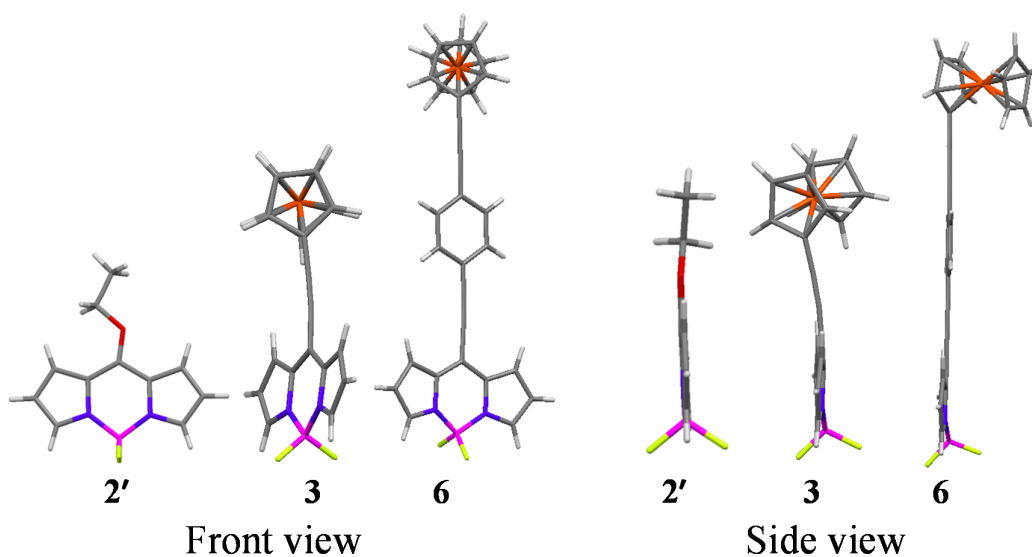


Figure 4.7. Crystal structures of **2'**, **3**, and **6** (a) Front view, (b) Side view.

The single crystal X-ray structures of **2'**, **3**, and **6** are shown in Figure 4.7. The crystal and refinement data are summarized in Table 4.2. The crystal structure of **2'** consists of two asymmetric units. The cyclopentadienyl ring of the ferrocenyl core and the BODIPY are non-planar with an interplanar angle of 64.06° and 31.77° for **3** and **6** respectively. The high electronegativity of fluoride atoms leads to multiple C–H...F intermolecular interactions forming interesting supramolecular

structural motifs. The intermolecular interactions in the crystals are displayed in Table 4.3.

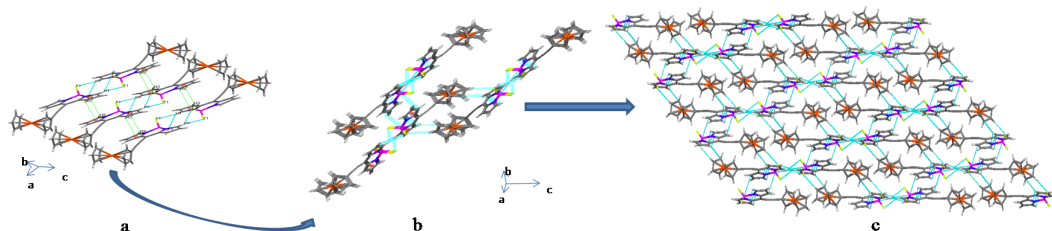


Figure 4.8. Crystal packing of **3** along tilted *b*-axis.

In the crystal packing of ferrocenyl BODIPY **3**, two molecules connect to each other in a head-to-head fashion *via* C(1)–H(1)···F(1) and C(1)–H(1)···F(2) interactions forming a dimeric structure (Figure 4.8a). Such a dimer connects to other two dimers *via* a C–H··· π interaction between H(9) and the π electron cloud of pyrrole (shown by the green dotted line), to form a staircase shaped sheet along the *b*-axis. The top side of this staircase shaped sheet is covered with another sheet by π ··· π stacking interactions between two BODIPY cores, while the bottom side of the sheet is connected to another sheet by C–H··· π and C–H···F interactions (Figure 4.8b), forming a brickwork type complex 3-D structure along the *b*-axis (Figure 4.8c).

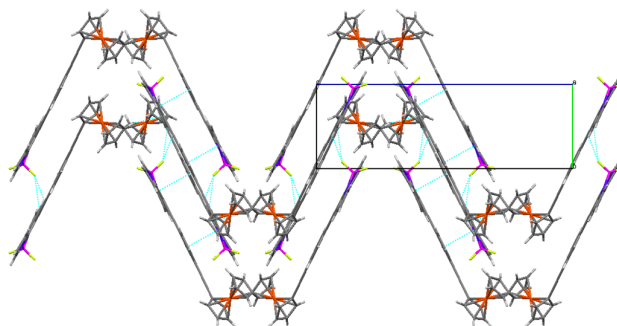


Figure 4.9. Zigzag arrangement of molecules in the crystal packing of **6** along *a*-axis.

In the crystal packing of ferrocenyl BODIPY **6**, the intermolecular hydrogen bonding interaction C(7)–H(7)···F(1) holds two molecules one above another. Similarly the C–H··· π interactions C(13)–H(13)··· π (pyrrole), and C(9)–H(9)··· π (phenyl) form a layer type arrangement, and such arrangements connect one another

Table 4.2. Crystal data and structure refinement parameters.

Compound	3	6	2'
Empirical formula	C ₂₁ H ₁₅ BF ₂ FeN ₂	C ₃₀ H ₁₉ BCl _{1.50} F ₂ FeN ₂	C ₂₂ H ₂₂ B ₂ F ₄ N ₄ O ₂
Formula weight	400.01	565.31	472.06
Temperature/K	150(2) K	150(2) K	150(2) K
Crystal system	Monoclinic	Monoclinic	Triclinic
Space group	<i>P</i> 2 ₁ / <i>c</i>	<i>P</i> 2/ <i>n</i>	<i>P</i> $\bar{1}$
Unit cell dimensions			
<i>a</i> /Å	10.4793(2)	15.2883(5)	7.7544(3)
α /°	90	90	89.693(4)
<i>b</i> /Å	7.70330(10)	7.3885(2)	11.5491(6)
β /°	100.674(2)	94.043	72.353(3)
<i>c</i> /Å	21.8524(4)	22.5986(6)	12.7800(5)
γ /°	90	90	78.713(4)
Volume/ Å ³	1733.52(5)	2546.33(13)	78.713(4)
<i>Z</i>	4	4	2
Calculated density/ Mg/m ³	1.533	1.475	1.468
Absorption coefficient/mm ⁻¹	0.898	0.787	0.118
<i>F</i> (000)	816	1150	488
Crystal size/mm	0.23 x 0.18 x 0.13	0.33 x 0.26 x 0.21	0.33 x 0.26 x 0.21
θ range from data collection/°	2.98 to 25.00	2.90 to 25.00	3.06 to 25.00
Reflections collected/unique	13355 / 3050 [<i>R</i> (int) = 0.0187]	20261 / 4480 [<i>R</i> (int) = 0.0511]	7798 / 3749 [<i>R</i> (int) = 0.0160]
Absorption correction	Semi-empirical from equivalents	Semi-empirical from equivalents	Semi-empirical from equivalents
Data/restraints/parameters	3050 / 0 / 244	4480 / 0 / 339	3749 / 0 / 309
Goodness-of-fit on <i>F</i> ²	1.076	1.058	1.112
Final <i>R</i> indices [<i>I</i> > 2σ (<i>I</i>)]	<i>R</i> ₁ = 0.0269, w <i>R</i> ₂ = 0.0685	<i>R</i> ₁ = 0.0738, w <i>R</i> ₂ = 0.2049	<i>R</i> ₁ = 0.0339, w <i>R</i> ₂ = 0.0858
<i>R</i> indices (all data)	<i>R</i> ₁ = 0.0296, w <i>R</i> ₂ = 0.0704	<i>R</i> ₁ = 0.0953, w <i>R</i> ₂ = 0.2274	<i>R</i> ₁ = 0.0373, w <i>R</i> ₂ = 0.0882
Largest diff. peak and hole/e Å ⁻³	0.189 and -0.339	2.355 and -1.091	0.161 and -0.233
CCDC number	934137	934138	934139

4.7. Experimental section

General methods- Chemicals were used as received unless otherwise indicated. All oxygen or moisture sensitive reactions were performed under a nitrogen/argon atmosphere using standard Schlenk techniques. ¹H NMR (400 MHz), and ¹³C NMR (100 MHz) spectra were recorded on the Bruker Avance (III) 400 MHz, using CDCl₃ as solvent. Chemical shifts are reported in parts per million (ppm) relative to the residual solvent peak (CDCl₃, 7.26 ppm for ¹H and 77.36 ppm

for ^{13}C). Multiplicities are given as: s (singlet), d (doublet), t (triplet), q (quartet), dd (doublet of doublets), m (multiplet), and the coupling constants, J , are given in Hz. Thermogravimetric analyses were performed on a Metler Toledo Thermal Analysis system. UV-visible absorption spectra of all compounds were recorded on a Cary-100 Bio UV-visible Spectrophotometer. Fluorescence spectra of all the compounds were recorded on a Horiba Jobin Yvon Floromax 4P spectrophotometer. Cyclic voltammograms (CVs) were recorded on a CHI620D electrochemical analyzer using Glassy carbon as the working electrode, Pt wire as the counter electrode, and a saturated calomel electrode (SCE) as the reference electrode. HRMS was recorded on a Bruker-Daltonics, micrOTOF-Q II mass spectrometer.

Synthesis and characterization

Generalised procedure for Sonogashira coupling reaction. *meso*-Chloro BODIPY **2** (190 mg, 0.845 mmol), and corresponding ferrocenyl alkyne (0.845 mmol) were dissolved in THF–triethylamine (10 : 1, v/v; 5 ml), and the mixture was cooled to 0 °C using an ice bath. The reaction mixture was purged with argon, and $\text{Pd}(\text{PPh}_3)_2\text{Cl}_2$ (29.6 mg, 5 mol%) and CuI (16 mg, 10 mol%) were added, followed by stirring at 0 °C for 30 min. Upon completion of the reaction, the mixture was evaporated to dryness, and the crude product was dissolved in CH_2Cl_2 , chromatographed on silica (1 : 1; hexanes– CHCl_3), and recrystallized from a chloroform–hexane–ethanol (7 : 2 : 1) mixture to give **3–6** (yield 40–60%) as purple crystalline solids.

8-(Ferrocenylethynyl)-4,4-difluoro-4-bora-3a,4a-diaza-s-indacene (3). Yield: 60% (201 mg). ^1H NMR (CDCl_3 , 400 MHz, ppm): δ 7.82 (s, 2H), 7.34 (d, 2H, J = 4 Hz), 6.53 (d, 2H, J = 3.8 Hz), 4.70 (t, 2H, J = 2 Hz), 4.53 (t, 2H, J = 2 Hz), 4.32 (s, 5H); ^{13}C NMR (CDCl_3 , 100 MHz, ppm): 142.46, 136.59, 128.54, 128.46, 118.24, 110.83, 83.27, 73.38, 71.92, 71.02, 61.93; HRMS (ESI) m/z = calculated for $\text{C}_{21}\text{H}_{15}\text{BF}_2\text{FeN}_2\text{Na}^+$ = 423.0542, measured 423.0548.

8-((3-Ferrocenyl)-phenylethynyl)-4,4-difluoro-4-bora-3a,4a-diaza-s-indacene (4). Yield: 65% (260 mg). ^1H NMR (CDCl_3 , 400 MHz, ppm): δ 7.84 (s, 2H), 7.69 (s, 2H), 7.62 (d, 2H, J = 8.04), 7.48 (d, 2H, J = 7.52), 7.43 (bs, 2H), 7.37 (dd, J = 7.52, J = 7.8), 6.57 (s, 2H), 4.70 (s, 2H), 4.39 (s, 2H), 4.08 (s, 5H); ^{13}C NMR (CDCl_3 , 100 MHz, ppm): 143.92, 141.05, 136.88, 130.40, 129.85, 129.49, 129.18, 129.03, 127.69, 121.22, 118.69, 106.48, 84.22, 83.71, 70.05, 69.83, 66.89; HRMS (ESI) m/z = calculated for $\text{C}_{27}\text{H}_{19}\text{FeBF}_2\text{N}_2$ = 476.0958, measured 476.0983.

8-((4-Ferrocenyl)-phenylethynyl)-4,4-difluoro-4-bora-3a,4a-diaza-s-indacene

(5). Yield: 50% (200 mg). ^1H NMR (CDCl_3 , 400 MHz, ppm): δ 7.83 (s, 2H), 7.57 (d, 2H, $J = 8$ Hz), 7.52 (d, 2H, $J = 8$ Hz), 7.41 (bs, 2H), 6.56 (bs, 2H), 4.73 (s, 2H), 4.44 (s, 2H), 4.06 (s, 5H) ppm; ^{13}C NMR (CDCl_3 , 100 MHz, ppm): 144.34, 143.48, 136.74, 133.29, 129.11, 128.05, 126.38, 118.53, 117.95, 107.74, 85.29, 83.37, 70.47, 70.27, 67.19; HRMS (ESI) m/z = calculated for $\text{C}_{27}\text{H}_{19}\text{FeBF}_2\text{N}_2$ = 476.0958, measured 476.0958.

8-((4-Ferrocenylethynyl)-phenylethynyl)-4,4-difluoro-4-bora-3a,4a-diaza-s-indacene (6).

Yield: 70% (294 mg). ^1H NMR (CDCl_3 , 400 MHz, ppm): δ 7.83 (s, 2H), 7.60 (d, 2H, $J = 8$ Hz), 7.54 (d, 2H, $J = 8$ Hz), 7.38 (s, 2H), 6.55 (s, 2H), 4.54 (s, 2H), 4.30 (s, 2H), 4.27 (s, 5H); ^{13}C NMR (CDCl_3 , 100 MHz, ppm): 143.94, 139.60, 136.79, 133.00, 131.89, 129.35, 127.34, 119.85, 118.72, 106.02, 93.72, 85.99, 85.73, 71.98, 70.42, 69.69, 64.62; HRMS (ESI) m/z = calculated for $\text{C}_{29}\text{H}_{19}\text{FeBF}_2\text{N}_2$ = 500.0959, measured 500.0964.

4.8. Conclusion

In summary we have synthesized a series of *meso*-alkynylated ferrocenyl BODIPYs by the Pd catalyzed Sonogashira cross-coupling reaction. The photophysical, and electrochemical properties of these ferrocenyl BODIPYs show considerable electronic interaction between the BODIPY core, and the ferrocenyl group. This electronic communication can be tuned by varying the length, and linkage of the spacer group. The alkynylation at meso position of BODIPY reveals the superior electronic communication between Donor and Acceptor BODIPY moiety compared to alkynylation at α and β positions.

References

-
- [1] (a) Nepomnyashchii, A. B., & Bard, A. J. (2012). Electrochemistry and Electrogenenerated Chemiluminescence of BODIPY Dyes. *Accounts of Chemical Research*, 45(11), 1844–1853. <http://doi.org/10.1021/ar200278b>; (b) Cheng, T., Wang, T., Zhu, W., Chen, X., Yang, Y., Xu, Y., & Qian, X. (2011). Red-Emission Fluorescent Probe Sensing Cadmium and Pyrophosphate Selectively in Aqueous Solution. *Organic Letters*, 13(14), 3656–3659. <http://doi.org/10.1021/ol201305d>; (c) Bozdemir, O. A., Guliyev, R., Buyukcakil, O., Selcuk, S.,

Kolemen, S., Gulseren, G., ... Akkaya, E. U. (2010). Selective Manipulation of ICT and PET Processes in Styryl-Bodipy Derivatives: Applications in Molecular Logic and Fluorescence Sensing of Metal Ions. *Journal of the American Chemical Society*, 132(23), 8029–8036. <http://doi.org/10.1021/ja1008163>; (d) Benstead, M., Mehl, G. H., & Boyle, R. W. (2011). 4,4'-Difluoro-4-bora-3a,4a-diaza-s-indacenes (BODIPYs) as components of novel light active materials. *Tetrahedron*, 67(20), 3573–3601. <http://doi.org/http://dx.doi.org/10.1016/j.tet.2011.03.028>; (e) Zhou, Y., Xiao, Y., Chi, S., & Qian, X. (2008). Isomeric Boron–Fluorine Complexes with Donor–Acceptor Architecture: Strong Solid/Liquid Fluorescence and Large Stokes Shift. *Organic Letters*, 10(4), 633–636. <http://doi.org/10.1021/ol702963w>; (f) Lord, S. J., Conley, N. R., Lee, H. D., Samuel, R., Liu, N., Twieg, R. J., & Moerner, W. E. (2008). A Photoactivatable Push–Pull Fluorophore for Single-Molecule Imaging in Live Cells. *Journal of the American Chemical Society*, 130(29), 9204–9205. <http://doi.org/10.1021/ja802883k>; (g) West, R., Panagabko, C., & Atkinson, J. (2010). Synthesis and Characterization of BODIPY- α -Tocopherol: A Fluorescent Form of Vitamin E. *The Journal of Organic Chemistry*, 75(9), 2883–2892. <http://doi.org/10.1021/jo100095n>; (h) Descalzo, A. B., Xu, H.-J., Xue, Z.-L., Hoffmann, K., Shen, Z., Weller, M. G., ... Rurack, K. (2008). Phenanthrene-Fused Boron-Dipyrromethenes as Bright Long-Wavelength Fluorophores. *Organic Letters*, 10(8), 1581–1584. <http://doi.org/10.1021/ol800271e>; (i) Marder, S. R., Kippelen, B., Jen, A. K.-Y., & Peyghambarian, N. (1997). Design and synthesis of chromophores and polymers for electro-optic and photorefractive applications. *Nature*, 388(6645), 845–851; (j) LeCours, S. M., Guan, H.-W., DiMagno, S. G., Wang, C. H., & Therien, M. J. (1996). Push–Pull Arylethynyl Porphyrins: New Chromophores That Exhibit Large Molecular First-Order Hyperpolarizabilities. *Journal of the American Chemical Society*, 118(6), 1497–1503. <http://doi.org/10.1021/ja953610l>.

- [2] (a) Erten-Ela, S., Yilmaz, M. D., Icli, B., Dede, Y., Icli, S., & Akkaya, E. U. (2008). A Panchromatic Boradiazaindacene (BODIPY) Sensitizer for Dye-Sensitized Solar Cells. *Organic Letters*, 10(15), 3299–3302. <http://doi.org/10.1021/ol8010612>; (b) Kumaresan, D., Thummel, R. P., Bura, T., Ulrich, G., &

-
- Ziessel, R. (2009). Color Tuning in New Metal-Free Organic Sensitizers (Bodipys) for Dye-Sensitized Solar Cells. *Chemistry – A European Journal*, 15(26), 6335–6339. <http://doi.org/10.1002/chem.200900518>; (c) Kolemen, S., Cakmak, Y., Erten-Ela, S., Altay, Y., Brendel, J., Thelakkat, M., & Akkaya, E. U. (2010). Solid-State Dye-Sensitized Solar Cells Using Red and Near-IR Absorbing Bodipy Sensitizers. *Organic Letters*, 12(17), 3812–3815. <http://doi.org/10.1021/ol1014762>.
- [3] (a) Whited, M. T., Djurovich, P. I., Roberts, S. T., Durrell, A. C., Schlenker, C. W., Bradforth, S. E., & Thompson, M. E. (2011). Singlet and Triplet Excitation Management in a Bichromophoric Near-Infrared-Phosphorescent BODIPY-Benzoporphyrin Platinum Complex. *Journal of the American Chemical Society*, 133(1), 88–96. <http://doi.org/10.1021/ja108493b>; (b) Iehl, J., Nierengarten, J.-F., Harriman, A., Bura, T., & Ziessel, R. (2012). Artificial Light-Harvesting Arrays: Electronic Energy Migration and Trapping on a Sphere and between Spheres. *Journal of the American Chemical Society*, 134(2), 988–998. <http://doi.org/10.1021/ja206894z>; (c) Flavin, K., Lawrence, K., Bartelmess, J., Tasior, M., Navio, C., Bittencourt, C., ... Giordani, S. (2011). Synthesis and Characterization of Boron Azadipyrromethene Single-Wall Carbon Nanotube Electron Donor–Acceptor Conjugates. *ACS Nano*, 5(2), 1198–1206. <http://doi.org/10.1021/nn102831x>; (d) Florian, A., Mayoral, M. J., Stepanenko, V., & Fernández, G. (2012). Alternated Stacks of Nonpolar Oligo(p-phenyleneethynylene)-BODIPY Systems. *Chemistry – A European Journal*, 18(47), 14957–14961. <http://doi.org/10.1002/chem.201203279>.
- [4] (a) Zheng, Q., Xu, G., & Prasad, P. N. (2008). Conformationally Restricted Dipyrromethene Boron Difluoride (BODIPY) Dyes: Highly Fluorescent, Multicolored Probes for Cellular Imaging. *Chemistry – A European Journal*, 14(19), 5812–5819. <http://doi.org/10.1002/chem.200800309>; (b) Didier, P., Ulrich, G., Mely, Y., & Ziessel, R. (2009). Improved push-pull-push E-Bodipy fluorophores for two-photon cell-imaging. *Organic & Biomolecular Chemistry*, 7(18), 3639–3642. <http://doi.org/10.1039/B911587K>; (c) Bouit, P.-A., Kamada, K., Feneyrou, P., Berginc, G., Toupet, L., Maury, O., & Andraud, C. (2009). Two-Photon Absorption-Related Properties of Functionalized BODIPY Dyes

in the Infrared Range up to Telecommunication Wavelengths. *Advanced Materials*, 21(10-11), 1151–1154. <http://doi.org/10.1002/adma.200801778>.

- [5] (a) Murtagh, J., Frimannsson, D. O., & O'Shea, D. F. (2009). Azide Conjugatable and pH Responsive Near-Infrared Fluorescent Imaging Probes. *Organic Letters*, 11(23), 5386–5389. <http://doi.org/10.1021/ol902140v>; (b) Coskun, A., Yilmaz, M. D., & Akkaya, E. U. (2007). Bis(2-pyridyl)-Substituted Boratriazaindacene as an NIR-Emitting Chemosensor for Hg(II). *Organic Letters*, 9(4), 607–609. <http://doi.org/10.1021/ol062867t>; (c) Han, J., Loudet, A., Barhoumi, R., Burghardt, R. C., & Burgess, K. (2009). A Ratiometric pH Reporter For Imaging Protein-dye Conjugates In Living Cells. *Journal of the American Chemical Society*, 131(5), 1642–1643. <http://doi.org/10.1021/ja8073374>; (d) Shi, W.-J., Liu, J.-Y., & Ng, D. K. P. (2012). A Highly Selective Colorimetric and Fluorescent Probe for Cu²⁺ and Hg²⁺ Ions Based on a Distyryl BODIPY with Two Bis(1,2,3-triazole)amino Receptors. *Chemistry – An Asian Journal*, 7(1), 196–200. <http://doi.org/10.1002/asia.201100598>; (e) Madhu, S., Gonnade, R., & Ravikanth, M. (2013). Synthesis of 3,5-Bis(acrylaldehyde) Boron-dipyrromethene and Application in Detection of Cysteine and Homocysteine in Living Cells. *The Journal of Organic Chemistry*, 78(10), 5056–5060. <http://doi.org/10.1021/jo4004597>.
- [6] (a) Yogo, T., Urano, Y., Ishitsuka, Y., Maniwa, F., & Nagano, T. (2005). Highly Efficient and Photostable Photosensitizer Based on BODIPY Chromophore. *Journal of the American Chemical Society*, 127(35), 12162–12163. <http://doi.org/10.1021/ja0528533>; (b) Ozlem, S., & Akkaya, E. U. (2009). Thinking Outside the Silicon Box: Molecular AND Logic As an Additional Layer of Selectivity in Singlet Oxygen Generation for Photodynamic Therapy. *Journal of the American Chemical Society*, 131(1), 48–49. <http://doi.org/10.1021/ja808389t>.
- [7] (a) Awuah, S. G., & You, Y. (2012). Boron dipyrromethene (BODIPY)-based photosensitizers for photodynamic therapy. *RSC Advances*, 2(30), 11169–11183. <http://doi.org/10.1039/C2RA21404K>; (b) Boens, N., Leen, V., & Dehaen, W. (2012). Fluorescent indicators based on BODIPY. *Chemical*

-
- Society Reviews*, 41(3), 1130–1172. <http://doi.org/10.1039/C1CS15132K>; (c) Kim, H. S., Pham, T. C. T., & Yoon, K. B. (2012). A novel class of nonlinear optical materials based on host-guest composites: zeolites as inorganic crystalline hosts. *Chemical Communications*, 48(39), 4659–4673. <http://doi.org/10.1039/C2CC30919J>; (d) Benniston, A. C., & Copley, G. (2009). Lighting the way ahead with boron dipyrromethene (Bodipy) dyes. *Physical Chemistry Chemical Physics*, 11(21), 4124–4131. <http://doi.org/10.1039/B901383K>.
- [8] (a) Chen, J., Mizumura, M., Shinokubo, H., & Osuka, A. (2009). Functionalization of Boron Dipyrin (BODIPY) Dyes through Iridium and Rhodium Catalysis: A Complementary Approach to α - and β -Substituted BODIPYs. *Chemistry – A European Journal*, 15(24), 5942–5949. <http://doi.org/10.1002/chem.200802541>; (b) Schmidt, E. Y., Trofimov, B. A., Mikhaleva, A. I., Zorina, N. V., Protzuk, N. I., Petrushenko, K. B., ... Pansu, R. B. (2009). Synthesis and Optical Properties of 2-(Benzo[b]thiophene-3-yl)pyrroles and a New BODIPY Fluorophore (BODIPY=4,4-Difluoro-4-bora-3a,4a-diaza-s-indacene). *Chemistry – A European Journal*, 15(23), 5823–5830. <http://doi.org/10.1002/chem.200802467>; (c) Ulrich, G., Ziessel, R., & Harriman, A. (2008). The Chemistry of Fluorescent Bodipy Dyes: Versatility Unsurpassed. *Angewandte Chemie International Edition*, 47(7), 1184–1201. <http://doi.org/10.1002/anie.200702070>; (d) Yin, X., Li, Y., Zhu, Y., Jing, X., Li, Y., & Zhu, D. (2010). A highly sensitive viscosity probe based on ferrocene-BODIPY dyads. *Dalton Transactions*, 39(41), 9929–9935. <http://doi.org/10.1039/C0DT00309C>.
- [9] (a) Loudet, A., & Burgess, K. (2007). BODIPY Dyes and Their Derivatives: Syntheses and Spectroscopic Properties. *Chemical Reviews*, 107(11), 4891–4932. <http://doi.org/10.1021/cr078381n>; (b) Zheng, Q., Xu, G., & Prasad, P. N. (2008). Conformationally Restricted Dipyrromethene Boron Difluoride (BODIPY) Dyes: Highly Fluorescent, Multicolored Probes for Cellular Imaging. *Chemistry – A European Journal*, 14(19), 5812–5819. <http://doi.org/10.1002/chem.200800309>.

-
- [10] (a) Lakshmi, V., & Ravikanth, M. (2012). Brominated boron dipyrins: synthesis, structure, spectral and electrochemical properties. *Dalton Transactions*, 41(19), 5903–5911. <http://doi.org/10.1039/C2DT00019A>; (b) Jiao, L., Pang, W., Zhou, J., Wei, Y., Mu, X., Bai, G., & Hao, E. (2011). Regioselective Stepwise Bromination of Boron Dipyrromethene (BODIPY) Dyes. *The Journal of Organic Chemistry*, 76(24), 9988–9996. <http://doi.org/10.1021/jo201754m>; (c) Godoy, J., Vives, G., & Tour, J. M. (2010). Synthesis of Highly Fluorescent BODIPY-Based Nanocars. *Organic Letters*, 12(7), 1464–1467. <http://doi.org/10.1021/ol100108r>; (d) Ortiz, M. J., Agarrabeitia, A. R., Duran-Sampedro, G., Bañuelos Prieto, J., Lopez, T. A., Massad, W. A., ... Lopez Arbeloa, I. (2012). Synthesis and functionalization of new polyhalogenated BODIPY dyes. Study of their photophysical properties and singlet oxygen generation. *Tetrahedron*, 68(4), 1153–1162. <http://doi.org/http://dx.doi.org/10.1016/j.tet.2011.11.070>; (e) Baruah, M., Qin, W., Basarić, N., De Borggraeve, W. M., & Boens, N. (2005). BODIPY-Based Hydroxyaryl Derivatives as Fluorescent pH Probes. *The Journal of Organic Chemistry*, 70(10), 4152–4157. <http://doi.org/10.1021/jo0503714>; (f) Yin, X., Li, Y., Li, Y., Zhu, Y., Tang, X., Zheng, H., & Zhu, D. (2009). Electrochromism based on the charge transfer process in a ferrocene–BODIPY molecule. *Tetrahedron*, 65(40), 8373–8377. <http://doi.org/http://dx.doi.org/10.1016/j.tet.2009.08.008>; (g) Khan, T. K., Pissurlenkar, R. R. S., Shaikh, M. S., & Ravikanth, M. (2012). Synthesis and studies of covalently linked *meso*-furyl boron-dipyrromethene-ferrocene conjugates. *Journal of Organometallic Chemistry*, 697(1), 65–73. <http://doi.org/http://dx.doi.org/10.1016/j.jorganchem.2011.10.016>.
- [11] (a) Baruah, M., Qin, W., Vallée, R. A. L., Beljonne, D., Rohand, T., Dehaen, W., & Boens, N. (2005). A Highly Potassium-Selective Ratiometric Fluorescent Indicator Based on BODIPY Azacrown Ether Excitable with Visible Light. *Organic Letters*, 7(20), 4377–4380. <http://doi.org/10.1021/ol051603o>; (b) Rohand, T., Baruah, M., Qin, W., Boens, N., & Dehaen, W. (2006). Functionalisation of fluorescent BODIPY dyes by nucleophilic substitution. *Chemical Communications*, (3), 266–268. <http://doi.org/10.1039/>

B512756D; (c) Rohand, T., Qin, W., Boens, N., & Dehaen, W. (2006). Palladium-Catalyzed Coupling Reactions for the Functionalization of BODIPY Dyes with Fluorescence Spanning the Visible Spectrum. *European Journal of Organic Chemistry*, 2006(20), 4658–4663. <http://doi.org/10.1002/ejoc.200600531>; (d) Leen, V., Braeken, E., Luckermans, K., Jackers, C., Van der Auweraer, M., Boens, N., & Dehaen, W. (2009). A versatile, modular synthesis of monofunctionalized BODIPY dyes. *Chemical Communications*, (30), 4515–4517. <http://doi.org/10.1039/B906164A>; (e) Leen, V., Leemans, T., Boens, N., & Dehaen, W. (2011). 2- and 3-Monohalogenated BODIPY Dyes and Their Functionalized Analogues: Synthesis and Spectroscopy. *European Journal of Organic Chemistry*, 2011(23), 4386–4396. <http://doi.org/10.1002/ejoc.201100324>; (f) Li, L., Nguyen, B., & Burgess, K. (2008). Functionalization of the 4,4-difluoro-4-bora-3a,4a-diaza-s-indacene (BODIPY) core. *Bioorganic & Medicinal Chemistry Letters*, 18(10), 3112–3116. <http://doi.org/http://dx.doi.org/10.1016/j.bmcl.2007.10.103>; (g) Han, J., Gonzalez, O., Aguilar-Aguilar, A., Pena-Cabrera, E., & Burgess, K. (2009). 3- and 5-Functionalized BODIPYs via the Liebeskind-Srogl reaction. *Organic & Biomolecular Chemistry*, 7(1), 34–36. <http://doi.org/10.1039/B818390B>; (h) Dilek, Ö., & Bane, S. L. (2008). Synthesis of boron dipyrromethene fluorescent probes for bioorthogonal labeling. *Tetrahedron Letters*, 49(8), 1413–1416. <http://doi.org/http://dx.doi.org/10.1016/j.tetlet.2007.12.052>; (i) Rao, M. R., Mobin, S. M., & Ravikanth, M. (2010). Boron–dipyrromethene based specific chemodosimeter for fluoride ion. *Tetrahedron*, 66(9), 1728–1734. <http://doi.org/http://dx.doi.org/10.1016/j.tet.2009.12.039>; (j) Khan, T. K., Rao, M. R., & Ravikanth, M. (2010). Synthesis and Photophysical Properties of 3,5-Bis(oxopyridinyl)- and 3,5-Bis(pyridinyloxy)-Substituted Boron-Dipyrromethenes. *European Journal of Organic Chemistry*, 2010(12), 2314–2323. <http://doi.org/10.1002/ejoc.200901460>.

- [12] Leen, V., Yuan, P., Wang, L., Boens, N., & Dehaen, W. (2012). Synthesis of *Meso*-Halogenated BODIPYs and Access to *Meso*-Substituted Analogues. *Organic Letters*, 14(24), 6150–6153. <http://doi.org/10.1021/ol3028225>.

-
- [13] Kusaka, S., Sakamoto, R., Kitagawa, Y., Okumura, M., & Nishihara, H. (2013). *meso*-Alkynyl BODIPYs: Structure, Photoproperties, π -Extension, and Manipulation of Frontier Orbitals. *Chemistry – An Asian Journal*, 8(4), 723–727. <http://doi.org/10.1002/asia.201201176>.
- [14] (a) Gautam, P., Dhokale, B., Shukla, V., Singh, C. P., Bindra, K. S., & Misra, R. (2012). Optical limiting performance of *meso*-tetraferrocenyl porphyrin and its metal derivatives. *Journal of Photochemistry and Photobiology A: Chemistry*, 239(0), 24–27. <http://doi.org/http://dx.doi.org/10.1016/j.jphotochem.2012.04.020>; (b) Dhokale, B., Gautam, P., & Misra, R. (2012). Donor–acceptor perylene-3,4,9,10-tetracarboxylic diimide–ferrocene conjugates: synthesis, photophysical, and electrochemical properties. *Tetrahedron Letters*, 53(18), 2352–2354. <http://doi.org/http://dx.doi.org/10.1016/j.tetlet.2012.02.107>; (c) Gautam, P., Dhokale, B., Mobin, S. M., & Misra, R. (2012). Ferrocenyl BODIPYs: synthesis, structure and properties. *RSC Advances*, 2(32), 12105–12107. <http://doi.org/10.1039/C2RA21964F>; (d) Maragani, R., Jadhav, T., Mobin, S. M., & Misra, R. (2012). Synthesis, structure, photophysical, and electrochemical properties of donor–acceptor ferrocenyl derivatives. *Tetrahedron*, 68(36), 7302–7308. <http://doi.org/http://dx.doi.org/10.1016/j.tet.2012.06.094>; (e) Dhokale, B., Gautam, P., Mobin, S. M., & Misra, R. (2013). Donor-acceptor, ferrocenyl substituted BODIPYs with marvelous supramolecular interactions. *Dalton Transactions*, 42(5), 1512–1518. <http://doi.org/10.1039/C2DT31632C>; (f) Maragani, R., Jadhav, T., Mobin, S. M., & Misra, R. (2013). C₃ symmetric ferrocenyl triazines: synthesis, structure, and properties. *RSC Advances*, 3(9), 2889–2892. <http://doi.org/10.1039/C2RA23153K>; (g) Misra, R., Gautam, P., Sharma, R., & Mobin, S. M. (2013). Donor– π –acceptor– π –donor ferrocenyl benzothiadiazoles: synthesis, structure, and properties. *Tetrahedron Letters*, 54(5), 381–383. <http://doi.org/http://dx.doi.org/10.1016/j.tetlet.2012.11.016>; (h) Jadhav, T., Maragani, R., Misra, R., Sreeramulu, V., Rao, D. N., & Mobin, S. M. (2013). Design and synthesis of donor-acceptor pyrazabole derivatives for multiphoton absorption. *Dalton Transactions*, 42(13), 4340–4342. <http://doi.org/10.1039/C3DT33065F>.

-
- [15] (a) Plater, M. J., Aiken, S., & Bourhill, G. (2002). A new synthetic route to donor–acceptor porphyrins. *Tetrahedron*, 58(12), 2405–2413. [http://doi.org/http://dx.doi.org/10.1016/S0040-4020\(02\)00109-6](http://doi.org/http://dx.doi.org/10.1016/S0040-4020(02)00109-6); (b) Kim, D., Yamamoto, K., & Ahn, K. H. (2012). A BODIPY-based reactive probe for ratiometric fluorescence sensing of mercury ions. *Tetrahedron*, 68(26), 5279–5282. <http://doi.org/http://dx.doi.org/10.1016/j.tet.2012.01.091>.
- [16] Misra, R., Kumar, R., Chandrashekar, T. K., Suresh, C. H., Nag, A., & Goswami, D. (2006). 22 π Smaragdyrin Molecular Conjugates with Aromatic Phenylacetylenes and Ferrocenes: Syntheses, Electrochemical, and Photonic Properties. *Journal of the American Chemical Society*, 128(50), 16083–16091. <http://doi.org/10.1021/ja0628295>.
- [17] (a) Rao, M. R., Kumar, K. V. P., & Ravikanth, M. (2010). Synthesis of boron-dipyrromethene–ferrocene conjugates. *Journal of Organometallic Chemistry*, 695(6), 863–869. <http://doi.org/http://dx.doi.org/10.1016/j.jorganchem.2010.01.009>; (b) Misra, R., Kumar, R., PrabhuRaja, V., & Chandrashekar, T. K. (2005). Modified push–pull expanded corroles: Syntheses, structure and nonlinear optical properties. *Journal of Photochemistry and Photobiology A: Chemistry*, 175(2–3), 108–117. <http://doi.org/http://dx.doi.org/10.1016/j.jphotochem.2005.04.024>; (c) Fery-Forgues, S., & Delavaux-Nicot, B. (2000). Ferrocene and ferrocenyl derivatives in luminescent systems. *Journal of Photochemistry and Photobiology A: Chemistry*, 132(3), 137–159. [http://doi.org/http://dx.doi.org/10.1016/S1010-6030\(00\)00213-6](http://doi.org/http://dx.doi.org/10.1016/S1010-6030(00)00213-6); (d) Nadtochenko, V. A., Denisov, N. N., Gak, V. Y., Abramova, N. V., & Loim, N. M. (1999). Photochemical and photophysical properties of *meso*-tetraferrocenylporphyrin. Quenching of *meso*-tetraphenylporphyrin by ferrocene. *Russian Chemical Bulletin*, 48(10), 1900–1903. <http://doi.org/10.1007/BF02494744>; (e) Barlow, S., & Marder, S. R. (2000). Electronic and optical properties of conjugated group 8 metallocene derivatives. *Chemical Communications*, (17), 1555–1562. <http://doi.org/10.1039/B004907G>.

-
- [18] Gritzner, G. & Kuta, J. (2009). Recommendations on reporting electrode potentials in nonaqueous solvents (Recommendations 1983). *Pure and Applied Chemistry*, 56 (4), 461-466. doi:10.1351/pac198456040461.
- [19] (a) Qian, G., Dai, B., Luo, M., Yu, D., Zhan, J., Zhang, Z., ... Wang, Z. Y. (2008). Band Gap Tunable, Donor–Acceptor–Donor Charge-Transfer Heteroquinoid-Based Chromophores: Near Infrared Photoluminescence and Electroluminescence. *Chemistry of Materials*, 20(19), 6208–6216. <http://doi.org/10.1021/cm801911n>; (b) Tahara, K., Fujita, T., Sonoda, M., Shiro, M., & Tobe, Y. (2008). Donors and Acceptors Based on Triangular Dehydrobenzo[12]annulenes: Formation of a Triple-Layered Rosette Structure by a Charge-Transfer Complex. *Journal of the American Chemical Society*, 130(43), 14339–14345. <http://doi.org/10.1021/ja804604y>.

Chapter 5

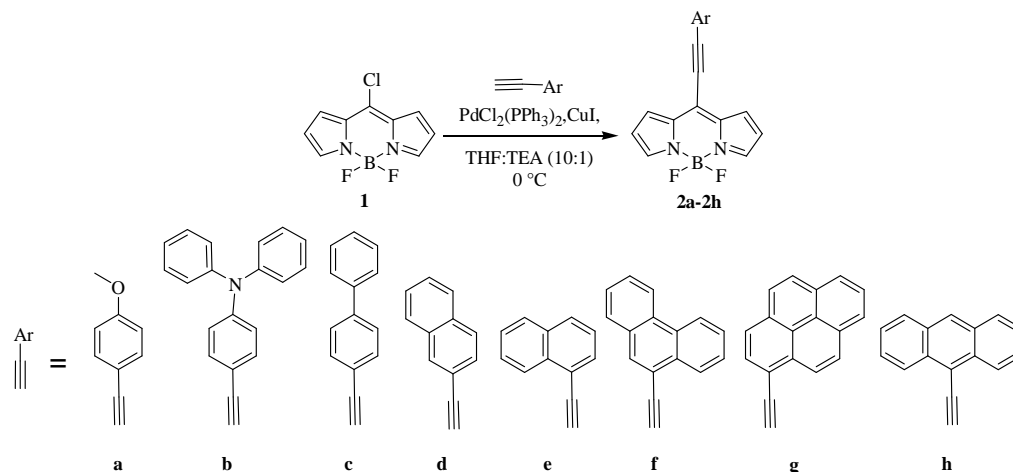
Quenching of fluorescence as an indicator of donor strength of *meso* arylethynyl BODIPYs

5.1. Introduction

In recent years BODIPY chemistry has gained momentum, which is reflected from their share in most of the journals.^[1] BODIPY dyes distinguish themselves from others due to strong absorption, sharp fluorescence and high thermal stability.^[2] These properties of the BODIPYs make them a potential candidate in organic electronics and photonics.^[3] Our group is interested in design of donor-acceptor molecular systems for photonic applications.^[4] The BODIPY unit acts as strong acceptor. Therefore functionalization of BODIPY dyes with donors will result in donor-acceptor (D-A) type molecular systems.^[5] Various strategies are reported in the literature for functionalization of the BODIPY dyes at *meso* as well as pyrrolic positions.^[6] In *meso* aryl functionalized BODIPY, the *meso* substituent adopts orthogonal orientation with respect to the BODIPY core, which hinders the electronic communication. One can overcome this problem by introducing the ethynyl linkage at the *meso* position, so that the substituent and the BODIPY will be planar, with respect to each other for better electronic communication. Wim Dehaen *et al.* have introduced efficient synthetic strategy for incorporation of the ethynyl linkage at the *meso* position.^[7]

Our previous report on ferrocenyl BODIPYs has established that the *meso* alkynylated BODIPYs show superior electronic communication than the pyrrolic alkynylated BODIPYs.^[8] This encouraged us to study the effect of various donors at the *meso* position of the BODIPY via ethynyl linkage. In this report we have incorporated various donors at the *meso* position of the BODIPY via ethynyl linkage and studied their structural, electronic, photophysical, and electrochemical properties.

5.2. Results and Discussion



Scheme 5.1. Synthesis of *meso*-arylethynyl BODIPYs **2a – 2h**.

The *meso*-arylethynyl BODIPYs **2a – 2h** were synthesized by the palladium catalyzed Sonogashira cross-coupling reaction of 8-chloro BODIPY **1** with respective arylethyne (**a – h**) as shown in Scheme 5.1. The 8-chloro BODIPY **1**, was synthesized from dipyrromethane.⁷ The dipyrromethane was reacted with POCl₃ followed by *in-situ* deprotonation by base and complexation with BF₃ etherate, which resulted 8-chloro BODIPY **1** in 59 % yield. The dipyrromethane was synthesized by the condensation reaction of thiophosgene, and pyrrole, followed by oxidation with H₂O₂ under basic condition.^[9] The arylethyne **a – h** were synthesized from reported procedures.^[10]

The Pd-catalyzed Sonogashira cross-coupling reaction of the 8-chloro BODIPY **1**, with the respective arylethyne at 0 °C resulted, BODIPYs **2a – 2h** in 44 to 77 % yields. These reactions were completed within half an hour due to the high reactivity of 8-chloro BODIPY. The BODIPYs **2a – 2h** were well characterized by ¹H NMR, ¹³C NMR, and HRMS techniques. The BODIPYs **2d** and **2e** were also characterized by single crystal X-ray diffraction technique.

The typical ¹H NMR spectrum of the BODIPY derivatives show two α pyrrolic protons as singlet at ~ 7.8 ppm, whereas the β and β' protons appear as doublet at ~ 6.6 and ~ 7.7 ppm. The protons of the aryl substituent appear in aromatic region.

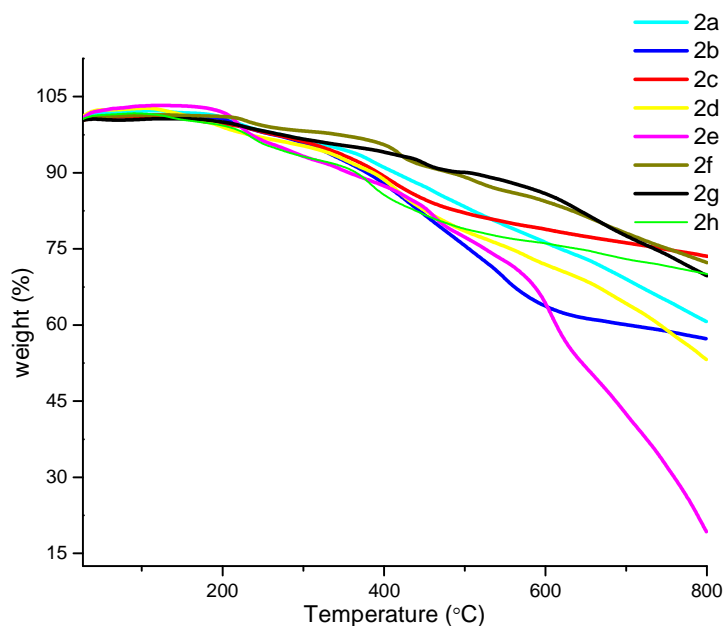


Figure 5.1. TGA plot of the *meso* arylethynyl BODIPYs **2a** – **2h**.

The thermal stability is one of the key criteria for optoelectronic applications. The thermal properties of the *meso*-arylethynyl BODIPYs (**2a** – **2h**) were investigated using thermogravimetric analysis (TGA) by heating the BODIPYs under nitrogen atmosphere at the heating rate of 10 °C per minute and monitoring the weight loss against temperature (Figure 5.1). The TGA analysis shows that the *meso*-arylethynyl BODIPYs were stable enough up to 350 °C. The decomposition temperature at 10 % weight loss is shown in Table 5.1, indicating good thermal stability of the BODIPYs.

5.3. Photophysical Properties

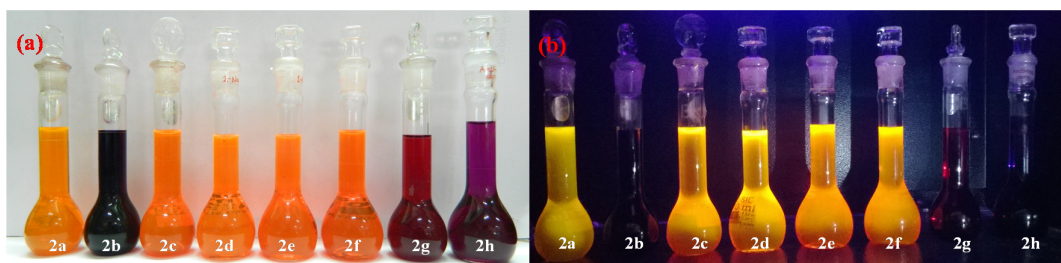


Figure 5.2. BODIPYs **2a** – **2h** in dichloromethane at concentration of 10^{-4} M (a) in day light and (b) in UV light.

The photograph of the BODIPYs **2a** – **2h** in dichloromethane solvent in day light and in UV light is displayed in Figure 5.2. The coloring pattern of the BODIPYs reflects the D-A interaction. The BODIPYs **2b**, **2g** and **2h** are non-fluorescent with dark purple color indicating strong D-A interaction, whereas the BODIPYs **2a** and **2c** – **2f** are fluorescent with yellow-red shade indicating moderate D-A interaction.

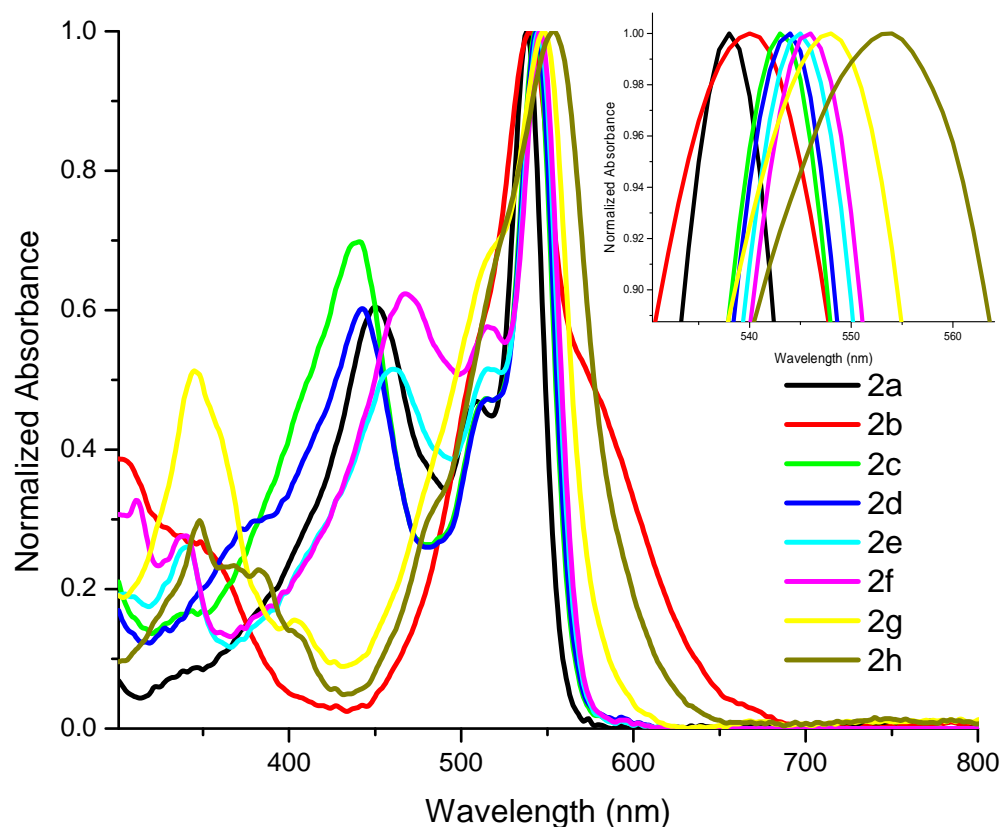


Figure 5.3. Normalized UV-vis absorption spectra of *meso*-arylethynyl BODIPYs **2a** – **2h** recorded in dichloromethane, inset show the enlarged view.

The UV-vis absorption spectra of the *meso*-arylethynyl BODIPYs **2a** – **2h** were recorded in dichloromethane (Figure 5.3), and the corresponding data are shown in Table 5.1. The BODIPYs **2a** – **2h** show strong absorption band between 538 to 553 nm region corresponding to the $S_0 \rightarrow S_1$ transition with high extinction coefficient, and a shoulder at higher energy region corresponding to the respective vibronic transition of the BODIPY. The BODIPYs **2a** – **2h** show red shift of 35 – 50 nm in the $S_0 \rightarrow S_1$ absorption band compared to 8-chloro BODIPY **1** (Table 5.1) due to enhanced conjugation. The red shift in the $S_0 \rightarrow S_1$ absorption band follows the order

of **2h**>**2g**>**2f**>**2e**>**2d**>**2c**>**2b**>**2a**. The BODIPY **2b** shows a shoulder in $S_0 \rightarrow S_1$ absorption band at low energy region, which can be attributed to charge transfer.^[11]

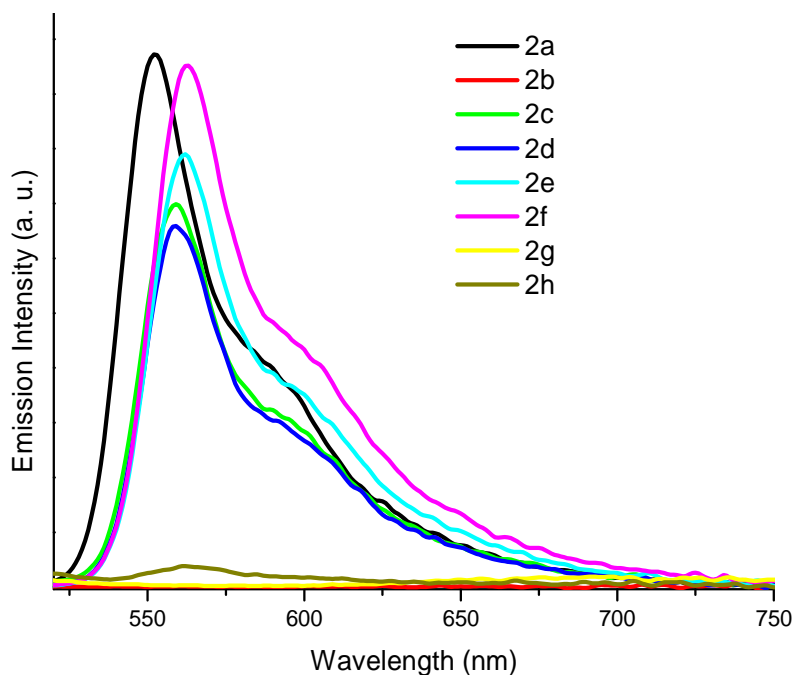


Figure 5.4. Emission spectra of the *meso*-arylethynyl BODIPYs **2a** – **2h**, recorded in dichloromethane.

The emission properties of the *meso*-arylethynyl BODIPYs **2a** – **2h** were studied in dichloromethane (Figure 5.4) and corresponding data is given in Table 5.1. The *meso* arylethynyl BODIPYs **2a**, **2c** – **2f** and **2h** emit in the 520 – 650 nm region with stokes shift ranging from 380 – 550 cm^{-1} . The fluorescence quantum yields of the BODIPYs **2a** – **2h** were decreased drastically compared to the 8-chloro BODIPY **1**. The BODIPYs **2b** and **2g** were non-emissive in nature. The quenching of the fluorescence is may be due to the intramolecular charge transfer from aryl moiety to the BODIPY.^[12] The trend in quenching of fluorescence can be correlated to the electron donating ability of the aryl substituent. More the electron donating ability lesser will be the quantum yield. From the quantum yield values the electron donating ability of the aryl substituent follows the order: **2b**>**2g**>**2h**>**2d**>**2c**>**2e**>**2f**>**2a**.

Table 5.1. Photophysical and thermal properties of *meso*-arylethynyl BODIPYs **2a** – **2h**.

BODIPY	$\lambda_{S_0 \rightarrow S_1}$ (nm)	$\epsilon/10^4$ (M ⁻¹ .cm ⁻¹) ^a	λ_{em} ^b (nm)	Stokes shift (cm ⁻¹)	Φ_F ^c	T _d ^d (°C)
2a	538	4.4	552	472	0.23	414
2b	540	5.0	- ^e	- ^e	- ^e	379
2c	543	3.8	558	495	0.18	392
2d	544	4.9	559	493	0.19	386
2e	545	3.5	561	523	0.19	357
2f	546	4.4	563	554	0.20	484
2g	548	4.5	- ^e	- ^e	- ^e	504
2h	553	4.6	565	384	0.02	365

^aRecorded at S₀→S₁, ^bExcited at $\lambda_{S_0 \rightarrow S_1}$, ^cDetermined by using Rhodamine 6G as standard ($\phi=0.88$, in ethanol), ^dDecomposition temperature at 10% weight loss, determined by TGA. ^e BODIPYs are non-emissive.

5.4. Electrochemical properties

The electrochemical properties of the *meso*-arylethynyl BODIPYs were investigated by the cyclic voltametric and differential pulse voltammetric (CV and DPV) techniques (Figure 5.5) and corresponding data is displayed in Table 5.2. The potentials were referenced against Fc/Fc⁺ as per IUPAC guidelines.^[13] The redox peaks were mostly irreversible or quasi reversible. The BODIPYs **2a** – **2h** show two oxidation and two reduction waves corresponding to the formation of dication and dianion radical respectively. Stronger the D-A interaction, better will be the delocalization of electrons from the donor aryl moiety to the acceptor BODIPY moiety, showing easier oxidation and difficult reduction of the BODIPYs.

Table 5.2. Electrochemical properties of the *meso*-arylethynyl BODIPYs **2a** – **2h**.^a

BODIPY	E ² oxid ^b	E ¹ oxid ^b	E ¹ red ^b	E ² red ^b
2a	1.28	1.07	-1	-1.35
2b	1.13	0.65 (broad)	-1.01	-1.29
2c	1.35	1.1	-0.98	-1.35
2d	1.28	1.07	-0.99	-1.28
2e	1.28	1.07	-1.01	-1.37
2f	1.32	0.99	-1.01	-1.32
2g	1.22 (broad)	0.85	-1	-1.37
2h	1.16 (broad)	0.89	-1	-1.4

^aelectrochemical analysis was performed, in 0.1 M solution of Bu₄NPF₆ in dichloromethane at 100 mV s⁻¹ scan rate, versus Fc/Fc⁺. ^birreversible wave.

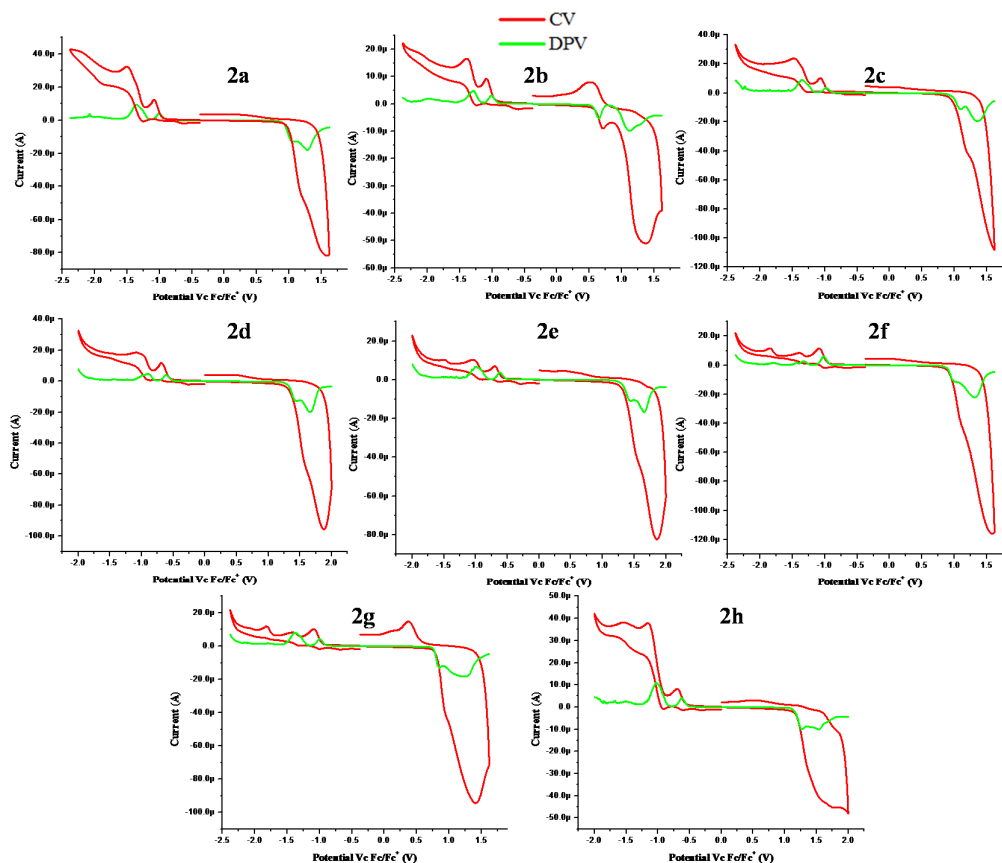


Figure 5.5. Overlaid CV and DPV plots of the *meso*-arylethynyl BODIPY **2a** – **2h**.

The BODIPY **2b** show easiest oxidation and harder reduction indicating the pronounced delocalization of the electron density of the donor triphenylamine moiety to the acceptor BODIPY. On the other hand, the BODIPY **2c** shows easiest reduction and harder oxidation indicating poor delocalization of the electrons of donor aryl group to the acceptor BODIPY. The other BODIPYs show redox peaks at intermediate potentials. The redox properties suggest strong D-A interaction in BODIPYs **2b**, **2g** and **2h**; and moderate D-A interactions in **2a** and **2c** – **2f**.

5.5. Theoretical Calculations

The electronic distribution of the *meso*-arylethynyl BODIPYs could be better understood by DFT calculations. The energy minimized structures show planar orientation of the BODIPY core with respect to the *meso* aryl substituent, which indicates better electronic communication. The energy optimized structures closely resemble with the single crystal structure. The frontier molecular orbital plots are

displayed in Figure 5.6. The LUMO in *meso*-arylethynyl BODIPYs **2b**, **2g** and **2h** is majorly contributed by the BODIPY moiety, and the HOMO is contributed by the arylethynyl moiety, supporting strong D-A interactions. In the *meso*-arylethynyl BODIPYs **2a**, **2c** – **2f** the HOMO is localized on the BODIPY unit and the LUMO is distributed on the whole molecule but majorly on the arylethynyl unit suggesting moderate D-A interactions.

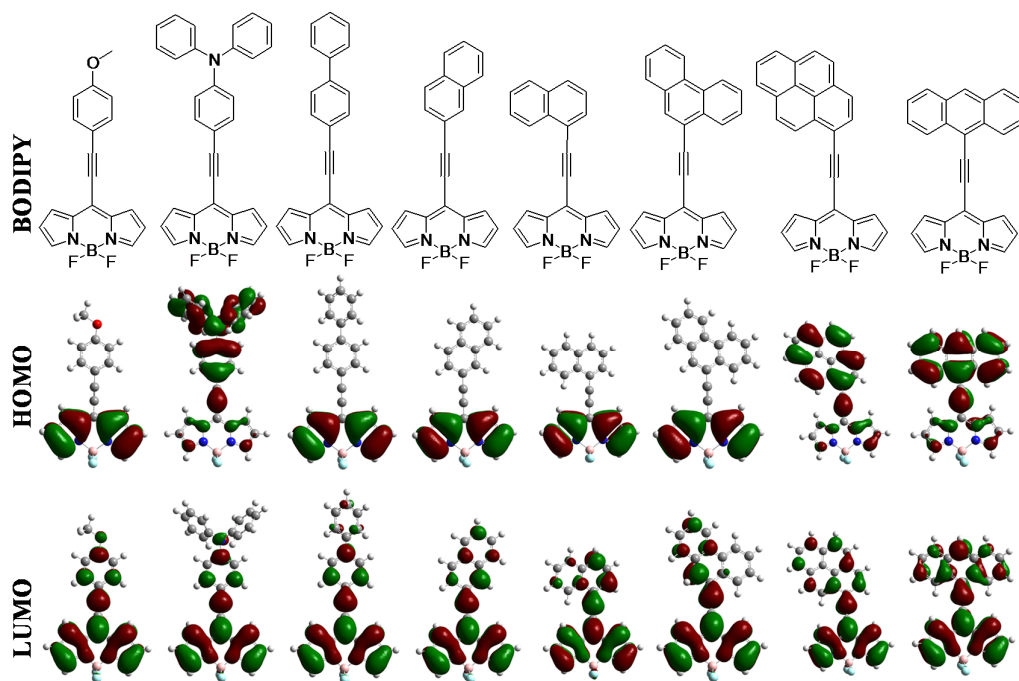


Figure 5.6. HOMO and LUMO frontier molecular orbitals of the *meso*-arylethynyl BODIPYs at the B3LYP/6-31G (d).

5.6. Single crystal X-ray diffraction studies

The single crystals of BODIPYs **2d** and **2e** were obtained by the slow evaporation of mixture of chloroform and hexane solution (1:3 ratio). The BODIPYs **2d** and **2e** crystallizes in the space groups $P2_12_12_1$ and $P2/c$ respectively. The crystal structure and data refinement parameters and the distances and angles of intermolecular interactions in the crystal structures are summarized in Table 5.3 and Table 5.4 respectively.

Table 5.3. Crystal structure and data refinement parameters.

BODIPY	2d	2e
Empirical formula	C ₂₁ H ₁₃ B F ₂ N ₂	C ₂₁ H ₁₃ B F ₂ N ₂
Formula weight	342.14	342.14
Temperature/K	150(2)	150(2)
Crystal system	Orthorhombic	Monoclinic
Space group	<i>P</i> 2 ₁ 2 ₁ 2 ₁	<i>P</i> 2/c
Unit cell dimensions		
a/Å	a = 5.5995(2)	a = 10.1059(3)
α /°	90	90
b/Å	13.5098(4)	b = 10.4411(3)
β /°	90	100.699(3)
c/Å	22.2683(8)	15.6091(5)
γ /°	90	90
Volume/ Å ³	1684.56(10)	1618.39(8)
Z	4	4
Calculated density/ Mg/m ³	1.349	1.404
Absorption coefficient/mm ⁻¹	0.779	0.811
<i>F</i> (000)	704	704
Crystal size/mm	0.21 x 0.18 x 0.13	0.33 x 0.26 x 0.19
θ range from data collection/°	3.83 to 72.10	4.23 to 72.16
Reflections collected/unique	11102 / 3269 [R(int) = 0.0166]	10226 / 3147 [R(int) = 0.0239]
Absorption correction	Semi-empirical from equivalents	Semi-empirical from equivalents
Data/restraints/parameters	3269 / 0 / 236	3147 / 0 / 236
Goodness-of-fit on <i>F</i> ²	1.023	1.090
Final <i>R</i> indices [<i>I</i> > 2 σ (<i>I</i>)]	R ₁ = 0.0281, wR ₂ = 0.0735	R ₁ = 0.0427, wR ₂ = 0.1244
<i>R</i> indices (all data)	R ₁ = 0.0336, wR ₂ = 0.0788	R ₁ = 0.0519, wR ₂ = 0.1387
Largest diff. peak and hole/e Å ⁻³	0.081 and -0.099	0.198 and -0.207
Absolute structure parameter	0.10(14)	-
CCDC number	967406	967407

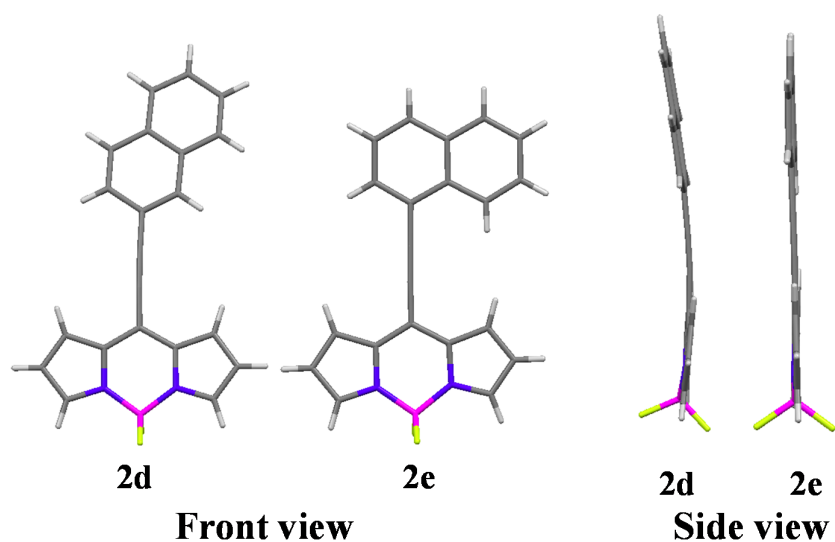


Figure 5.7. Single crystals of BODIPYs **2d** and **2e**, front view and side view.

The crystal structure of the BODIPYs **2d** and **2e** are shown in Figure 5.7. The side view of crystal structures show highly planar orientation of the aryl moiety and BODIPY unit.

Table 5.4. Distance and angle of intermolecular of interactions in the crystal structures.

Interaction	Distance (Å)	Angle of Interaction (°)
2d		
F(1)---H(7)-C(7)	2.355	131.08
F(1)---H(21)-C(21)	2.285	128.27
F(2)---H(9)-C(9)	2.627	119.94
C(17)-H(17)--- π (pyrrolic)	3.044	
π --- π between two BODIPY units	3.383	
2e		
F(1)---H(9)-C(9)	2.467	160.18
F(2)---H(18)-C(18)	2.527	156.97
π --- π between two BODIPY units	3.384	

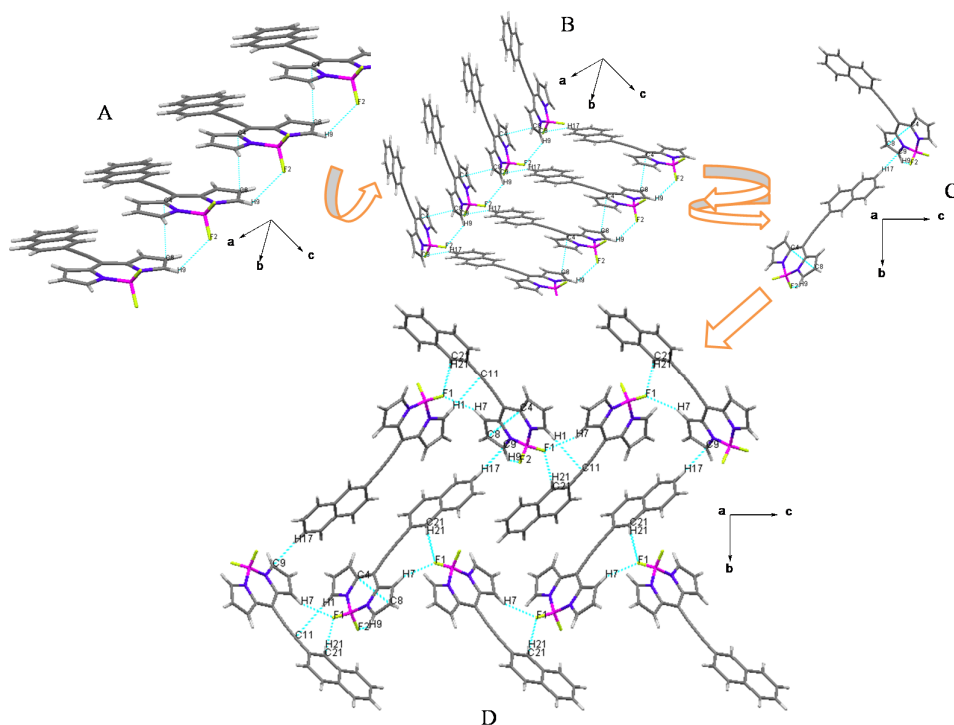


Figure 5.8. Crystal packing of **2d**.

In the packing of BODIPY **2d**, the π - π staking interaction between the two BODIPY units forms staircase like structure. Such a staircase like structure connects another stair case like structure in perpendicular direction via C(17)-H(17)--- π (pyrrolic) interaction, if flipped to view along *a*-axis it looks L-shaped, hiding behind the π -stacked molecules. The L-shaped structure further grows to form complex 3-D structural motif (Figure 5.8).

Similarly in the crystal structure of **2e** two molecules connect to each other in head to tail fashion via another molecule by two mutual F(1)---H(9)-C(9); and a F(2)---H(18)-C(18) interactions forming 2D chain. Such two chains connect to another chain in anti-parallel fashion by face to face π --- π staking interactions between two BODIPY units (Figure 5.9a), these chains further cross links to other chains forming complex 3D packing diagram along tilted *c*-axis. In the packing diagram the molecules orient in such a way that the aryl part of the BODIPY units is at the centre and surrounded by the BODIPY moiety (Figure 5.9b).

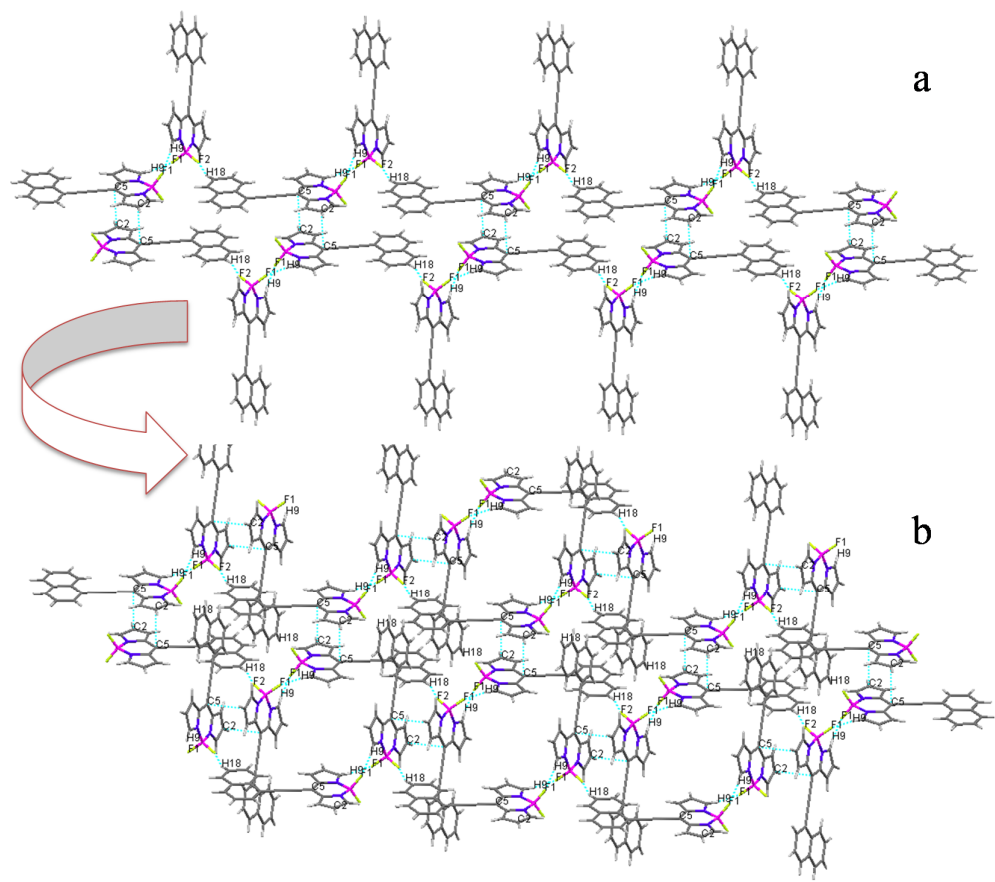


Figure 5.9. Crystal packing of **2e** along tilted *b*-axis

5.7. Experimental section

Generalized procedure for Sonogashira coupling reaction- 8-chloro BODIPY **1** (190 mg, 0.845 mmol), and corresponding arylethyne (0.845 mmol) were dissolved in THF:triethylamine (10:1,v/v; 5 ml), and the mixture was cooled to 0 °C using an ice bath. The reaction mixture was purged with argon, and Pd(PPh₃)₂Cl₂ (29.6 mg, 5 mol%), and CuI (16 mg, 10 mol%) were added, followed by stirring at 0 °C for 30 min. Upon completion of reaction, the mixture was evaporated to dryness, and the crude product was dissolved in CH₂Cl₂, chromatographed on silica (1:1; hexanes:CHCl₃), and recrystallized from chloroform: hexane (1:3) mixture to give **2a – 2h** (yield 44 – 77%) as purple crystalline solid.

BODIPY 2a

Yellow-red crystalline solid. Yield: 77% (110 mg); ^1H NMR (CDCl_3 , 400 MHz, ppm): δ 7.81 (s, 2H), 7.61 (d, $J = 8\text{Hz}$, 2H), 7.38 (d, $J = 4\text{Hz}$, 2H), 6.96 (d, $J = 8\text{Hz}$, 2H), 6.34 (d, $J = 4\text{Hz}$, 2H) 3.88 (s, 3H); ^{13}C NMR (CDCl_3 , 100 MHz, ppm): 162.2, 143.1, 136.5, 135.0, 128.9, 128.3, 118.2, 114.8, 113.0, 107.7, 84.4, 55.7; HRMS (ESI-TOF) m/z = calculated for $\text{C}_{18}\text{H}_{13}\text{BF}_2\text{N}_2\text{O}+\text{Na}^+$ = 345.0984, measured 345.0988.

BODIPY 2b

Dark purple crystalline solid. Yield: 44% (90 mg); ^1H NMR (CDCl_3 , 400 MHz, ppm): δ 7.79 (s, 1H), 7.47 (d, $J = 9\text{Hz}$, 2H), 7.34 (m, 6H), 7.17 (m, 6H), 7.01 (d, $J = 8.8\text{Hz}$, 2H) 6.52 (d, $J = 3\text{Hz}$, 2H); ^{13}C NMR (CDCl_3 , 100 MHz, ppm): 150.8, 146.3, 142.6, 136.3, 134.5, 129.9, 128.4, 126.2, 125.1, 120.5, 118.00, 112.1, 109.3, 85.6; HRMS (ESI-TOF) m/z = calculated for $\text{C}_{29}\text{H}_{20}\text{BF}_2\text{N}_3+\text{Na}^+$ = 482.1616, measured 482.1615.

BODIPY 2c

Red crystalline solid. Yield: 64% (105 mg); ^1H NMR (CDCl_3 , 400 MHz, ppm): δ 7.84 (s, 2H), 7.74 (d, $J = 8\text{Hz}$, 2H), 7.69 (d, $J = 8\text{Hz}$, 2H) 7.65 (m, 2H), 7.49 (m, 2H), 7.42 (m, 3H), 6.56 (d, $J = 4\text{Hz}$, 2H); ^{13}C NMR (CDCl_3 , 100 MHz, ppm): 144.0, 143.7, 139.8, 136.7, 133.4, 129.2, 128.5, 127.6, 127.5, 127.27, 119.7, 118.5, 106.1, 85.1; HRMS (ESI-TOF) m/z = $[\text{M}+\text{Na}]^+$ calculated for $\text{C}_{23}\text{H}_{15}\text{BF}_2\text{N}_2+\text{Na}^+$ = 391.1193, measured 391.1197.

BODIPY 2d

Red crystalline solid. Yield: 73% (110 mg); ^1H NMR (CDCl_3 , 400 MHz, ppm): δ 8.23 (s, 2H), 7.88 (m, 5H), 7.65 (dd, $J = 1.50\text{Hz}$ and $J = 8.54\text{Hz}$, 1H), 7.59 (m, 2H), 7.47 (d, $J = 4\text{Hz}$, 4H), 6.58 (d, $J = 4\text{Hz}$, 2H); ^{13}C NMR (CDCl_3 , 100 MHz, ppm): 143.8, 136.7, 134.2, 134.1, 132.9, 129.2, 128.9, 128.4, 128.2, 128.1, 127.6, 127.4, 118.5, 118.2, 106.6, 84.7; HRMS (ESI-TOF) m/z = calculated for $\text{C}_{21}\text{H}_{13}\text{BF}_2\text{N}_2+\text{Na}^+$ = 365.1036, measured 365.1039.

BODIPY 2e

Red crystalline solid. Yield: 65% (99 mg); ^1H NMR (CDCl_3 , 400 MHz, ppm): δ 8.35 (dd, $J = 8\text{Hz}$, 1H), 7.02 (d, $J = 8\text{Hz}$, 1H), 7.94 (m, 2H), 7.87 (s, 2H), 7.71 (m, 1H), 7.62 (m, 1H), 7.56 (dd, $J = 8\text{Hz}$, 1H), 7.51 (d, $J = 4\text{Hz}$, 2H); ^{13}C NMR (CDCl_3 , 100 MHz, ppm): 143.8, 136.7, 133.4, 133.3, 133.2, 132.0, 129.2, 129.0, 128.1, 127.5, 127.2, 125.6, 125.5, 118.64, 118.60, 104.4, 89.0; HRMS (ESI-TOF) m/z = calculated for $\text{C}_{21}\text{H}_{13}\text{BF}_2\text{N}_2+\text{Na}^+$ = 365.1036, measured 365.1036.

BODIPY 2f

Red crystalline solid. Yield: 57% (99 mg); ^1H NMR (CDCl_3 , 400 MHz, ppm): δ 8.73 (m, 1H), 8.69 (d, $J = 8\text{Hz}$, 1H), 8.40 (m, 1H), 8.24 (s, 1H), 7.93 (d, $J = 8\text{Hz}$, 1H), 7.88 (s, 2H), 7.77 (m, 3H), 7.67 (m, 1H), 7.52 (d, $J = 2\text{Hz}$, 2H), 6.60 (d, $J = 4\text{Hz}$, 2H); ^{13}C NMR (CDCl_3 , 100 MHz, ppm): 143.8, 136.8, 135.7, 131.6, 130.8, 130.6, 130.3, 129.4, 129.3, 127.9, 127.9, 127.6, 127.4, 126.5, 123.4, 123.0, 118.6, 117.6, 104.7, 88.6; HRMS (ESI-TOF) m/z = calculated for $\text{C}_{25}\text{H}_{15}\text{BF}_2\text{N}_2+\text{Na}^+$ = 515.1193, measured 515.1190.

BODIPY 2g

Dark purple crystalline solid. Yield: 47% (87 mg); ^1H NMR (CDCl_3 , 400 MHz, ppm): δ 8.52 (d, $J = 8\text{Hz}$, 2H), 8.22 (m, 6H), 8.08 (m, 2H), 7.88 (s, 2H), 7.54 (d, $J = 4\text{Hz}$, 2H), 6.61 (d, $J = 8\text{Hz}$, 2H); ^{13}C NMR (CDCl_3 , 100 MHz, ppm): 143.4, 136.6, 133.6, 133.5, 131.2, 131.1, 130.9, 130.1, 130.0, 128.9, 127.7, 127.3, 127.0, 126.9, 124.9, 124.8, 124.5, 124.1, 118.5, 114.9, 106.3; HRMS (ESI-TOF) m/z = calculated for $\text{C}_{27}\text{H}_{15}\text{BF}_2\text{N}_2+\text{Na}^+$ = 439.1193, measured 439.1194.

BODIPY 2h

Dark purple crystalline solid. Yield: 62% (108 mg); ^1H NMR (CDCl_3 , 400 MHz, ppm): δ 8.62 (s, 1H), 8.56 (m, 2H), 8.09 (d, $J = 8\text{Hz}$, 2H), 7.90 (s, 2H), 7.73 (m, 2H), 7.60 (m, 4H), 6.65 (d, $J = 4\text{Hz}$, 2H); ^{13}C NMR (CDCl_3 , 100 MHz, ppm): 143.4, 136.5, 134.1, 132.0, 131.2, 129.5, 129.0, 128.5, 127.5, 126.3, 126.0, 118.6, 114.5, 103.8, 95.9; HRMS (ESI-TOF) m/z = calculated for $\text{C}_{25}\text{H}_{15}\text{BF}_2\text{N}_2+\text{Na}^+$ = 415.1193, measured 415.1198.

5.8. Conclusion

In summary, we have synthesized *meso*-arylethynyl BODIPYs. The photophysical and electrochemical properties of the BODIPYs can be tuned by varying the strength of donor. The DFT calculations, photophysical and electrochemical properties suggest strong donor-acceptor interactions in the BODIPYs **2b**, **2g** and **2h**, and moderate interactions in **2a**, and **2c** – **2f**. The quenching of fluorescence can be used as a measure of the relative electron donating strength of the aryl substituent. The crystal structures show interesting supramolecular interactions.

References

-
- [1] (a) Nepomnyashchii, A. B., & Bard, A. J. (2012). Electrochemistry and Electrogenated Chemiluminescence of BODIPY Dyes. *Accounts of Chemical Research*, 45(11), 1844–1853. <http://doi.org/10.1021/ar200278b>; (b) Nepomnyashchii, A. B., & Bard, A. J. (2012). Electrochemistry and Electrogenated Chemiluminescence of BODIPY Dyes. *Accounts of Chemical Research*, 45(11), 1844–1853. <http://doi.org/10.1021/ar200278b>; (c) Boens, N., Leen, V., & Dehaen, W. (2012). Fluorescent indicators based on BODIPY. *Chemical Society Reviews*, 41(3), 1130–1172. <http://doi.org/10.1039/C1CS15132K>.
- [2] (a) Chen, J., Mizumura, M., Shinokubo, H., & Osuka, A. (2009). Functionalization of Boron Dipyrin (BODIPY) Dyes through Iridium and Rhodium Catalysis: A Complementary Approach to α - and β -Substituted BODIPYs. *Chemistry – A European Journal*, 15(24), 5942–5949. <http://doi.org/10.1002/chem.200802541>; (b) Schmidt, E. Y., Trofimov, B. A., Mikhaleva, A. I., Zorina, N. V., Protzuk, N. I., Petrushenko, K. B., ... Pansu, R. B. (2009). Synthesis and Optical Properties of 2-(Benzo[b]thiophene-3-yl)pyrroles and a New BODIPY Fluorophore (BODIPY=4,4-Difluoro-4-bora-3a,4a-diaza-s-indacene). *Chemistry – A European Journal*, 15(23), 5823–5830. <http://doi.org/10.1002/chem.200802467>; (c) Ulrich, G., Ziesse, R., & Harriman, A. (2008). The Chemistry of Fluorescent Bodipy Dyes: Versatility Unsurpassed. *Angewandte Chemie International Edition*, 47(7), 1184–1201.

-
- <http://doi.org/10.1002/anie.200702070>; (d) Yin, X., Li, Y., Zhu, Y., Jing, X., Li, Y., & Zhu, D. (2010). A highly sensitive viscosity probe based on ferrocene-BODIPY dyads. *Dalton Transactions*, 39(41), 9929–9935. <http://doi.org/10.1039/C0DT00309C>.
- [3] (a) Baruah, M., Qin, W., Vallée, R. A. L., Beljonne, D., Rohand, T., Dehaen, W., & Boens, N. (2005). A Highly Potassium-Selective Ratiometric Fluorescent Indicator Based on BODIPY Azacrown Ether Excitable with Visible Light. *Organic Letters*, 7(20), 4377–4380. <http://doi.org/10.1021/ol051603o>; (b) Rohand, T., Baruah, M., Qin, W., Boens, N., & Dehaen, W. (2006). Functionalisation of fluorescent BODIPY dyes by nucleophilic substitution. *Chemical Communications*, (3), 266–268. <http://doi.org/10.1039/B512756D>; (c) Rohand, T., Qin, W., Boens, N., & Dehaen, W. (2006). Palladium-Catalyzed Coupling Reactions for the Functionalization of BODIPY Dyes with Fluorescence Spanning the Visible Spectrum. *European Journal of Organic Chemistry*, 2006(20), 4658–4663. <http://doi.org/10.1002/ejoc.200600531>; (d) Leen, V., Braeken, E., Luckermans, K., Jackers, C., Van der Auweraer, M., Boens, N., & Dehaen, W. (2009). A versatile, modular synthesis of monofunctionalized BODIPY dyes. *Chemical Communications*, (30), 4515–4517. <http://doi.org/10.1039/B906164A>; (e) Leen, V., Leemans, T., Boens, N., & Dehaen, W. (2011). 2- and 3-Monohalogenated BODIPY Dyes and Their Functionalized Analogues: Synthesis and Spectroscopy. *European Journal of Organic Chemistry*, 2011(23), 4386–4396. <http://doi.org/10.1002/ejoc.201100324>; (f) Li, L., Nguyen, B., & Burgess, K. (2008). Functionalization of the 4,4-difluoro-4-bora-3a,4a-diaza-s-indacene (BODIPY) core. *Bioorganic & Medicinal Chemistry Letters*, 18(10), 3112–3116. <http://doi.org/http://dx.doi.org/10.1016/j.bmcl.2007.10.103>; (g) Han, J., Gonzalez, O., Aguilar-Aguilar, A., Pena-Cabrera, E., & Burgess, K. (2009). 3- and 5-Functionalized BODIPYs via the Liebeskind-Srogl reaction. *Organic & Biomolecular Chemistry*, 7(1), 34–36. <http://doi.org/10.1039/B818390B>.
- [4] (a) Gautam, P., Dhokale, B., Shukla, V., Singh, C. P., Bindra, K. S., & Misra, R. (2012). Optical limiting performance of *meso*-tetraferrocenyl porphyrin and its metal derivatives. *Journal of Photochemistry and Photobiology A: Chemistry*, 239(0), 24–27. <http://doi.org/http://dx.doi.org/10.1016/j.jphotochem.2012>.

04.020; (b) Dhokale, B., Gautam, P., & Misra, R. (2012). Donor-acceptor perylenediimide-ferrocene conjugates: synthesis, photophysical, and electrochemical properties. *Tetrahedron Letters*, 53(18), 2352–2354. <http://doi.org/http://dx.doi.org/10.1016/j.tetlet.2012.02.107>; (c) Gautam, P., Dhokale, B., Mobin, S. M., & Misra, R. (2012). Ferrocenyl BODIPYs: synthesis, structure and properties. *RSC Advances*, 2(32), 12105–12107. <http://doi.org/10.1039/C2RA21964F>; (d) Maragani, R., Jadhav, T., Mobin, S. M., & Misra, R. (2012). Synthesis, structure, photophysical, and electrochemical properties of donor-acceptor ferrocenyl derivatives. *Tetrahedron*, 68(36), 7302–7308. <http://doi.org/http://dx.doi.org/10.1016/j.tet.2012.06.094>; (e) Dhokale, B., Gautam, P., Mobin, S. M., & Misra, R. (2013). Donor-acceptor, ferrocenyl substituted BODIPYs with marvelous supramolecular interactions. *Dalton Transactions*, 42(5), 1512–1518. <http://doi.org/10.1039/C2DT31632C>; (f) Dhokale, B., Gautam, P., Mobin, S. M., & Misra, R. (2013). Donor-acceptor, ferrocenyl substituted BODIPYs with marvelous supramolecular interactions. *Dalton Transactions*, 42(5), 1512–1518. <http://doi.org/10.1039/C2DT31632C>; (g) Misra, R., Gautam, P., Sharma, R., & Mobin, S. M. (2013). Donor- π -acceptor- π -donor ferrocenyl benzothiadiazoles: synthesis, structure, and properties. *Tetrahedron Letters*, 54(5), 381–383. <http://doi.org/http://dx.doi.org/10.1016/j.tetlet.2012.11.016>; (h) Jadhav, T., Maragani, R., Misra, R., Sreeramulu, V., Rao, D. N., & Mobin, S. M. (2013). Design and synthesis of donor-acceptor pyrazabole derivatives for multiphoton absorption. *Dalton Transactions*, 42(13), 4340–4342. <http://doi.org/10.1039/C3DT33065F>; (i) Sharma, R., Gautam, P., Mobin, S. M., & Misra, R. (2013). [small beta]-Substituted ferrocenyl porphyrins: synthesis, structure, and properties. *Dalton Transactions*, 42(15), 5539–5545. <http://doi.org/10.1039/C3DT00003F>; (j) Misra, R., Gautam, P., Jadhav, T., & Mobin, S. M. (2013). Donor-Acceptor Ferrocenyl-Substituted Benzothiadiazoles: Synthesis, Structure, and Properties. *The Journal of Organic Chemistry*, 78(10), 4940–4948. <http://doi.org/10.1021/jo4005734>; (j) Sharma, R., Margani, R., Mobin, S. M., & Misra, R. (2013). Ferrocenyl substituted calixarenes: synthesis, structure and properties. *RSC Advances*, 3(17), 5785–5788. <http://doi.org/10.1039/C3RA00146F>; (k) Misra, R., Jadhav,

-
- T., & Mobin, S. M. (2013). Aryl pyrazaboles: a new class of tunable and highly fluorescent materials. *Dalton Transactions*, 42(47), 16614–16620. <http://doi.org/10.1039/C3DT52154K>; (l) Maragani, R., & Misra, R. (2013). Donor–acceptor ferrocenyl triazines: synthesis and properties. *Tetrahedron Letters*, 54(39), 5399–5402. <http://doi.org/http://dx.doi.org/10.1016/j.tetlet.2013.07.119>.
- [5] Yin, X., Li, Y., Li, Y., Zhu, Y., Tang, X., Zheng, H., & Zhu, D. (2009). Electrochromism based on the charge transfer process in a ferrocene–BODIPY molecule. *Tetrahedron*, 65(40), 8373–8377. <http://doi.org/http://dx.doi.org/10.1016/j.tet.2009.08.008>.
- [6] (a) Jiao, L., Pang, W., Zhou, J., Wei, Y., Mu, X., Bai, G., & Hao, E. (2011). Regioselective Stepwise Bromination of Boron Dipyrromethene (BODIPY) Dyes. *The Journal of Organic Chemistry*, 76(24), 9988–9996. <http://doi.org/10.1021/jo201754m>; (b) Godoy, J., Vives, G., & Tour, J. M. (2010). Synthesis of Highly Fluorescent BODIPY-Based Nanocars. *Organic Letters*, 12(7), 1464–1467. <http://doi.org/10.1021/ol100108r>; (c) Ortiz, M. J., Agarrabeitia, A. R., Duran-Sampedro, G., Bañuelos Prieto, J., Lopez, T. A., Massad, W. A., ... Lopez Arbeloa, I. (2012). Synthesis and functionalization of new polyhalogenated BODIPY dyes. Study of their photophysical properties and singlet oxygen generation. *Tetrahedron*, 68(4), 1153–1162. <http://doi.org/http://dx.doi.org/10.1016/j.tet.2011.11.070>; (d) Baruah, M., Qin, W., Basarić, N., De Borggraeve, W. M., & Boens, N. (2005). BODIPY-Based Hydroxyaryl Derivatives as Fluorescent pH Probes. *The Journal of Organic Chemistry*, 70(10), 4152–4157. <http://doi.org/10.1021/jo0503714>.
- [7] Leen, V., Yuan, P., Wang, L., Boens, N., & Dehaen, W. (2012). Synthesis of *Meso*-Halogenated BODIPYs and Access to *Meso*-Substituted Analogues. *Organic Letters*, 14(24), 6150–6153. <http://doi.org/10.1021/ol3028225>.
- [8] (a) Kusaka, S., Sakamoto, R., Kitagawa, Y., Okumura, M., & Nishihara, H. (2013). *meso*-Alkynyl BODIPYs: Structure, Photoproperties, π -Extension, and Manipulation of Frontier Orbitals. *Chemistry – An Asian Journal*, 8(4), 723–727. <http://doi.org/10.1002/asia.201201176>; (b) Graf, K., Korzdorfer, T., Kummel, S., & Thelakkat, M. (2013). Synthesis of donor-substituted *meso*-phenyl and *meso*-ethynylphenyl BODIPYs with broad absorption. *New Journal*

-
- of Chemistry*, 37(5), 1417–1426. <http://doi.org/10.1039/C3NJ00157A>; (c) Misra, R., Dhokale, B., Jadhav, T., & Mobin, S. M. (2013). Donor-acceptor *meso*-alkynylated ferrocenyl BODIPYs: synthesis, structure, and properties. *Dalton Transactions*, 42(37), 13658–13666. <http://doi.org/10.1039/C3DT51374B>.
- [9] (a) Plater, M. J., Aiken, S., & Bourhill, G. (2002). A new synthetic route to donor-acceptor porphyrins. *Tetrahedron*, 58(12), 2405–2413. [http://doi.org/http://dx.doi.org/10.1016/S0040-4020\(02\)00109-6](http://doi.org/http://dx.doi.org/10.1016/S0040-4020(02)00109-6); (b) Kim, D., Yamamoto, K., & Ahn, K. H. (2012). A BODIPY-based reactive probe for ratiometric fluorescence sensing of mercury ions. *Tetrahedron*, 68(26), 5279–5282. <http://doi.org/http://dx.doi.org/10.1016/j.tet.2012.01.091>.
- [10] (a) Feng, Y.-S., Xie, C.-Q., Qiao, W.-L., & Xu, H.-J. (2013). Palladium-Catalyzed Trifluoroethylation of Terminal Alkynes with 1,1,1-Trifluoro-2-iodoethane. *Organic Letters*, 15(4), 936–939. <http://doi.org/10.1021/ol400099h>; (b) Panthi, K., Adhikari, R. M., & Kinstle, T. H. (2010). Aromatic Fumaronitrile Core-Based Donor-Linker-Acceptor-Linker-Donor (D- π -A- π -D) Compounds: Synthesis and Photophysical Properties. *The Journal of Physical Chemistry A*, 114(13), 4542–4549. <http://doi.org/10.1021/jp9115589>; (c) Hachiya, S., Asai, K., & Konishi, G. (2013). Unique solvent-dependent fluorescence of nitro-group-containing naphthalene derivatives with weak donor-strong acceptor system. *Tetrahedron Letters*, 54(14), 1839–1841. <http://doi.org/http://dx.doi.org/10.1016/j.tetlet.2013.01.096>; (d) Yang, Y., Ji, S., Zhou, F., & Zhao, J. (2009). Synthesis of novel bispyrene diamines and their application as ratiometric fluorescent probes for detection of DNA. *Biosensors and Bioelectronics*, 24(12), 3442–3447. <http://doi.org/http://dx.doi.org/10.1016/j.bios.2009.04.018>; (e) Nierth, A., Kobitski, A. Y., Nienhaus, G. U., & Jäschke, A. (2010). Anthracene-BODIPY Dyads as Fluorescent Sensors for Biocatalytic Diels-Alder Reactions. *Journal of the American Chemical Society*, 132(8), 2646–2654. <http://doi.org/10.1021/ja9084397>; (f) Sarobe, M., Jenneskens, L. W., Wesseling, J., Snoeijer, J. D., & Zwikker, J. W. (1997). Thermal Interconversions of the C₁₆H₁₀ Cyclopenta-Fused Polycyclic Aromatic Hydrocarbons Fluoranthene, Acephenanthrylene and Aceanthrylene

-
- Revisited. *Liebigs Annalen*, 1997(6), 1207–1213. <http://doi.org/10.1002/jlac.199719970624>.
- [11] Ziessel, R., Retailleau, P., Elliott, K. J., & Harriman, A. (2009). Boron Dipyrin Dyes Exhibiting “Push–Pull–Pull” Electronic Signatures. *Chemistry – A European Journal*, 15(40), 10369–10374. <http://doi.org/10.1002/chem.200901725>.
- [12] Yang, P., Zhao, J., Wu, W., Yu, X., & Liu, Y. (2012). Accessing the Long-Lived Triplet Excited States in Bodipy-Conjugated 2-(2-Hydroxyphenyl) Benzothiazole/Benzoxazoles and Applications as Organic Triplet Photosensitizers for Photooxidations. *The Journal of Organic Chemistry*, 77(14), 6166–6178. <http://doi.org/10.1021/jo300943t>.
- [13] Gritzner G, & Kuta J. (1984). Recommendations on reporting electrode potentials in nonaqueous solvents (Recommendations 1983). *Pure and Applied Chemistry*. <http://doi.org/10.1351/pac198456040461>.

Chapter 6

***Meso* Heteroatom connected ferrocenyl BODIPYs**

6.1. Introduction

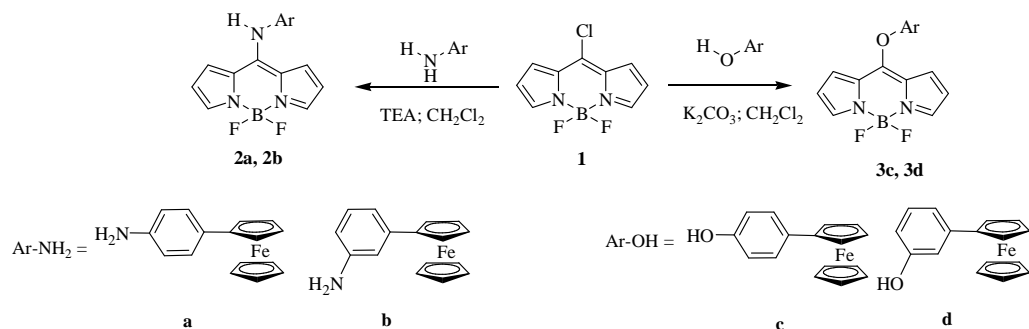
BODIPY dyes have attracted the attention of the scientific community because of its unique photophysical properties such as strong electronic absorption with high extinction coefficient, high luminescence efficiency, high thermal and photochemical stability, and their potential applications in laser dyes, chemosensors, organogelators, NIR-absorbing dyes, organic photovoltaics, and two-photon absorbing materials.^[1]

In recent years various strategies have been developed for the functionalization of the BODIPYs at α , β and *meso* positions.^[2] The halogenations at these positions are straight forward route for the functionalisation of the BODIPY. Usually the halogenation of the dipyrromethane results in α -halogenated BODIPYs whereas direct halogenation of the BODIPY results in β -halogenated BODIPYs.^[3]

Wim Dehaen *et al.* have developed the synthetic route for the halogenation at the *meso* position of the BODIPY (8-halogenated BODIPYs).^[4] The halogen group at the *meso* position of the BODIPY undergoes rapid substitution and coupling reactions. We have studied the Sonogashira coupling reaction at the *meso* position of the BODIPY.^[5] We were further interested in the nucleophilic aromatic substitution reaction of 8-chloro BODIPYs **1** with substituted phenols and anilines and to see the effect of heteroatom and aromatic substituents on the photophysical and electrochemical properties. The ferrocenyl derivatives are of great interest because of their applications in nonlinear optics, sensors and asymmetric catalysis.^[6] Our group is interested in the ferrocene based molecular systems for various photonic applications.^[7] In this context we have chosen the *para* and *meta* linked ferrocenyl anilines (**a** and **b**) and ferrocenyl phenols (**c** and **d**), and treated them with 8-chloro BODIPY **1**. The heteroatoms (O and N) at the *meso* position are known to destabilize the LOMO energy level of the BODIPYs.^[8] Therefore use of substituted anilines and phenols will have pronounced effect on the energy levels and optoelectronic properties of the BODIPY. We were interested to explore the effect

of heteroatom (O versus N) and ferrocenyl group on the photophysical, electrochemical and structural properties of these molecular systems.

6.2. Results and Discussion



Scheme 6.1. Synthesis of heteroatom connected ferrocenyl BODIPYs **2a**, **2b**, **3c** and **3d**.

The heteroatom connected ferrocenyl BODIPYs **2a**, **2b**, **3c** and **3d** were synthesized by the $\text{S}_{\text{N}}\text{Ar}$ type substitution reactions of 8-chloro BODIPY **1** with the corresponding ferrocenyl anilines (**a** and **b**) and ferrocenyl phenols (**c** and **d**) (Scheme 6.1). The precursors, ferrocenyl anilines (**a** and **b**) were synthesized by the diazotization reaction of nitroanilines with ferrocene followed by reduction with Sn/HCl , whereas the ferrocenyl phenols (**c** and **d**) were synthesized by the diazotization reaction of the aminophenols with ferrocene.^[9] The reaction of 8-chloro BODIPY **1** with 4-ferrocenyl aniline (**a**) and 3-ferrocenyl aniline (**b**) in the presence of triethylamine as base in CH_2Cl_2 resulted **2a** and **2b** in 64% and 60% yields respectively. On the other hand, the reaction of the 8-chloro BODIPY **1** with 4-ferrocenylphenol (**c**) and 3-ferrocenylphenol (**d**) in the presence of K_2CO_3 as base in CH_2Cl_2 resulted **3c** and **3d** in 62% and 60% yields respectively. BODIPY **4** was synthesized by previously reported procedure.^[4]

All the ferrocenyl BODIPYs were well characterized by ^1H , ^{13}C , ^{11}B and ^{19}F NMR, HRMS, elemental analysis and single crystal X - ray crystallographic techniques. The ^1H NMR spectra of the heteroatom connected ferrocenyl BODIPYs **2a**, **2b**, **3c** and **3d** exhibit the ferrocenyl protons in the 4.0 - 4.7 ppm region, and the phenyl protons in the 7.0 - 7.8 ppm region with typical di - substitution splitting pattern. The α pyrrolic protons appear at ~ 7.7 ppm as singlet, while the β and β' protons appear at ~ 6.4 and 6.7 ppm as doublets. All the ferrocenyl BODIPYs show as usual triplet at ~ 0 ppm in ^{11}B NMR.

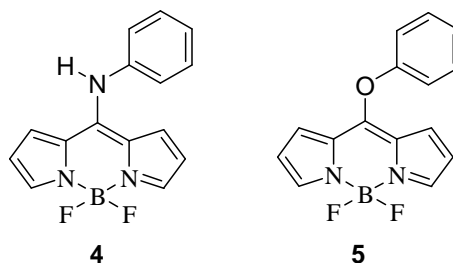


Chart 6.1. Previously reported aniline and phenol substituted BODIPYs.

6.3. Thermogravimetric Analysis

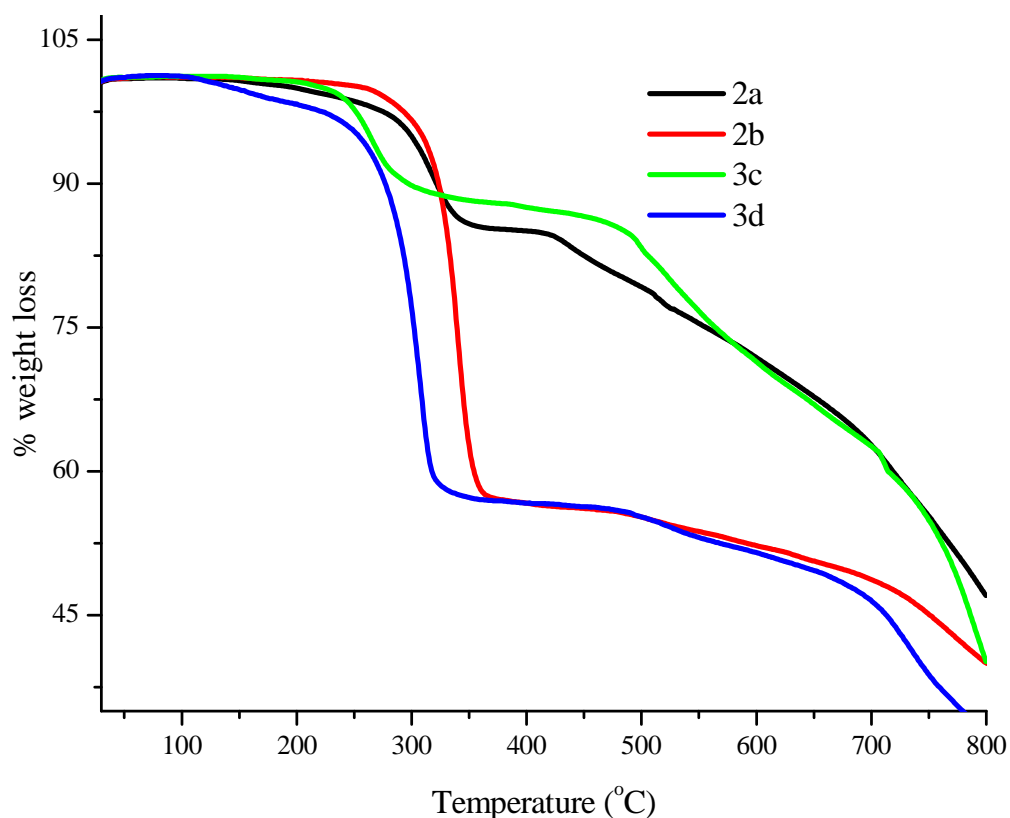


Figure 6.1. TGA plots of the heteroatom connected ferrocenyl BODIPYs **2a**, **2b**, **3c** and **3d** recorded at the heating rate of $10\text{ }^{\circ}\text{C min}^{-1}$ under nitrogen atmosphere.

The thermal stability is one of the key criterions for the optoelectronic applications of any material. The thermal properties of the heteroatom connected ferrocenyl BODIPYs **2a**, **2b**, **3c** and **3d** were investigated by thermogravimetric analysis (TGA), at $10\text{ }^{\circ}\text{C min}^{-1}$ heating rate under inert atmosphere (Figure 6.1). The thermal decomposition temperatures (T_d) at 5 % weight loss are shown in Table 6.1. The trend in thermal stability follows the order **2a-2b**>**3c**>**3d**. The BODIPYs **2b** and **3d** show sudden weight loss of 60 % at 360 °C and 310 °C respectively. This

suggests that the *para* isomers are thermally more stable than their *meta* isomers. The heteroatom connected ferrocenyl BODIPYs (**2a**, **2b**, **3c** and **3d**) possess good thermal stability up to 275 °C. Our previously reported *meso*-alkynylated ferrocenyl BODIPYs exhibit thermal stability up to 400 °C. This shows that the substitution at the *meso* position via heteroatom lowers the thermal stability of BODIPY.

6.4. Photophysical Properties

Figure 6.2 displays the color of the BODIPYs **1**, **2a**, **2b**, **3c** and **3d**, in dichloromethane. The BODIPY **1** show lime green color. The *meta* substituted BODIPYs **2b** and **3d** show yellow color, while *para* substituted BODIPYs **2a** and **3c** show yellowish-red color in solution. The UV-vis absorption spectra of the BODIPYs **1**, **2a**, **2b**, **3c** and **3d** were recorded in dichloromethane at room temperature (Figure 6.3) and the corresponding data are listed in Table 6.1.

Table 6.1. Optical, electrochemical and thermal properties of the BODIPYs **1**, **2a**, **2b**, **3c** and **3d**.

BODIPY	Optical data ^a		Electrochemical data ^d				T _d ^e (°C)
	λ_{abs} (max) ^b (nm)	$\epsilon/10^4$ (Mol ⁻¹ .cm ⁻¹) ^c	E ² _{oxi} (BODIPY)	E ¹ _{oxi} (Fc)	E ¹ _{red} (BODIPY)	E ² _{red} (BODIPY)	
1	503	9.8	1.31	--	-0.96	-1.32	193
2a	418	5.2	1.06	0.06	-1.19	-1.39	300
2b	419	5.1	1.12	0.03	-1.21	-1.39	309
3c	455	5.7	1.07	0.06	-1.14	-1.25	264
3d	455	6.5	1.12	0.10	-1.24	-1.28	254

^aMeasured in CH₂Cl₂. ^bAbsorption maxima. ^cExtinction coefficient recorded at λ_{abs} (max),

^dElectrochemical analysis was performed in 0.1 M solution of Bu₄NPF₆ in CH₂Cl₂ at 100 mVs⁻¹ scan rate versus Fc/Fc⁺, all potentials are expressed in unit volt (V). ^eThermal decomposition temperature at 5% weight loss, determined by TGA.

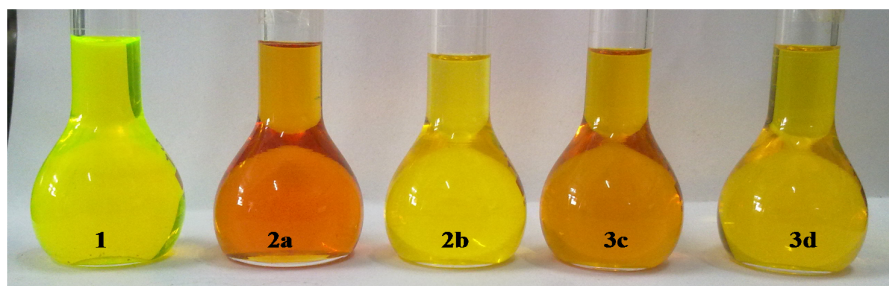


Figure 6.2. 8-chloro BODIPY **1**, and heteroatom connected ferrocenyl BODIPYs **2a**, **2b**, **3c** and **3d** in dichloromethane at 10^{-4} M concentration.

The 8-chloro BODIPY **1**, show strong absorption band at 503 nm due to $S_0 \rightarrow S_1$ absorption, whereas the heteroatom connected ferrocenyl BODIPYs **2a**, **2b**, **3c** and **3d** show blue shifted absorption band at 418, 419, 455 and 455 nm respectively, which was assigned to HOMO-2 \rightarrow LUMO and HOMO-3 \rightarrow LUMO transitions (TD-DFT calculations). The blue shift in the absorption is attributed to the delocalization of the lone pair electrons of *meso* substituted heteroatom into the electron deficient BODIPY to form cross-conjugated hemicyanine or merocyanine resonance structures.^[8] The higher electron releasing ability of the nitrogen than oxygen resulted more pronounced blue shift in the absorption band of the ferrocenyl BODIPYs **2a** and **2b** than **3c** and **3d**. In order to explore the effect of ferrocenyl group on the photonic properties of the BODIPYs (**2a**, **2b**, **3c** and **3d**), their properties were compared with the aniline and phenol substituted BODIPY derivatives **4** and **5** (chart 6.1). The BODIPYs **2a**, **2b** and **4** ($\lambda_{\text{max}} = 419\text{nm}$)^[10] absorb at the similar wavelength, similarly the BODIPYs **3c**, **3d** and **5** ($\lambda_{\text{max}} = 455\text{nm}$) absorb at the similar wavelength. This indicates that the ferrocenyl group has negligible effect on the electronic absorption. The heteroatom connected ferrocenyl BODIPYs **2a**, **2b**, **3c** and **3d** are non-emissive in nature. The phenol substituted BODIPY **5** (Chart 1) show high fluorescence ($\phi = 0.88$). Therefore the quenching of fluorescence can be attributed to the fast non radiative deactivation of the excited state with intramolecular charge transfer from the donor ferrocenyl unit to the acceptor BODIPY moiety.^[11]

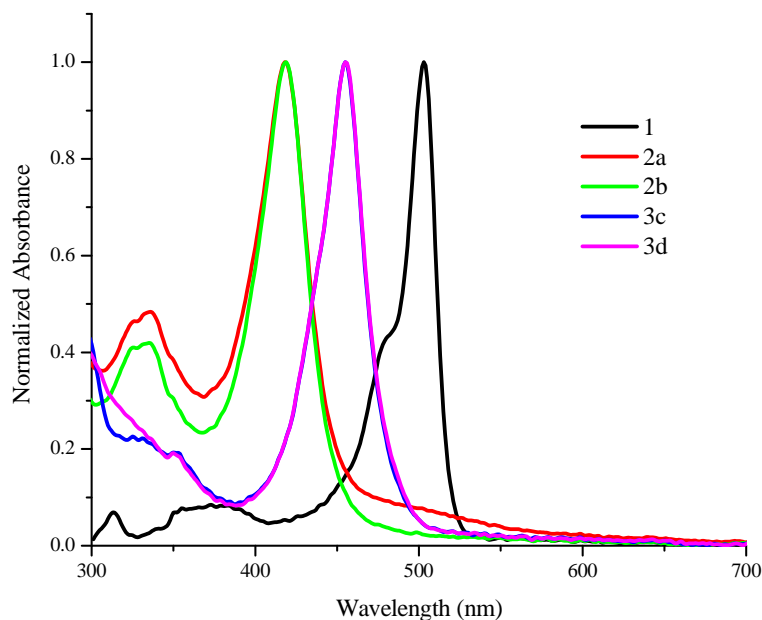


Figure 6.3. Normalized electronic absorption spectra of the 8-chloro BODIPY **1** and the heteroatom connected ferrocenyl BODIPYs **2a**, **2b**, **3c** and **3d** in dichloromethane.

6.5. Electrochemical properties

The electrochemical properties of the heteroatom connected ferrocenyl BODIPYs **2a**, **2b**, **3c** and **3d** were explored by the cyclic voltammetric (CV) and differential pulse voltammetric (DPV) analyses. The overlaid CV and DPV are shown in Figure 6.4 and the corresponding data are given in Table 6.1. The heteroatom connected ferrocenyl BODIPYs exhibit two reduction waves corresponding to the reduction of BODIPY moiety, and two oxidation waves, one attributed to the oxidation of ferrocenyl unit and another due to the BODIPY unit. The redox waves due to the BODIPY moiety are irreversible, while the ferrocenyl oxidation wave is reversible. The first oxidation potentials are similar in BODIPYs **2a** and **3c**, on the other hand it varies substantially in **2b** and **3d**. The first oxidation indicates the removal of an electron from π (HOMO) orbital and first reduction indicates the addition of an electron to the π^* (LUMO) orbital. The first oxidation potentials of the BODIPYs **2a** and **3c** indicate similar energies of HOMOs, whereas the first reduction potential indicate the easier reduction of the BODIPY **3c** than BODIPY **2a** indicating the lowering of LUMO in **3c** than **2a**. In case of **3c** the poor

electron delocalization on the BODIPY favors the easier reduction. The BODIPY **3d** shows exceptionally harder oxidation and reduction.

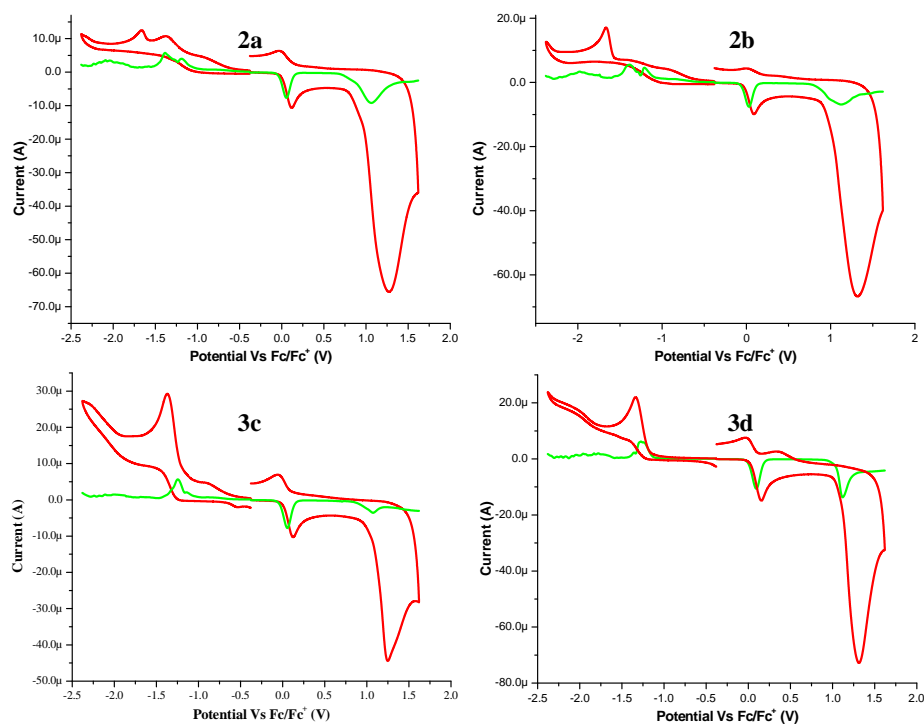


Figure 6.4. Cyclic voltammogram and differential pulse voltammogram of the heteroatom connected ferrocenyl BODIPY **2a**, **2b**, **3c** and **3d**.

6.6. Theoretical Calculations

Table 6.2. Computed vertical transitions and their oscillator strengths and configurations of BODIPY **3c**.

BODIPY	DCM		
	$\lambda_{\text{max}}[\text{nm}]$	f	Configuration
3c	423.65	0.0509	HOMO-2→LUMO (0.55073)
			HOMO-3→LUMO (-0.42994)
	409.28	0.6567	HOMO-2→LUMO (0.42888)
			HOMO-3→LUMO (0.55294)

To gain insight into the geometrical and electronic structures of the heteroatom connected ferrocenyl BODIPYs **2a**, **2b**, **3c** and **3d** computational studies were performed using density functional theory (DFT) at B3LYP/6-31G** for C, N, B, F, H, O and Lan12DZ for Fe level. The DFT optimized structures closely resemble to the crystal structures, with slight variation in bond lengths and bond angles. The comparison of the selected bond lengths of the DFT optimized structures and crystal structures are shown in Figure 6.5. In the DFT optimized structures the boron atom is away from the average plane of BODIPY central ring whereas in the crystal structures it lies in the plane of the BODIPY. Figure 6.6 visualizes the difference in planarity in the crystal structure and DFT optimized structure.

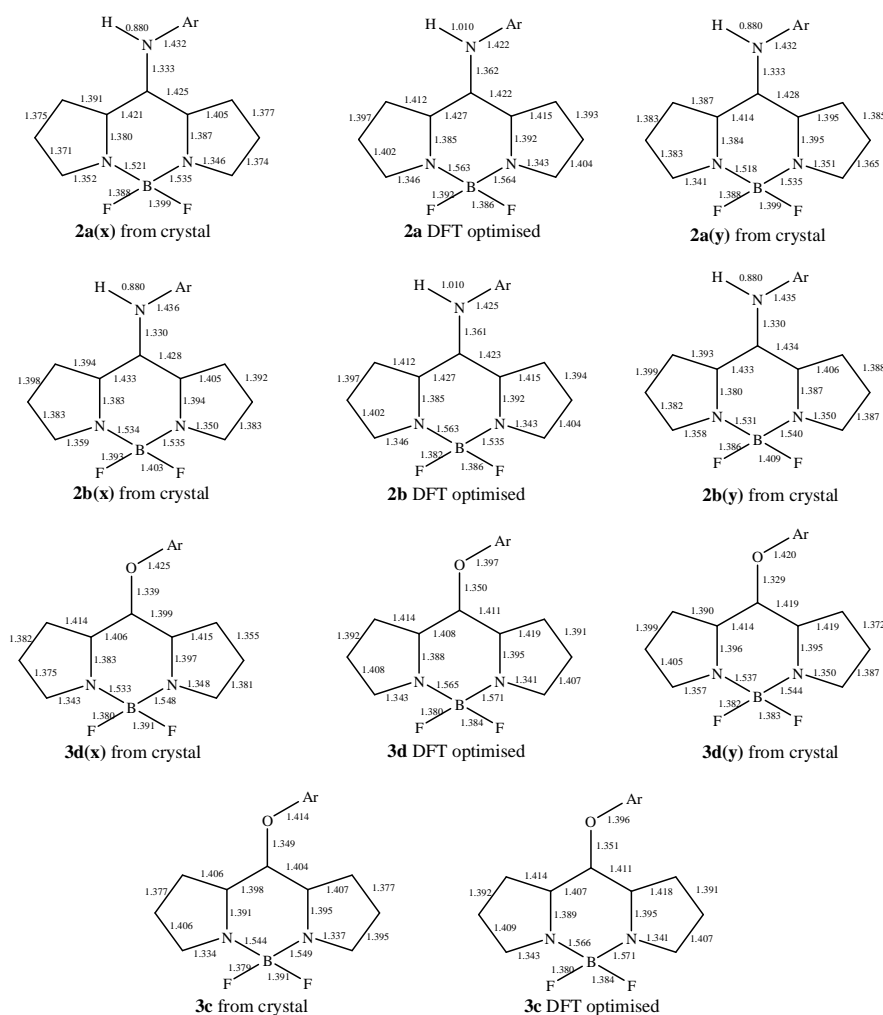


Figure 6.5. Comparison of selected bond lengths of the crystal structures and DFT optimized structures of the heteroatom connected ferrocenyl BODIPYs **2a**, **2b**, **3c** and **3d** (x and y represents two different molecules in an asymmetric unit).

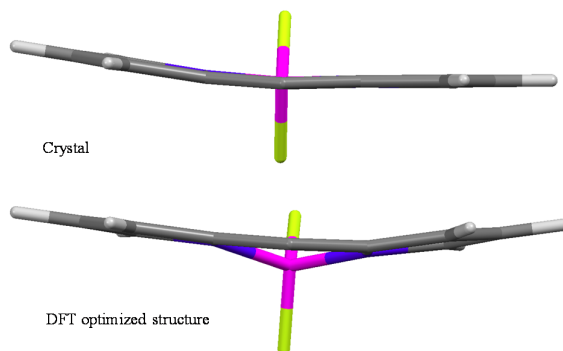


Figure 6.6. Comparison of the planarity of the BODIPY central ring in the crystal structure and the DFT optimized structure of **2a** (top view).

The energy level diagram of the frontier molecular orbitals of the BODIPYs **1**, **2a**, **2b**, **3c**, **3d**, **4** and **5**, estimated by DFT calculations are shown in Figure 6.7. In the BODIPYs **2a** and **3c** the HOMOs are at the same energy level, but the LUMO in **3c** is lower in energy compared to **2a**. Similar trend was observed in the BODIPYs **2b** and **3d**, and in the BODIPYs **4** and **5**. This indicates that the nature of heteroatom at the *meso* position does not affect the HOMO energy level considerably, but show pronounced effect on the LUMO. The O-atom at the *meso* position of the BODIPY stabilizes the LUMO better than N-atom. The delocalization of the lone pair of electrons of the *meso* substituted heteroatom is more pronounced in (N-) **2a** and **2b**, than (O-) **3c** and **3d**, which is also evident from the molecular electrostatic potential maps, shown in Figure 6.8. The *meso* substituted nitrogen atom carries positive potential (blue color), and the fluorines show negative potentials (brown color). These observations are in good agreement with the optical and electrochemical properties. The first oxidation potential in the BODIPYs **2a** and **3c** are similar (similar HOMO), but the first reduction in **3c** is easier than **2a** (lowering of LUMO in **3c** than **2a**).^[12]

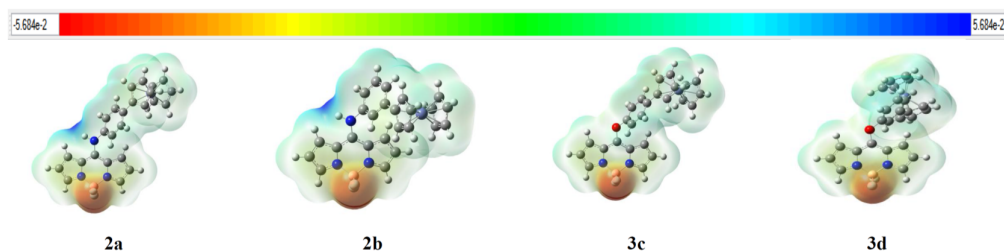


Figure 6.8. Electrostatic potential map of heteroatom connected ferrocenyl BODIPYs **2a**, **2b**, **3c** and **3d**. Red = lowest potential (electron-rich) and blue = highest potential (electron-poor). Calculated by Gaussian 09W.

The energy level diagram (Figure 6.7) reveals that the LUMO energy level of BODIPYs **2a**, **2b** and **4** are almost at same energy level but the HOMO of BODIPYs **2a** and **2b** destabilized than BODIPY **4**, and the extent of destabilization is more pronounced in case of HOMO-1 and HOMO-2. Similar trend was observed in the BODIPYs **3c**, **3d** and **5**. This observation indicates that the ferrocenyl group has negligible effect on the LUMO but shows pronounced effect on the energy of HOMOs.

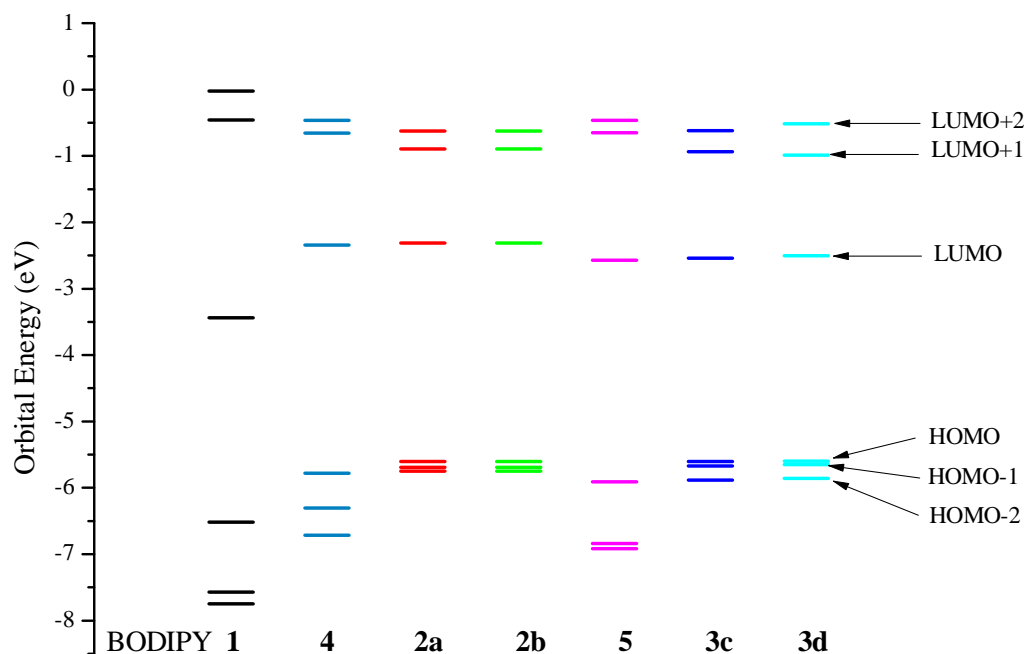


Figure 6.7. Energy level diagram of the frontier molecular orbitals of the BODIPYs **1**, **4**, **2a**, **2b**, **5**, **3c** and **3d** estimated by DFT calculations.

The frontier molecular orbitals of the BODIPYs **2a**, **2b**, **3c**, **3d**, **4** and **5** are displayed in Figure 6.9. In the BODIPYs **2a**, **2b**, **3c** and **3d** the HOMO is localized on the ferrocenyl group, whereas the LUMO is located on the BODIPY moiety. The HOMO-LUMO distribution reflects the strong donor-acceptor interactions. The major absorption band in the electronic absorption spectrum of BODIPYs **2a**, **2b**, **3c** and **3d** corresponds to the BODIPY absorption, but the HOMO is localized on the ferrocenyl part, which suggests the origin of major absorption band from HOMO-n energy levels. To get detailed analysis of the origin of the absorption bands in the BODIPYs (**2a**, **2b**, **3c** and **3d**) TD-DFT calculations was performed on BODIPY **3c** at the B3LYP/6-31 G** for C, N, B, F, H, O and Lanl2DZ for Fe level in

dichloromethane solvent using IEFPCM formulation for solvent effect.^[13] Computed vertical transitions and their oscillator strengths and configurations are shown in Table 6.2. The TD-DFT calculations show good agreement with the experimental spectra, and reveals that the main transition (λ_{max}) is from HOMO-2→LUMO and HOMO-3→LUMO.

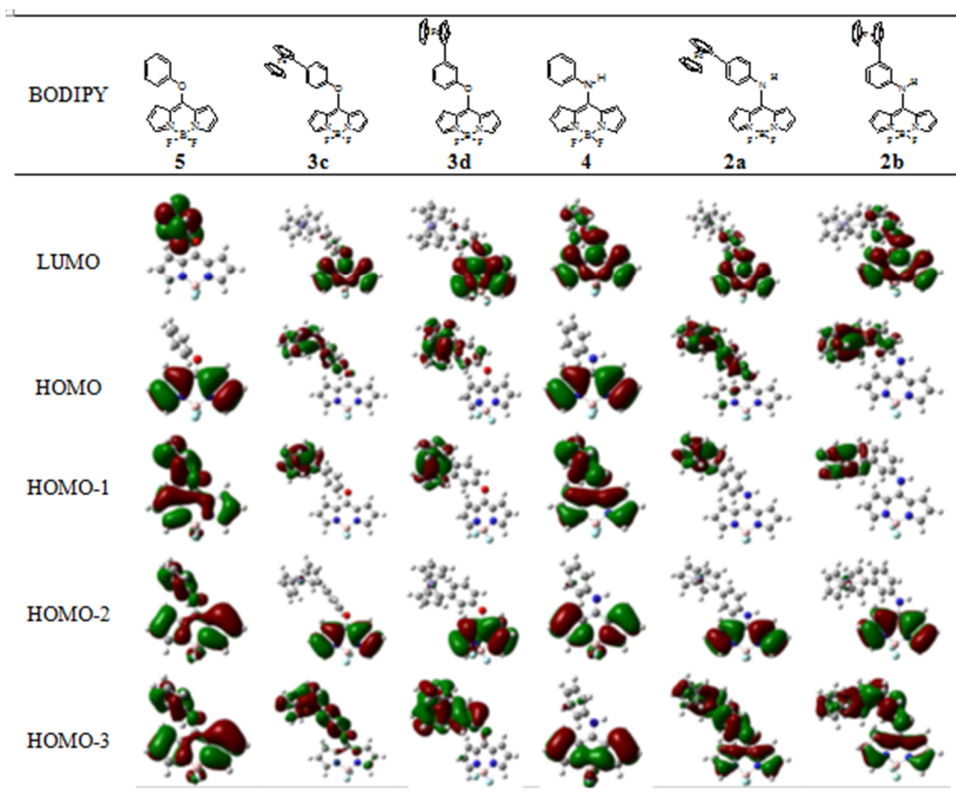


Figure 6.9. Frontier molecular orbitals of BODIPYs **5**, **3c**, **3d**, **4**, **2a** and **2b** at the B3LYP/6-31 G** for C, N, B, F, H, O and Lanl2DZ for Fe level.

6.7. Single crystal X-ray diffraction studies

The single crystals of the heteroatom connected ferrocenyl BODIPYs **2a**, **2b**, **3c** and **3d** were obtained by slow diffusion of hexane into the chloroform solution at room temperature. The BODIPYs **2a** and **3c** crystallize into monoclinic $P2_1c$ space group, **2b** crystallizes into triclinic $P\bar{1}$ space group and **3d** crystallizes into orthorhombic $P2_12_12_1$ space group. The crystal structure and data refinement parameters are shown in Table 6.3. The crystal structures of **2a**, **2b** and **3d** contain two molecules (x and y) in an asymmetric unit. The front view and side view of the crystal structures are shown in Figure 6.10. In the crystal structures of the

heteroatom connected ferrocenyl BODIPYs **2a**, **2b** and **3d** there are two molecules in an asymmetric unit which differ in the torsional angles of the cyclopentadienyl rings. In **2a** the cyclopentadienyl rings of ferrocene unit are staggered in both the molecules of asymmetric unit. In BODIPYS **2b** and **3d**, one molecule in asymmetric unit show staggered conformation whereas another show eclipsed conformation (Figure 6.11).

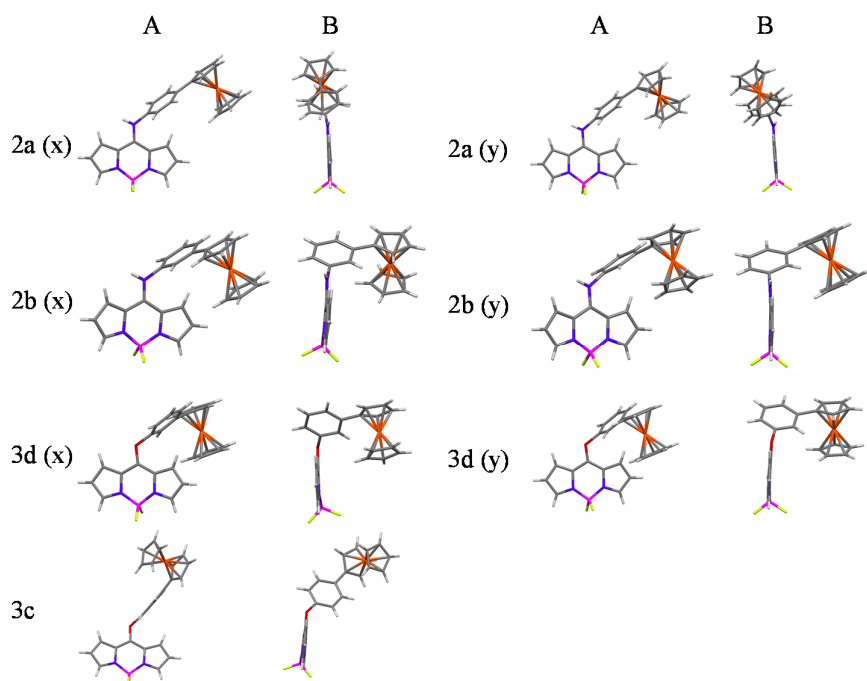


Figure 6.10. Crystal structures of the BODIPY **2a**, **2b**, **2c** and **3d**, (A) front view and (B) side view (x and y represents two different molecules in an asymmetric unit).

The supramolecular interactions in the crystal structures lead to the marvelous structural motifs. The distance and angle of the supramolecular interactions are shown in Table 6.4.

In the packing diagram of **2a**, two molecules in an asymmetric unit are interconnected to each other via B(1)-F(2)--- π (pyrrolic) interaction. One molecule in asymmetric unit independently form 2-D flat sheet (red colored) via C(11)-H(11)---F(1) and N(3)-H(3A)---F(2) interactions, similarly another molecule in asymmetric unit form another sheet (green colored) via C(32)-H(32)---F(4) and N(6)-H(6)---F(4) interactions along *c*-axis. In both the sheets the ferrocenyl part is oriented at the periphery and the BODIPY part lies at the centre of sheet. These sheets connect to others via C(21)-H(21)--- π (BODIPY), C(45)-H(45)--- π (Fc), C(1)-H(1)--- π (Fc),

C(47)-H(47)--- π (pyrrolic), C(46)-H(46)---N(5) and C(26)-H(26)--- π (Fc) interactions to form complex 3D structural motifs. The sheets are arranged in aabbaa fashion along *a*-axis (Figure 6.12).

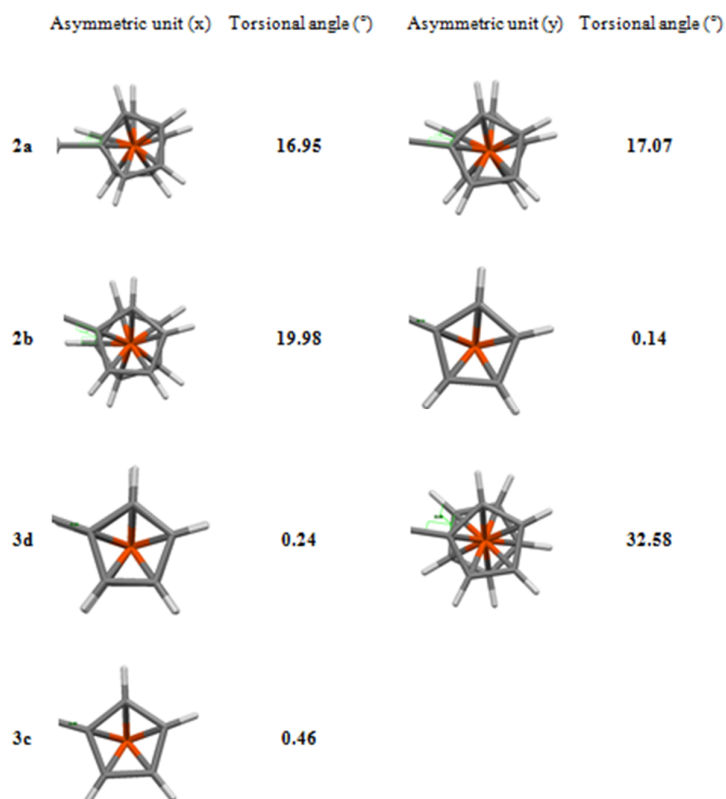


Figure 6.11. Torsional angles in cyclopentadienyl ring in the crystal structures of heteroatom connected ferrocenyl BODIPYs **2a**, **2b**, **3c** and **3d**.

The crystal structure of **2b** contains two molecules in an asymmetric unit. These two molecules are interconnected by C(15)-H(15)--- π (pyrrolic) interaction. Two pairs of two molecules in an asymmetric unit connect to each other in head to head fashion to form a stair shaped 3-D tetrameric structure via N(6)-H(6)---F(1), C(9)-H(9)--- π (phenyl) and C(40)-H(40)--- π (pyrrolic) interactions. This stair shaped tetramer further connects to other tetramers via C(2)-H(2)--- π (Fc), N(3)-H(3)---F(3), C(19)-H(19)---F(3), C(49)-H(49)--- π (Fc) and C(39)-H(39)--- π (Fc) interactions to form complex 2D sheet, which show the alternate bands of ferrocene and BODIPY (Figure 6.13).

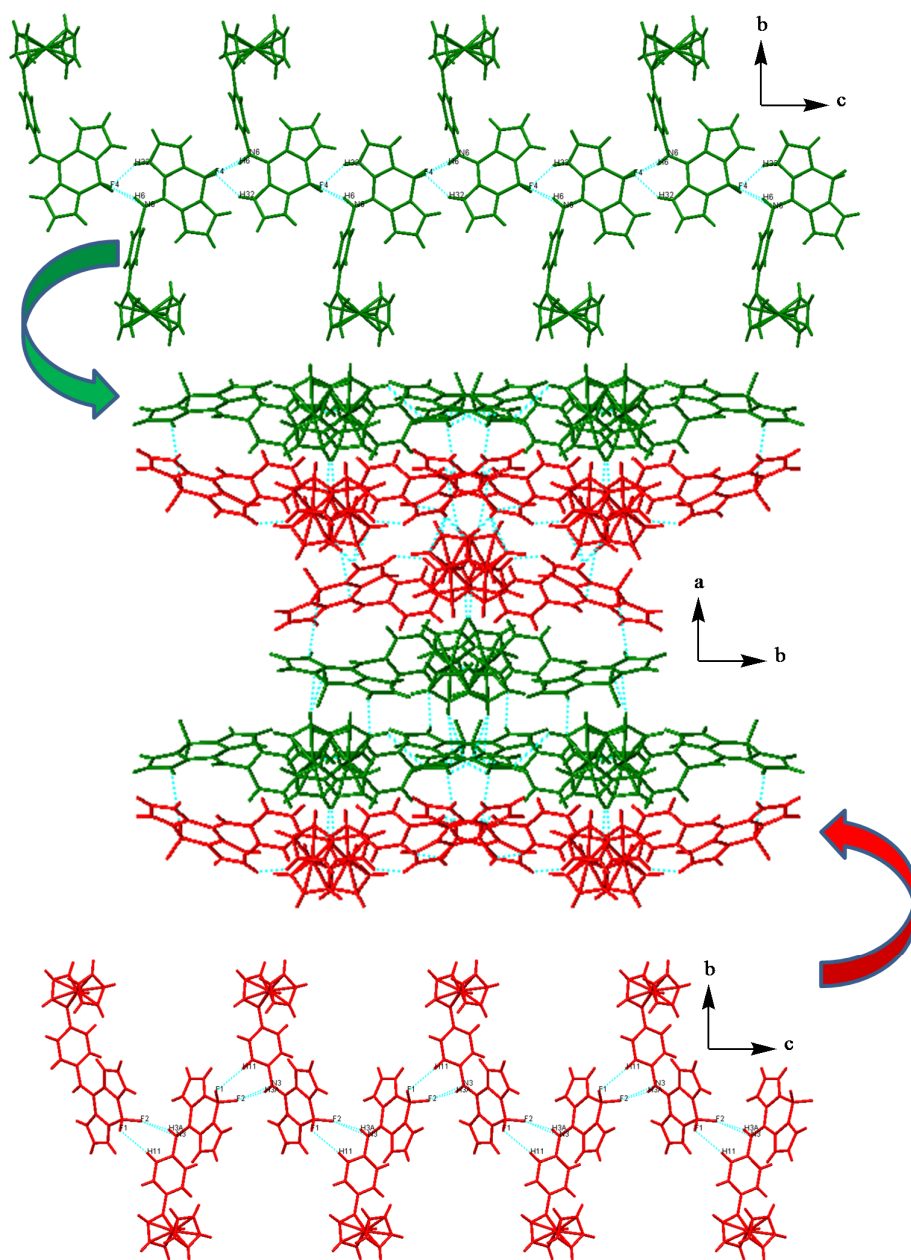


Figure 6.12. Packing diagram of the heteroatom connected ferrocenyl BODIPY **2a** (red and green color represent two different molecules in asymmetric unit).

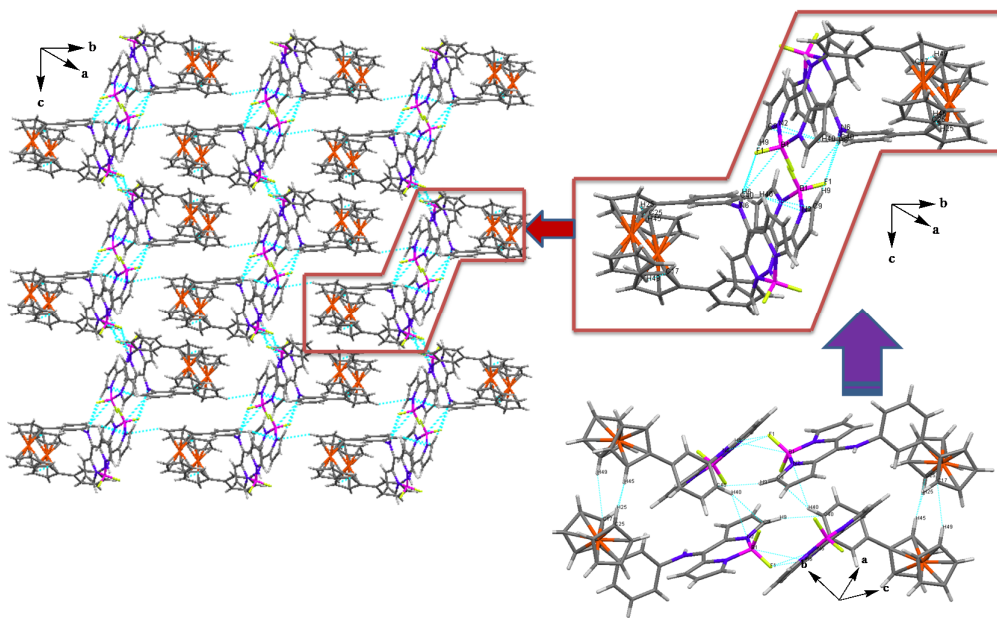


Figure 6.13. Packing diagram of the heteroatom connected ferrocenyl BODIPY **2b**.

In the packing diagram of **3c** the two mutual C(15)-H(15)---F(1) interactions and π --- π staking interaction between two BODIPY units form a dimer like structure. Such dimer like structures connects each other via C(18)-H(18)---F(2), C(17)-H(17)---F(2), C(2)-H(2)--- π (ph), C(25)-H(25)--- π (py), C(14)-H(14)--- π (Fc), C(19)-H(19)--- π (Fc) interactions to form thick sheet like structure along *b*-axis, which looks zigzag along *a*-axis (Figure 6.14).

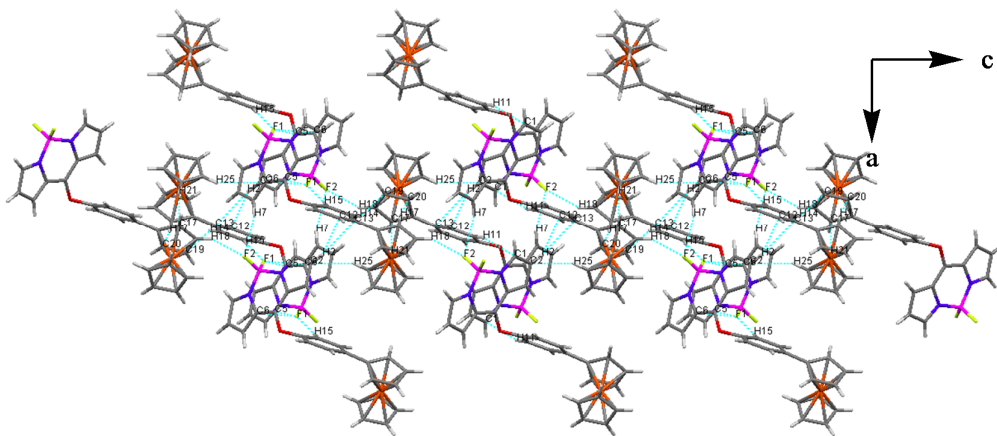


Figure 6.14. Packing diagram of the heteroatom connected ferrocenyl BODIPY **3c**.

In the packing diagram of **3d**, two molecules in asymmetric unit connects to each other via C(17)-H(17)--- π (Fc) interaction. A pair of two molecules connects

another pair in head to head fashion via C(36)-H(36)--- π (BODIPY), C(15)-H(15)--- π (BODIPY), C(44)-H(44)--- π (BODIPY), C(2)-H(2)---F(4) and C(15)-H(15)---F(4) to form a tetramer, and such tetramers connects to each other via C(8)-H(8)---O(2), C(33)-H(33)---F(2) and C(2)-H(2)---F(4) interactions forming a sheet. This sheet contains bands of ferrocene and BODIPY moiety alternately (Figure 6.15).

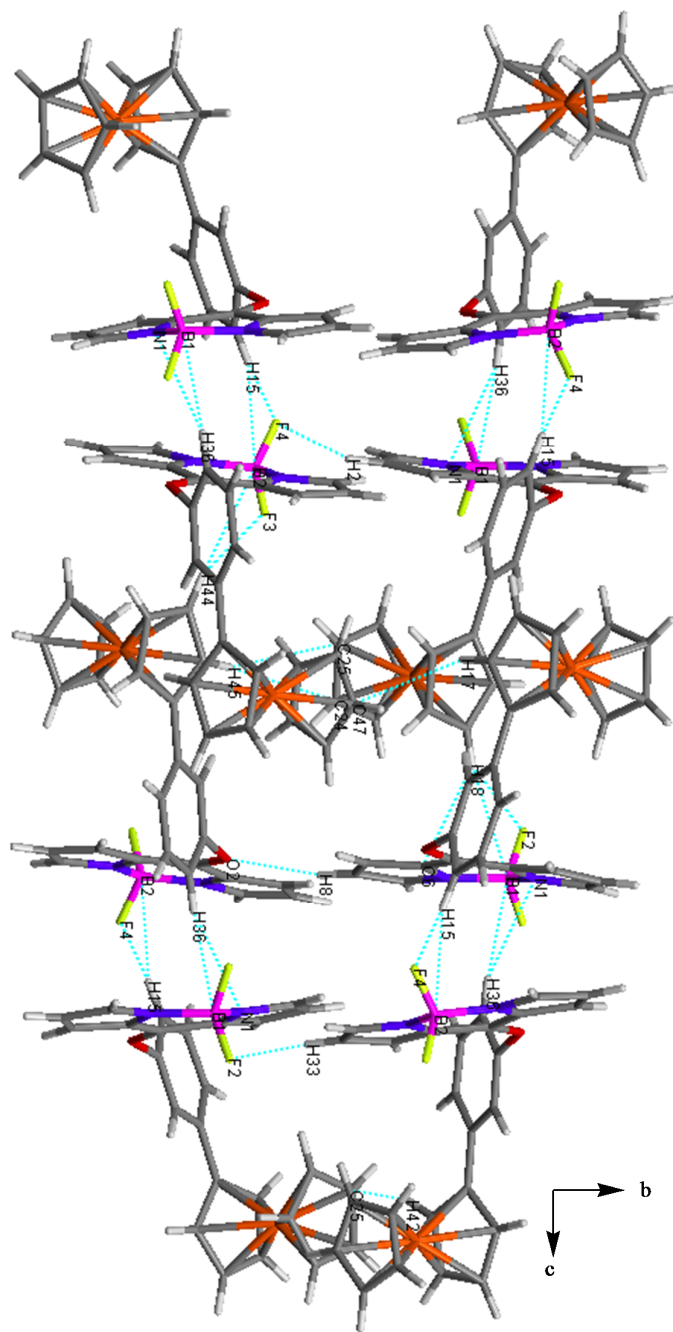


Table 6.3. Crystal structure and data refinement parameters.

BODIPY	2a	2b	3c	3d
Empirical formula	C ₅₀ H ₄₀ B ₂ F ₄ Fe ₂ N ₆	C ₅₀ H ₄₀ B ₂ F ₄ Fe ₂ N ₆	C ₅₀ H ₃₈ B ₂ F ₄ Fe ₂ N ₄ O ₂	C ₅₀ H ₃₈ B ₂ F ₄ Fe ₂ N ₄ O ₂
Formula weight	934.20	934.20	936.16	936.16
Temperature/K	150(2)	150(2)	150(2)	150(2)
Crystal system	Monoclinic	Triclinic	Monoclinic	Orthorhombic
Space group	<i>P</i> 2 ₁ / <i>c</i>	<i>P</i> $\bar{1}$	<i>P</i> 2 ₁ / <i>c</i>	<i>P</i> 2 ₁ 2 ₁ 2 ₁
Unit cell dimensions				
<i>a</i> /Å	20.5133(6)	11.3486(3)	7.88490(10)	11.0633(4)
α /°	90	88.981(2)	90	90
<i>b</i> /Å	15.1810(4)	13.7482(3)	10.0374(2)	14.4288(6)
β /°	110.808(3)	88.659(2)	94.228(2)	90
<i>c</i> /Å	14.5953(4)	13.9193(4)	26.0231(5)	26.8755(13)
γ /°	90	69.607(2)	90	90
Volume/ Å ³	4248.7(2)	2034.95(9)	2053.96(6)	4290.1(3)
<i>Z</i>	4	2	2	4
Calculated density/ Mg/m ³	1.460	1.525	1.514	1.449
Absorption coefficient/mm ⁻¹	0.745	0.778	0.773	5.957
<i>F</i> (000)	1920	960	960	1920
Crystal size/mm	0.23 x 0.18 x 0.13	0.36 x 0.32 x 0.24	0.23 x 0.15 x 0.12	0.33 x 0.27 x 0.21
θ range from data collection/°	3.10 to 25.00	3.16 to 25.00	3.11 to 25.00	3.29 to 71.89
Reflections collected/unique	27023 / 7447 [<i>R</i> (int) = 0.0450]	16060 / 7157 [<i>R</i> (int) = 0.0146]	16172 / 3617 [<i>R</i> (int) = 0.0275]	30197 / 8322 [<i>R</i> (int) = 0.0949]
Absorption correction	Semi- empirical from equivalents	Semi- empirical from equivalents	Semi- empirical from equivalents	Semi- empirical from equivalents
Data/restraints/parameters	7447 / 0 / 577	7157 / 0 / 577	3617 / 0 / 289	8322 / 0 / 578
Goodness-of-fit on <i>F</i> ²	1.099	1.109	1.054	0.987
Final <i>R</i> indices [<i>I</i> > 2σ (<i>I</i>)]	<i>R</i> ₁ = 0.0450, w <i>R</i> ₂ = 0.1082	<i>R</i> ₁ = 0.0293, w <i>R</i> ₂ = 0.0759	<i>R</i> ₁ = 0.0270, w <i>R</i> ₂ = 0.0675	<i>R</i> ₁ = 0.0619, w <i>R</i> ₂ = 0.1514
<i>R</i> indices (all data)	<i>R</i> ₁ = 0.0618, w <i>R</i> ₂ = 0.1202	<i>R</i> ₁ = 0.0309, w <i>R</i> ₂ = 0.0768	<i>R</i> ₁ = 0.0284, w <i>R</i> ₂ = 0.0685	<i>R</i> ₁ = 0.0956, w <i>R</i> ₂ = 0.1823
Largest diff. peak and hole/e Å ⁻³	0.370 and - 0.323	0.383 and - 0.378	0.288 and - 0.319	0.743 and - 0.696
CCDC number	973244	973245	973246	973247

Table 6.4. Distance and angle of intermolecular interactions in the crystal structure of BODIPYs **2a**, **2b**, **3c** and **3d**.

Interaction	Distance (Å)	Angle (°)
2a		
B(1)-F(2)--- π (pyrrolic)	3.509 (weak)	
C(11)-H(11)---F(1)	2.598	150.00
N(3)-H(3A)---F(2)	2.148	144.33
C(32)-H(32)---F(4)	2.622	131.16
N(6)-H(6)---F(4)	1.958	157.52
C(21)-H(21)--- π (BODIPY),	3.107	
C(45)-H(45)--- π (Fc),	3.017	
C(1)-H(1)--- π (Fc),	2.684	
C(47)-H(47)--- π (pyrrolic),	3.337	
C(46)-H(46)---N(5)	2.660	168.69
C(26)-H(26)--- π (Fc)	2.993	
2b		
C(15)-H(15)--- π (pyrrolic)	2.761	
N(6)-H(6)---F(1)	2.218	145.50
C(9)-H(9)--- π (phenyl)	3.680 (weak)	
C(40)-H(40)--- π (pyrrolic)	2.785	
C(2)-H(2)--- π (Fc)	3.275	
N(3)-H(3)---F(3)	2.134	152.82
C(19)-H(19)---F(3)	2.578	153.78
C(49)-H(49)--- π (Fc)	3.609 (weak)	
C(39)-H(39)--- π (Fc)	3.410 (weak)	
3c		
C(15)-H(15)---F(1)	2.412	163.20
C(18)-H(18)---F(2)	2.547	149.54
C(17)-H(17)---F(2)	2.587	156.57
C(2)-H(2)--- π (phenyl)	2.638	
C(25)-H(25)--- π (pyrrolic)(weak)	3.585	
C(14)-H(14)--- π (Fc)	3.238	
C(19)-H(19)--- π (Fc)	2.896	
3d		
C(17)-H(17)--- π (Fc)	3.674	
C(26)-H(26)---F(1)	2.229	166.01
C(13)-H(13)---F(2)	2.426	138.85
C(18)-H(18)---F(2)	2.445	148.14
C(33)-H(33)---F(2)	2.450	113.32
C(9)-H(9)---F(4)	2.607	140.20
C(8)-H(8)---O(2)	2.652	168.55
C(2)-H(2)---F(4)	2.610	157.15
C(18)-H(18)--- π (BODIPY)	2.713	
C(36)-H(36)--- π (BODIPY)	2.673	
C(15)-H(15)---F(4)	2.612	121.60
C(42)-H(42)--- π (Fc)	2.754	
C(44)-H(44)---F(3)	2.502	155.80
C(38)-H(38)---F(3)	2.487	128.49
C(15)-H(15)--- π (BODIPY)	2.799	
C(44)-H(44)--- π (BODIPY)	2.727	

6.8. Experimental section

Synthesis and Characterization of heteroatom connected ferrocenyl BODIPYs

2a and 2b: 8-chloro BODIPY **1** (100 mg, 0.44 mmol) was dissolved in dichloromethane (10 ml), and respective ferrocenyl aniline (122 mg, 0.44 mmol) and TEA (124 μ L, 0.88 mmol) were added. The reaction mixture was purged with nitrogen and stirred at ~ 20 $^{\circ}$ C for 7 hr. Upon completion of reaction, the mixture was evaporated to dryness, and the crude product was dissolved in CH_2Cl_2 , chromatographed on silica (1:3; hexanes: CHCl_3), and recrystallized from chloroform: hexane: ethanol (7:2:1) mixture to give **2a** and **2b** (yield 64 % and 60 %) as yellow-red crystalline solid.

BODIPY 2a

Yellow-red crystalline solid. Yield: 64% (132 mg); m. p: 236-237 $^{\circ}$ C. ^1H NMR (CDCl_3 , 400 MHz, ppm): δ 8.15 (bs, 1H), 7.60 (m, 4H), 7.30 (d, J = 8 Hz, 2H), 6.60 (bs, 2H), 6.34 (m, 2H), 4.72 (t, J = 1.76 Hz, 2H), 4.41 (t, J = 1.76, 2H), 4.06 (s, 5H). ^{13}C NMR (Acetone- d_6 , 100 MHz, ppm): 149.5, 142.1, 136.6, 134.5, 128.2, 127.9, 125.0, 121.4, 114.6, 84.1, 70.6, 70.5, 67.6. ^{11}B NMR (CDCl_3 , 96.3 MHz, , ppm) 0.2 (t, $J_{\text{B-F}}$ = 19.6 Hz); HRMS (ESI-TOF) m/z = calculated for $\text{C}_{25}\text{H}_{20}\text{BF}_2\text{N}_3$ = 467.1067 $[\text{M}]^+$, measured 467.1085 $[\text{M}]^+$. Elemental analysis calcd (%): C, 64.28; H, 4.32; N, 9.00. Found: C, 64.66; H, 4.36; N, 8.85. UV/vis (DCM): λ_{max} (ϵ [$\text{M}^{-1}\text{cm}^{-1}$]) 418 (5.2×10^4),

BODIPY 2b

Yellow-red crystalline solid. Yield: 60% (123 mg); m. p: above 290 $^{\circ}$ C. ^1H NMR (CDCl_3 , 400 MHz, ppm): δ 7.87 (bs, 1H), 7.61 (m, 3H), 7.51 (s, 1H), 7.46 (t, J = 8 Hz, 1H), 7.20 (d, J = 8 Hz, 1H). 6.62 (bs, 2H), 6.36 (m, 2H), 4.69 (t, J = 2 Hz, 2H), 4.38 (t, J = 2 Hz, 2H), 4.04 (s, 5H) ^{13}C NMR (Acetone- d_6 , 100 MHz, ppm): 149.5, 143.5, 139.5, 134.5, 131.2, 127.2, 125.1, 124.8, 121.4, 114.6, 84.01, 70.4, 70.36, 67.3. ^{11}B NMR (CDCl_3 , 96.3 MHz, ppm) 0.22 (t, $J_{\text{B-F}}$ = 21.2 Hz); HRMS (ESI-TOF) m/z = calculated for $\text{C}_{25}\text{H}_{20}\text{BF}_2\text{N}_3$ = 467.1067 $[\text{M}]^+$, found 467.1067 $[\text{M}]^+$. Elemental analysis calcd (%): C, 64.28; H, 4.32; N, 9.00. Found: C, 64.46; H, 4.40; N, 8.75. UV/vis (DCM): λ_{max} (ϵ [$\text{M}^{-1}\text{cm}^{-1}$]) 419 (5.1×10^4),

Synthesis and Characterization of heteroatom connected ferrocenyl BODIPYs

3c and 3d: 8-chloro BODIPY **1** (100 mg, 0.44 mmol) was dissolved in dichloromethane (7 ml), and respective ferrocenyl phenol (123 mg, 0.44 mmol) and

K₂CO₃ (121 mg, 0.88 mmol) were added. The reaction mixture was purged with nitrogen and stirred at ~20 °C for 7 hr. Upon completion of reaction, the mixture was evaporated to dryness, and the crude product was dissolved in CH₂Cl₂, chromatographed on silica (2:1; hexanes:CHCl₃), and recrystallized from chloroform: hexane: ethanol (7:2:1) mixture to give **3c** and **3d** (yield 67 % and 60 %) as yellow-red crystalline solid.

BODIPY **3c**

Yellow-red crystalline solid. Yield: 62% (85 mg); m. p: 188 °C. ¹H NMR (CDCl₃, 400 MHz, ppm): δ 7.75 (s, 2H), 7.57 (d, *J* = 8 Hz, 2H), 7.17 (d, *J* = 8 Hz, 2H), 6.74 (d, *J* = 4.04 Hz, 2H), 6.41 (m, 2H), 4.69 (t, *J* = 1.76, 2H), 4.39 (t, *J* = 1.76, 2H), 4.06 (s, 5H) ¹³C NMR (CDCl₃, 100 MHz, ppm): 159.7, 153.6, 140.7, 139.0, 127.6, 126.8, 126.2, 120.3, 116.8, 83.4, 69.9, 69.7, 66.6. ¹¹B NMR (CDCl₃, 96.3 MHz, ppm) 0.16 (t, *J*_{B-F} = 21.2 Hz); HRMS (ESI-TOF) *m/z* = calculated for C₂₅H₁₉BF₂N₂O = 468.0907 [M]⁺, measured 468.0911 [M]⁺. Elemental analysis calcd (%): C, 64.15; H, 4.09; N, 5.98; O, 3.42. Found: C, 64.62; H, 4.24; N, 5.66. UV/vis (DCM): λ_{max} (ε [M⁻¹cm⁻¹]) 455 (5.7 × 10⁴).

BODIPY **3d**

Yellow-red crystalline solid. Yield: 60% (71 mg); m. p: 138 °C. ¹H NMR (CDCl₃, 400 MHz, ppm): δ 7.76 (s, 2H), 7.48 (m, 1H), 7.40 (t, *J* = 8 Hz, 1H), 7.33 (t, *J* = 2 Hz, 1H), 7.06 (m, 1H), 6.77 (d, *J* = 2.28 Hz, 2H), 6.42 (m, 2H), 4.67 (t, *J* = 1.76, 2H), 4.37 (t, *J* = 1.76, 2H), 4.03 (s, 5H). ¹³C NMR (CDCl₃, 100 MHz, ppm): 159.8, 155.9, 143.3, 140.8, 130.5, 126.8, 126.3, 124.5, 117.35, 117.32, 116.9, 82.9, 69.87, 69.83, 66.7. ¹¹B NMR (CDCl₃, 96.3 MHz, ppm) 0.20 (t, *J*_{B-F} = 19.6 Hz); HRMS (ESI-TOF) *m/z* = calculated for C₂₅H₁₉BF₂N₂O = 468.0907 [M]⁺, measured 468.0906 [M]⁺. Elemental analysis calcd (%): C, 64.15; H, 4.09; N, 5.98; O, 3.42. Found: C, 64.52; H, 4.35; N, 5.61. UV/vis (DCM): λ_{max} (ε [M⁻¹cm⁻¹]) 455 (6.5 × 10⁴).

6.9. Conclusion

In summary heteroatom connected ferrocenyl BODIPYs (**2a**, **2b**, **3c** and **3d**) were synthesized by the nucleophilic aromatic substitution reaction. The nature of heteroatom perturbs the optical, electrochemical, and thermal properties of the BODIPYs substantially. The extent of blue shift in the absorption spectra of the

BODIPYs is due to the delocalization of the lone pair electrons of the heteroatom to the electron deficient BODIPY, which is supported by DFT calculations. The computational calculations show strong donor-acceptor interactions. The heteroatom at the *meso* position of BODIPY destabilizes the LUMO energy level whereas the ferrocenyl group destabilizes the HOMO, HOMO-1 and HOMO-2 energy levels. The crystal structures of the BODIPYs **2a**, **2b**, **3c** and **3d** show interesting interactions in crystal packing.

References

-
- [1] (a) Cheng, T., Wang, T., Zhu, W., Chen, X., Yang, Y., Xu, Y., & Qian, X. (2011). Red-Emission Fluorescent Probe Sensing Cadmium and Pyrophosphate Selectively in Aqueous Solution. *Organic Letters*, 13(14), 3656–3659. <http://doi.org/10.1021/ol201305d>; (b) Bozdemir, O. A., Guliyev, R., Buyukcakil, O., Sencuk, S., Kolenen, S., Gulseren, G., ... Akkaya, E. U. (2010). Selective Manipulation of ICT and PET Processes in Styryl-Bodipy Derivatives: Applications in Molecular Logic and Fluorescence Sensing of Metal Ions. *Journal of the American Chemical Society*, 132(23), 8029–8036. <http://doi.org/10.1021/ja1008163>; (c) Kim, H. S., Pham, T. C. T., & Yoon, K. B. (2012). A novel class of nonlinear optical materials based on host-guest composites: zeolites as inorganic crystalline hosts. *Chemical Communications*, 48(39), 4659–4673. <http://doi.org/10.1039/C2CC30919J>; (d) Benstead, M., Mehl, G. H., & Boyle, R. W. (2011). 4,4'-Difluoro-4-bora-3a,4a-diaza-s-indacenes (BODIPYs) as components of novel light active materials. *Tetrahedron*, 67(20), 3573–3601. <http://doi.org/http://dx.doi.org/10.1016/j.tet.2011.03.028>; (e) Zhou, Y., Xiao, Y., Chi, S., & Qian, X. (2008). Isomeric Boron–Fluorine Complexes with Donor–Acceptor Architecture: Strong Solid/Liquid Fluorescence and Large Stokes Shift. *Organic Letters*, 10(4), 633–636. <http://doi.org/10.1021/ol702963w>; (f) Lord, S. J., Conley, N. R., Lee, H. D., Samuel, R., Liu, N., Twieg, R. J., & Moerner, W. E. (2008). A Photoactivatable Push–Pull Fluorophore for Single-Molecule Imaging in Live Cells. *Journal of the American Chemical Society*, 130(29), 9204–9205. <http://doi.org/10.1021/ja802883k>; (g) West, R., Panagabko, C., & Atkinson, J. (2010). Synthesis and Characterization of BODIPY- α -Tocopherol: A

-
- Fluorescent Form of Vitamin E. *The Journal of Organic Chemistry*, 75(9), 2883–2892. <http://doi.org/10.1021/jo100095n>; (h) Descalzo, A. B., Xu, H.-J., Xue, Z.-L., Hoffmann, K., Shen, Z., Weller, M. G., ... Rurack, K. (2008). Phenanthrene-Fused Boron–Dipyrromethenes as Bright Long-Wavelength Fluorophores. *Organic Letters*, 10(8), 1581–1584. <http://doi.org/10.1021/ol800271e>; (i) Marder, S. R., Kippelen, B., Jen, A. K.-Y., & Peyghambarian, N. (1997). Design and synthesis of chromophores and polymers for electro-optic and photorefractive applications. *Nature*, 388(6645), 845–851; (j) LeCours, S. M., Guan, H.-W., DiMagno, S. G., Wang, C. H., & Therien, M. J. (1996). Push–Pull Arylethynyl Porphyrins: New Chromophores That Exhibit Large Molecular First-Order Hyperpolarizabilities. *Journal of the American Chemical Society*, 118(6), 1497–1503. <http://doi.org/10.1021/ja953610l>; (k) Yin, X., Li, Y., Li, Y., Zhu, Y., Tang, X., Zheng, H., & Zhu, D. (2009). Electrochromism based on the charge transfer process in a ferrocene–BODIPY molecule. *Tetrahedron*, 65(40), 8373–8377. <http://doi.org/http://dx.doi.org/10.1016/j.tet.2009.08.008>; (l) Yin, X., Li, Y., Zhu, Y., Jing, X., Li, Y., & Zhu, D. (2010). A highly sensitive viscosity probe based on ferrocene-BODIPY dyads. *Dalton Transactions*, 39(41), 9929–9935. <http://doi.org/10.1039/C0DT00309C>; (m) Ulrich, G., Ziessel, R., & Harriman, A. (2008). The Chemistry of Fluorescent Bodipy Dyes: Versatility Unsurpassed. *Angewandte Chemie International Edition*, 47(7), 1184–1201. <http://doi.org/10.1002/anie.200702070>; (n) El-Khouly, M. E., Fukuzumi, S., & D’Souza, F. (2014). Photosynthetic Antenna–Reaction Center Mimicry by Using Boron Dipyrromethene Sensitizers. *ChemPhysChem*, 15(1), 30–47. <http://doi.org/10.1002/cphc.201300715>.
- [2] (a) Baruah, M., Qin, W., Vallée, R. A. L., Beljonne, D., Rohand, T., Dehaen, W., & Boens, N. (2005). A Highly Potassium-Selective Ratiometric Fluorescent Indicator Based on BODIPY Azacrown Ether Excitable with Visible Light. *Organic Letters*, 7(20), 4377–4380. <http://doi.org/10.1021/ol051603o>; (b) Rohand, T., Baruah, M., Qin, W., Boens, N., & Dehaen, W. (2006). Functionalisation of fluorescent BODIPY dyes by nucleophilic substitution. *Chemical Communications*, (3), 266–268. <http://doi.org/10.1039/B512756D>;

-
- (c) Rohand, T., Qin, W., Boens, N., & Dehaen, W. (2006). Palladium-Catalyzed Coupling Reactions for the Functionalization of BODIPY Dyes with Fluorescence Spanning the Visible Spectrum. *European Journal of Organic Chemistry*, 2006(20), 4658–4663. <http://doi.org/10.1002/ejoc.200600531>; (d) Leen, V., Braeken, E., Luckermans, K., Jackers, C., Van der Auweraer, M., Boens, N., & Dehaen, W. (2009). A versatile, modular synthesis of monofunctionalized BODIPY dyes. *Chemical Communications*, (30), 4515–4517. <http://doi.org/10.1039/B906164A>; (e) Leen, V., Leemans, T., Boens, N., & Dehaen, W. (2011). 2- and 3-Monohalogenated BODIPY Dyes and Their Functionalized Analogues: Synthesis and Spectroscopy. *European Journal of Organic Chemistry*, 2011(23), 4386–4396. <http://doi.org/10.1002/ejoc.201100324>; (f) Li, L., Nguyen, B., & Burgess, K. (2008). Functionalization of the 4,4-difluoro-4-bora-3a,4a-diaza-s-indacene (BODIPY) core. *Bioorganic & Medicinal Chemistry Letters*, 18(10), 3112–3116. <http://doi.org/http://dx.doi.org/10.1016/j.bmcl.2007.10.103>; (g) Han, J., Gonzalez, O., Aguilar-Aguilar, A., Pena-Cabrera, E., & Burgess, K. (2009). 3- and 5-Functionalized BODIPYs via the Liebeskind-Srogl reaction. *Organic & Biomolecular Chemistry*, 7(1), 34–36. <http://doi.org/10.1039/B818390B>; (h) Dilek, Ö., & Bane, S. L. (2008). Synthesis of boron dipyrromethene fluorescent probes for bioorthogonal labeling. *Tetrahedron Letters*, 49(8), 1413–1416. <http://doi.org/http://dx.doi.org/10.1016/j.tetlet.2007.12.052>.
- [3] (a) Loudet, A., & Burgess, K. (2007). BODIPY Dyes and Their Derivatives: Syntheses and Spectroscopic Properties. *Chemical Reviews*, 107(11), 4891–4932. <http://doi.org/doi:10.1021/cr078381n>; (b) Gautam, P., Dhokale, B., Mobin, S. M., & Misra, R. (2012). Ferrocenyl BODIPYs: synthesis, structure and properties. *RSC Advances*, 2(32), 12105–12107. <http://doi.org/10.1039/C2RA21964F>.
- [4] Leen, V., Yuan, P., Wang, L., Boens, N., & Dehaen, W. (2012). Synthesis of Meso-Halogenated BODIPYs and Access to Meso-Substituted Analogues. *Organic Letters*, 14(24), 6150–6153. <http://doi.org/10.1021/ol3028225>.

-
- [5] (a) Misra, R., Dhokale, B., Jadhav, T., & Mobin, S. M. (2013). Donor-acceptor meso-alkynylated ferrocenyl BODIPYs: synthesis, structure, and properties. *Dalton Transactions*, 42(37), 13658–13666. <http://doi.org/10.1039/C3DT51374B>. (b) Misra, R., Dhokale, B., Jadhav, T., & Mobin, S. M. (2014). The quenching of fluorescence as an indicator of donor-strength in meso arylethynyl BODIPYs. *Dalton Transactions*, 43(12), 4854–4861. <http://doi.org/10.1039/C3DT53056F>.
- [6] (a) Marder, S. R., Kippelen, B., Jen, A. K.-Y., & Peyghambarian, N. (1997). Design and synthesis of chromophores and polymers for electro-optic and photorefractive applications. *Nature*, 388(6645), 845–851. (b) Fabre, B. (2010). Ferrocene-Terminated Monolayers Covalently Bound to Hydrogen-Terminated Silicon Surfaces. Toward the Development of Charge Storage and Communication Devices. *Accounts of Chemical Research*, 43(12), 1509–1518. <http://doi.org/10.1021/ar100085q>. (c) Tucker, J. H. R., & Collinson, S. R. (2002). Recent developments in the redox-switched binding of organic compounds. *Chemical Society Reviews*, 31(3), 147–156. <http://doi.org/10.1039/A804251I>.
- [7] (a) Gautam, P., Dhokale, B., Shukla, V., Singh, C. P., Bindra, K. S., & Misra, R. (2012). Optical limiting performance of meso-tetraferrocenyl porphyrin and its metal derivatives. *Journal of Photochemistry and Photobiology A: Chemistry*, 239(0), 24–27. <http://doi.org/http://dx.doi.org/10.1016/j.jphotochem.2012.04.020>. (b) Dhokale, B., Gautam, P., & Misra, R. (2012). Donor-acceptor perylenediimide-ferrocene conjugates: synthesis, photophysical, and electrochemical properties. *Tetrahedron Letters*, 53(18), 2352–2354. <http://doi.org/http://dx.doi.org/10.1016/j.tetlet.2012.02.107>; (c) Maragani, R., Jadhav, T., Mobin, S. M., & Misra, R. (2012). Synthesis, structure, photophysical, and electrochemical properties of donor-acceptor ferrocenyl derivatives. *Tetrahedron*, 68(36), 7302–7308. <http://doi.org/http://dx.doi.org/10.1016/j.tet.2012.06.094>; (d) Dhokale, B., Gautam, P., Mobin, S. M., & Misra, R. (2013). Donor-acceptor, ferrocenyl substituted BODIPYs with marvelous supramolecular interactions. *Dalton Transactions*, 42(5), 1512–1518. <http://doi.org/10.1039/C2DT31632C>; (e) Maragani, R., Jadhav, T., Mobin, S.

M., & Misra, R. (2013). C 3 symmetric ferrocenyl triazines: synthesis, structure, and properties. *RSC Advances*, 3(9), 2889–2892. <http://doi.org/10.1039/C2RA23153K>; (f) Misra, R., Gautam, P., Sharma, R., & Mobin, S. M. (2013). Donor- π -acceptor- π -donor ferrocenyl benzothiadiazoles: synthesis, structure, and properties. *Tetrahedron Letters*, 54(5), 381–383. <http://doi.org/http://dx.doi.org/10.1016/j.tetlet.2012.11.016>; (g) Jadhav, T., Maragani, R., Misra, R., Sreeramulu, V., Rao, D. N., & Mobin, S. M. (2013). Design and synthesis of donor-acceptor pyrazabole derivatives for multiphoton absorption. *Dalton Transactions*, 42(13), 4340–4342. <http://doi.org/10.1039/C3DT33065F>; (h) Sharma, R., Gautam, P., Mobin, S. M., & Misra, R. (2013). [small beta]-Substituted ferrocenyl porphyrins: synthesis, structure, and properties. *Dalton Transactions*, 42(15), 5539–5545. <http://doi.org/10.1039/C3DT00003F>; (i) Misra, R., Gautam, P., Jadhav, T., & Mobin, S. M. (2013). Donor-Acceptor Ferrocenyl-Substituted Benzothiadiazoles: Synthesis, Structure, and Properties. *The Journal of Organic Chemistry*, 78(10), 4940–4948. <http://doi.org/10.1021/jo4005734>; (j) Sharma, R., Margani, R., Mobin, S. M., & Misra, R. (2013). Ferrocenyl substituted calixarenes: synthesis, structure and properties. *RSC Advances*, 3(17), 5785–5788. <http://doi.org/10.1039/C3RA00146F>; (k) Maragani, R., & Misra, R. (2013). Donor-acceptor ferrocenyl triazines: synthesis and properties. *Tetrahedron Letters*, 54(39), 5399–5402. <http://doi.org/http://dx.doi.org/10.1016/j.tetlet.2013.07.119>; (l) Misra, R., Jadhav, T., & Mobin, S. M. (2014). Ferrocenyl pyrazaboles: design, synthesis, structure, and properties. *Dalton Transactions*, 43(5), 2013–2022. <http://doi.org/10.1039/C3DT52315B>; (m) Misra, R., Gautam, P., & Mobin, S. M. (2013). Aryl-Substituted Unsymmetrical Benzothiadiazoles: Synthesis, Structure, and Properties. *The Journal of Organic Chemistry*, 78(24), 12440–12452. <http://doi.org/10.1021/jo402111q>; (n) Misra, R., Sharma, R., & Mobin, S. M. (2014). Star shaped ferrocenyl truxenes: synthesis, structure and properties. *Dalton Transactions*, 43(18), 6891–6896. <http://doi.org/10.1039/C4DT00210E>.

- [8] Flores-Rizo, J. O., Esnal, I., Osorio-Martínez, C. A., GómezDurán, C. F. A., Bañuelos, J., López Arbeloa, I., ... Peña-Cabrera, E. (2013). 8-Alkoxy- and 8-

-
- Aryloxy-BODIPYs: Straightforward Fluorescent Tagging of Alcohols and Phenols. *The Journal of Organic Chemistry*, 78(12), 5867–5877. <http://doi.org/10.1021/jo400417h>.
- [9] (a) H. Ping, K.-Q. Zhao, H. -B. Xu, (2001). 4-Ferrocenylaniline. *Molecules*, 6, M250; (b) H. Ping, K.-Q. Zhao, H. -B. Xu, (2001). 4-nitrophenylferrocene. *Molecules*, 6, M249.
- [10] Boens, N., Wang, L., Leen, V., Yuan, P., Verbelen, B., Dehaen, W., ... Alvarez-Pez, J. M. (2014). 8-HaloBODIPYs and Their 8-(C, N, O, S) Substituted Analogues: Solvent Dependent UV–Vis Spectroscopy, Variable Temperature NMR, Crystal Structure Determination, and Quantum Chemical Calculations. *The Journal of Physical Chemistry A*, 118(9), 1576–1594. <http://doi.org/10.1021/jp412132y>.
- [11] Nadtochenko, V. A., Denisov, N. N., Gak, V. Y., Abramova, N. V., & Loim, N. M. (1999). Photochemical and photophysical properties of meso-tetraferrocenylporphyrin. Quenching of meso-tetraphenylporphyrin by ferrocene. *Russian Chemical Bulletin*, 48(10), 1900–1903. <http://doi.org/10.1007/BF02494744>.
- [12] Kusaka, S., Sakamoto, R., Kitagawa, Y., Okumura, M., & Nishihara, H. (2013). meso-Alkynyl BODIPYs: Structure, Photoproperties, π -Extension, and Manipulation of Frontier Orbitals. *Chemistry – An Asian Journal*, 8(4), 723–727. <http://doi.org/10.1002/asia.201201176>.
- [13] Mennucci, B., Cancès, E., & Tomasi, J. (1997). Evaluation of Solvent Effects in Isotropic and Anisotropic Dielectrics and in Ionic Solutions with a Unified Integral Equation Method: Theoretical Bases, Computational Implementation, and Numerical Applications. *The Journal of Physical Chemistry B*, 101(49), 10506–10517. <http://doi.org/10.1021/jp971959k>.

Chapter 7

Oxidation of aliphatic *tert*-amines by 8-chloro BODIPY and *in situ* cross-coupling

7.1. Introduction

The research on BODIPY dyes have gained momentum, which is reflected from their large number of publications.^[1] The BODIPY dyes are fluorophore of choice due to their strong electronic absorption, high fluorescence quantum yield and excellent thermal and photochemical stability.^[2] The photonic properties of the BODIPYs can be tuned by incorporating diverse functionalities.^[3] In recent years various methods have been developed for the functionalization of BODIPYs at α , β and *meso* positions.^[4]

Our group is involved in the development of donor-acceptor (D-A) materials for various optoelectronic applications.^[5] We have introduced a variety of donors at the *meso* as well as at the β pyrrolic positions of the BODIPY.^[6] The functionalization at the *meso* position is of interest as it exhibits better electronic communication.^[7]

The 8-chloro BODIPY (**1**) is a versatile precursor for the *meso* functionalization. It undergoes rapid Pd-catalyzed coupling and substitution reactions.^[8] We have explored variety of Sonogashira cross-coupling reactions of BODIPY **1**.^[6c,7b] During these coupling reactions, we observed sudden change in the color of BODIPY **1** solution on addition of triethylamine. While monitoring the progress of the reaction via TLC, we observed trace amount of yellow colored impurity below the expected cross coupled major product. The pursuit of our curiosity to explore the formation of same impurity in different reactions leads to surprising results.

The reaction of BODIPY **1** with triethylamine resulted in enamine adduct at the *meso* position of the BODIPY. Usually the enamines are synthesized by catalysts like FeCl₃, Pd(OAc)₂ and pincer-ligated iridium complex.^[9] Here they are incorporated into the BODIPY moiety without any catalyst. Thus the 8-chloro BODIPY (**1**) itself might be promoting the oxidation of triethylamine and C-C bond formation. Similar transformation was reported for the reaction of *p*-chloranil with

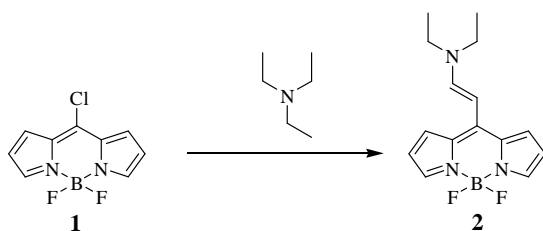
triethylamine, leading to the enamine substituted quinone.^[10]

In this chapter we discuss the novel methodology for C-C bond formation and synthesis of enamine substituted BODIPYs via catalyst free oxidation of tertiary amines and coupling with 8-chloro BODIPY and their optical properties.

7.2. Results and Discussion

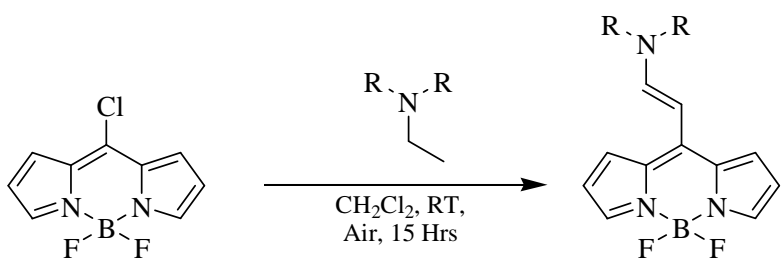
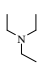
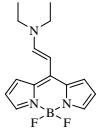
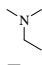
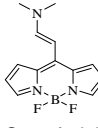
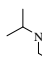
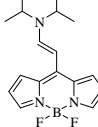
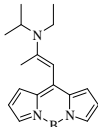
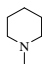
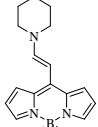
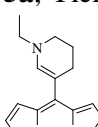
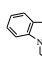
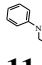
The reaction of triethylamine with 8-chloro BODIPY **1** in dichloromethane solvent at room temperature resulted enamine substituted BODIPY **2** (Table 7.1). The BODIPY **2** was purified by column chromatography and characterized by ¹H, ¹³C, ¹¹B and ¹⁹F NMR, HRMS and single crystal X-ray diffraction techniques. The reaction conditions were optimized to achieve better yield (Table 7.1). The reaction yield and time was found to be independent of solvents and catalysts like Pd(OAc)₂ or CuI. The reaction was fast in open atmosphere (15 hrs) but sluggish under argon atmosphere (48 hrs). The dichloromethane was optimal solvent for the reaction and purification. The reaction works well in dichloromethane solvent, with four equivalents of triethylamine in air and completes within 15 hrs.

Table 7.1. Screening results of reaction optimization.



Entry	Conditions	Temperature	Yield %	Reaction Time
1	DCM, in Ar atmosphere	RT	31	48 hrs
2	THF, in Ar atmosphere	RT	30	48 hrs
3	DCM + CuI, in Ar atmosphere	RT	30	48 hrs
4	DCM + Pd(OAc) ₂ , in Ar atmosphere	RT	32	48 hrs
5	DCM + Pd(OAc) ₂ , in Ar atmosphere	60 °C	31	48 hrs
6	DCM, in air	RT	31	15 hrs

Table 7.2. Screening of the substrates and optical properties of the BODIPYs **1** – **5**.

			
Entry	Substrate	Product/s ^a	λ_{max} (nm) ^b [ϵ / 10 ⁴ (Mol ⁻¹ .cm ⁻¹)] ^c
1		 2 , Yield- 31 %	476 [3.34]
2		 3 , Yield- 18%	477 [3.38]
3		 4a , Yield- 13%	477 [3.87]
		 4b , Yield- 9%	504 [3.40] 466 [2.99]
4		 5a , Yield- 12%	477 [3.14]
		 5b , Yield- 7%	447 [3.9]
5		No expected product, Starting decomposed	
6		No expected product, Starting decomposed	

(a) Isolated yields. (b) Absorbance measured in dichloromethane at 10⁻⁶ M concentration. (c) Recorded at λ_{max} .

In order to explore the scope of the reaction under optimized conditions, the reaction was carried out with different *tert*-amines (Table 7.2). The reaction of 8-chloro BODIPY (**1**) with *N,N*-dimethylethylamine (**7**), resulted BODIPY **3** in 18% yield (Entry 2), whereas the reaction of BODIPY **1** with triethylamine (**6**) gave BODIPY **2** in 31 % yield (Entry 1). The better yield of BODIPY **2** compared to BODIPY **3** indicates that the *N*-methyl substituents are not involved in the reaction and more the number of *N*-ethyl substituents better will be the yield.

Further the reaction of 8-chloro BODIPY (**1**) with *N,N*-diisopropylethylamine (DIPEA) (**8**) (Entry 3), resulted two products, BODIPY **4a** and **4b**. The BODIPY **4a** was obtained from the reaction of *N*-ethyl part whereas **4b** from the reaction with *N*-isopropyl part of DIPEA (**8**). The better yield of BODIPY **4a** than **4b** indicates the higher reactivity of *N*-ethyl group than the *N*-isopropyl group. Similarly the reaction of 8-chloro BODIPY **1** with *N*-ethyl piperidine (**9**) resulted BODIPYs **5a** and **5b** from the reaction with *N*-ethyl and *N*-CH₂-CH₂- groups respectively (Entry 4). The reaction with *N,N*-diisopropylethyl amine (**8**) and *N*-ethylpiperidine (**9**) proves that the *N*-(CH-CH-) group is essential for the reaction by this methodology. All the reactions yielded exclusively *E* isomers.

After successful reactions with aliphatic amines we checked the feasibility of the reaction for aromatic amines, *N*-ethyl carbazole (**10**) and *N*-ethyl-*N*-phenylaniline (**11**) (Entry 5 and 6). The reactions with these aryl substrates were not feasible even after addition of external bases like pyridine, K₂CO₃ or CsCO₃ and leads to the decomposition of the BODIPY (**1**). The inert nature of these substrates may be due to steric crowding or better electron delocalizing ability of the aromatic substituents. In all the reactions the blackish-green, sticky polar compound was observed, which was difficult to purify and characterize.

The enamine substituted BODIPYs were well characterized by ¹H NMR, ¹³C NMR and HRMS techniques. The ¹H NMR spectra of the BODIPYs exhibits α , β and β' protons at 7.6, 6.4 and 7.0 ppm respectively. In BODIPYs **2**, **3**, **4a** and **5a** the *trans* protons of vinyl bond appears at 5.9 and 7.8 ppm, with the coupling constant *J* = 12 Hz. In BODIPYs **3** and **4a** the *N*-alkyl protons appear separately at 3.1-3.8 ppm, whereas in BODIPYs **2** and **5a** they appear at 3.5 ppm collectively.

7.3. Single crystal X-ray diffraction studies

The BODIPYs **2**, **4a**, **4b** and **5a** were also characterized by single crystal X-ray diffraction technique. Crystal data and structure refinement parameters are listed in Table 7.3. The front view and side view of the crystal structures are shown in Figure 7.1. The side view of the crystals reveals non planar conformation of the BODIPYs.

Table 7.3. Single crystal data and structure refinement parameters.

BODIPY	2	4a	4b	5a
Empirical formula	C ₁₅ H ₁₈ B F ₂ N ₃	C ₁₇ H ₂₂ B F ₂ N ₃	C ₁₇ H ₂₂ B F ₂ N ₃	C ₁₆ H ₁₈ B F ₂ N ₃
Formula weight	289.13	317.19	317.19	301.14
Temperature/K	150(2)	150(2)	150(2)	150(2)
Crystal system	Monoclinic	Monoclinic	Monoclinic	Monoclinic,
Space group	<i>P</i> 2 ₁ / <i>n</i>	<i>P</i> 2 ₁ / <i>c</i>	<i>P</i> 2 ₁ / <i>n</i>	<i>P</i> 2 ₁ / <i>c</i>
Unit cell dimensions				
<i>a</i> /Å	<i>a</i> = 8.3942(3)	9.2376(16)	11.1777(8)	<i>a</i> = 7.8218(4)
<i>α</i> /°	90	90	90	90
<i>b</i> /Å	12.6829(4)	14.7140(12)	11.3773(5)	<i>b</i> = 23.1144(9)
<i>β</i> /°	95.074(3)	127.73(3)	109.830(8)	110.867(6)
<i>c</i> /Å	14.0136(4)	15.929(3)	14.4649(9)	<i>c</i> = 8.5337(4)
<i>γ</i> /°	90	90	90	90
Volume/ Å ³	1486.08(8)	1712.2(5)	1730.45(18)	1441.66(11)
<i>Z</i>	4	4	4	4
Calculated density/ Mg/m ³	1.292	1.230	1.217	1.387
Absorption coefficient/mm ⁻¹	0.785	0.088	0.087	0.101
<i>F</i> (000)	608	672	672	632
Crystal size/mm	0.26 x 0.18 x 0.13	0.33 x 0.26 x 0.21	0.33 x 0.28 x 0.21	0.33 x 0.26 x 0.21
<i>θ</i> range from data collection/°	4.71 to 72.08	3.02 to 24.99	3.34 to 25.00	3.10 to 25.00
Reflections collected/unique	9691 / 2895 [<i>R</i> (int) = 0.0210]	13178 / 3000 [<i>R</i> (int) = 0.0417]	9413 / 3022 [<i>R</i> (int) = 0.0609]	11087 / 2523 [<i>R</i> (int) = 0.0371]
Absorption correction	Semi-empirical from equivalents	Semi-empirical from equivalents	Semi-empirical from equivalents	Semi-empirical from equivalents
Data/restraints/parameters	2895 / 0 / 190	3000 / 0 / 212	3022 / 0 / 212	2523 / 0 / 199
Goodness-of-fit on <i>F</i> ²	1.044	1.108	1.020	1.127
Final <i>R</i> indices [<i>I</i> > 2σ (<i>I</i>)]	<i>R</i> ₁ = 0.0550, <i>wR</i> ₂ = 0.1567	<i>R</i> ₁ = 0.0515, <i>wR</i> ₂ = 0.1262	<i>R</i> ₁ = 0.0550, <i>wR</i> ₂ = 0.1179	<i>R</i> ₁ = 0.0374, <i>wR</i> ₂ = 0.0857
<i>R</i> indices (all data)	<i>R</i> ₁ = 0.0606, <i>wR</i> ₂ = 0.1627	<i>R</i> ₁ = 0.0632, <i>wR</i> ₂ = 0.1352	<i>R</i> ₁ = 0.0979, <i>wR</i> ₂ = 0.1443	<i>R</i> ₁ = 0.0445, <i>wR</i> ₂ = 0.0889
Largest diff. peak and hole/e Å ⁻³	0.300 and -0.261	0.302 and -0.261	0.186 and -0.202	0.198 and -0.209
CCDC number	1001550	1001551	1001552	1001553

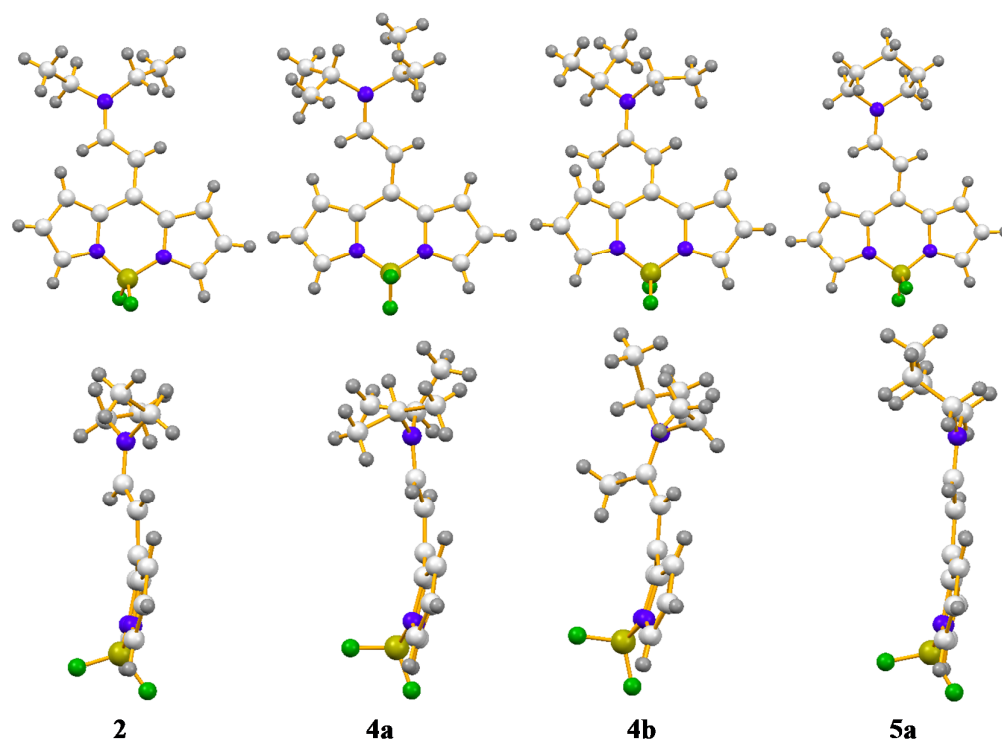


Figure 7.1 Single crystal structures of BODIPYs **2**, **4a**, **4b** and **5a**. Front view (above) and Side view (below).

7.4. Photophysical Properties

The electronic absorption spectra of the BODIPYs **1** – **5** were recorded in dichloromethane (Figure 7.2) and the corresponding data are presented in Table 7.2. The BODIPYs **2**, **3**, **4a** and **5a** show blue shift of ~27 nm compared to 8-chloro BODIPY **1**. The blue shift in the absorption spectra can be attributed to the cross conjugation due to the delocalization of lone pair electrons of the nitrogen atom into the electron deficient BODIPY.^[11] The BODIPYs **4b** and **5b** behaves differently from rest of the BODIPYs. The BODIPY **4b**, bearing the methyl substituent at the double bonded carbon shows broad absorption band at 504 nm with a shoulder at 466 nm, whereas the BODIPY **5b** bearing the piperidine ring at the double bonded carbon shows highly blue shifted broad absorption band at 447 nm. The higher blue shift in BODIPY **5b** compared to **4b** can be attributed to the more planar conformation of the enamine with respect to the BODIPY. The BODIPYs **2** – **5** are poorly emissive in dichloromethane.

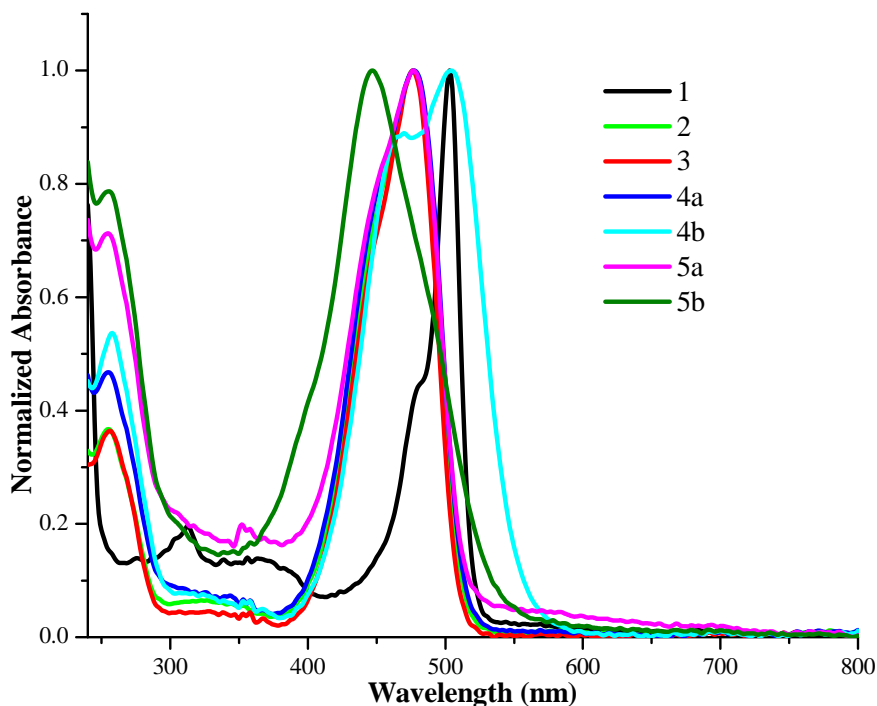


Figure 7.2. Normalized electronic absorption spectra of BODIPYs **1** – **5** in dichloromethane.

7.5. Experimental section

Reaction Procedure- 8-chloro BODIPY (200mg, 0.88 mmol), was dissolved in the 20 ml dry DCM and, respective tertiary amine (3.54 mmol) was added. The reaction mixture was stirred at room temperature; and the progress of the reaction was monitored by TLC. After completion of reaction the solvent was removed at the reduced pressure without heating, and the crude product was purified by column chromatography by using DCM: hexane (2:1).

Characterization data

BODIPY 2

Yellow-red crystalline solid. Yield: 31% (79 mg); ^1H NMR (CDCl_3 , 400 MHz, ppm): δ 8.89 (d, J = 12 Hz, 1H), 7.60 (s, 2H), 6.98 (d, J = 4 Hz, 2H), 6.41 (m, 2H), 6.03 (d, J = 12 Hz, 1H), 3.50 (m, 4H), 1.35 (t, J = 8 Hz, 6H). ^{13}C NMR (CDCl_3 , 100 MHz, ppm): 155.4, 147.7, 134.5, 131.3, 121.0, 114.4, 96.3, 52.0, 44.2, 15.0, 12.7. ^{11}B NMR (CDCl_3 , 128 MHz, ppm) 0.41 (t, $J_{\text{B-F}}$ = 29.5 Hz); UV/vis (DCM): λ_{max} (ϵ

[M⁻¹cm⁻¹]) 477 (3.38× 10⁴). HRMS (ESI-TOF) m/z = calculated for C₁₅H₁₈BF₂N₃ = 312.1457 [M+Na]⁺, measured 312.1471 [M+Na]⁺.

BODIPY 3

Yellow-red crystalline solid. Yield: 18% (42 mg); ¹H NMR (CDCl₃, 400 MHz, ppm): δ 8.83 (d, *J* = 12 Hz, 1H), 7.61 (s, 2H), 6.99 (d, *J* = 4 Hz, 2H), 6.41 (m, 2H), 5.93 (d, *J* = 12 Hz, 1H), 3.29 (s, 3H), 3.12 (s, 3H). ¹³C NMR (CDCl₃, 100 MHz, ppm): 156.0, 147.7, 134.3, 131.2, 120.7, 114.3, 96.4, 53.8, 27.5, 24.4. UV/vis (DCM): λ_{max} (ε [M⁻¹cm⁻¹]) 476 (3.34× 10⁴). HRMS (ESI-TOF) m/z = calculated for C₁₃H₁₄BF₂N₃ = 284.1143 [M+Na]⁺, measured 284.1147 [M+Na]⁺.

BODIPY 4a

Yellow-red crystalline solid. Yield: 13% (36 mg); ¹H NMR (CDCl₃, 400 MHz, ppm): δ 8.01 (d, *J* = 12 Hz, 1H), 7.60 (s, 2H), 6.94 (d, *J* = 4 Hz, 2H), 6.42 (m, 2H), 6.21 (d, *J* = 12 Hz, 1H), 4.32 (m, 1H), 4.82 (m, 1H), 1.38 (d, *J* = 4 Hz, 12H). ¹³C NMR (CDCl₃, 100 MHz, ppm): 153.0, 147.9, 134.0, 131.1, 120.6, 114.2, 96.8, 51.4, 49.2, 23.8, 20.3; UV/vis (DCM): λ_{max} (ε [M⁻¹cm⁻¹]) 477 (3.87× 10⁴). HRMS (ESI-TOF) m/z = calculated for C₁₆H₁₈BF₂N₃ = 340.1770 [M+Na]⁺, measured 340.1763 [M+Na]⁺.

BODIPY 4b

Yellow-red crystalline solid. Yield: 9% (25 mg); ¹H NMR (CDCl₃, 400 MHz, ppm): δ 7.56 (s, 2H), 6.84 (s, 2H), 6.37 (s, 2H), 6.03 (s, 1H), 4.38 (m, 1H), 3.54 (m, 1H), 2.45 (s, 1H), 1.37 (m, 9H). ¹³C NMR (CDCl₃, 100 MHz, ppm): 145.0, 139.6, 134.0, 132.3, 121.6, 119.1, 114.1, 52.0, 40.2, 34.6, 21.6, 20.9, 14.9. UV/vis (DCM): λ_{max} (ε [M⁻¹cm⁻¹]) 504 (3.40× 10⁴) and 466 (2.99× 10⁴). HRMS (ESI-TOF) m/z = calculated for C₁₇H₂₂BF₂N₃ = 340.1770 [M+Na]⁺, measured 340.1771 [M+Na]⁺.

BODIPY 5a

Yellow-red crystalline solid. Yield: 12% (32 mg); ¹H NMR (CDCl₃, 400 MHz, ppm): δ 7.84 (d, *J* = 12 Hz, 1H), 7.59 (s, 2H), 6.97 (d, *J* = 4 Hz, 2H), 6.40 (m, 2H), 6.06 (d, *J* = 12 Hz, 1H), 3.54 (m, 4H), 1.77 (m, 6H). ¹³C NMR (CDCl₃, 100 MHz, ppm): 156.0, 147.7, 134.3, 131.2, 120.9, 114.3, 96.0, 53.8, 27.1, 24.0. UV/vis

(DCM): λ_{max} (ϵ [$M^{-1}cm^{-1}$]) 477 (3.14×10^4). HRMS (ESI-TOF) m/z = calculated for $C_{16}H_{18}BF_2N_3$ = 324.1457 $[M+Na]^+$, measured 324.1444 $[M+Na]^+$.

BODIPY 5b

Yellow-red crystalline solid. Yield: 7% (18 mg); 1H NMR ($CDCl_3$, 400 MHz, ppm): δ 7.78 (s, 1H), 7.61 (s, 2H), 6.84 (d, J = 4 Hz, 2H), 6.41 (m, 2H), 3.44 (m, 4H), 2.80 (t, J = 8 Hz, 2H), 2.15 (p, J = 8 Hz, 2H), 1.33 (t, J = 8 Hz, 3H). ^{13}C NMR ($CDCl_3$, 100 MHz, ppm): 155.6, 147.7, 133.8, 131.4, 123.8, 113.9, 110.2, 52.6, 47.0, 25.7, 21.8, 14.0; UV/vis (DCM): λ_{max} (ϵ [$M^{-1}cm^{-1}$]) 447 (3.9×10^4). HRMS (ESI-TOF) m/z = calculated for $C_{16}H_{18}BF_2N_3$ = 324.1457 $[M+Na]^+$, measured 324.1556 $[M+Na]^+$.

7.6. Conclusion

In Summary, a novel route for the introduction of enamines at the *meso* position of the BODIPYs was developed via oxidation of *tert*-amines and *in situ* cross coupling with 8-chloro BODIPY. The reaction resembles with the reaction of *p*-chloranil with triethyl amine and indicates the electron deficient nature of 8-chloro BODIPY. The *N*-ethyl substituents are more reactive compared to the *N*-(CH_2-CH_2-) and *N*-($CH(CH_3)_2$) substituents. The electronic absorption of *meso* enamine substituted BODIPYs show blue shift of ~ 27 nm than the 8-chloro BODIPY (**1**). The alkyl substituents at the vinyl carbons have strong influence on the photophysical properties of these BODIPYs.

References

-
- [1] (a) Lu, H., Mack, J., Yang, Y., & Shen, Z. (2014). Structural modification strategies for the rational design of red/NIR region BODIPYs. *Chemical Society Reviews*, 43(13), 4778–4823. <http://doi.org/10.1039/C4CS00030G>; (b) Nepomnyashchii, A. B., & Bard, A. J. (2012). Electrochemistry and Electrogenated Chemiluminescence of BODIPY Dyes. *Accounts of Chemical Research*, 45(11), 1844–1853. <http://doi.org/10.1021/ar200278b>; (c) Boens, N., Leen, V., & Dehaen, W. (2012). Fluorescent indicators based on BODIPY. *Chemical Society Reviews*, 41(3), 1130–1172. <http://doi.org/10.1039/C1CS15132K>; (d) Bozdemir, O. A., Guliyev, R., Buyukcakil, O., Selcuk, S.,

-
- Kolemen, S., Gulseren, G., ... Akkaya, E. U. (2010). Selective Manipulation of ICT and PET Processes in Styryl-Bodipy Derivatives: Applications in Molecular Logic and Fluorescence Sensing of Metal Ions. *Journal of the American Chemical Society*, 132(23), 8029–8036. <http://doi.org/10.1021/ja1008163>.
- [2] (a) Chen, J., Mizumura, M., Shinokubo, H., & Osuka, A. (2009). Functionalization of Boron Dipyrin (BODIPY) Dyes through Iridium and Rhodium Catalysis: A Complementary Approach to α - and β -Substituted BODIPYs. *Chemistry – A European Journal*, 15(24), 5942–5949. <http://doi.org/10.1002/chem.200802541>; (b) Ulrich, G., Ziesel, R., & Harriman, A. (2008). Die vielseitige Chemie von Bodipy-Fluoreszenzfarbstoffen. *Angewandte Chemie*, 120(7), 1202–1219. <http://doi.org/10.1002/ange.200702070>; (c) Baruah, M., Qin, W., Vallée, R. A. L., Beljonne, D., Rohand, T., Dehaen, W., & Boens, N. (2005). A Highly Potassium-Selective Ratiometric Fluorescent Indicator Based on BODIPY Azacrown Ether Excitable with Visible Light. *Organic Letters*, 7(20), 4377–4380. <http://doi.org/10.1021/ol051603o>; (d) Han, J., Gonzalez, O., Aguilar-Aguilar, A., Pena-Cabrera, E., & Burgess, K. (2009). 3- and 5-Functionalized BODIPYs via the Liebeskind-Srogl reaction. *Organic & Biomolecular Chemistry*, 7(1), 34–36. <http://doi.org/10.1039/B818390B>.
- [3] (a) Bessette, A., & Hanan, G. S. (2014). Design, synthesis and photophysical studies of dipyrromethene-based materials: insights into their applications in organic photovoltaic devices. *Chemical Society Reviews*, 43(10), 3342–3405. <http://doi.org/10.1039/C3CS60411J>; (b) Loudet, A., & Burgess, K. (2007). BODIPY Dyes and Their Derivatives: Syntheses and Spectroscopic Properties. *Chemical Reviews*, 107(11), 4891–4932. <http://doi.org/10.1021/cr078381n>; (c) Yokoi, H., Wachi, N., Hiroto, S., & Shinokubo, H. (2014). Oxidation of 2-amino-substituted BODIPYs providing pyrazine-fused BODIPY trimers. *Chemical Communications*, 50(21), 2715–2717. <http://doi.org/10.1039/C3CC48738E>; (d) Tamgho, I.-S., Hasheminasab, A., Engle, J. T., Nemykin, V. N., & Ziegler, C. J. (2014). A New Highly Fluorescent and Symmetric Pyrrole–

BF2 Chromophore: BOPHY. *Journal of the American Chemical Society*, 136(15), 5623–5626. <http://doi.org/10.1021/ja502477a>.

- [4] (a) Jiao, L., Pang, W., Zhou, J., Wei, Y., Mu, X., Bai, G., & Hao, E. (2011). Regioselective Stepwise Bromination of Boron Dipyrromethene (BODIPY) Dyes. *The Journal of Organic Chemistry*, 76(24), 9988–9996. <http://doi.org/10.1021/jo201754m>; (b) Godoy, J., Vives, G., & Tour, J. M. (2010). Synthesis of Highly Fluorescent BODIPY-Based Nanocars. *Organic Letters*, 12(7), 1464–1467. <http://doi.org/10.1021/ol100108r>; (c) Ortiz, M. J., Agarrabeitia, A. R., Duran-Sampedro, G., Bañuelos Prieto, J., Lopez, T. A., Massad, W. A., ... Lopez Arbeloa, I. (2012). Synthesis and functionalization of new polyhalogenated BODIPY dyes. Study of their photophysical properties and singlet oxygen generation. *Tetrahedron*, 68(4), 1153–1162. <http://doi.org/http://dx.doi.org/10.1016/j.tet.2011.11.070>; (d) Baruah, M., Qin, W., Basarić, N., De Borggraeve, W. M., & Boens, N. (2005). BODIPY-Based Hydroxyaryl Derivatives as Fluorescent pH Probes. *The Journal of Organic Chemistry*, 70(10), 4152–4157. <http://doi.org/10.1021/jo0503714>.
- [5] (a) Gautam, P., Dhokale, B., Shukla, V., Singh, C. P., Bindra, K. S., & Misra, R. (2012). Optical limiting performance of meso-tetraferrocenyl porphyrin and its metal derivatives. *Journal of Photochemistry and Photobiology A: Chemistry*, 239(0), 24–27. <http://doi.org/http://dx.doi.org/10.1016/j.jphotochem.2012.04.020>; (b) Dhokale, B., Gautam, P., & Misra, R. (2012). Donor–acceptor perylenediimide–ferrocene conjugates: synthesis, photophysical, and electrochemical properties. *Tetrahedron Letters*, 53(18), 2352–2354. <http://doi.org/http://dx.doi.org/10.1016/j.tetlet.2012.02.107>; (c) Maragani, R., Jadhav, T., Mobin, S. M., & Misra, R. (2013). C 3 symmetric ferrocenyl triazines: synthesis, structure, and properties. *RSC Advances*, 3(9), 2889–2892. <http://doi.org/10.1039/C2RA23153K>; (d) Misra, R., Gautam, P., Sharma, R., & Mobin, S. M. (2013). Donor– π –acceptor– π –donor ferrocenyl benzothiadiazoles: synthesis, structure, and properties. *Tetrahedron Letters*, 54(5), 381–383. <http://doi.org/http://dx.doi.org/10.1016/j.tetlet.2012.11.016>; (e) Misra, R., Gautam, P., Jadhav, T., & Mobin, S. M. (2013). Donor–Acceptor Ferrocenyl-Substituted Benzothiadiazoles: Synthesis, Structure, and Properties.

-
- The Journal of Organic Chemistry*, 78(10), 4940–4948. <http://doi.org/10.1021/jo4005734>; (f) Jadhav, T., Maragani, R., Misra, R., Sreeramulu, V., Rao, D. N., & Mobin, S. M. (2013). Design and synthesis of donor-acceptor pyrazabole derivatives for multiphoton absorption. *Dalton Transactions*, 42(13), 4340–4342. <http://doi.org/10.1039/C3DT33065F>; (g) Sharma, R., Gautam, P., Mobin, S. M., & Misra, R. (2013). [small beta]-Substituted ferrocenyl porphyrins: synthesis, structure, and properties. *Dalton Transactions*, 42(15), 5539–5545. <http://doi.org/10.1039/C3DT00003F>; (h) Sharma, R., Margani, R., Mobin, S. M., & Misra, R. (2013). Ferrocenyl substituted calixarenes: synthesis, structure and properties. *RSC Advances*, 3(17), 5785–5788. <http://doi.org/10.1039/C3RA00146F>; (i) Misra, R., Jadhav, T., & Mobin, S. M. (2013). Aryl pyrazaboles: a new class of tunable and highly fluorescent materials. *Dalton Transactions*, 42(47), 16614–16620. <http://doi.org/10.1039/C3DT52154K>.
- [6] (a) Dhokale, B., Gautam, P., Mobin, S. M., & Misra, R. (2013). Donor-acceptor, ferrocenyl substituted BODIPYs with marvelous supramolecular interactions. *Dalton Transactions*, 42(5), 1512–1518. <http://doi.org/10.1039/C2DT31632C>; (b) Gautam, P., Dhokale, B., Mobin, S. M., & Misra, R. (2012). Ferrocenyl BODIPYs: synthesis, structure and properties. *RSC Advances*, 2(32), 12105–12107. <http://doi.org/10.1039/C2RA21964F>; (c) Misra, R., Dhokale, B., Jadhav, T., & Mobin, S. M. (2014). The quenching of fluorescence as an indicator of donor-strength in meso arylethynyl BODIPYs. *Dalton Transactions*, 43(12), 4854–4861. <http://doi.org/10.1039/C3DT53056F>. (d) Misra, R., Dhokale, B., Jadhav, T., & Mobin, S. M. (2014). Heteroatom-Connected Ferrocenyl BODIPYs: Synthesis, Structure, and Properties. *Organometallics*, 33(7), 1867–1877. <http://doi.org/10.1021/om5002292>.
- [7] (a) Kusaka, S., Sakamoto, R., Kitagawa, Y., Okumura, M., & Nishihara, H. (2013). meso-Alkynyl BODIPYs: Structure, Photoproperties, π -Extension, and Manipulation of Frontier Orbitals. *Chemistry – An Asian Journal*, 8(4), 723–727. <http://doi.org/10.1002/asia.201201176>; (b) Misra, R., Dhokale, B., Jadhav, T., & Mobin, S. M. (2013). Donor-acceptor meso-alkynylated ferrocenyl

BODIPYs: synthesis, structure, and properties. *Dalton Transactions*, 42(37), 13658–13666. <http://doi.org/10.1039/C3DT51374B>.

- [8] Leen, V., Yuan, P., Wang, L., Boens, N., & Dehaen, W. (2012). Synthesis of Meso-Halogenated BODIPYs and Access to Meso-Substituted Analogues. *Organic Letters*, 14(24), 6150–6153. <http://doi.org/10.1021/ol3028225>.
- [9] Morigaki, A., Kawamura, M., Arimitsu, S., Ishihara, T., & Konno, T. (2013). Application of Tertiary Amines Synthesized by Catalytic Dehydrogenation of Enamines as Nucleophilic C2 Synthons for 1,4-Conjugate Addition with Fluoroalkylated Olefins. *Asian Journal of Organic Chemistry*, 2(3), 239–243. <http://doi.org/10.1002/ajoc.201300007>; (b) Barluenga, J., Fernandez, M. A., Aznar, F., & Valdes, C. (2002). Novel method for the synthesis of enamines by palladium catalyzed amination of alkenyl bromides. *Chemical Communications*, (20), 2362–2363. <http://doi.org/10.1039/B207524E>; (c) Zhang, X., Fried, A., Knapp, S., & Goldman, A. S. (2003). Novel synthesis of enamines by iridium-catalyzed dehydrogenation of tertiary amines. *Chemical Communications*, (16), 2060–2061. <http://doi.org/10.1039/B304357F>; (d) Takasu, N., Oisaki, K., & Kanai, M. (2013). Iron-Catalyzed Oxidative C(3)–H Functionalization of Amines. *Organic Letters*, 15(8), 1918–1921. <http://doi.org/10.1021/ol400568u>.
- [10] Buckley, D., Dunstan, S., & Henbest, H. B. (1957). 981. Amine oxidation. Part II. Reactions of aliphatic tertiary amines with quinones. Detection of dehydrogenation by the formation of coloured dialkylaminovinylquinones. *Journal of the Chemical Society (Resumed)*, (0), 4880–4891. <http://doi.org/10.1039/JR9570004880>.
- [11] Boens, N., Wang, L., Leen, V., Yuan, P., Verbelen, B., Dehaen, W., ... Alvarez-Pez, J. M. (2014). 8-HaloBODIPYs and Their 8-(C, N, O, S) Substituted Analogues: Solvent Dependent UV–Vis Spectroscopy, Variable Temperature NMR, Crystal Structure Determination, and Quantum Chemical Calculations. *The Journal of Physical Chemistry A*, 118(9), 1576–1594. <http://doi.org/10.1021/jp412132y>.

Conclusions and scope for future work

Conclusions

In recent years BODIPY based Donor-acceptor (D-A) systems have gained immense attention of scientific community. The nature of D-A interaction depends on the electron donating ability of donor, electron withdrawing strength of acceptor and nature of the spacer connecting them. The BODIPY fluorophores are one of the strong acceptor. They exhibit strong absorption and high fluorescence quantum yield. The photonic properties of BODIPYs can be tuned by slight variation in the nature of substituents.

The BODIPYs can be functionalized at α , β and *meso* positions. We have functionalized various positions of BODIPYs with ferrocenyl group through varying spacers and evaluated different positions of BODIPY for their superior electronic communication, and explored into efficient D-A systems.

In chapter 3, the BODIPYs were functionalized at the β -position with ferrocenyl group through varying length of spacers. The conformation between two cyclopentadienyl rings of ferrocene was found to be the function of conjugation length and steric hindrance. The cyclopentadienyl rings of ferrocene exhibits staggered conformation in sterically crowded ferrocenyl BODIPY with short conjugation length, whereas they exhibit eclipsed conformation in ferrocenyl BODIPY with lower steric crowding and elongated conjugation length. The photonic properties of ferrocenyl BODIPYs were function of the spacer between BODIPY and ferrocene. The nature of spacers determine the strength of D-A and charge transfer interaction. The β alkynylated ferrocenyl BODIPYs exhibit blue shifted absorption than the previously reported α alkynylated ferrocenyl BODIPYs, which suggests the superior electronic communication in α -alkynylated ferrocenyl BODIPYs.

In Chapter 4, we have designed and synthesized the *meso*-alkynylated ferrocenyl BODIPYs with varying conjugation lengths. The *meso* alkynylated ferrocenyl BODIPYs exhibit the red shifted absorption and higher extinction coefficient than α and β alkynylated BODIPYs. The trend in red shift follows the order *meso* > α > β alkynylated BODIPYs. This suggests the superior electronic communication in *meso*

alkynylated ferrocenyl BODIPYs. The photonic properties of *meso* alkynylated ferrocenyl BODIPYs were also the function of the spacer between ferrocene and BODIPY core.

In chapter 5, we have synthesized various *meso* aryl alkyne substituted BODIPYs by Sonogashira cross-coupling reaction. The photophysical and electrochemical properties of the BODIPYs can be tuned by varying the strength of donor. These aryl alkynylated BODIPYs show gradual red shift in the absorption with increasing conjugation length. The quenching of fluorescence was correlated with the electron donating strength of the donor. Stronger the donor poor will be the quantum yield and *vice versa*. The anthracene, pyrene and triphenylamine moieties were found to have stronger electron donating ability than *p*-methoxyphenyl, phenanthrene, 1-naphthalene, biphenyl, and 2-naphthalene moieties. This was further supported by computational calculations and electrochemical analysis.

In chapter 6, the series of heteroatom connected ferrocenyl BODIPYs were designed and synthesized by the nucleophilic aromatic substitution reaction of 8-chloro BODIPY, with ferrocenyl anilines and ferrocenyl phenols. The effects of heteroatom substitution at the *meso* position on the optical and electrochemical properties of the BODIPY were studied. The absorption spectra of the BODIPYs containing nitrogen at the *meso* position show blue shift of 80 nm, whereas the BODIPYs containing oxygen at the *meso* position show blue shift of 50 nm compared to 8-chloro BODIPY. The DFT calculations reveal strong donor acceptor interactions. The TD-DFT studies indicate that the ferrocenyl group perturbs the HOMO energy levels and induces the absorption from HOMO-*n* energy levels, whereas the nature of heteroatom does not affect the HOMO but perturbs the LUMO energy level significantly.

In chapter 7, the electron deficient nature of 8-chloro BODIPY was used for the oxidation of aliphatic amines to enamines and *in situ* cross-coupling. This has been explored for the synthesis of various *meso* enamine substituted BODIPYs. The reaction conditions were optimized to achieve better yields. The reaction works well with aliphatic *tert*-amines bearing *N*-(CH-CH-) backbone. The *N*-alkyl substituents have strong influence on the properties of enamine substituted BODIPYs. The incorporation of enamines quenches the fluorescence of BODIPYs through intramolecular charge-transfer from enamine to the BODIPY.

Scope for future work

The thesis highlights the superior electronic communication of the *meso* alkynylated BODIPYs and explored the *meso* position for various D-A systems. Wide range of donors were incorporated at the *meso* position of BODIPY. The theoretical studies by Acebal *et al.* indicates the great potential of *meso*-alkynylated BODIPYs as NLO materials.^[1] Thus the various aryl substituted *meso* alkynylated BODIPYs can be used for NLO applications.

The incorporation of donor at the *meso* position of BODIPY results in blue shifted absorption and poor quantum yields. This suggests that the incorporation of acceptors at the *meso* position of BODIPYs may result the red shifted absorption and emission with higher fluorescence quantum yields. The photonic properties of BODIPYs can be tuned effectively by incorporating various acceptors through varying length of spacers. This can be further explored as a measure of relative acceptor strength of different acceptors.

The *meso* enamine substituted BODIPYs are non-fluorescent due to the charge transfer from donor enamine to the acceptor BODIPY. The protonation of enamines can regain the fluorescence of these BODIPYs, thus the enamine substituted BODIPYs can be used as ‘fluorescence ON’ sensor for acid.

[1] Acebal, P., Blaya, S., & Carretero, L. (2003). Dipyrromethene-BF₂ complexes with optimized electrooptic properties. *Chemical Physics Letters*, 382(5–6), 489–495. <http://doi.org/http://dx.doi.org/10.1016/j.cplett.2003.10.125>.